



# Acoustic and Laser Doppler Anemometer Results for Confluent and 12-Lobed $E^3$ Mixer Exhaust Systems for Subsonic Jet Noise Reduction

M. Salikuddin, R.R. Babbitt, H. Shin, S. Wisler, B.A. Janardan, and R.K. Majjigi  
General Electric Aircraft Engines Company, Cincinnati, Ohio

## The NASA STI Program Office . . . in Profile

Since its founding, NASA has been dedicated to the advancement of aeronautics and space science. The NASA Scientific and Technical Information (STI) Program Office plays a key part in helping NASA maintain this important role.

The NASA STI Program Office is operated by Langley Research Center, the Lead Center for NASA's scientific and technical information. The NASA STI Program Office provides access to the NASA STI Database, the largest collection of aeronautical and space science STI in the world. The Program Office is also NASA's institutional mechanism for disseminating the results of its research and development activities. These results are published by NASA in the NASA STI Report Series, which includes the following report types:

- **TECHNICAL PUBLICATION.** Reports of completed research or a major significant phase of research that present the results of NASA programs and include extensive data or theoretical analysis. Includes compilations of significant scientific and technical data and information deemed to be of continuing reference value. NASA's counterpart of peer-reviewed formal professional papers but has less stringent limitations on manuscript length and extent of graphic presentations.
- **TECHNICAL MEMORANDUM.** Scientific and technical findings that are preliminary or of specialized interest, e.g., quick release reports, working papers, and bibliographies that contain minimal annotation. Does not contain extensive analysis.
- **CONTRACTOR REPORT.** Scientific and technical findings by NASA-sponsored contractors and grantees.

- **CONFERENCE PUBLICATION.** Collected papers from scientific and technical conferences, symposia, seminars, or other meetings sponsored or cosponsored by NASA.
- **SPECIAL PUBLICATION.** Scientific, technical, or historical information from NASA programs, projects, and missions, often concerned with subjects having substantial public interest.
- **TECHNICAL TRANSLATION.** English-language translations of foreign scientific and technical material pertinent to NASA's mission.

Specialized services that complement the STI Program Office's diverse offerings include creating custom thesauri, building customized databases, organizing and publishing research results . . . even providing videos.

For more information about the NASA STI Program Office, see the following:

- Access the NASA STI Program Home Page at <http://www.sti.nasa.gov>
- E-mail your question via the Internet to [help@sti.nasa.gov](mailto:help@sti.nasa.gov)
- Fax your question to the NASA Access Help Desk at 301-621-0134
- Telephone the NASA Access Help Desk at 301-621-0390
- Write to:  
NASA Access Help Desk  
NASA Center for AeroSpace Information  
7121 Standard Drive  
Hanover, MD 21076



# Acoustic and Laser Doppler Anemometer Results for Confluent and 12-Lobed $E^3$ Mixer Exhaust Systems for Subsonic Jet Noise Reduction

M. Salikuddin, R.R. Babbitt, H. Shin, S. Wisler, B.A. Janardan, and R.K. Majjigi  
General Electric Aircraft Engines Company, Cincinnati, Ohio

Prepared under Contract NAS3-26617

National Aeronautics and  
Space Administration

Glenn Research Center

## Acknowledgments

This report is prepared by GE Aircraft Engines, Cincinnati, Ohio for NASA Glenn Research Center, Cleveland, Ohio under LET Contract NAS3-26617, Task Order 31. Mr. Gene Krejsa was the Project Manager for NASA Glenn Research Center and Dr. R.K. Majjigi was the Program Manager for GEAE. The authors are thankful to Mr. J. Brausch for his contributions in designing and acquiring the model hardware and helping the installation of the hardware in GEAE's Cell 41 for testing. The authors are also thankful to Mr. J. Hencheck and Ms. S. Thomson for running the test facility. The authors are particularly thankful to Dr. C.E. Whitfield for her involvement in acoustic testing and data analysis during the course of this work

Trade names or manufacturers' names are used in this report for identification only. This usage does not constitute an official endorsement, either expressed or implied, by the National Aeronautics and Space Administration.

Available from

NASA Center for Aerospace Information  
7121 Standard Drive  
Hanover, MD 21076

National Technical Information Service  
5285 Port Royal Road  
Springfield, VA 22100

Available electronically at <http://gltrs.grc.nasa.gov>



## SUMMARY

The research described in this report has been funded by NASA Lewis Research Center as part of the Advanced Subsonic Technologies (AST) initiative. The program operates under the Large Engine Technologies (LET) as Task Order #31. Task Order 31 is a three year research program divided into three subtasks. Subtask A develops the experimental acoustic and aerodynamic subsonic mixed flow exhaust system data bases. Subtask B seeks to develop and assess CFD-based aero-acoustic methods for subsonic mixed flow exhaust systems. Subtask B relies on the data obtained from Subtask A to direct and calibrate the aero-acoustic methods development. Subtask C then seeks to utilize both the aero-acoustic data bases developed in Subtask A and the analytical methods developed in Subtask B to define improved subsonic mixed-flow exhaust systems. The mixed flow systems defined in Subtask C will be experimentally demonstrated for improved noise reduction in a scale model aero-acoustic test conducted similarly to the test performed in Subtask A. The overall object of this Task Order is to develop and demonstrate the technology to define a -3EPNdB exhaust system relative to 1992 exhaust system technology.

### **Specific functions to be performed in conjunction with the contractual execution of Subtask A include:**

- Identify E3 mixer hardware for test in GE Cell 41 anechoic test facility
- Procure the design, refurbishment, and fabrication of E3 scale model test hardware
- Develop a detailed test plan for acoustic and LV data measurement
- Perform acoustic and aero-flowfield measurements per the Test Plan
- Process all acoustic data for scaling, flight transformation and extrapolation to FAR 36 Stage 3
- Process the aero-flowfield data
- Analyze the data to establish aero and acoustic databases, and
- Perform pre-test aero CFD predictions for test planning and data comparison.

### **The activities to be performed in conjunction with Subtask B include:**

- Performing CFD aero analyses on the E3 configurations to assess CFD code enhancements
- Modify the MGB jet noise predictions to assess internal as well as external jet noise
- Perform acoustic predictions with CFD/MGB unified analysis on the E3 configurations, and compare to data
- Document assessment of the CFD/MGB unified analysis.

### **The Subtask C specific functions include:**

- Design aero-flowpaths for LDMF configurations
- Assess technical and viability of a separate flow nozzle with a core nozzle suppressor

- Seek NASA test configuration approval
- Develop detailed drawings for instrumentation and model design
- Procure model design and fabrication
- Develop a detailed test plan for acoustic and aero-flowfield testing
- Perform acoustic and aero-flowfield measurements per the test plan
- Process all acoustic data for scaling, flight transformation and extrapolation to

#### FAR 36 Stage 3

- Process the aero-flowfield data
- Perform detailed test analysis to
  - a) Enhance the understanding of subsonic mixed-flow exhaust system jet noise characteristics
  - b) Improve the existing aero and acoustic design databases
  - c) Develop design approaches to meet the jet noise reduction goal (-3 EPNdB), and
- Perform pre-test aero and acoustic predictions and compare to data.

The information reported on in this document pertains to the activities associated with Subtask A of Task Order 31. The details associated with the E<sup>3</sup> test configurations, the scale model test program, the data analysis, and discussion of the data results are all detailed in this report.

## TABLE OF CONTENTS

Section	Page
SUMMARY	iii
1.0 INTRODUCTION	1
2.0 MODEL DESCRIPTION AND INSTRUMENTATION	9
2.1 Selection of E <sup>3</sup> Mixer Configurations	9
2.2 Cell 41 Adapter and Model Hardware Design	18
2.3 Model Instrumentation	21
3.0 TEST FACILITY	35
4.0 TEST PLAN	45
5.0 ACOUSTIC DATA	51
5.1 Cell 41 Acoustic Testing	51
5.2 Repeatability of Acoustic Data	53
5.3 Comparison of Mixer, Confluent, and Conic Nozzle Data	53
5.4 Effect of Mixing Duct Length	66
5.5 Effect of Variations from Engine Baseline Operating Cycle	69
5.6 Effect of Flight Mach Number	75
5.7 Acoustic Conclusions	75
6.0 AERO-FLOWFIELD DATA	81
6.1 Nozzle Exit Total Pressure and Total Temperature Survey	81
6.2 Velocity Measurements	86
6.2.1 Velocity Measurements of V1 (Confluent Mixer)	92
6.2.2 Velocity Measurements of V2 (Scalloped Mixer)	103
6.2.3 Velocity Measurements of V2A (Scalloped Mixer with Extended Tailpipe)	112
6.2.4 Velocity Measurements of F12A (Skewed Mixer)	119
6.2.5 Velocity Measurements of F9B (Scalloped and Staggered Mixer)	119
6.3 Nozzle Exit Plane Velocity Comparison	126
6.4 Conclusions	126

7.0	ANALYSIS COMPARED TO DATA	129
7.1	CFD - PAB3D (Ps-Distribution)	132
7.2	CFD - PAB3D (Exit PT & TT Profiles)	132
7.3	Flowfield Mean and Turbulent Velocities	136
7.3.1	Confluent Mixer (V1)	136
	Velocity Data Comparison	
7.3.2	ICLS Scaloped Lobe Mixer (V2)	136
	Velocity Data Comparison	
7.3.3	ICLS Scaloped Lobe Mixer (V2A)	147
	Velocity Data Comparison	
7.3.4	Skewed Lobe Mixer (F12A)	147
	Velocity Data Comparison	
8.0	REFERENCES	153
	Appendix A-Acoustic Data	155

## 1.0 INTRODUCTION

Jet mixing noise limits the amount of engine noise reduction that can be achieved at high power settings for current high bypass engines, and for advanced engines with bypass ratios less than 10. Methods for reducing jet mixing noise are therefore needed for engines with bypass ratios less than 10 that do not introduce significant performance and weight penalties.

Current production engines have bypass ratios in the range of 4 to 8. One certainty is that future noise certification rules will become more stringent. The question is by how much, from Stage 3 to Stage 3 - 3dB?, or - 4dB? The development of jet noise reduction concepts that are applicable to, and practical for, the current class of engines, therefore, becomes ever more significant. Because of the long lead time required to introduce new engines into the marketplace with sufficient fleet penetration to have a significant impact on community noise exposure, only by reducing the noise of current production engine models can it be hoped to reduce community noise impact in the next 15 to 20 years.

As part of the NASA Advanced Subsonic Technology (AST) program Noise Reduction charter, *GE Aircraft Engines* is involved in a three year research program sponsored under the NASA Large Engine Technology (LET) Contract NAS3-26617. The objective of the NASA/GEAE LET Task Order 31, *Subsonic Jet Noise Reduction*, is to develop high bypass exhaust system technology to reduce jet noise by 3 EPNdB relative to 1992 technology.

Subtask A under Task Order 31 calls for exhaust system acoustic testing in the GE Aircraft Engines Cell 41 anechoic free jet test facility. The scale models tested in Cell 41 were selected Energy Efficient Engine, E<sup>3</sup> Long Duct Mixed Flow (LDMF) exhaust system configurations with multi-lobed mixers. Subtask A establishes an aero and acoustic diagnostic database from which to calibrate and refine current aero and acoustic prediction tools.

Subtask A aero-acoustic testing utilizes select exhaust mixer systems from the Energy Efficient Engine, E<sup>3</sup>, engine development program. The E<sup>3</sup> engine (Figures 1.1 and 1.2), was developed under NASA contract in the 1970's and early 1980's as a demonstrator of advanced engine technologies [Ref. 1]. Part of the E<sup>3</sup> engine development was the design of the E<sup>3</sup> LDMF exhaust system. The E<sup>3</sup> exhaust system was developed in three phases of design/analyses, scale model development, and scale model test. Figures 1.3 through 1.5 show cross-sections from the three phases of E<sup>3</sup> scale models [Ref. 2].

Subtask A uses four 12-lobed mixers and one free/confluent mixer from the E<sup>3</sup> data base of LDMF configurations. Some refurbishment of the existing hardware was required. New hardware was also fabricated. New scale model hardware included, Cell 41 model adapters, upstream flow path hardware, including the E<sup>3</sup> fan and core ducts, two new nozzles, and laser velocimeter glass windows for viewing the mixing process for one of the nozzles.

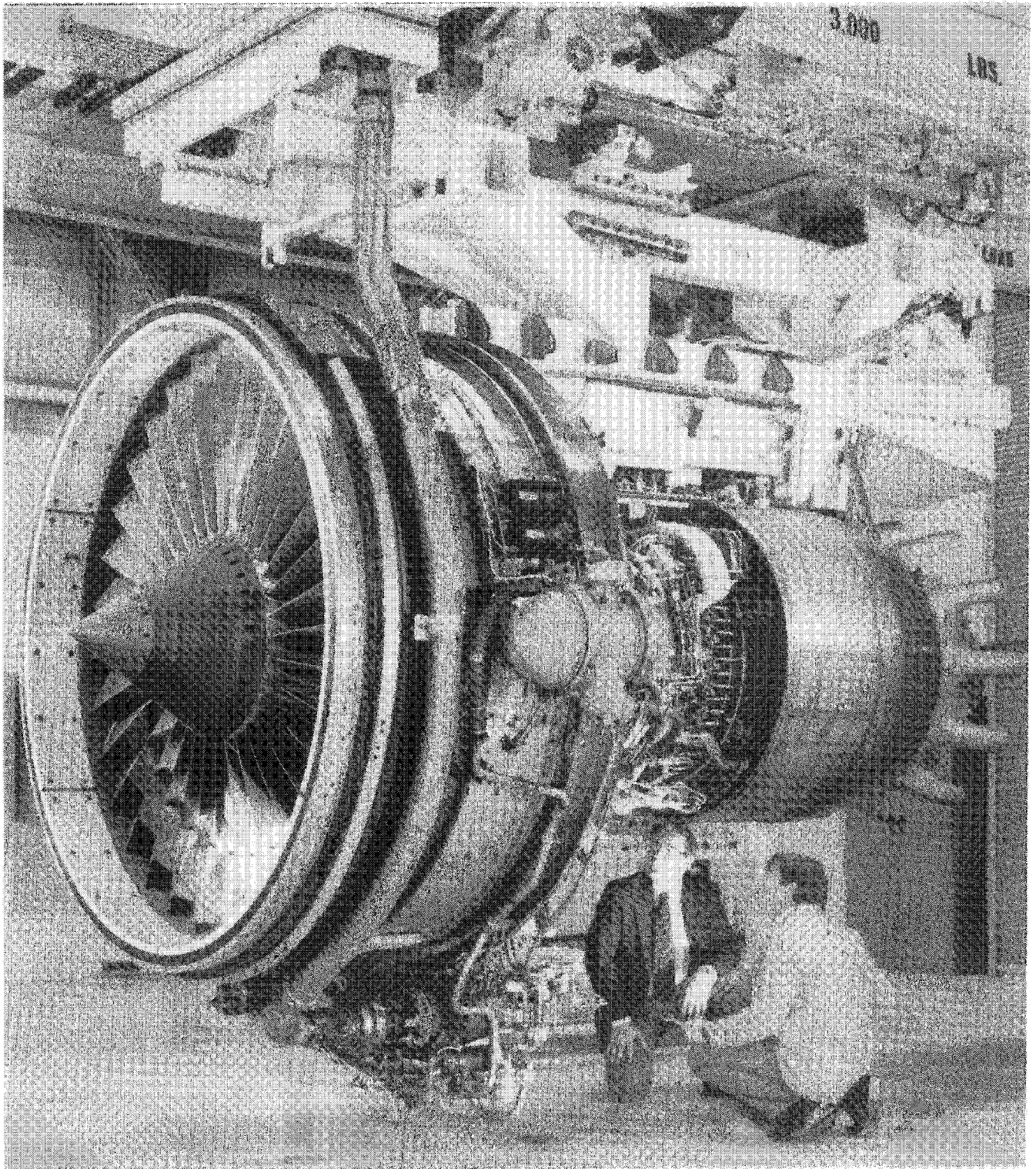


Figure 1.1. NASA-GE Energy Efficient Engine (E<sup>3</sup>).



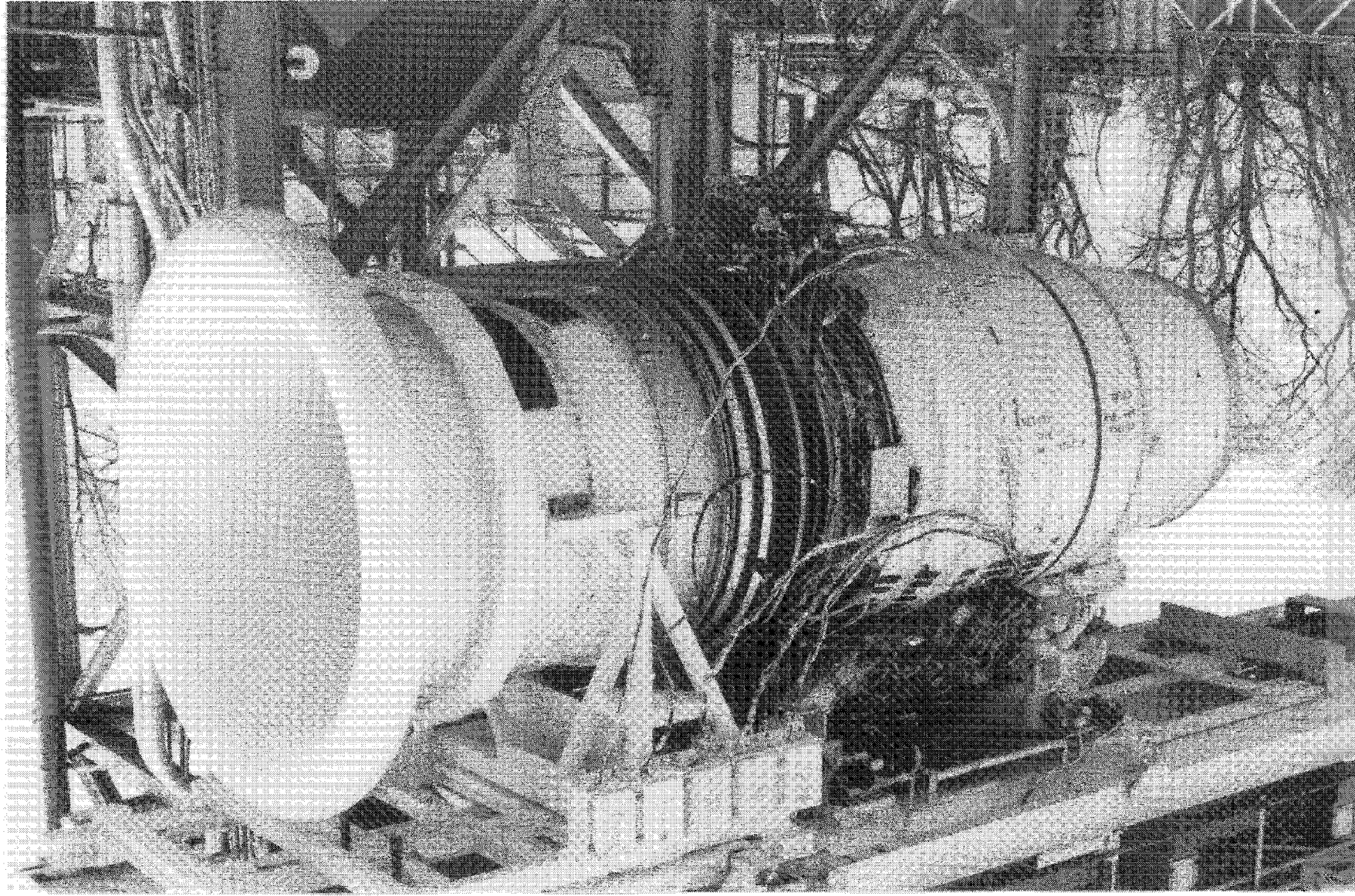


Figure 1.2. NASA-GE Energy Efficient Engine (E<sup>3</sup>) installed at the test site.

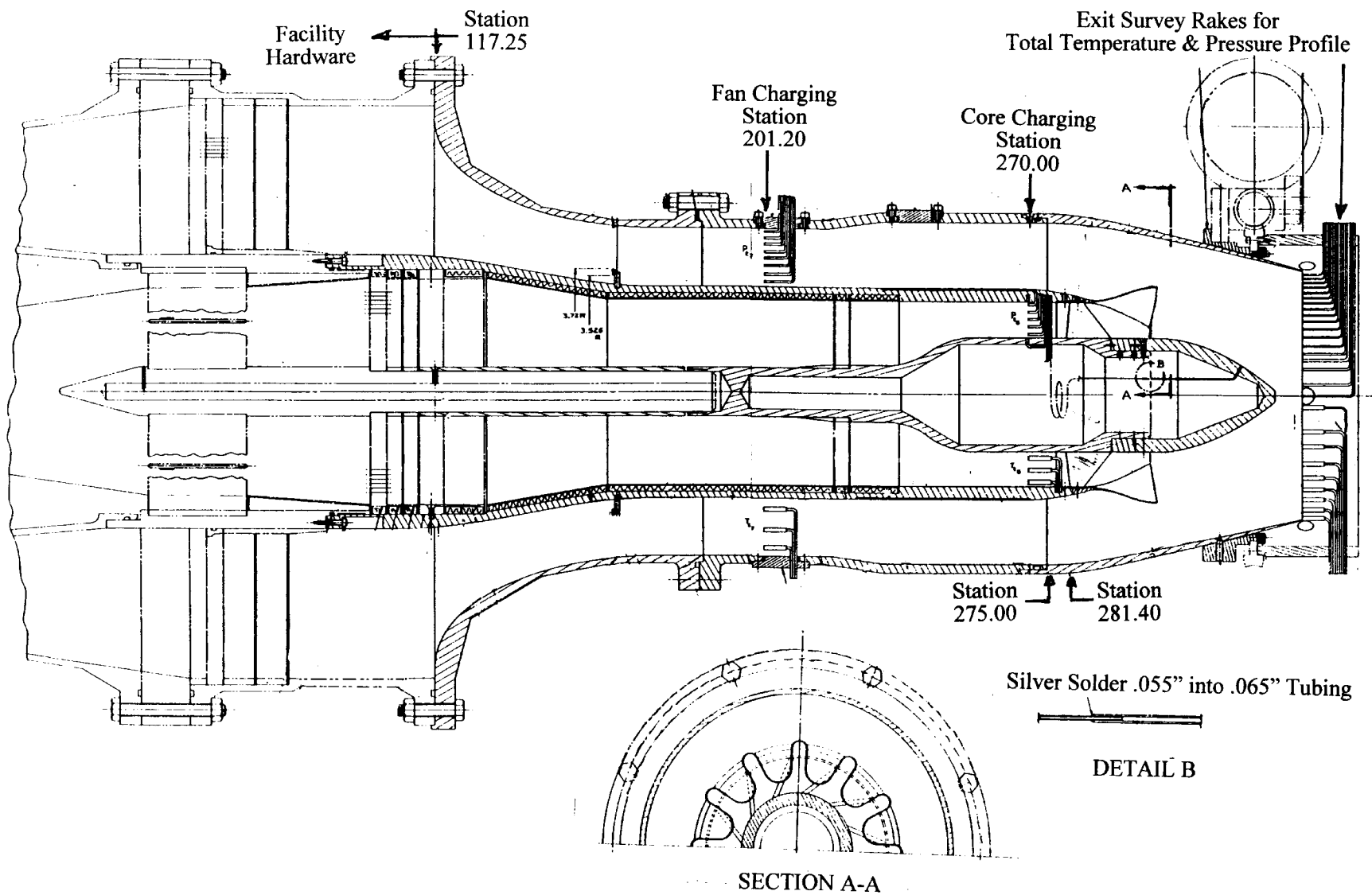


Figure 1.3. Phase I scale model test flowpath



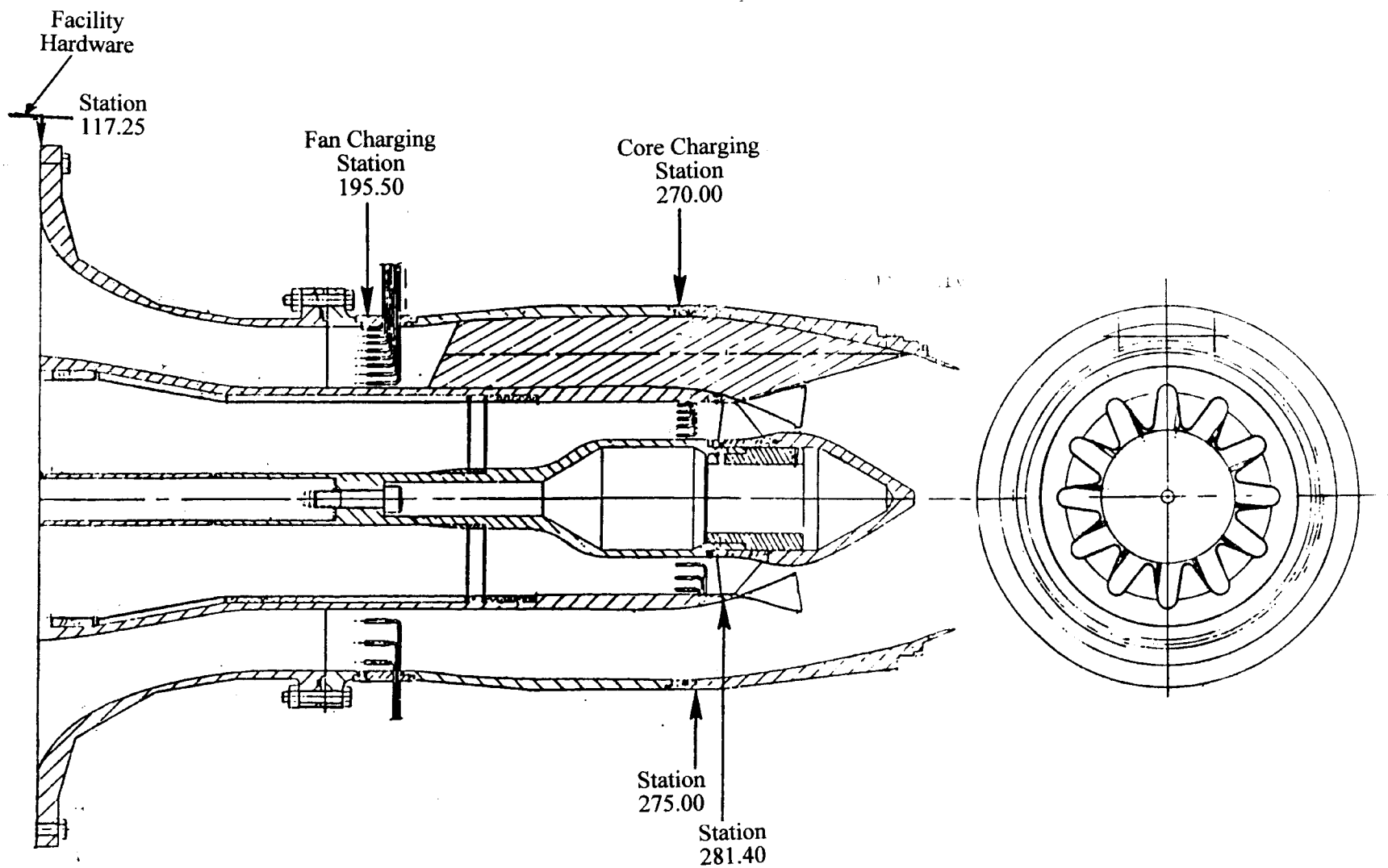


Figure 1.4. Phase II scale model test flowpath.

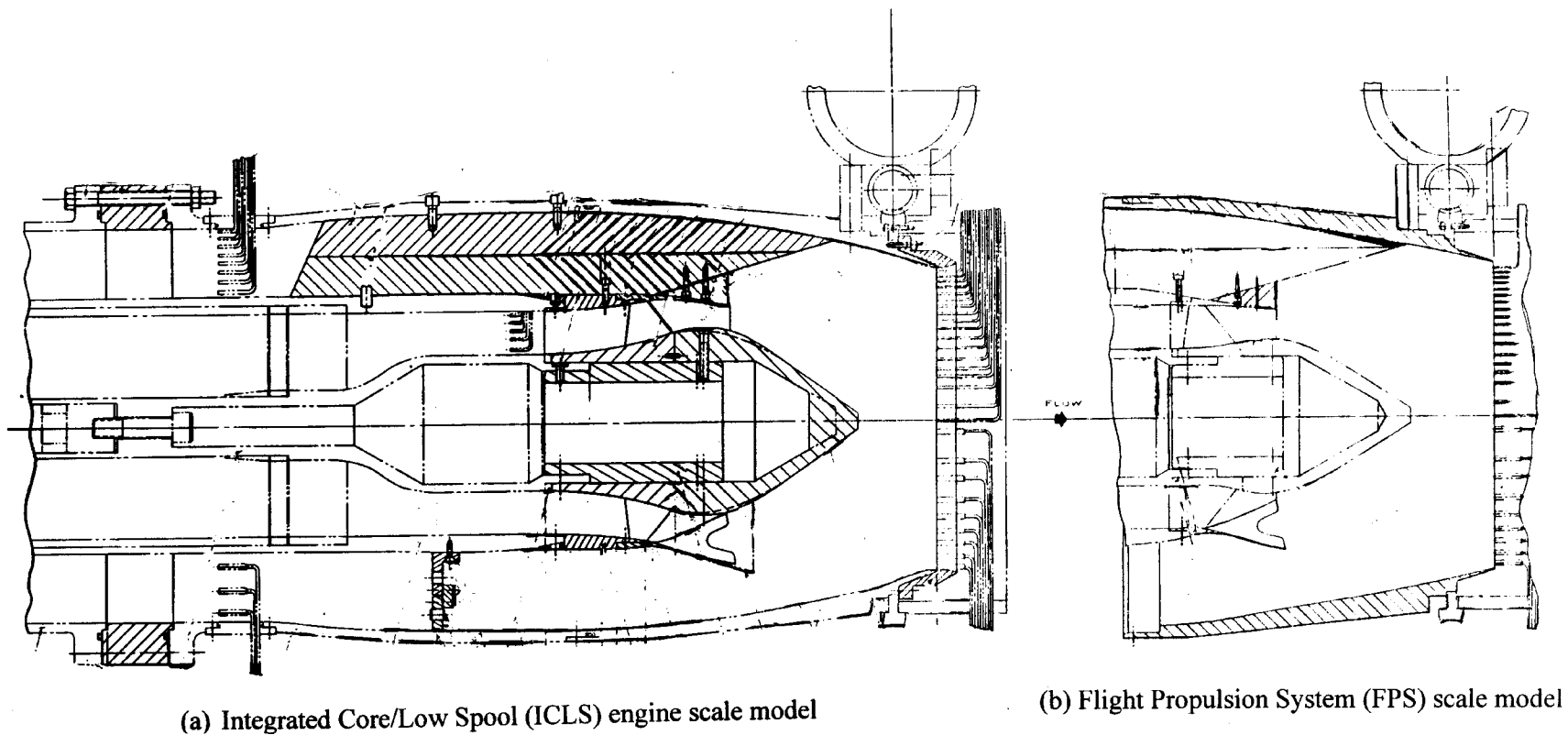


Figure 1.5. Phase III (a) Integrated Core/Low Spool (ICLS) engine and (b) Flight Propulsion System (FPS) scale model flowpaths.

Specific program objectives of the Subtask A aero-acoustic testing were to:

- Obtain acoustic data on various mixed flow exhaust systems that exhibit variations in mixer geometric characteristics and mixing performance.
- Quantify internal mixing noise relative to uniform mixed-flow conditions with a reference conic nozzle.
- Perform Laser Velocimeter measurements both of the external jet plume and internal mixing process to measure the jet flow velocities and turbulence intensity.
- Measure nozzle exit total pressure and temperature profiles.
- Measure surface pressure distributions on the fan duct, core duct and internal nozzle contours along with the fan and core side pressures on one of the lobed mixers.
- Establish the 1992 jet noise bench-mark based on a free (confluent) mixer configuration. The confluent mixers will be the basis from which the goal of reducing jet noise by 3 EPNdB will be measured.

CFD based aero flowfield pretest predictions were performed on several of the Subtask A test configurations. These predictions have been compared with the measured pressure, temperature, velocity, and turbulence intensity data for evaluating the quality of the CFD prediction.



## 2.0 MODEL DESCRIPTION

### 2.1 Selection of E<sup>3</sup> Mixer Configurations:

The cross section of the GE E<sup>3</sup> engine-nacelle design in Figure 2.1 shows the relationship of the mixer to the overall engine flowpath. The engine has a fan-to-core exhaust system bypass ratio of 7.3 at take-off conditions.

The E<sup>3</sup> model exhaust system is a 12% geometric scale model of the NASA/GE development engine. The scale was maintained at 12% for the Cell 41 test hardware for consistency between the new hardware and previously tested E<sup>3</sup> configurations. Geometric simulation of the exhaust system flowpath in the 12% scale model included the fan duct, core flow duct, mixer, centerbody, and exhaust nozzle.

Existing E<sup>3</sup> model hardware that was reused in Cell 41 include four multi-lobed mixers and a confluent (annular) mixer, two core plugs, and removable 2 fan duct total pressure (P<sub>T</sub>) rakes.

Key geometric characteristic of the five mixer configurations tested are summarized below in Table 2.1. All Cell 41 lobed mixers had 12 lobes. This simplified data sampling and configuration comparison. Sufficient geometric and aero-characteristic variation was obtained from these mixers through the variation of the other mixer geometric parameters (e.g., lobe penetration, mixer length and lobe shaping).

Table 2.1 Geometric characteristic of the mixer configurations

Configuration Number	Mixer	No. Of Lobes	Lobe Description	Lobe Height Penetration	Mixer Spread Angle (°)	$L_{\text{mixer}}/D_{\text{plane}}$
1	V1	N/A	Confluent	N/A	N/A	N/A
2	V2	12	Scalloped	0.43	38.9	0.18
2A	V2A	12	V2 Mixer + 2"extension	0.43	38.9	0.18
3	F9B	12	Scalloped + Staggered	0.48	31.2	0.22
4	F12A	12	Skewed	0.38	35.6	0.19
5	F8	12	Scalloped (Ps-Inst)	0.39	36.5	0.19

Configuration V2A is the V2-Integrated Core/Low Spool (ICLS) mixer and centerbody but with a 2 inch model scale (16.67 inches full scale) cylindrical spacer inserted into the outer fan duct upstream of the mixer. The spacer translated the tailpipe and nozzle aft thereby increasing both the mixing area and mixing length.

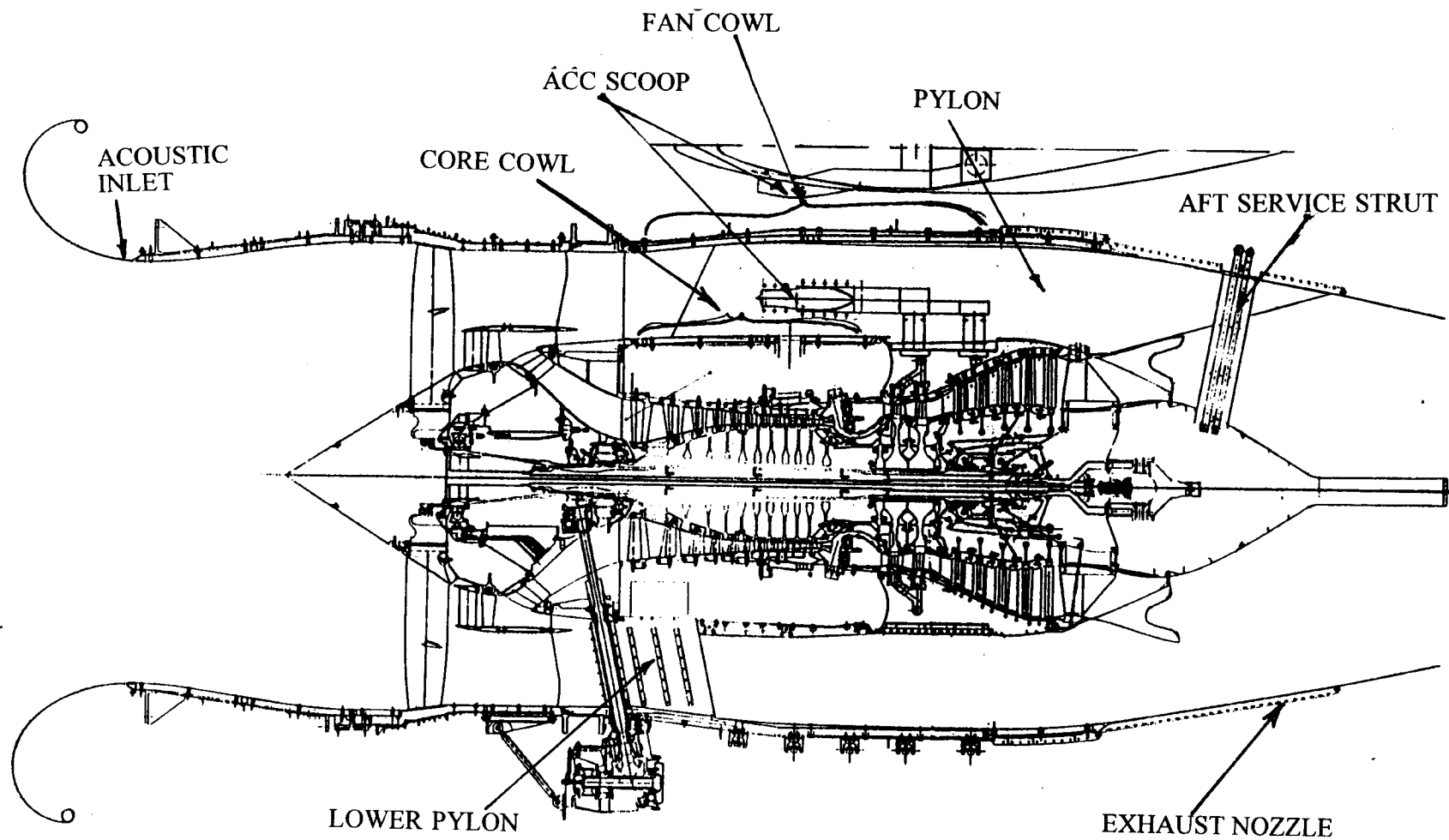


Figure 2.1. E<sup>3</sup> Integrated Core/Low Spool (ICLS) engine cross section.

Figures 2.2 through 2.6 illustrate the acoustically tested Cell 41 mixer configurations. Figure 2.7 shows a photo of the four acoustically tested mixers (Mixers V1, V2, F12A, & F9B).

#### *Mixer Performance -*

The mixer performance characteristics at a typical cruise condition for the selected E<sup>3</sup> mixer configurations are shown in Table 2.2. The performance characteristics shown are mixing effectiveness, %K4, mixer pressure loss,  $\% \Delta P_T / P_T$ , and an overall performance benefit quoted as % $\Delta$ CT relative to a unmixed, cold-flow configuration. These are empirically derived values obtained from nozzle thrust measurements performed at FluidDyne Engineering Corporation during the E<sup>3</sup> development test programs [Ref. 2].

Table 2.2 Performance characteristic of the mixer configurations

Mixer	Mixing Effectiveness, %K4	Mixer Pressure Loss, $\% \Delta P_T / P_T$	Mixer Overall Performance, % $\Delta$ CT
V1 - Confluent	18	0	.24
V2 - ICLS	67	.66	.65
V2A <sup>1</sup> - Extended Tailpipe	>67	<.66	≈.80
F9B - Quarter Periodic	61	.56	.63
F12A - Skewed	85	1.80	.35
F8 <sup>2</sup> -	70	.38	.80
F8 - Adjusted	60	.50	≈.65

<sup>1</sup> Note: Configuration V2A (2-inch tailpipe extension), was never performance tested.

<sup>2</sup> Note: Data based on extended tailpipe configuration.

Mixing Effectiveness, K4, is defined as the percent of actual thrust gain due to thermal mixing divided by the ideal gain in thrust for a fully-mixed flow. Mixing Effectiveness is a measure, as a percentage, of how well the overall temperature of the exhaust system is raised based on measured thrust.

The mixer pressure loss is obtained from the change in measured cold, i.e., non-heated core flow, thrust coefficient with and without the lobed mixer. The without configuration is represented with a confluent mixer. It is measured at cold-flow conditions to remove any thermal mixing benefit thereby isolating the lobe mixer pressure loss (correcting for changes in Reynold's number due to temperature). The mixer pressure loss is a measure of how much additional pressure loss the mixer creates in the process of achieving increased temperature mixing.

The % $\Delta$ CT is an overall performance efficiency term combining the benefit of thermal

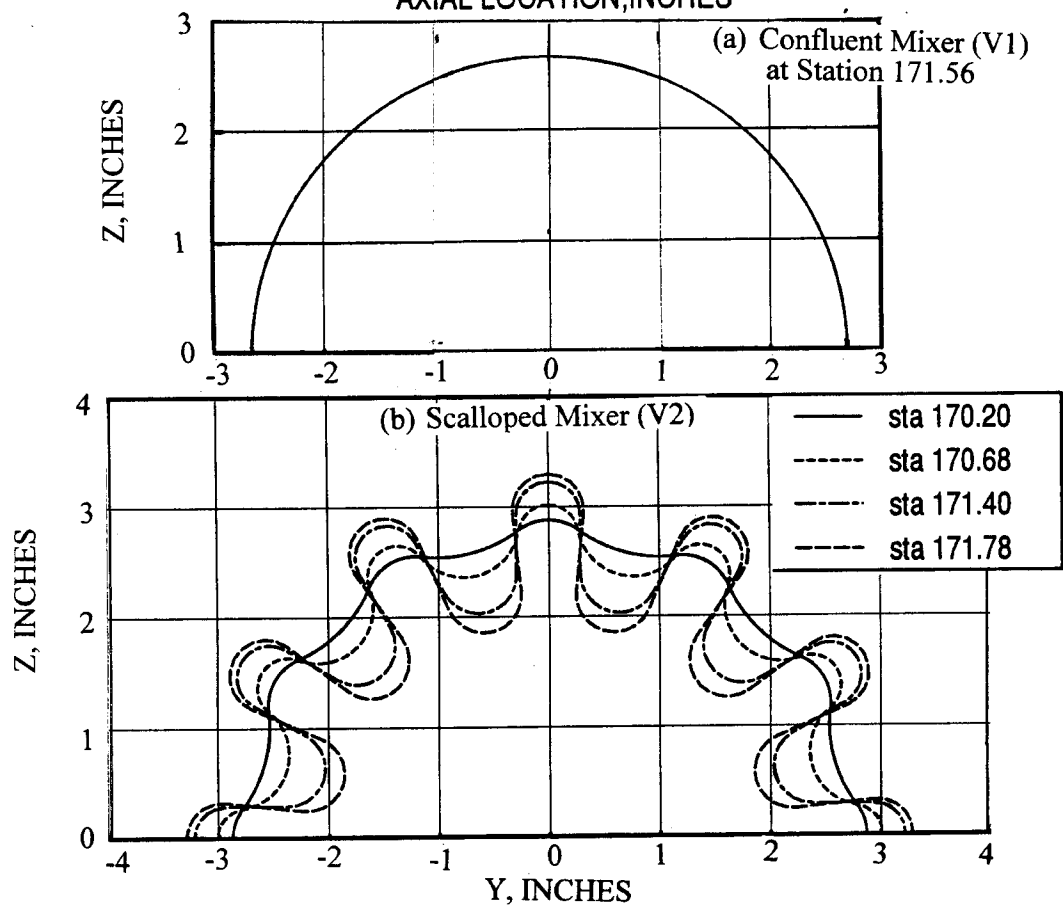
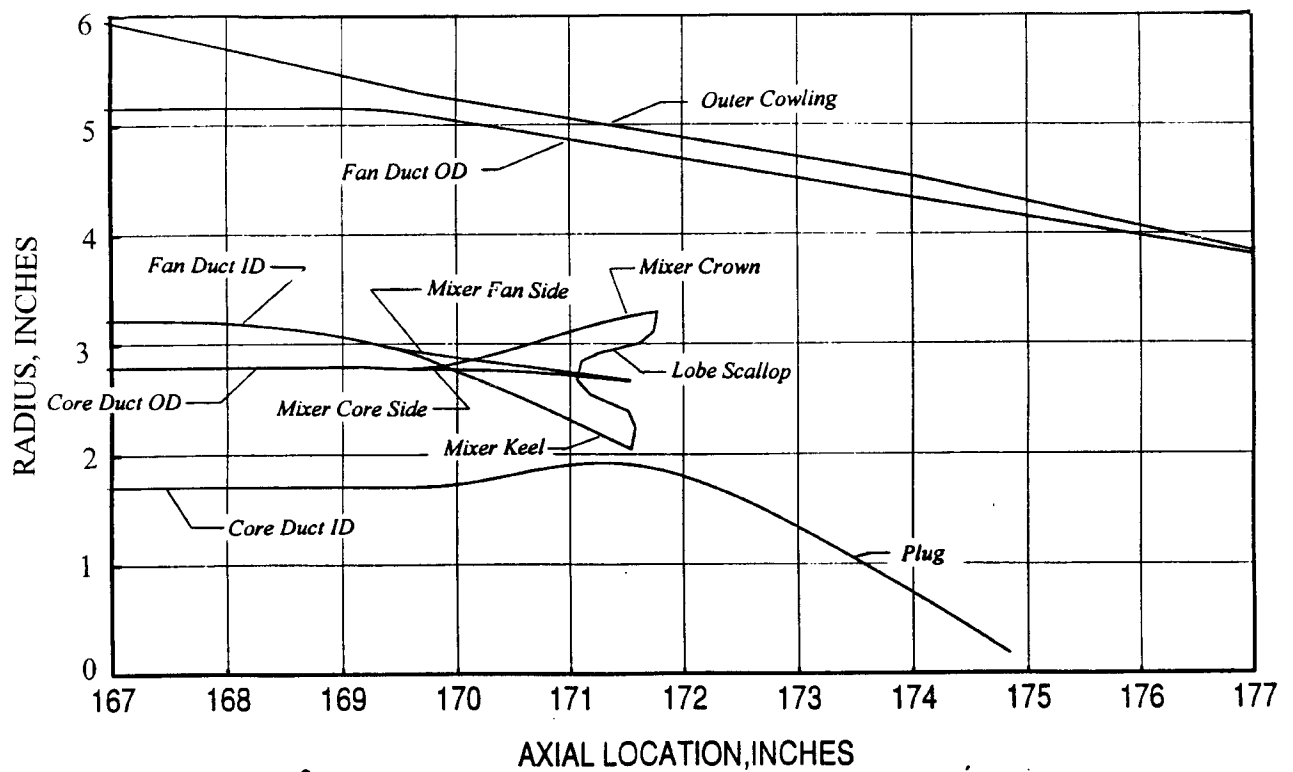


Figure 2.2. ICLS configurations with (a) Confluent (V1) and (b) 12-lobed Scalloped (V2) mixers.



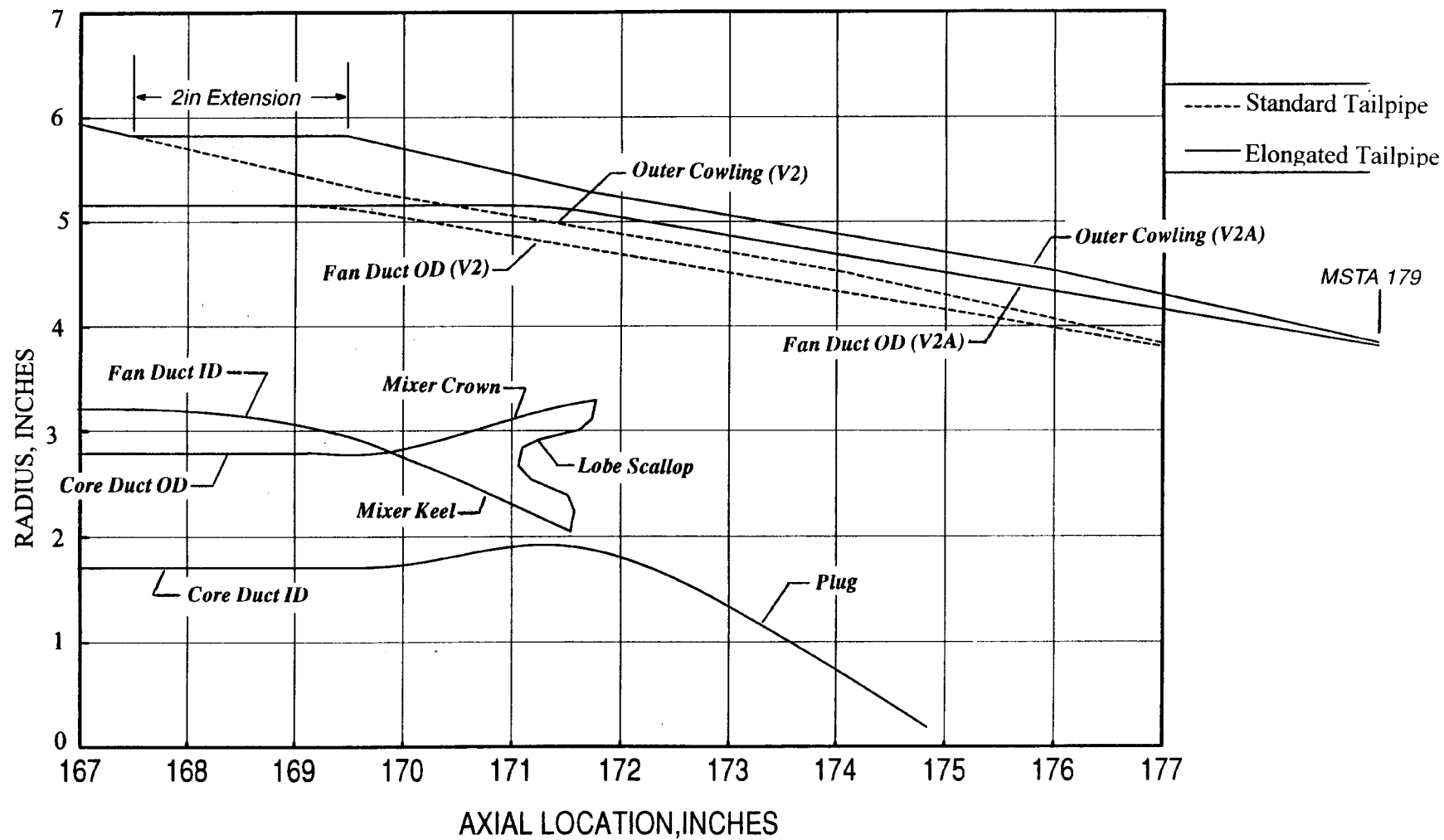


Figure 2.3. ICLS configurations with a 12-lobed scalloped mixers, (a) standard tailpipe (V2).and (b) 2" elongated tailpipe (V2A).

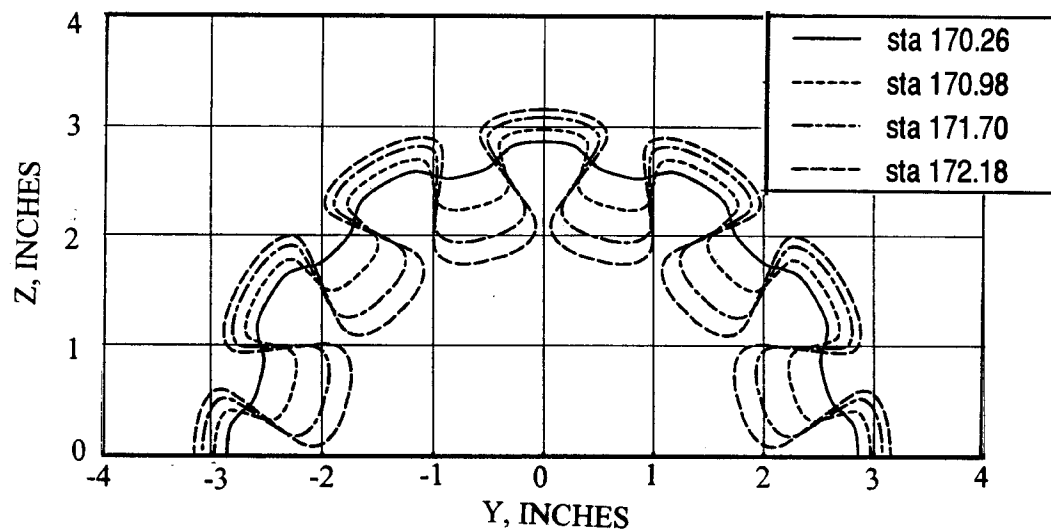
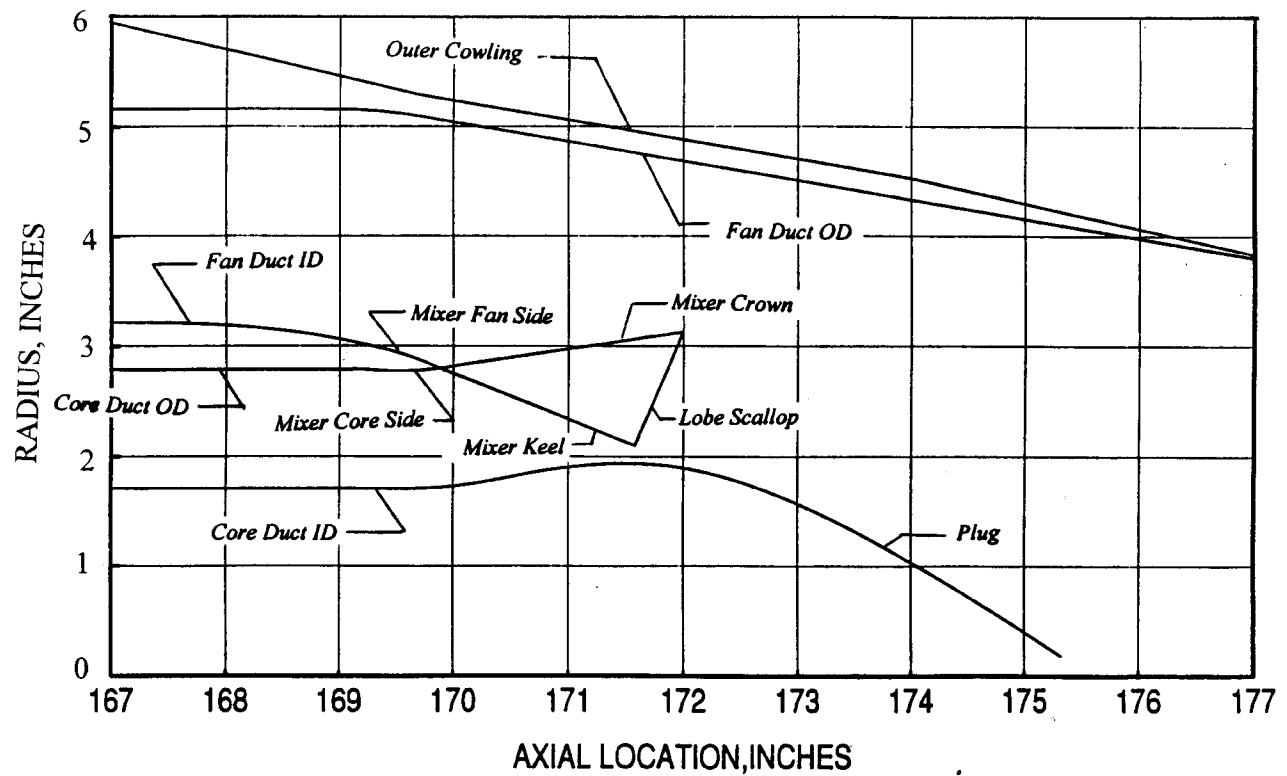


Figure 2.4. ICLS configuration with a 12-lobed skewed mixer (F12A).

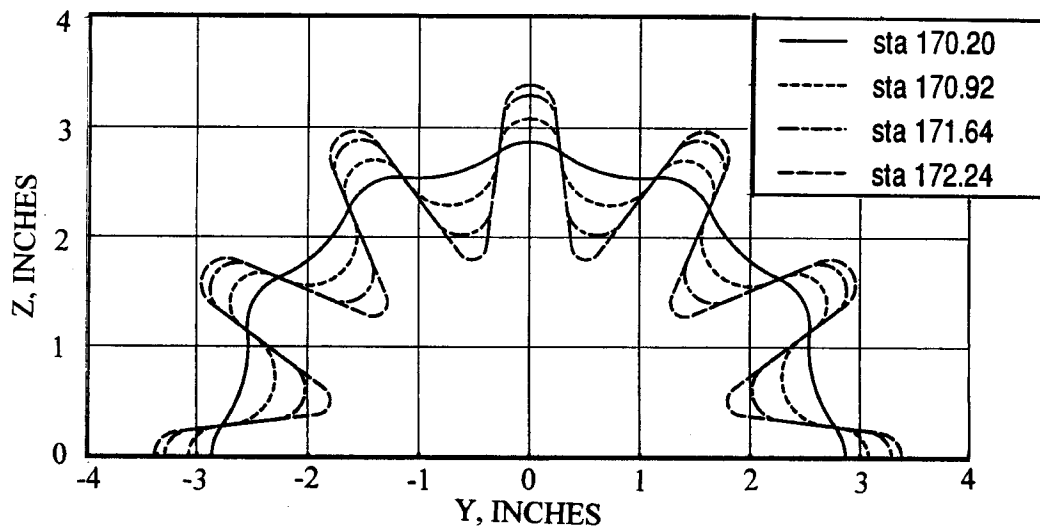
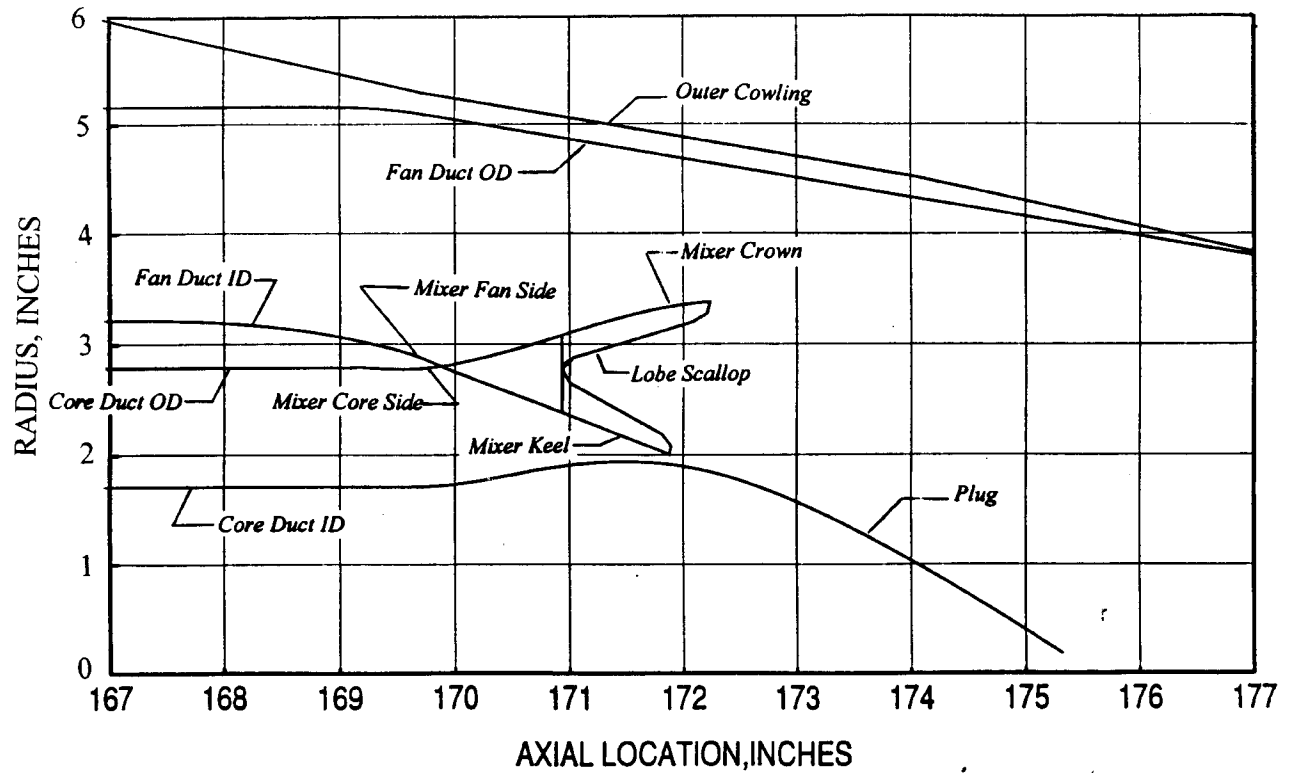


Figure 2.5. ICLS configuration with a 12-lobed scalloped and staggered mixer (F9B).

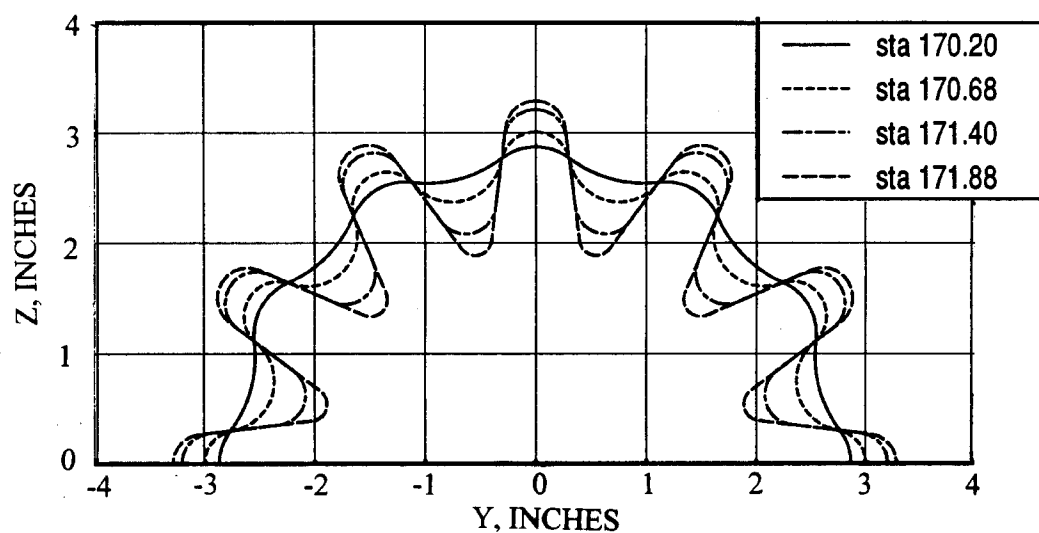
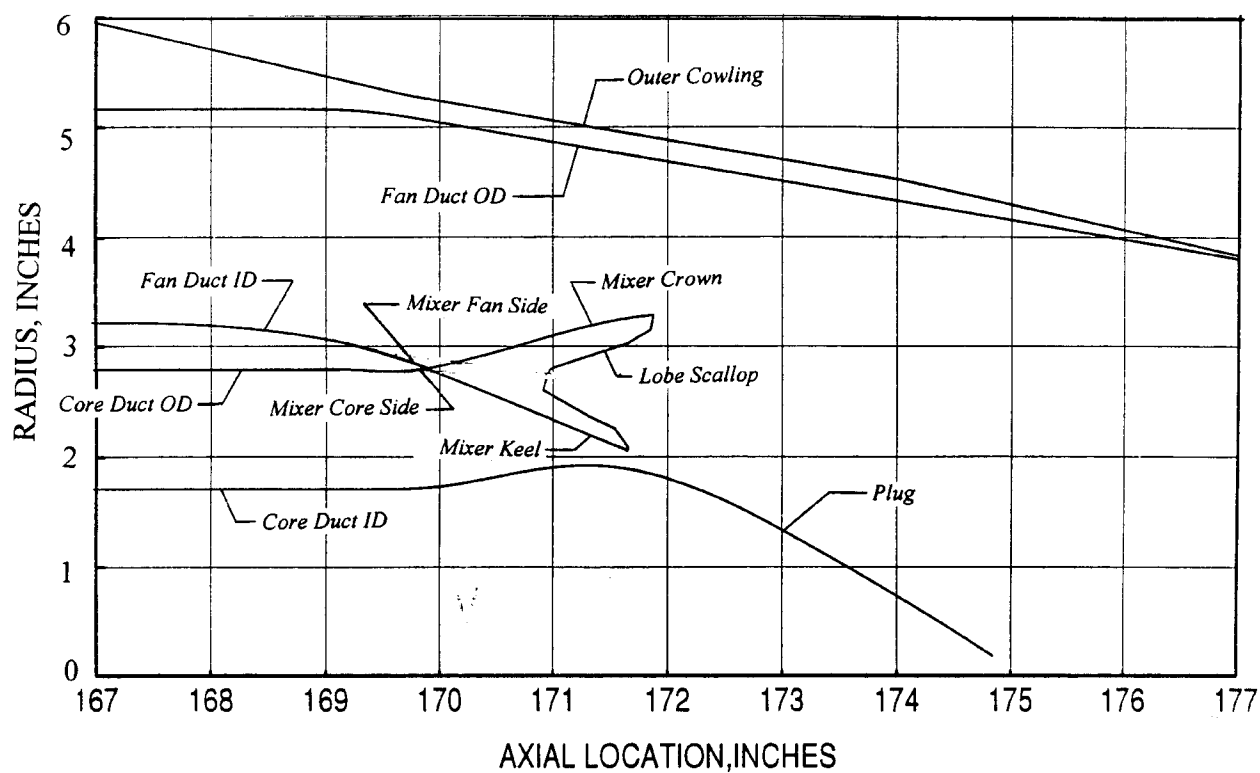


Figure 2.6. ICLS configuration with an instrumented 12-lobed scalloped mixer (F8).

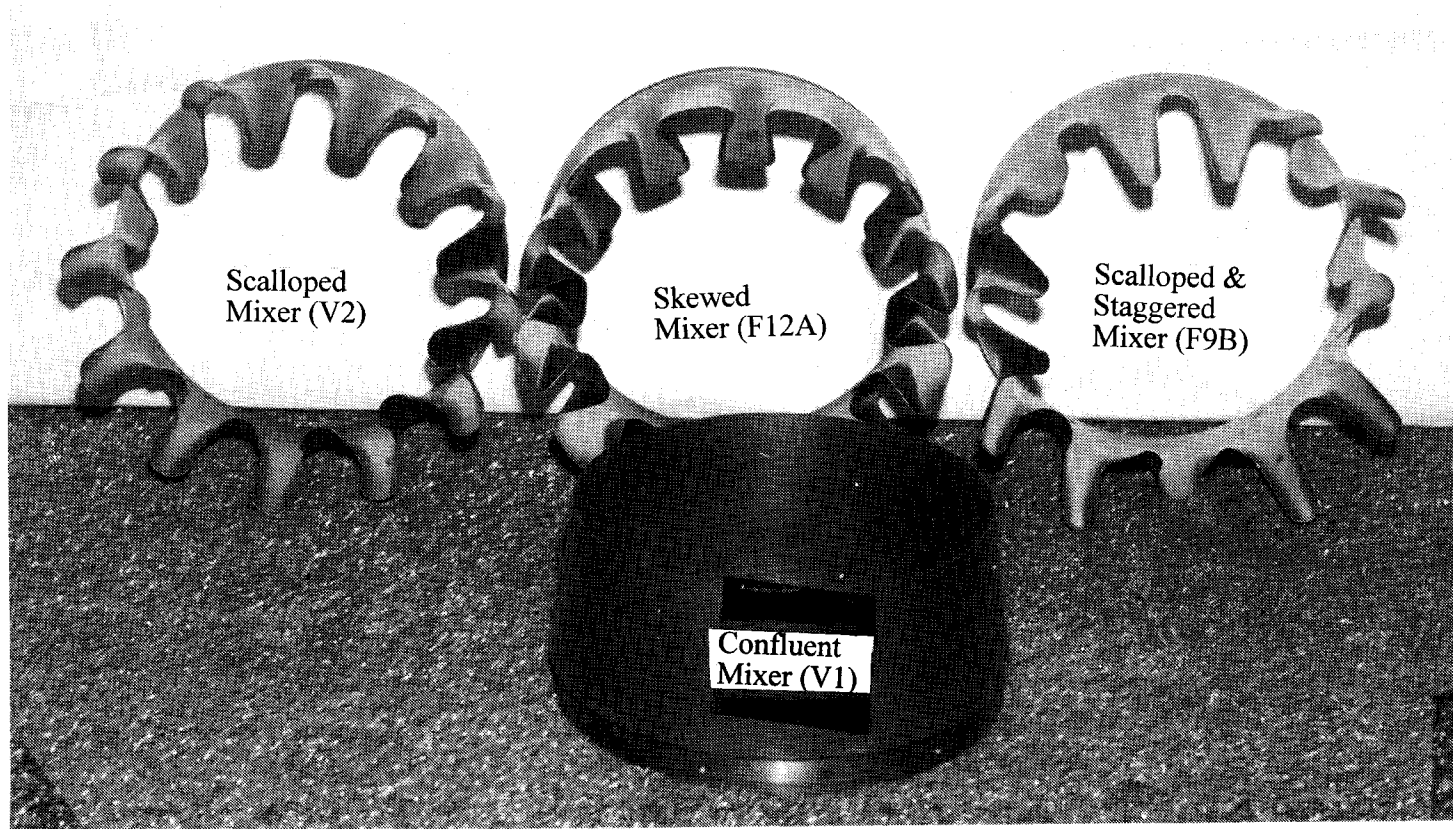


Figure 2.7. Confluent and 12-lobed  $E^3$  mixers tested in Cell 41 Anechoic Free Jet Facility.

mixing and the penalty of mixer pressure loss. It is obtained by comparing the hot core flow thrust coefficient to the cold-flow confluent mixer thrust coefficient.

The best overall performance configuration, therefore, is assumed to be the extended tailpipe V2A mixer. Acoustically tested mixers V2 and F9B both provide similar thrust performance. Mixer F8 is assumed to also have similar thrust performance to mixers V2 and F9B. Recall, however, that mixer F8 was not tested acoustically due to the pressure instrumentation tubing on the mixer lobes. Mixer F12A, while providing a high amount of thrust based thermal mixing, does so at the expense of significant internal pressure loss and consequently, provides relatively poor overall thrust efficiency for a lobe mixer. The confluent (free) mixer offers improved performance potential relative to an unmixed exhaust system based on the nominal level of thermal mixing.

## **2.2 Cell 41 Adapter and Model Hardware Design -**

New scale model hardware fabricated for the Cell 41 test include Cell 41 model adapters, upstream flow path hardware, new nozzles, and laser velocimeter glass windows for viewing the mixing process in the nozzle.

The Cell 41 adapters integrate the model to the Cell 41 facility. The hardware was designed to allow for differential thermal growth. Regions between the core and fan streams were thermal insulated where feasible to minimize the amount of heat transfer from the core to the fan.

The Subtask A model geometry did not include fan duct bifurcations. This was to minimize the 3-D cross-flow effects and to simplify the flowfield in the mixing region. In place of bifurcations, the model was designed with upstream fan and core duct support struts (Figure 2.8). The core duct struts supported the cantilevered core plug and provided routing passages for the core duct pressure instrumentation. The fan duct struts provided for routing of the core duct pressure instrumentation and the fan duct inner surface pressure instrumentation. The fan duct struts also provided the model with a means of maintaining fan-to-core duct concentricity and centering.

The support strut system consisted of 3 equally spaced symmetrical struts. The struts are NACA 63018 *hybrid* airfoils with a constant chord length of 4 inches and maximum thickness of .68 inches. The struts are considered *hybrid* NACA 63018 airfoils because the actual airfoil thickness-to-chord ratio ( $t/c$ ), is 17% not 18%. The 17% airfoil was generated by scaling the NACA 63018 airfoil thickness to 17% while maintaining the 4 inch chord length. Figure 2.9 (a) illustrates the 17% *hybrid* airfoil cross-section. Flow analysis performed on this airfoil showed acceptable strut trailing edge wake characteristics.

The design requirements of the support struts were to have minimum wake shedding while providing model structural rigidity and allowing for routing of the pressure instrumentation. The final strut airfoil thickness was dictated by the pressure

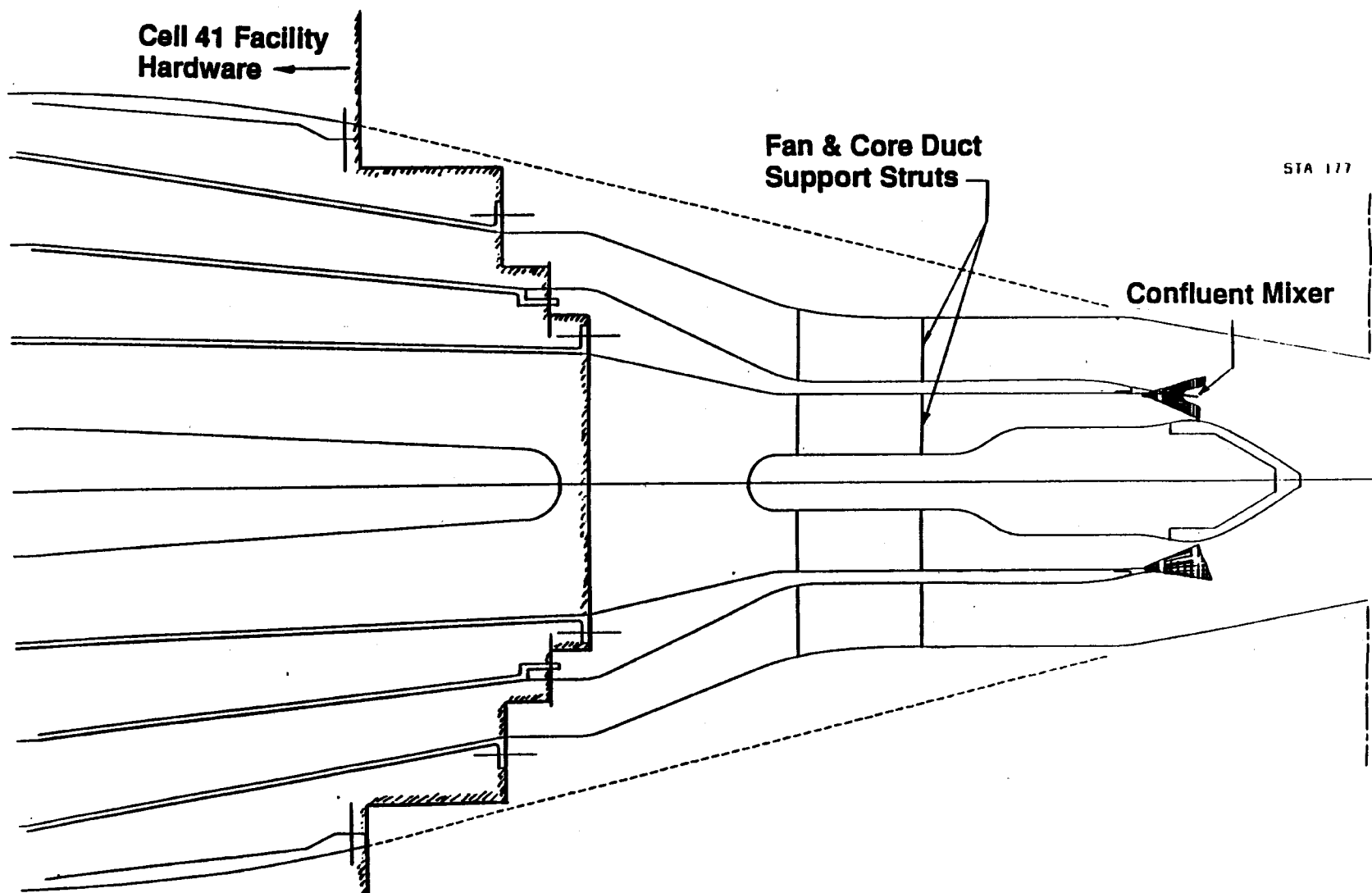


Figure 2.8. Model flowpath for E<sup>3</sup> mixers tested in Cell 41 Anechoic Free Jet Facility.

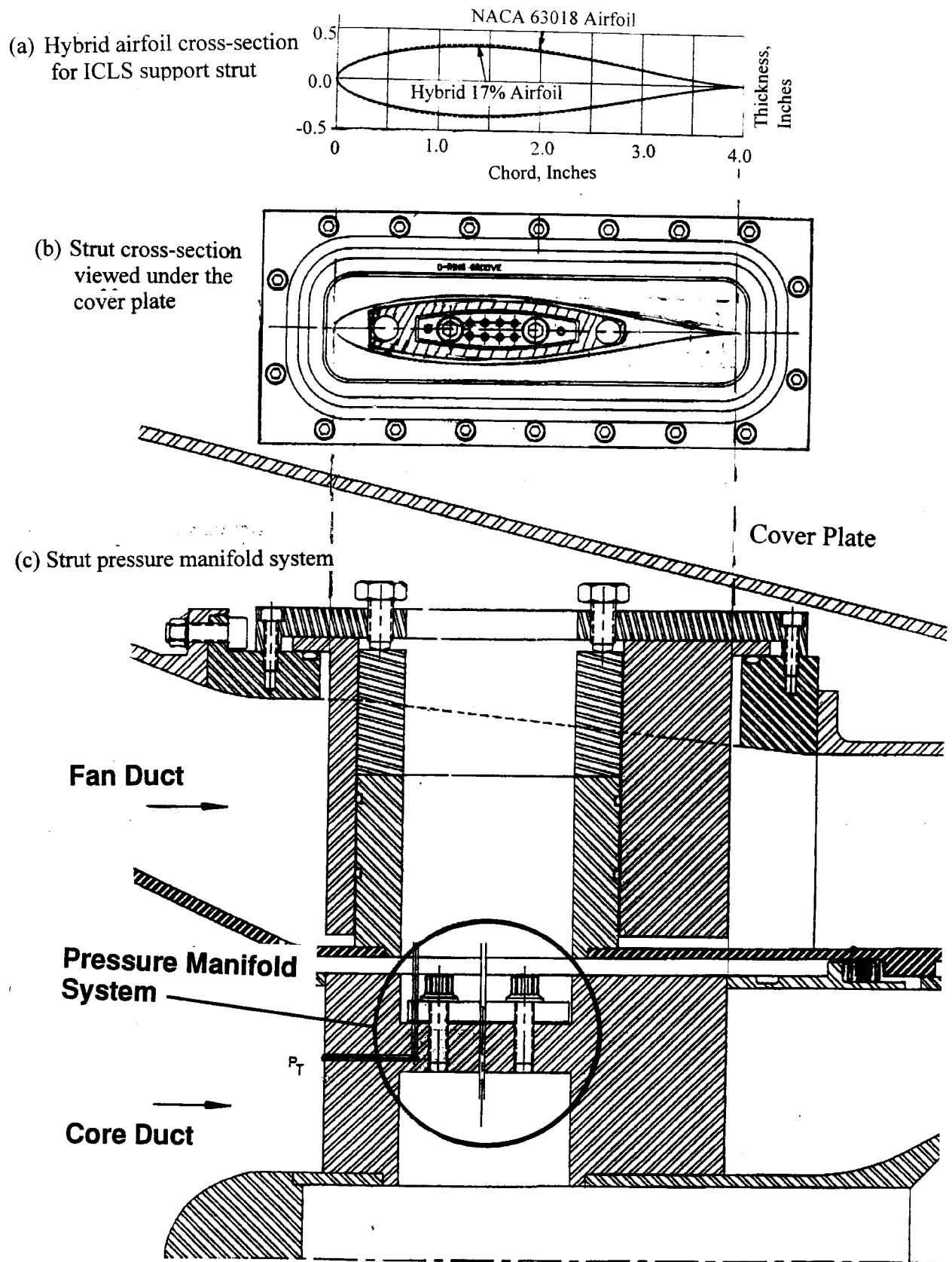


Figure 2.9. Strut aerofoil cross sections and the strut pressure manifold system for E<sup>3</sup> mixers tested in Cell 41 Anechoic Free Jet Facility.



instrumentation routing requirements. For ease of model installation and model change-out, the core duct pressure instrumentation was manifolded in the core struts. Figures 2.9 (b) and 2.9 (c) illustrate the strut manifold design.

The aero-flowpaths aft of the struts are consistent with the E<sup>3</sup>/FluiDyne performance test geometry except for the fan duct outer contour and nozzle, and the absence of fan duct bifurcations. The fan duct and nozzle contour is different to accommodate the planar (flat) Laser Velocimeter windows. Figure 2.10 illustrates the contour differences between the FluiDyne performance geometry and the Cell 41 acoustic configuration. The differences are small. Analysis of the two geometries indicate that the flow characteristics and fan-to-core bypass ratios very nearly match.

To accomplish the Subtask A test objectives, two nozzles were fabricated and tested. Both nozzles were manufactured to the same internal contour. One nozzle was dedicated to internal Laser Velocimeter (LV) measurements by incorporating three planar LV windows. This nozzle has external brackets that secure the LV windows. Figure 2.11 illustrates the circumferential orientation of the three LV windows in the Cell 41 test facility. Figure 2.12 illustrates the LV nozzle in Cell 41. This nozzle is used for static ( $M=0$ ), LV measurement testing only. There are no surface pressure instrumentation for the LV nozzle. The second nozzle, which is instrumented with two rows of surface static pressure taps oriented 195-degrees apart and is externally clean, is for aero-acoustic testing.

The Cell 41 model assembly is detailed in Figure 2.13. Figures 2.14 through 2.16 are the photographic views of the model assembly in Cell 41.

### **2.3 Model Instrumentation:**

The Cell 41 Subtask A hardware has 108 surface pressure taps. Generally, two axially rows of pressure taps were located circumferentially in line with a lobe chute and valley. This was consistent throughout the test configuration variations since all the lobed mixers have the same number of lobes (12). Model surfaces that were pressure instrumented were the fan duct outer contour, fan duct inner contour, core plug and a mixer crown and keel (both fan and core side). Figure 2.17 illustrates the model surface pressure measurement locations.

One mixer was pressure instrumented in the lobe region, mixer F8 (Figure 2.18). The lobed mixer pressure instrumentation tubing was bundled aft of the mixer and routed out through the nozzle. The pressure tubing was bundled and routed aft so as to not compromise the fan and core duct contours ahead of the mixer and for ease of mixer installation (Figures 2.19 and 2.20). All other surface pressure instrumentation were inlaid to the flow surface. The surface pressure data were measured throughout the test program.

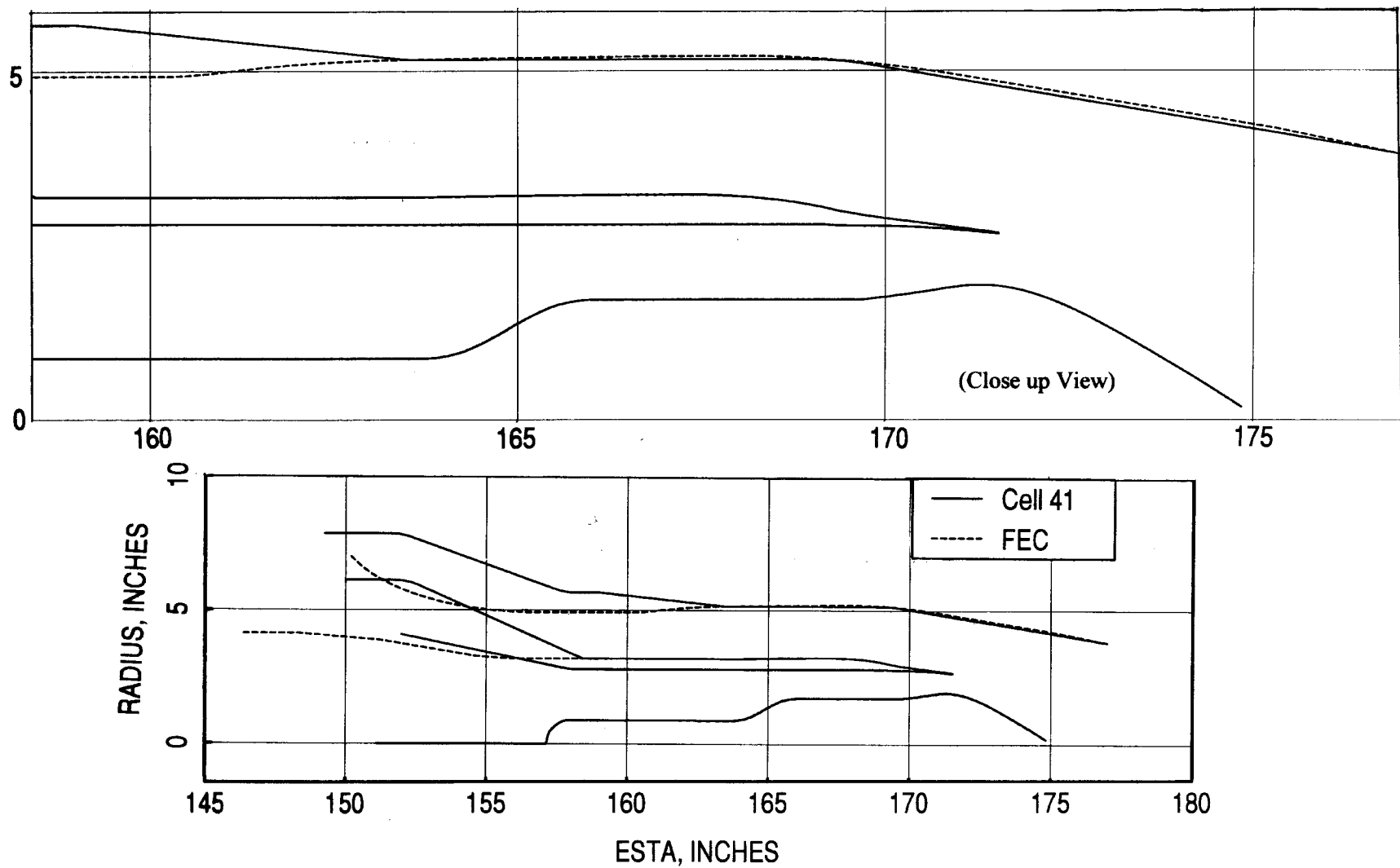


Figure 2.10. Flow path comparison between  $E^3$  performance model and the  $E^3$  Cell 41 acoustic model.

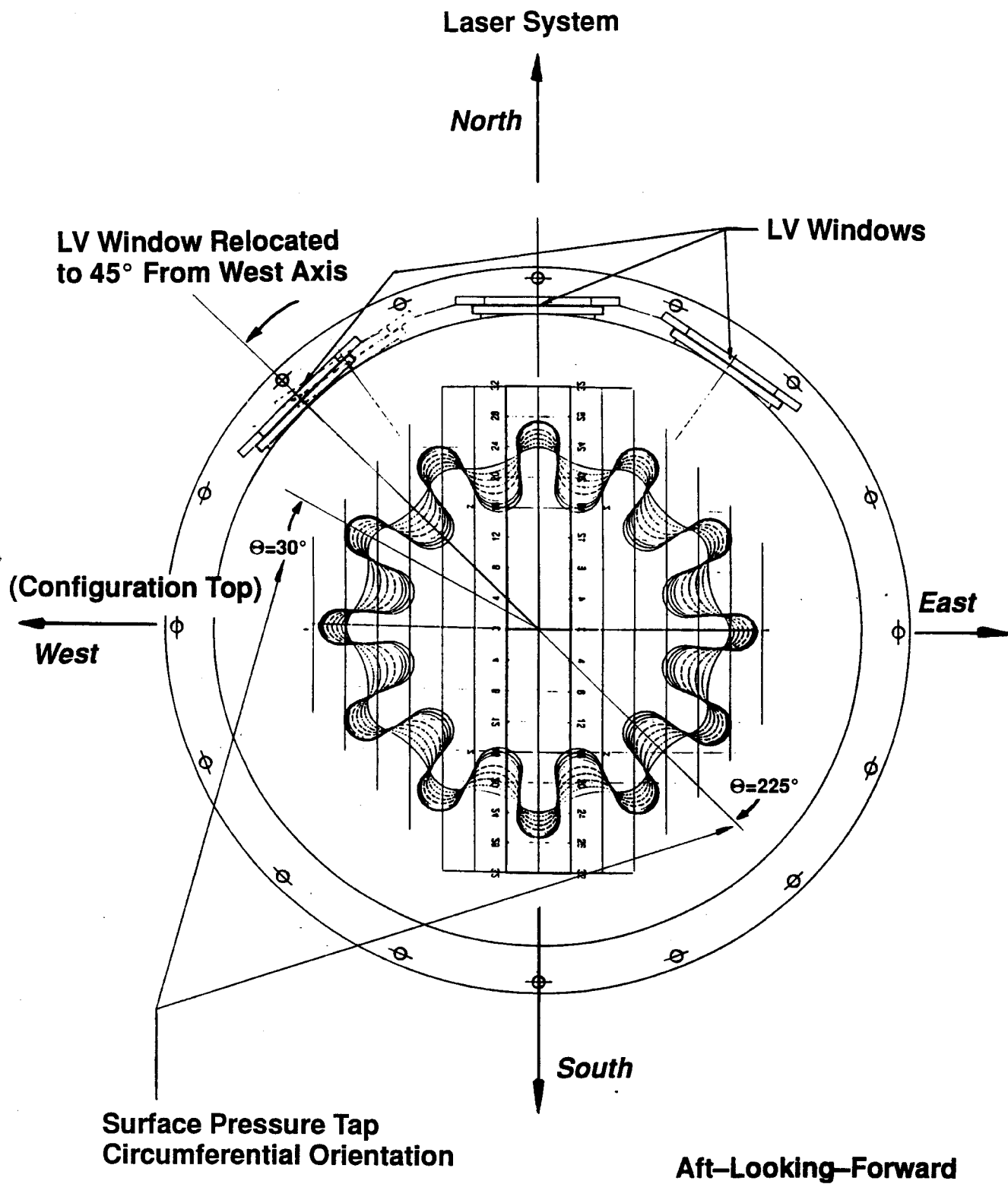


Figure 2.11. Circumferential Orientation of the nozzle LV windows.

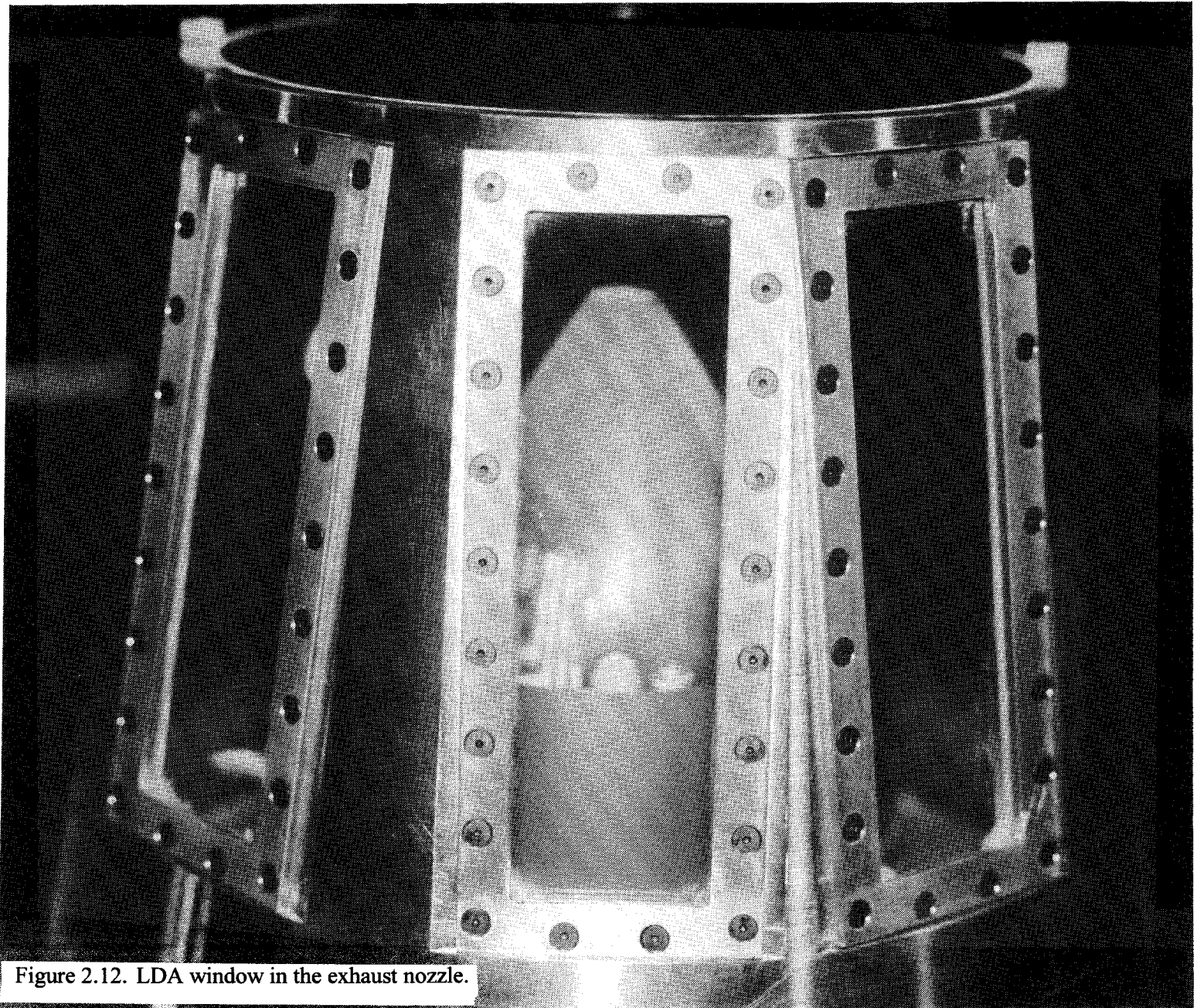


Figure 2.12. LDA window in the exhaust nozzle.

Figure 2.13 was unavailable at time of printing.

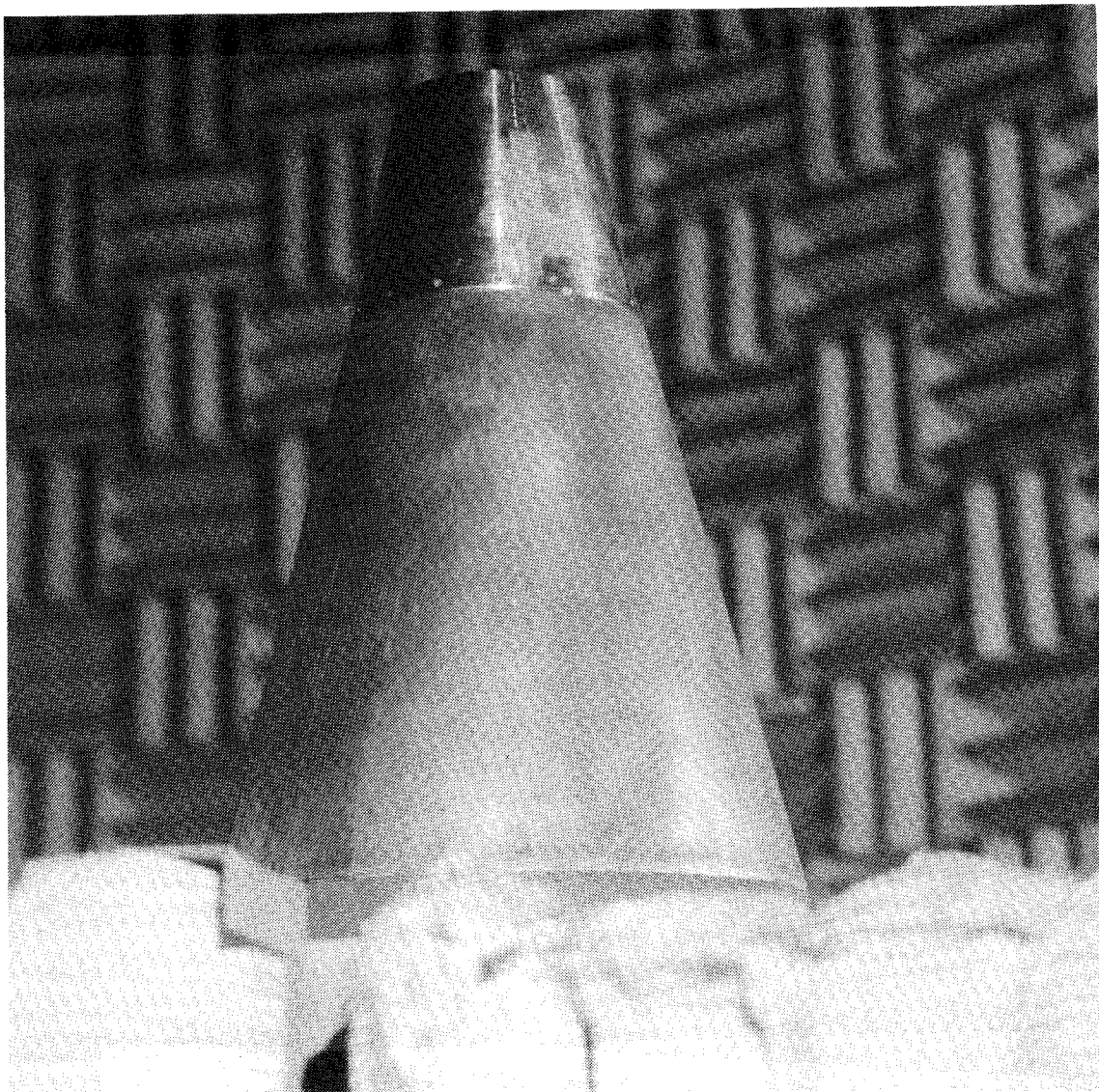


Figure 2.14. E<sup>3</sup> acoustic model installed in Cell 41 anechoic free jet facility.

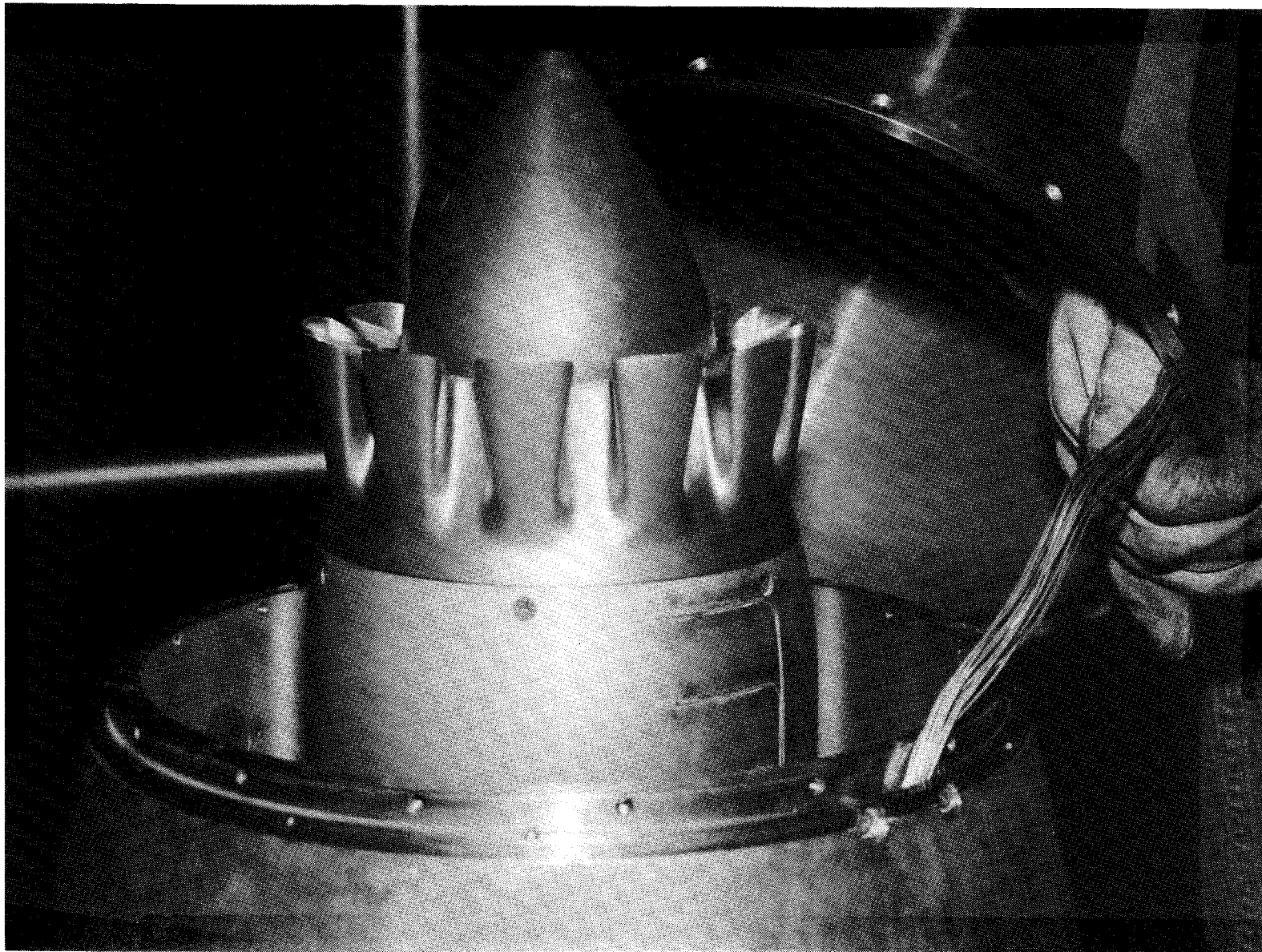


Figure 2.15. E<sup>3</sup> acoustic model with skewed 12-lobed mixer (F12A) is being installed in Cell 41 anechoic free jet facility.



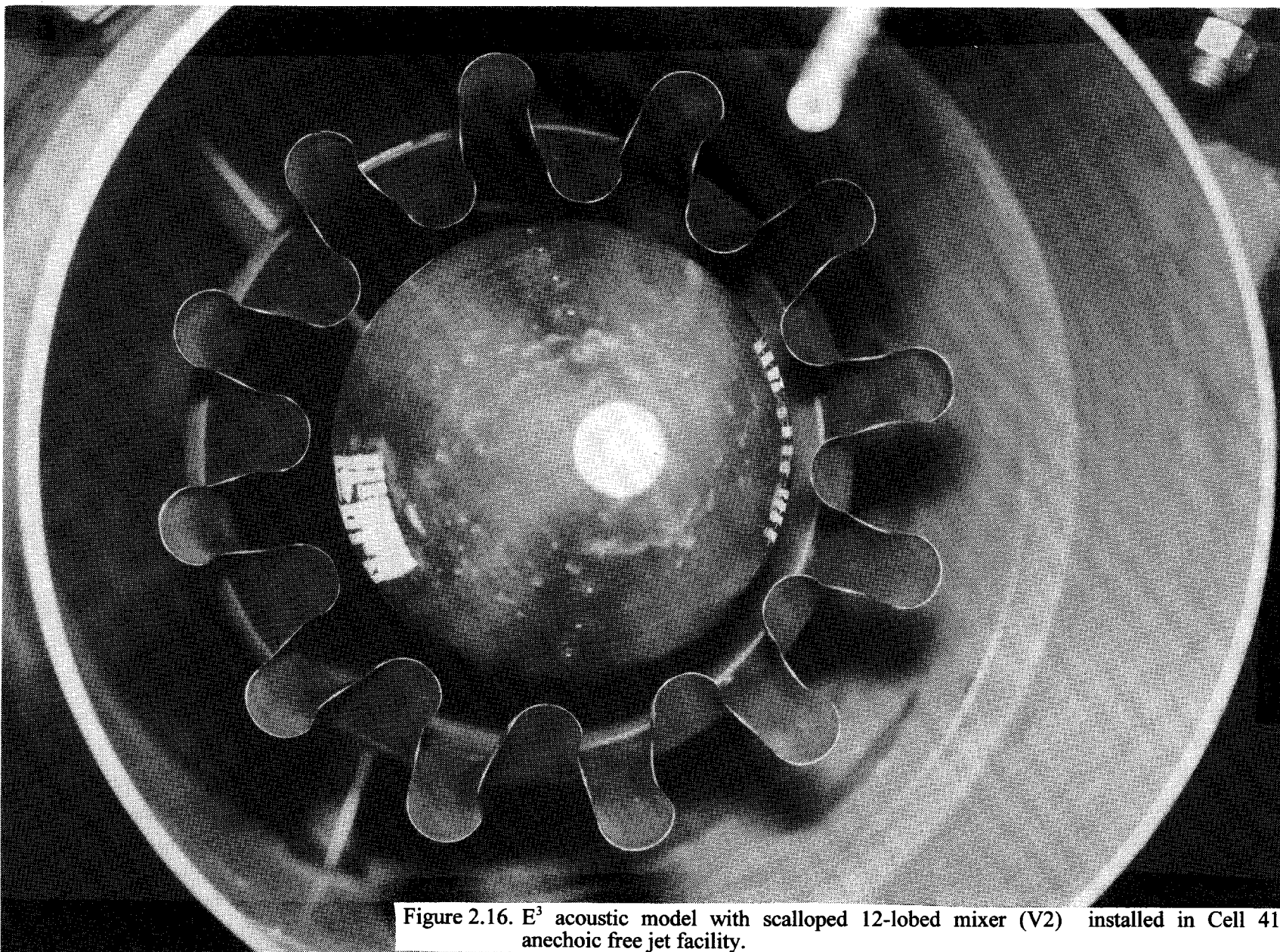
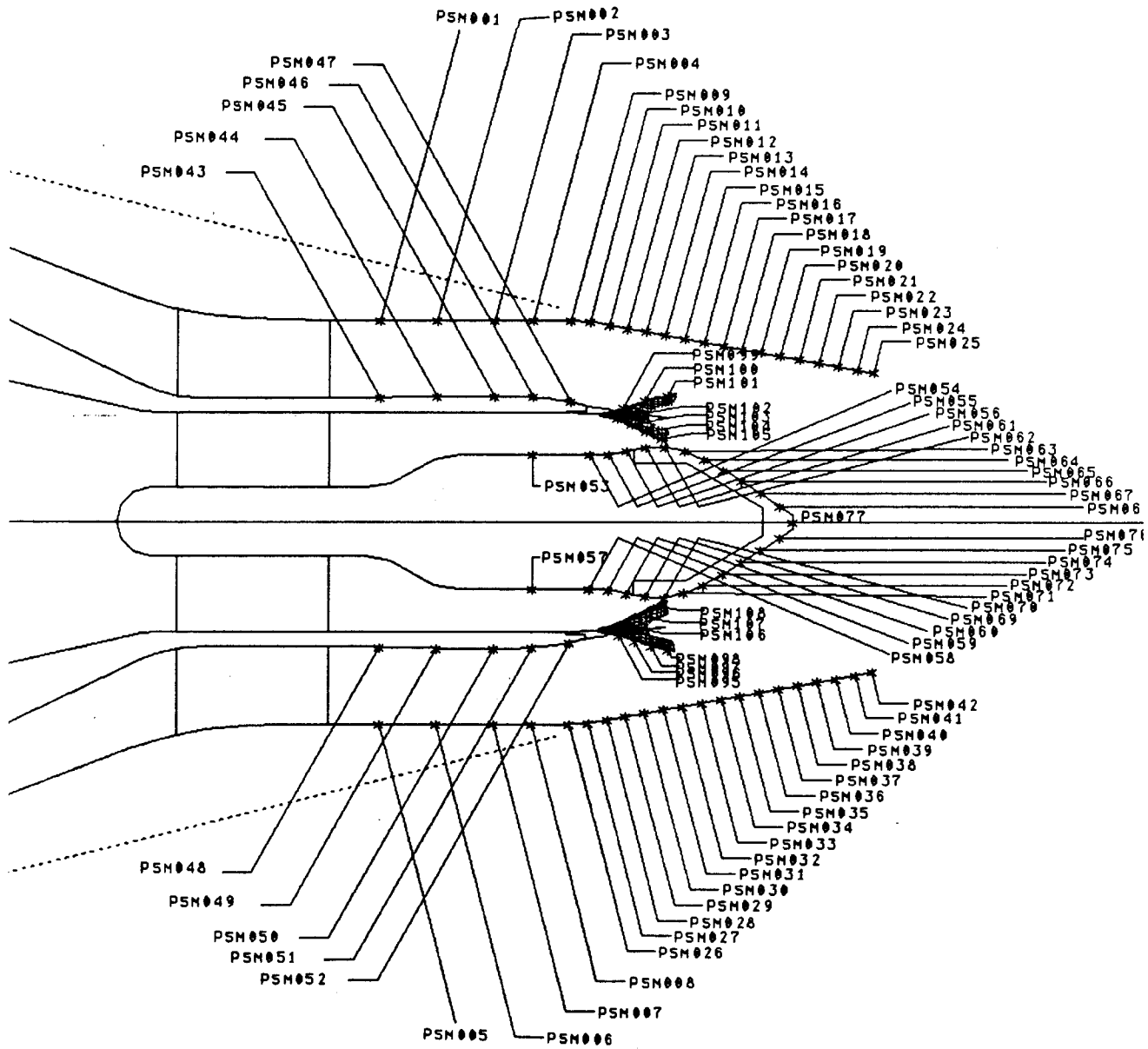


Figure 2.16. E<sup>3</sup> acoustic model with scalloped 12-lobed mixer (V2) installed in Cell 41 anechoic free jet facility.



Figure 2.17. Model surface pressure measurement locations.



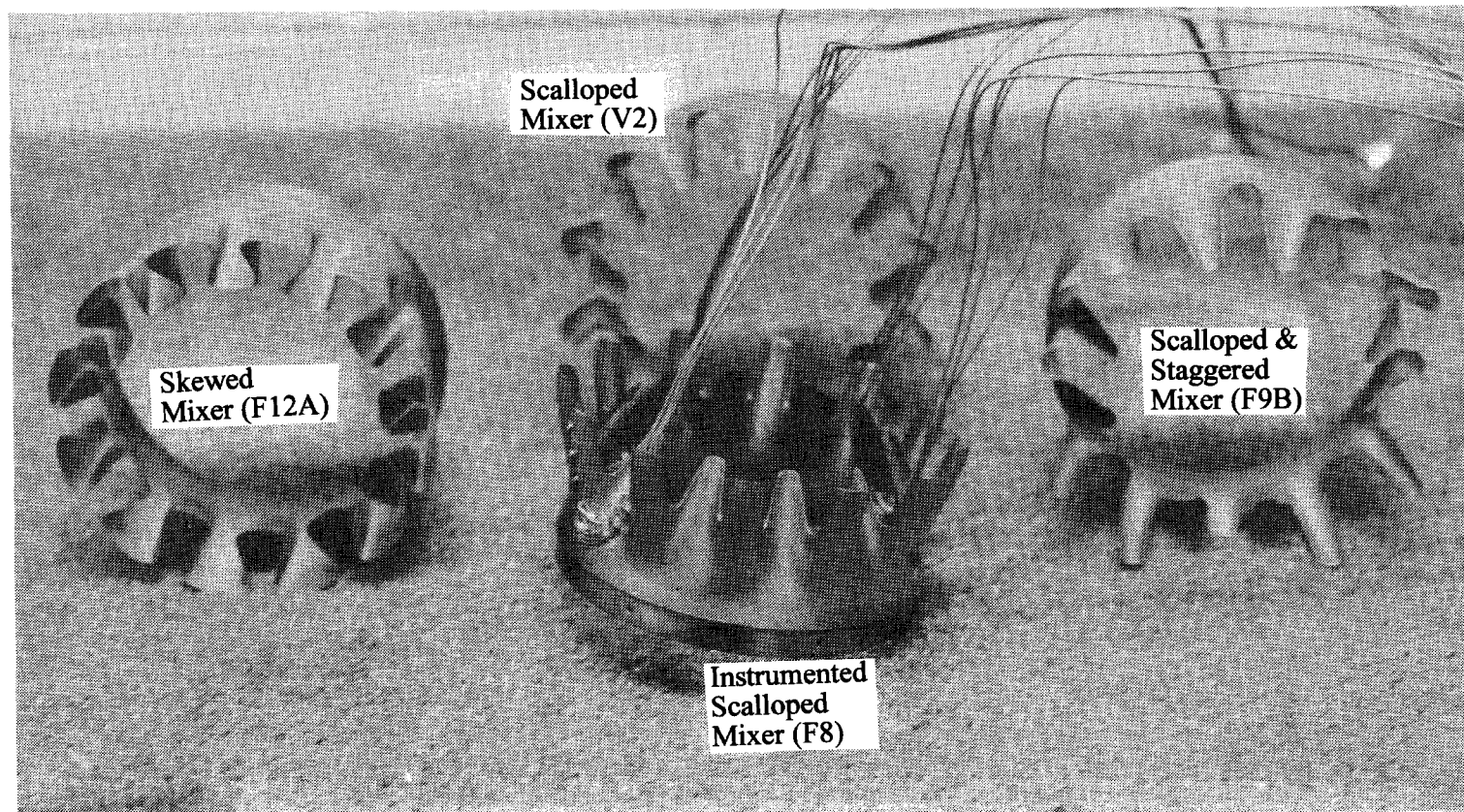


Figure 2.18. A number of 12-lobed mixer including the one instrumented for pressure measurement.

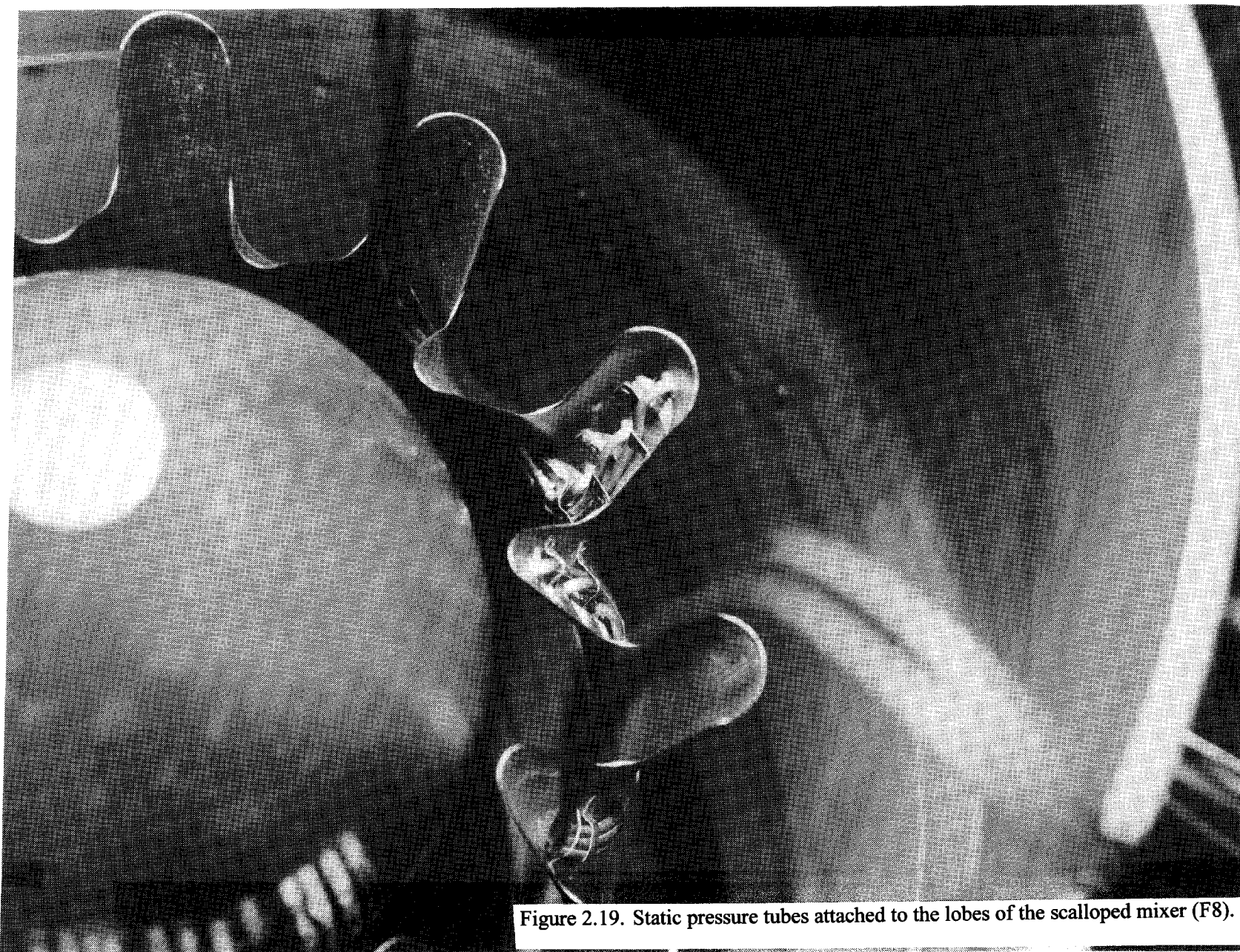


Figure 2.19. Static pressure tubes attached to the lobes of the scalloped mixer (F8).

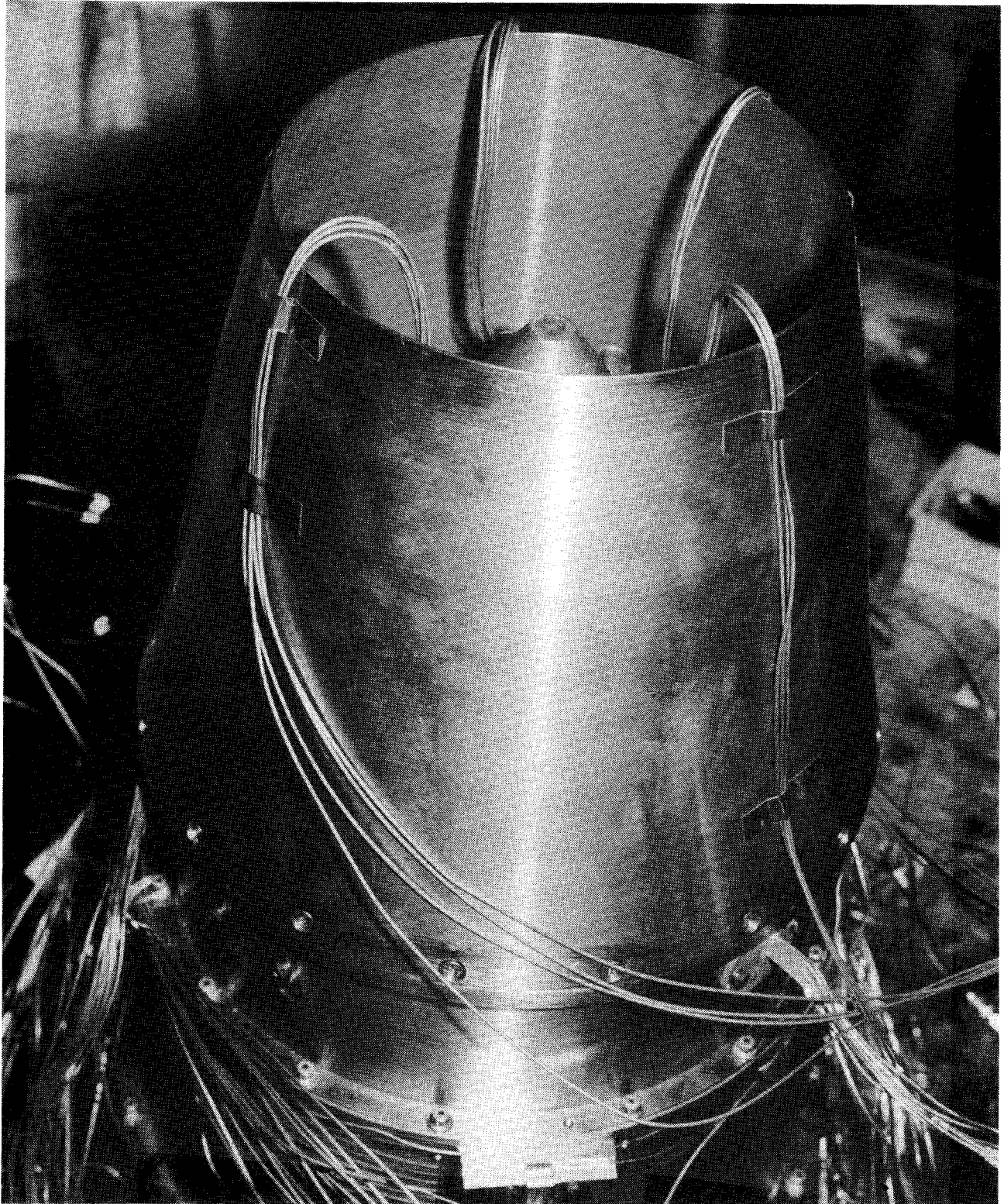


Figure 2.20. Static pressure tubes routed for least interference.

The fan duct total pressure profile could be measured by two removable PT rakes (reference Figure 2.13). The fan duct PT rakes were installed and tested at certain select times of testing for comparison with upstream facility charging station total pressures. All acoustic testing, however, was performed without the fan duct rakes.

A single PT probe extends from the leading edge of all three core support struts. The PT probe was permanently attached to the strut to measure the core total pressure as a reference check with the Cell 41 facility core charging station pressures.

Nozzle exit total pressures and temperatures were measured with a kiel-temperature probe (Figure 2.21). The exit survey probe was mounted to the model nozzle with a bracket designed to support a two-axis actuator that positioned the Kiel probe.

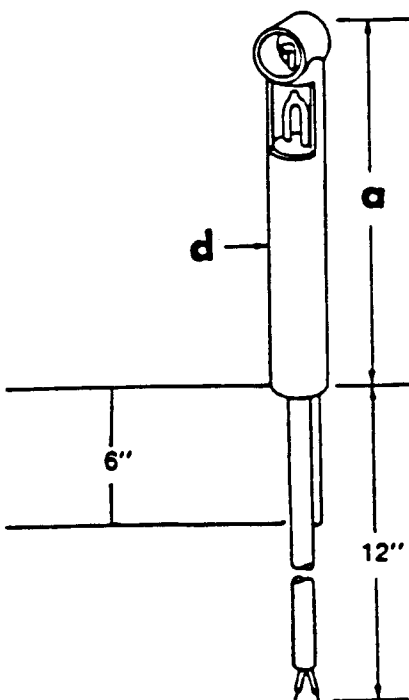


Figure 2.21. Kiel-Temperature probe (KT-36-228-CH/CON-F) for nozzle exit total pressure and temperature survey,  $a=36"$ ,  $d=0.25"$ .



### 3.0 TEST FACILITY

#### *Anechoic Free-Jet Noise Facility -*

The GEAE Cell-41 anechoic free-jet jet noise facility, shown in Figure 3.1 is a cylindrical chamber 43ft. in diameter and 72ft. tall. The inner surfaces of the chamber are lined with anechoic wedges made of fiberglass wool to render the facility anechoic above 220 Hz. The facility can accommodate single flow and dual flow model configurations. The corresponding throat areas for these streams are 22 and 24 square inches. The streams of heated air for the dual flow arrangement, produced by two separate natural gas burners, flow through silencers and plenum chambers before entering the test nozzle. The operating domain of the facility in terms of total temperature, pressure ratio, mass flow rate and jet velocity is indicated in Figure 3.2 for single and dual flow operation and for static and simulated flight operation. Each stream can be heated to a maximum of 1960°R with nozzle pressure ratios as high as 5.5, resulting in a maximum jet velocity of 3000 feet/second.

For this test program both single flow and dual flow nozzle set-up is required. For all dual flow configurations, the core flow will be provided through the core burner and flow delivery plenum system. Fan flow will be provided through the fan burner and flow delivery plenum system. For the conic nozzle, a single stream is required which will be provided through the fan burner/flow delivery plenum system. The tertiary air stream system (freejet simulation) consists of a 250,000 scfm (at 50in. of water column static pressure) fan and a 3,500 horsepower electric motor. The transition duct work and silencer route the air from the fan discharge through the 48in. diameter free-jet exhaust. The silencer reduces the fan noise by 30 dB to 50 dB. Tertiary flow at its maximum delivery rate permits simulation up to a free jet Mach number of about 0.4. Mach number variation is achieved by adjusting the fan inlet vanes. The combined model, free-jet and entrained airflow is exhausted through a 'T' stack silencer aligned directly over the model in the ceiling of the chamber. The 'T' stack is acoustically treated to reduce noise transfer from the facility to the surrounding community.

The facility is equipped with two systems of microphone arrays (see Figure 3.3) to measure the acoustic characteristics of the test models in the farfield; a fixed array of microphones and an array on a traversing tower. The fixed array has 17 microphones mounted from the false floor, the wall and the ceiling of the test cell. These provide measurements at a minimum distance of 26.75ft. from the nozzle reference location and cover the polar angle range from  $\theta_i = 50^\circ$  to  $155^\circ$ . The traversing tower contains 13 microphones, mounted at polar angles ranging from  $\theta_i = 45^\circ$  to  $155^\circ$ , and provides measurements at a minimum distance of 22ft. from the nozzle reference location. The traversing tower can be physically positioned at any azimuthal angle ( $\phi$ ) between  $\pm 55^\circ$  with respect to the fixed microphone array. However, to ensure non-interference from close proximity to wedges in its extreme positions, data acquisition is normally limited to  $\pm 45^\circ$  relative to the fixed microphone array. The azimuthal angle  $\phi = 0$  is defined as the

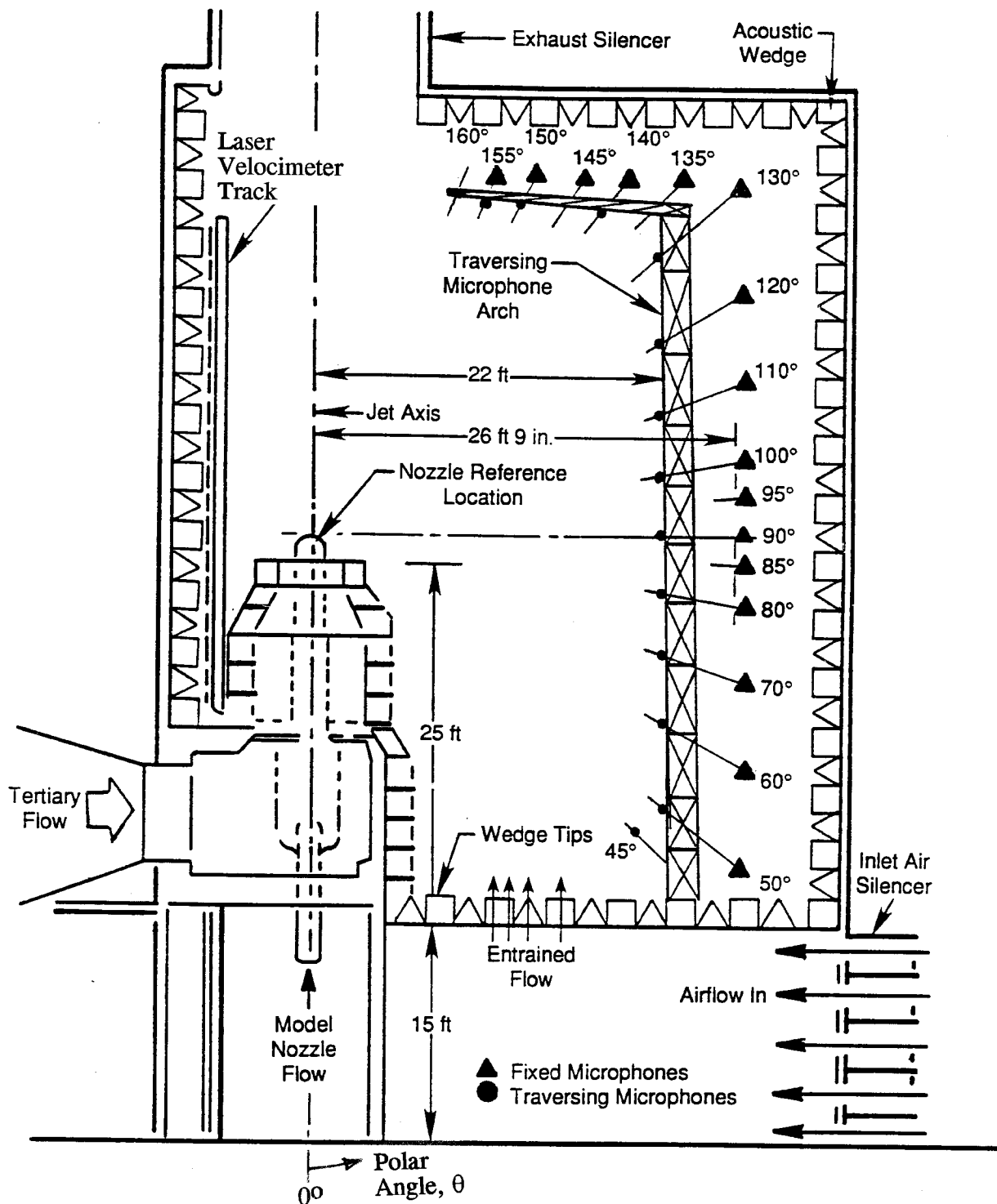


Figure 3.1. Side view of Cell 41 Anechoic Free Jet Facility in the azimuthal plane of  $\phi = 45^\circ$ .



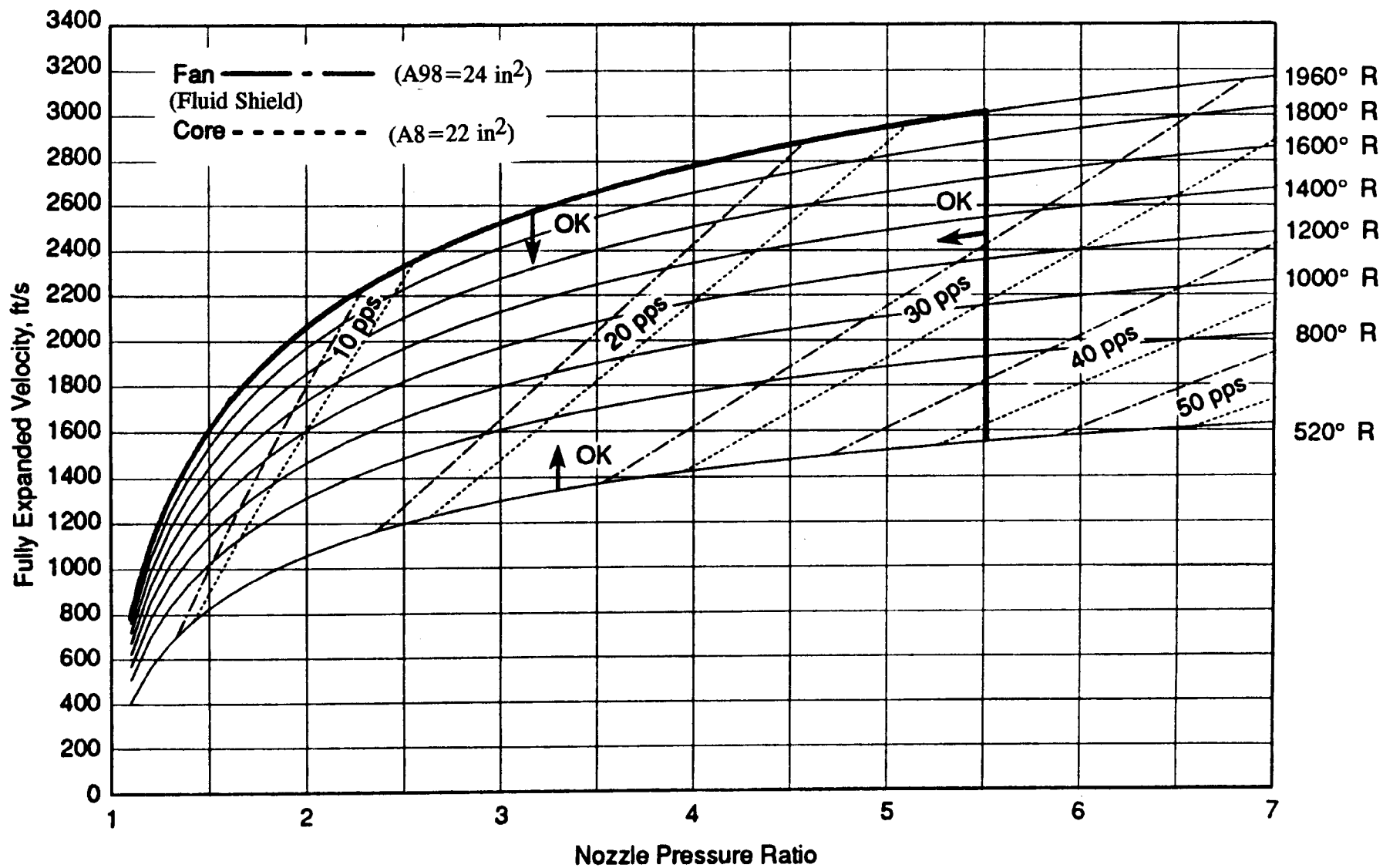


Figure 3.2. Operating domain of the Cell 41 Anechoic Free Jet Facility.

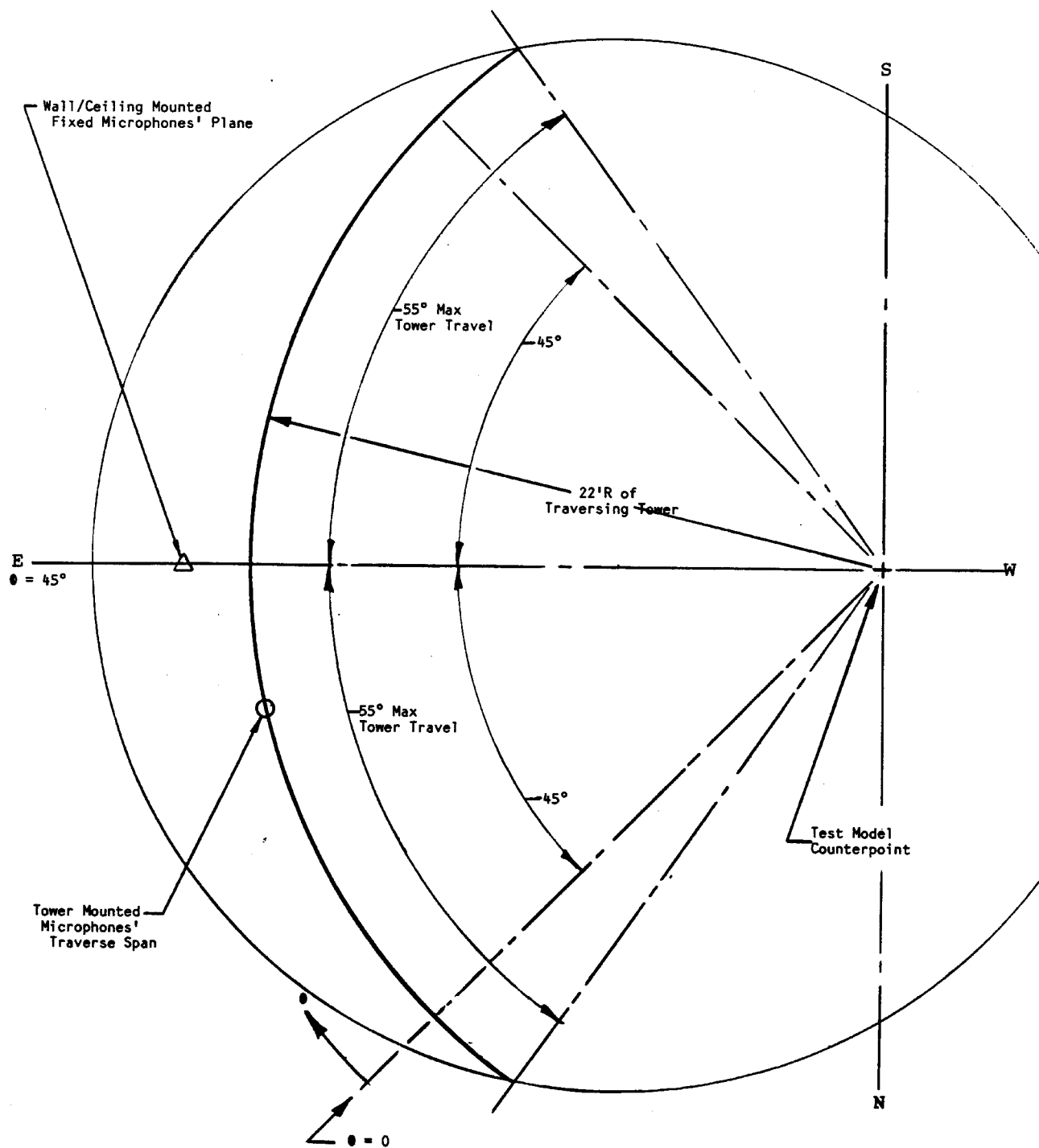


Figure 3.3. Plan view of Cell 41 Anechoic Freejet Facility showing tower microphone traverse capability.

45° (N-E) position. For the E<sup>3</sup> nozzle acoustic test program, the axisymmetric character of the nozzle implies that its orientation is irrelevant, therefore the traversing tower remains in the  $\phi = 10^\circ$  location throughout the test. Acoustic data is acquired from both the fixed (at  $\phi = 45^\circ$ ) and tower microphones.

#### ***Laser Doppler Velocimeter (LDV) System-***

The facility is also equipped with a laser Doppler velocimeter (LDV) system. The LDV system, illustrated in Figure 3.4, is a three dimensional Laser Fiber Flow system. The optical system consists of a 60 mm diameter fiber optic probe, a 1.9 beam expander, and a 1.5 beam expander with 140 mm diameter front lens. The focal length of this lens is 2000 mm. The optical system has 3.27234° beam angle, 114.2572 mm beam distance, 36 fringes, and 9.0096 micron fringe spacing. The Laser Doppler Anemometer (LDA) system is modified to obtain online data from a counter processor with x-y plotter using a Fluke 1752A computer. The seeding to each flow stream is provided using individual 100 psi vacuum pump. For high temperature flow, one micron alumina powder is used for seeding. A photograph of the fiber flow probe of the LDV system mounted on a 3-dimensional actuator table system and the LV window nozzle in Cell 41 are shown in Figure 3.5.

Velocity histogram data are obtained from a counter processor through D/A converter, which provides a voltage related Doppler frequency and a Bragg cell frequency of 40 mega Hz. The measured voltage is converted to velocity using the following relationship:

Velocity, m/sec. = (volt x amplification factor - 40 mega Hz.) x fringe spacing, micron

The amplification factor for the present system is 100. The measured data and the corresponding laser locations are digitized simultaneously and averaged with 20 readings and stored in the Fluke computer, while instantaneous data are plotted on the x-y plotter.

#### ***Data Acquisition Systems -***

Cell 41 is supported by well-calibrated acoustic and aerodynamic data acquisition systems. Acoustic data is analyzed by an on-line system, which computes 1/3-octave band data for model scale at a 40' arc corrected to standard day conditions (i.e., 59°F and 70 % relative humidity) and narrowband data as measured. In addition, this data is recorded on magnetic tapes for post processing.

All static and total pressures including model surface pressures are measured using an aerodynamic data acquisition system consisting of multiport scanivalve contained pressure transducers, signal conditioner, and analog/digital converters. The pressure signals are supplied to a Micro VAX computer system where it can be analyzed or down-loaded to GE's mainframe computer system.

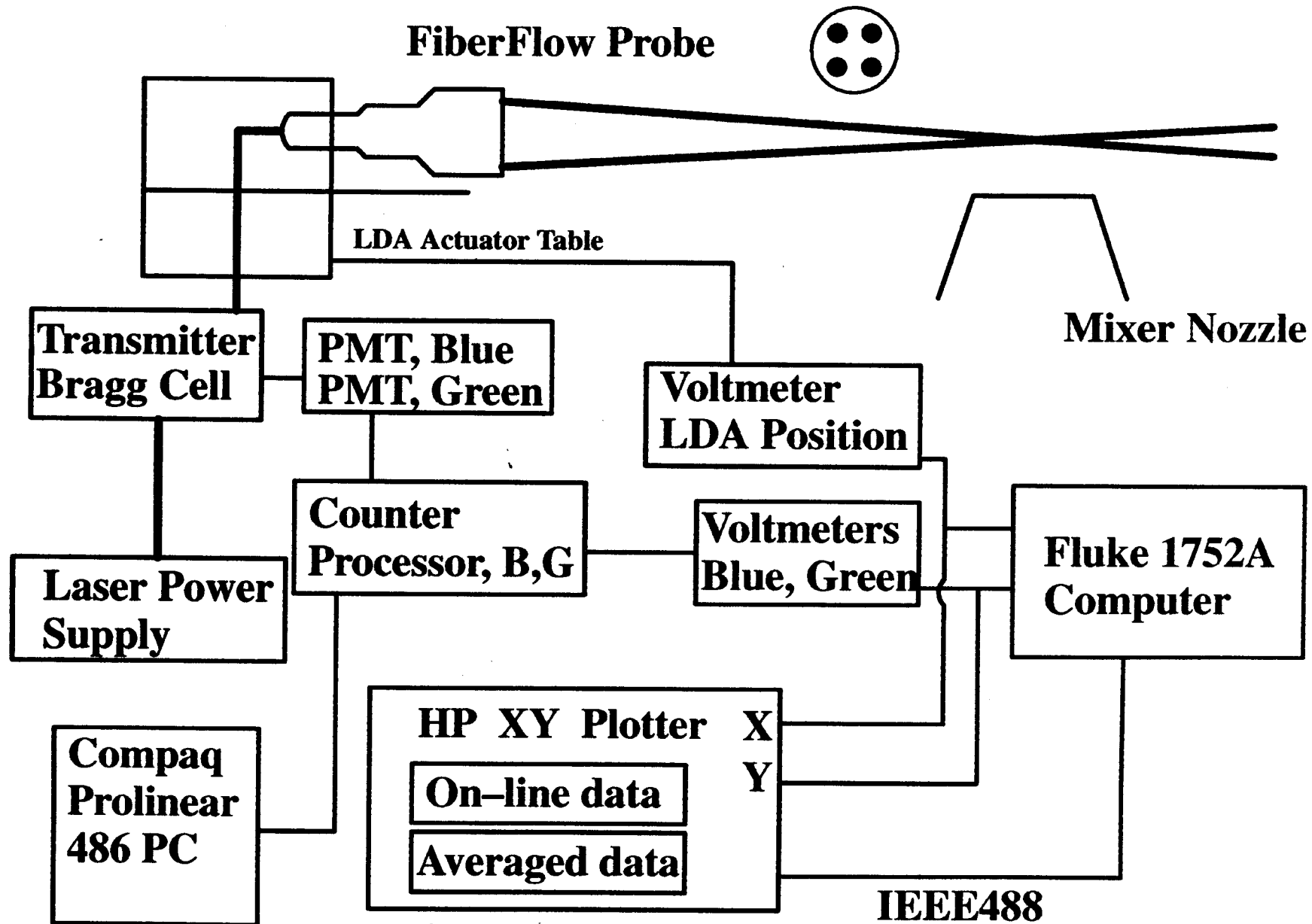


Figure 3.4. On-line LDA data acquisition system.

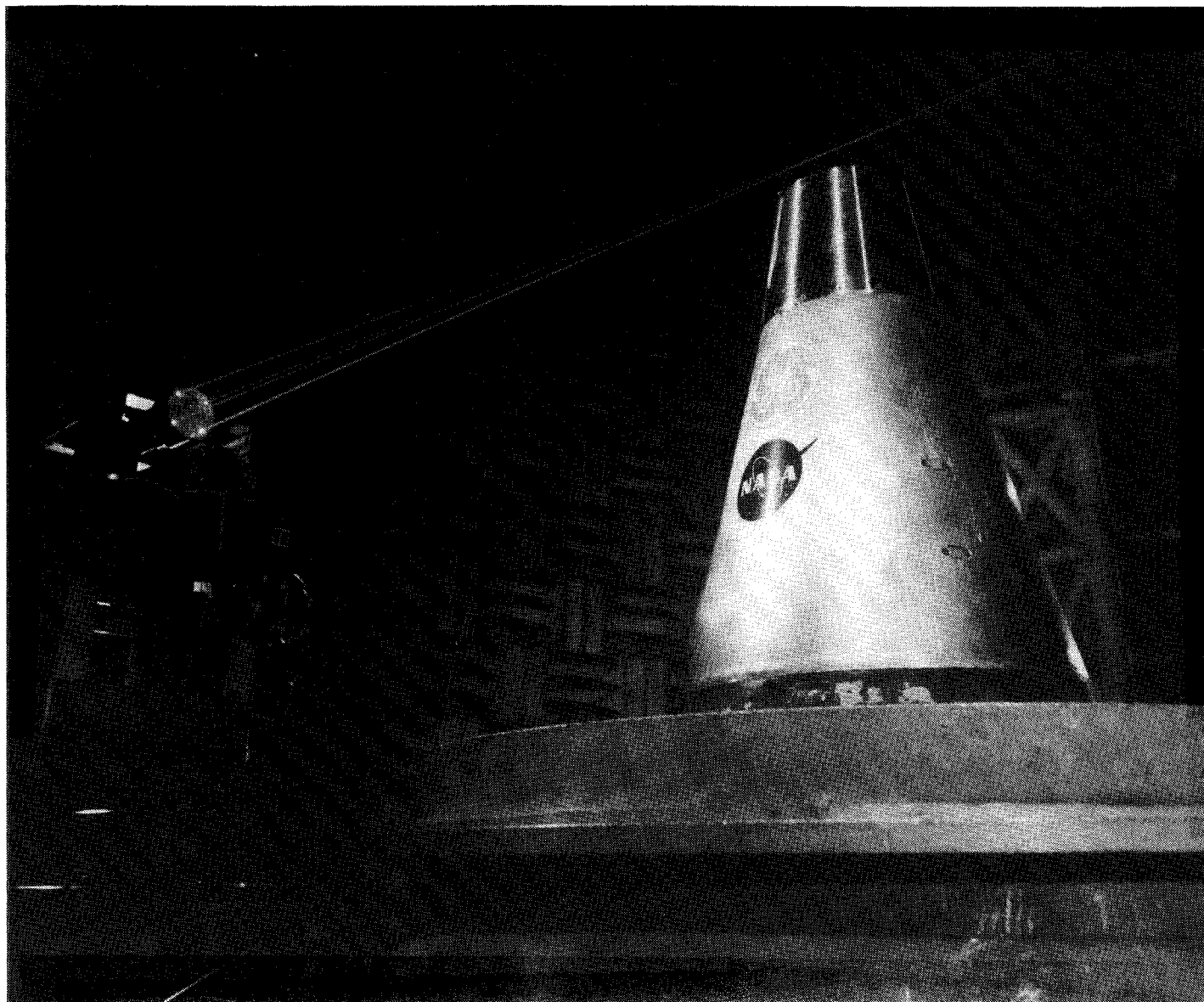


Figure 3.5. LDA system with fiber flow probe focused on  $E^3$  acoustic model installed in Cell 41 anechoic free jet facility.

A front-end computer with touch-screen application is used for signal and facility control and for real time data monitoring. Temperature data (thermocouple signals) are fed directly to the front-end computer.

On-line 1/3-octave data or post processed acoustic data are further analyzed per the flow chart of Figure 3.6 for scaling, flight transformation, and extrapolation to any sideline (or arc) location.

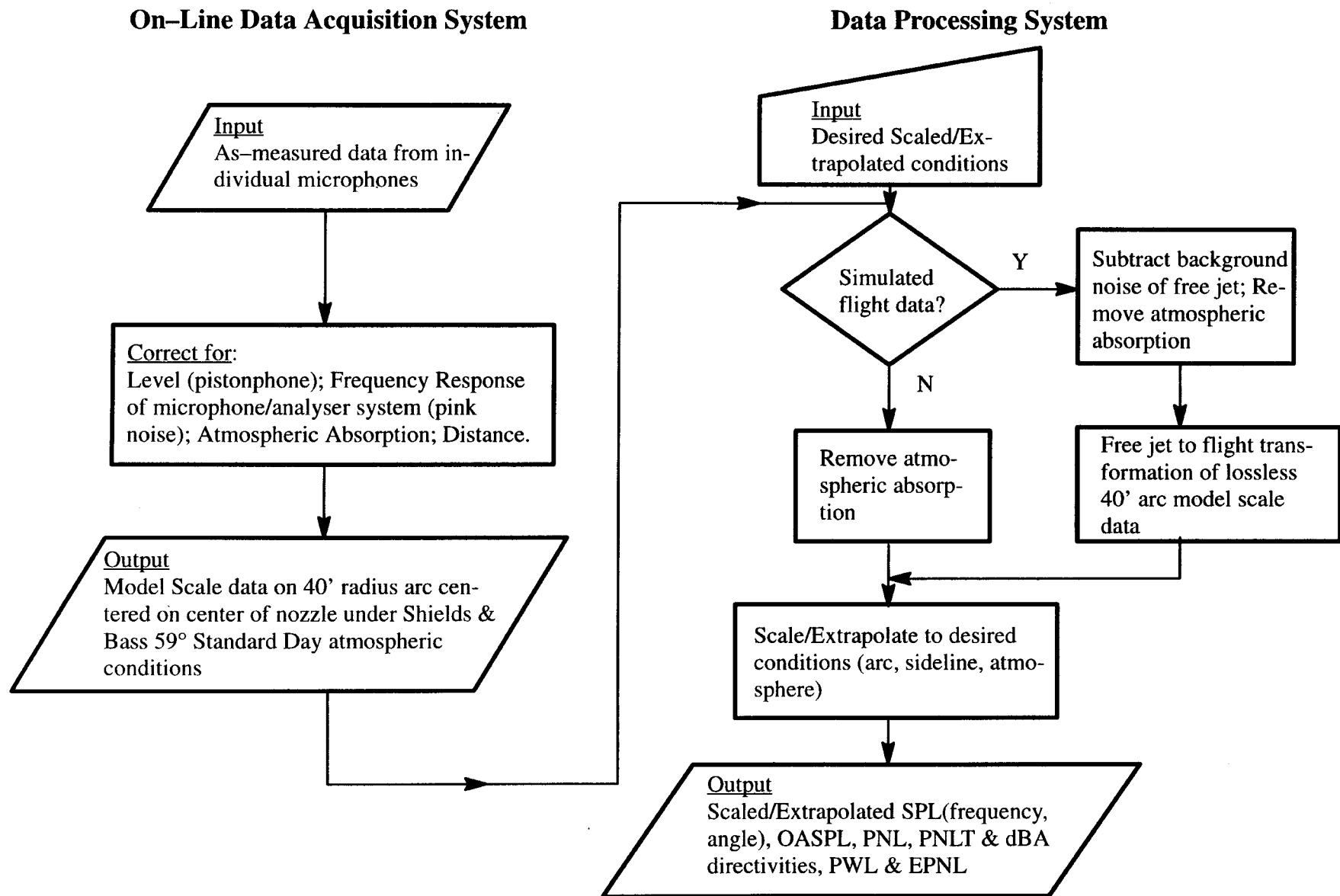


Figure 3.6. Cell 41 acoustic data acquisition and processing flow chart.





## 4.0 TEST PLAN

### *Acoustic Testing -*

The acoustic test matrix was patterned to follow two typical engine cycle operating lines for take-off and climb. The cycles represented are the E<sup>3</sup> high bypass ratio *mixed-flow* operating cycle and a high bypass ratio engine *separate flow* exhaust system cycle. The typical take-off and climb characteristics of these two engine cycles are listed in Table 4.1 and illustrated in Figures 4.1 and 4.2. Refer to Tables A1 through A6 (Appendix) for exact test conditions for each nozzle configuration.

Table 4.1. Typical Test Conditions

Point	NPR <sub>F</sub>	NPR <sub>C</sub>	TT <sub>F</sub> (°R)	V <sub>jF</sub> (f/s)	TT <sub>C</sub> /TT <sub>F</sub>	TT <sub>C</sub> (°R)	V <sub>jC</sub> (f/s)	V <sub>mix</sub> (f/s)	F <sub>GI</sub> (lb)
Mixed Flow Cycle									
1	1.4	1.365	540	771	2.513	1357	1179	819	418
2	1.45	1.428	540	808	2.559	1382	1270	863	467
3	1.5	1.493	540	842	2.602	1405	1354	903	515
4	1.55	1.560	540	874	2.648	1430	1435	941	562
5	1.6	1.631	540	903	2.693	1454	1513	977	608
6	1.65	1.703	540	930	2.738	1479	1586	1010	654
7	1.70	1.776	540	955	2.782	1502	1657	1041	698
Separate Flow Cycle									
8	1.483	1.293	540	831	2.333	1260	1036	852	468
9	1.589	1.389	540	897	2.390	1291	1181	926	561
10	1.698	1.505	540	954	2.457	1327	1328	994	656

A key distinction between the two engine cycles, from a jet noise standpoint, is that for a constant exhaust system gross thrust, the separate flow cycle operates at a higher bypass ratio than the mixed flow cycle. Consequently, the corresponding mixed flow velocity, a correlation parameter for jet noise, is lower for a separate flow cycle than for a mixed flow cycle at ideal constant thrust conditions.

Conducting the test along both mixed and separate flow engine cycle conditions enabled the thermodynamic effects of engine cycle design on jet noise to be investigated. The impact of mixer lobe shape on jet noise was assessed at constant cycle conditions, while the impact of cycle condition is investigated for a given mixer configuration.

A single flow conic nozzle was tested at the fully-mixed average test conditions. The conic nozzle represents a fully mixed near-uniform nozzle exit flow configuration. It is the ideal scenario being strived for by the lobed mixer configurations (in terms of complete, 100% mixing).

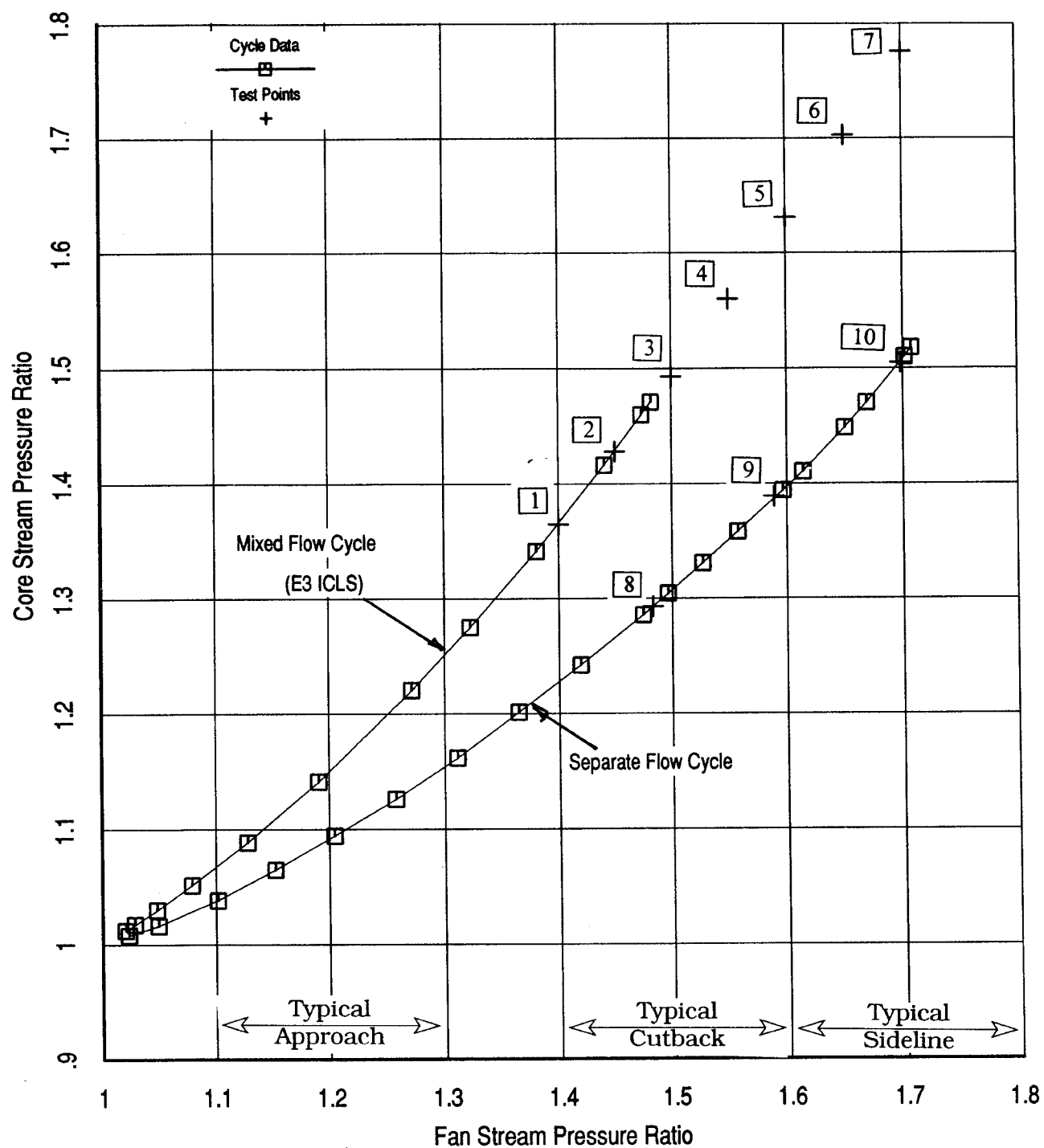


Figure 4.1. Aerothermodynamic test conditions with respect to core stream pressure ratio as a function of fan stream pressure ratio.

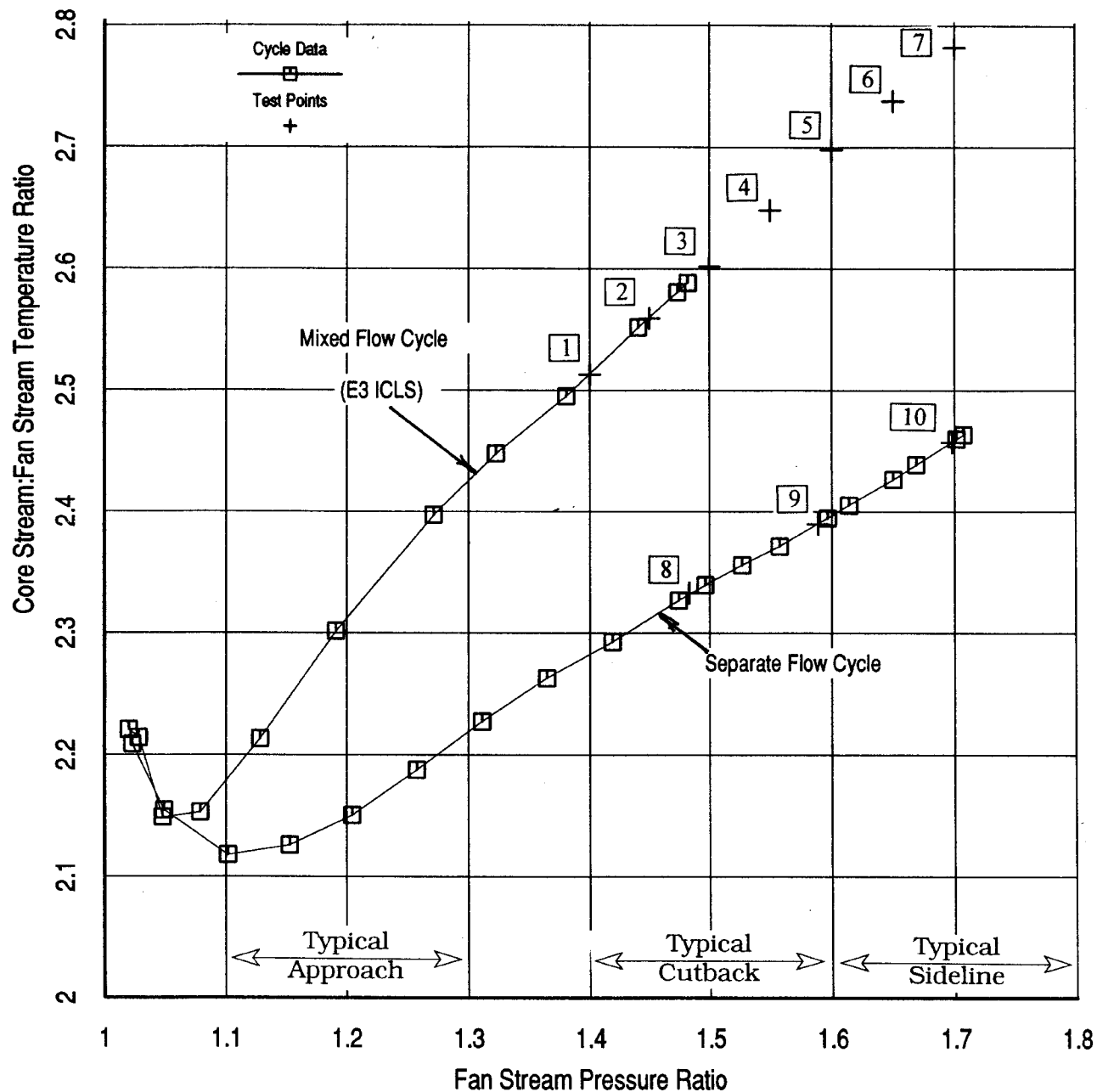


Figure 4.2. Aerothermodynamic test conditions with respect to the temperature ratio between core and fan streams as a function of fan stream pressure ratio.

Acoustic data was measured both statically, and at simulated flight conditions of Mach=0.24 and 0.28. Free jet back-ground noise, (jet off / wind on operation), was evaluated to ensure sufficient jet signal-to-(back-ground) noise ratio. With the exception of the lowest test condition, this ratio was generally greater than 10 across the measurement range of 10Hz to 100kHz.

The acoustic test configurations are summarized in Figure 4.3. A total of 6 distinct nozzle configurations were tested. Each of the configurations was tested under both static and simulated flight (free jet Mach number = 0.24 and 0.28) conditions. The tabulated reading numbers identify the individual test points.

#### ***Aero-Flowfield Measurements-***

Nozzle exit total pressure and temperature surveys were performed for two conditions statically. The LV data measured on the jet plume was performed both statically and wind-on. Figure 4.4 illustrates what configurations were tested acoustically, exit surveyed, and LV measured.

Test Date	Config Number	Config Designation	Test Nozzle Description	Test Mach Number	Test Reading Number	Aeroacoustic Data Summary
Jan-95	0		Conic	0	42-47,49-51,96	Appendix A Table A1
				0.24	74,75,78,79,82,83,87,91,92,95	
				0.28	73,76,77,80,81,84,89,90,93,94	
Feb-95	1	V1	Confluent	0	139-148	Appendix A Table A2
				0.24	120,121,124,125,127,130,131,134,135,138	
				0.28	119,122,123,126,128,129,132,133,136,137	
Feb-95	2	V2 (ICLS)	Scalloped Mixer	0	152,174,178,179,180-185	Appendix A Table A3
				0.24	153,158,159,163,164,167,168,171,172,186	
				0.28	155,157,160,162,165,166,169,170,173,187	
Mar-95	2R (Repeat)	V2 (ICLS)	Scalloped Mixer	0	317-320	Appendix A Table A3
				0.24	322-325	
Feb-95	2A	V2	Scalloped Mixer with Extended Tailpipe	0	190,201-205	Appendix A Table A4
				0.24	191-193,196,197,200	
				0.28	194,195,198,199	
Feb-95	3	F9B	Scalloped & Staggered Mixer	0	242,258-266	Appendix A Table A5
				0.24	244-247,250,251,254-257	
				0.28	248,249,252,253	
Feb-95	4	F12A	Skewed Mixer	0	228-235,239,315	Appendix A Table A6
				0.24	216,217,220,221,224-227,236,238	
				0.28	218,219,222,223	

Figure 4.3. Vsummary of scale model acoustic tests.



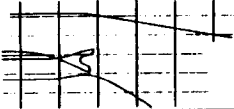
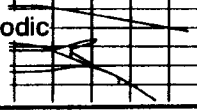
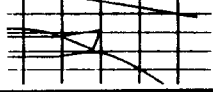

Config #	Configuration	Type of Testing				
		S/N Calib's	Acoustics	Laser Vel.	Exit PT/TT	Mixer Ps
0	Conic Nozzle(s)	✓	✓			
1	Confluent (V1) 		✓	✓	✓	
2	ICLS (V2) 		✓	✓	✓	
2A	ICLS w/ 2" Nozzle Extension 		✓	✓	✓	
3	Quarter-Periodic (F9B) 		✓	✓		
4	Skewed (F12A) 		✓	✓	✓	
5	Lobed Mixer (F8) 					✓

Figure 4.4. Various exhaust nozzle configurations and the types of tests conducted for each.

## 5.0 ACOUSTIC DATA

Acoustic tests were conducted as per engine core nozzle vs. fan nozzle pressure ratio operating lines shown in Figure 5.1a. Series-1 operating line simulates ICLS E<sup>3</sup> engine with LDMF. The mixer and confluent configurations were all tested at selected conditions on this line. Limited acoustic tests were also conducted on series-2 operating line that is typical of an engine with a separate flow nozzle. The conditions selected on the series-2 line match the ideal thrust of the corresponding test point on the mixed flow series-1 line.

For ease of identifying acoustic data of different configurations at comparable nozzle flow conditions, the selected test aero condition on each of the operating lines is specified by a number referred to as point number. Point numbers 1-7 signify test conditions on series-1 mixer operating line and point numbers 8-10 signify test conditions on series-2 separate flow operating line. The test point sets 2 and 8, 4 and 9, and 6 and 10 have equal ideal thrust but at different  $V_{mix}$ . Actual test conditions of confluent flow nozzle (Table A2) are used in Figure 5.1 b to illustrate data.

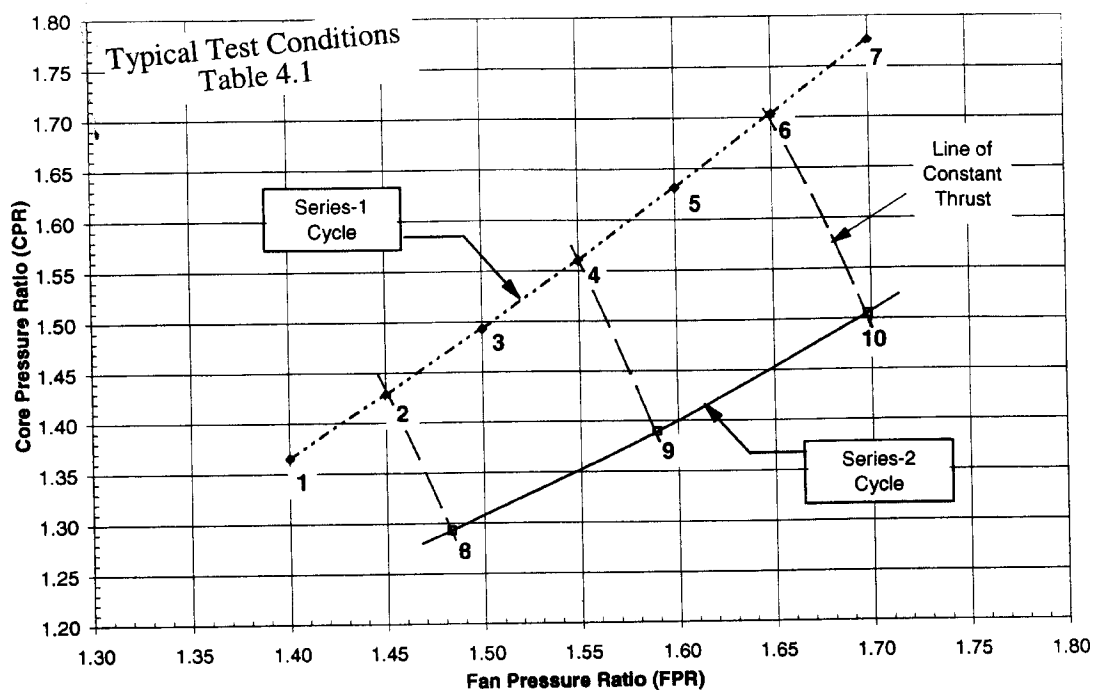
The test conditions are also shown in Figure 5.1b in terms of fan-to-core exhaust velocity ratio plotted against ideal mixed velocity,  $V_{mix}$ . Points 1 and 8, 3 and 9, and 5 and 10 are conditions at  $V_{mix}$  approximately equal to 850, 930, and 1000 fps but at different fan-to-core exhaust velocity ratios and thrust values.

The reference conic nozzle was tested at flow conditions that match the mass averaged mixed conditions of the series-1 and series-2 test points.

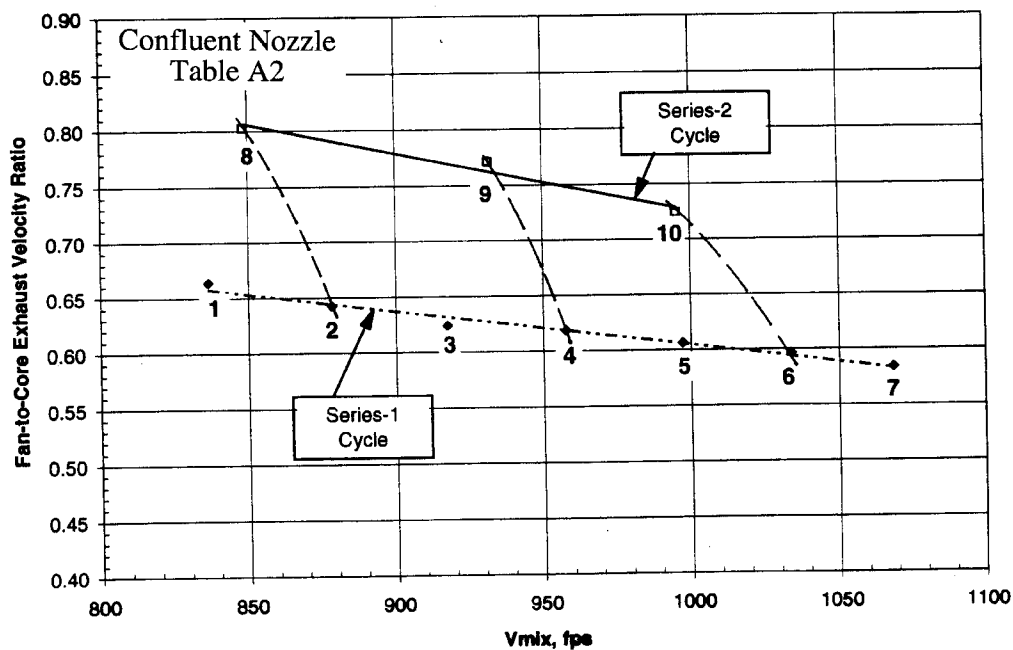
The aeroacoustic data are summarized in Tables A1-A6 of Appendix A. The aerodynamic nozzle flow conditions include ideal flow calculations based on the measured temperature and pressure information. The summarized acoustic data contain an engine scale aft quadrant  $PNL_{max}$  of all test points and EPNL of flight points. To be consistent with the earlier E<sup>3</sup> acoustic data, the model data were scaled to an engine nozzle size of 3078 sq in (scale factor = 8) and extrapolated to a 1500 ft altitude. The reading number identifies the unique test point and the point number defines the specific test condition on the operating line.

### 5.1 Cell 41 Acoustic Testing -

Acoustic testing of the E<sup>3</sup> model hardware in the GEAE Cell 41 anechoic free-jet facility required that extreme care be taken with regard to background noise levels and signal-to-noise ratios. The matrix of test conditions, along with the high bypass ratios of the model systems, results in nozzle conditions that have fully mixed velocities considerably lower than data recently acquired in this facility. Consequently, considerable time and effort was devoted to establishing the optimum techniques for acquiring high quality acoustic data.



a) Core Pressure Ratio vs Fan Pressure Ratio



b) Fan-to-Core Exhaust Velocity Ratio vs  $V_{MIX}$

Figure 5.1 Typical test operating line and conditions of scale model confluent and lobed-mixer nozzles.



Signal-to-noise ratios were monitored throughout the test when the free-jet was running through use of the on-line acoustic data acquisition system.

The microphone data has been reviewed for signal-to-noise ratio, calibration, etc. The acoustic data has been scaled to full scale E<sup>3</sup> nozzle exit area ( $A_8=3078 \text{ in}^2$ ), and extrapolated to 1500 feet side-line. The GEAE flight transformation technique has been applied to the simulated flight conditions.

The presented acoustic results are model data scaled to an engine nozzle size of 3078 sq in and extrapolated to 1500 ft altitude. The results are mostly discussed by comparing aft angle  $\text{PNL}_{\text{max}}$  for the static test conditions and EPNL for simulated flight cases plotted against ideal mixed velocity  $V_{\text{mix}}$ . The data will be presented against ideal net thrust during the discussion on the effect of operating cycles as the test conditions on the two cycles generate different thrust for a given  $V_{\text{mix}}$ . PNL-directivity and sound pressure level spectra at selected conditions are also presented in this section. The selected comparisons correspond to test conditions 2 and 6 on series-1 and test conditions 8 and 10 on series-2 operating line. These conditions provide engine static thrust  $\cong 33000$  and  $48000 \text{ lb}$ , respectively. The engine net thrust for these cases under simulated flight conditions ( $M=0.24$ ) are  $\cong 23000$  and  $34000 \text{ lb}$ , respectively. These test points, in this analyses, are considered to define the nozzle flow conditions at typical cutback and takeoff of an E<sup>3</sup>-class engine application.

## 5.2 Repeatability of Acoustic Data

The repeatability of the measured data, under both static and flight conditions, is demonstrated in Figure 5.2 by comparing the  $\text{PNL}_{\text{max}}$  (for static) and EPNL (for simulated flight) obtained with the scalloped mixer nozzle (config-2) on two different occasions. The data are generally within 1.0 dB of each other.

## 5.3 Comparison of Mixer, Confluent and Conical Nozzle Data

To determine the acoustic benefits of the mixer configurations, results of the three test mixers are compared in this section with data obtained with the confluent flow and the conical nozzles. No pylon hardware was installed with the test configurations. All mixer and confluent flow configurations were tested with nominal length fan exhaust shroud. The mixer and confluent flow nozzles data were obtained with series-1 operating line, simulating LDMF cycle conditions. The conical nozzle data correspond to test conditions that match the mass averaged mixed conditions of the series-1 test points.

The static  $\text{PNL}_{\text{max}}$  data are provided in Figure 5.3 as a function of ideal mixed velocity  $V_{\text{mix}}$ . While cycle test points 1-6 lie along a line, a shift is noted in data trend with test point 7. This is due to change in the angle at which the peak PNL was noted along the sideline. The EPNL results under the simulated flight conditions ( $M = 0.24$  and  $0.28$ ) are presented in Figures 5.4 and 5.5. As expected, the EPNL data now show a smooth trend.

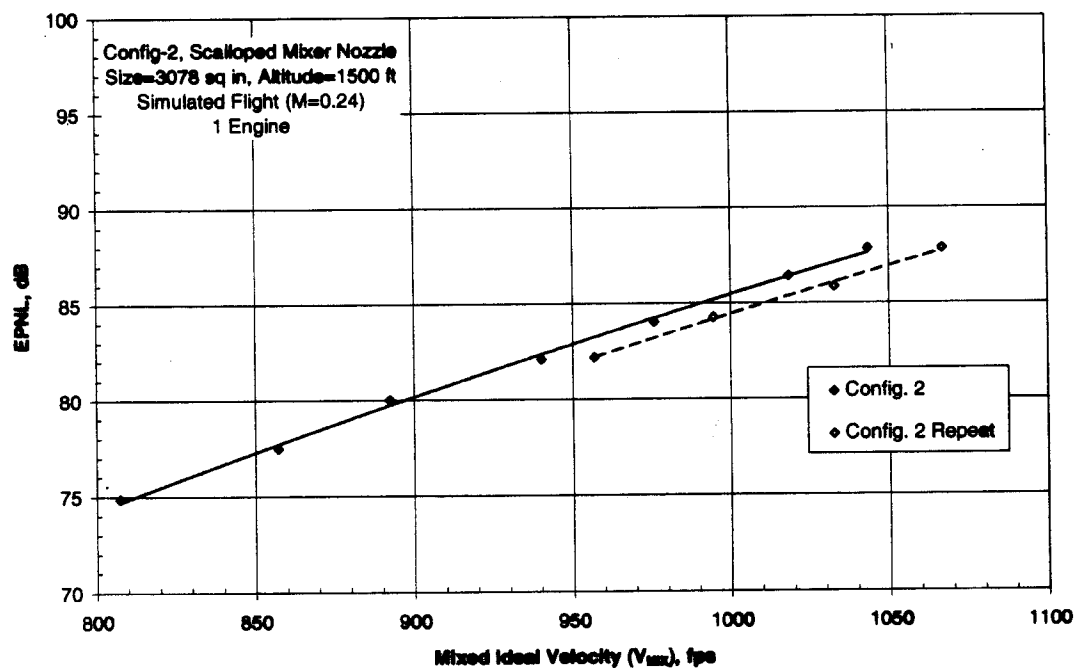
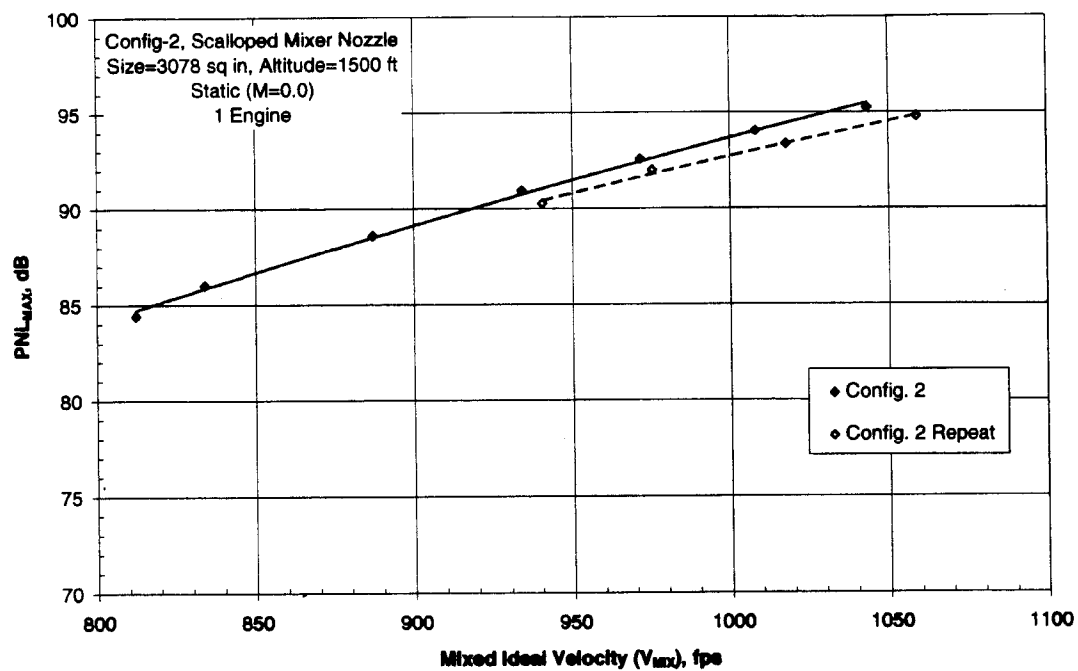


Figure 5.2 Repeatability of measured aeroacoustic data.

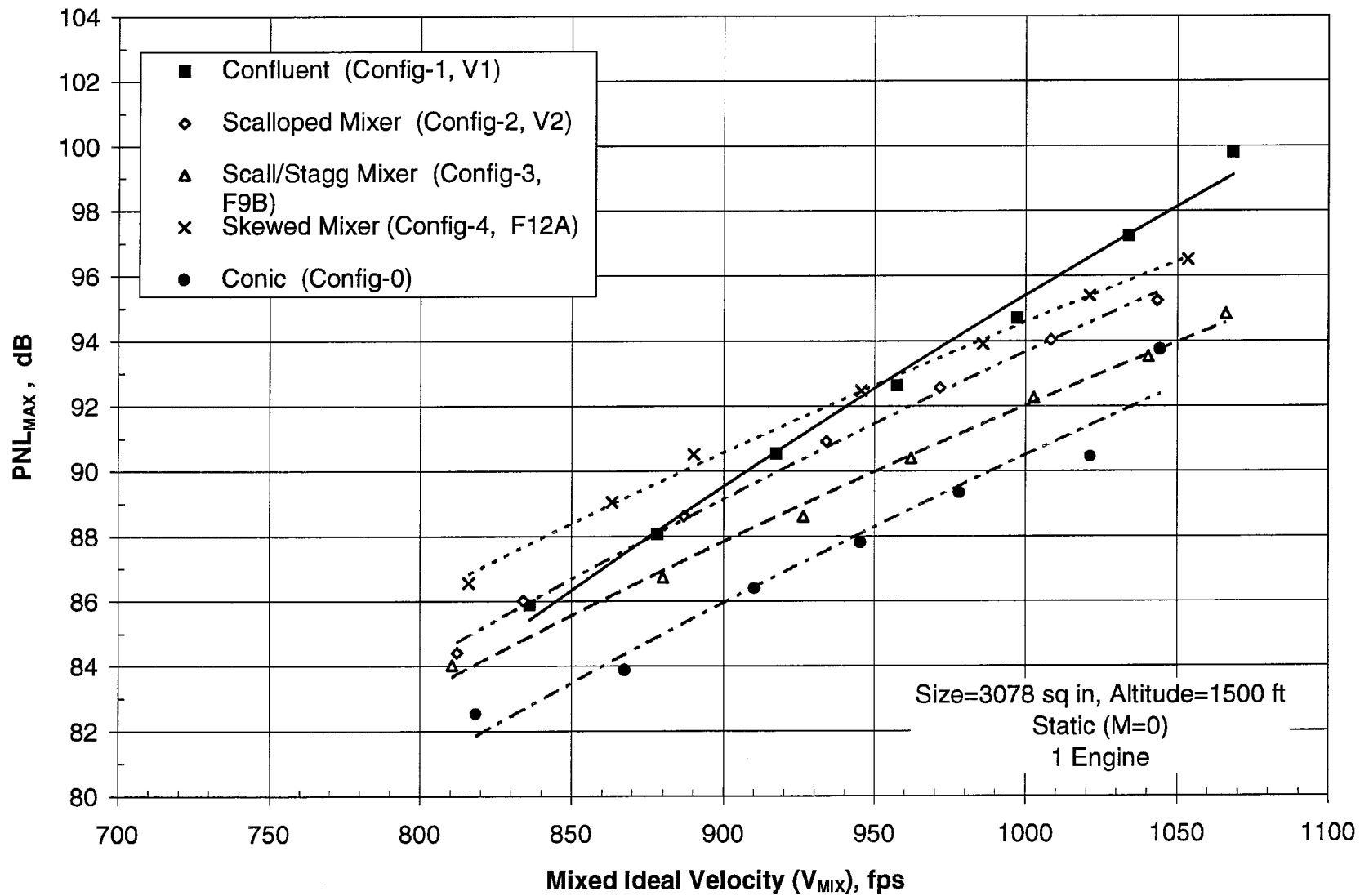


Figure 5.3 Comparison of confluent, 12-lobed mixers, and conic nozzle acoustic data, static.

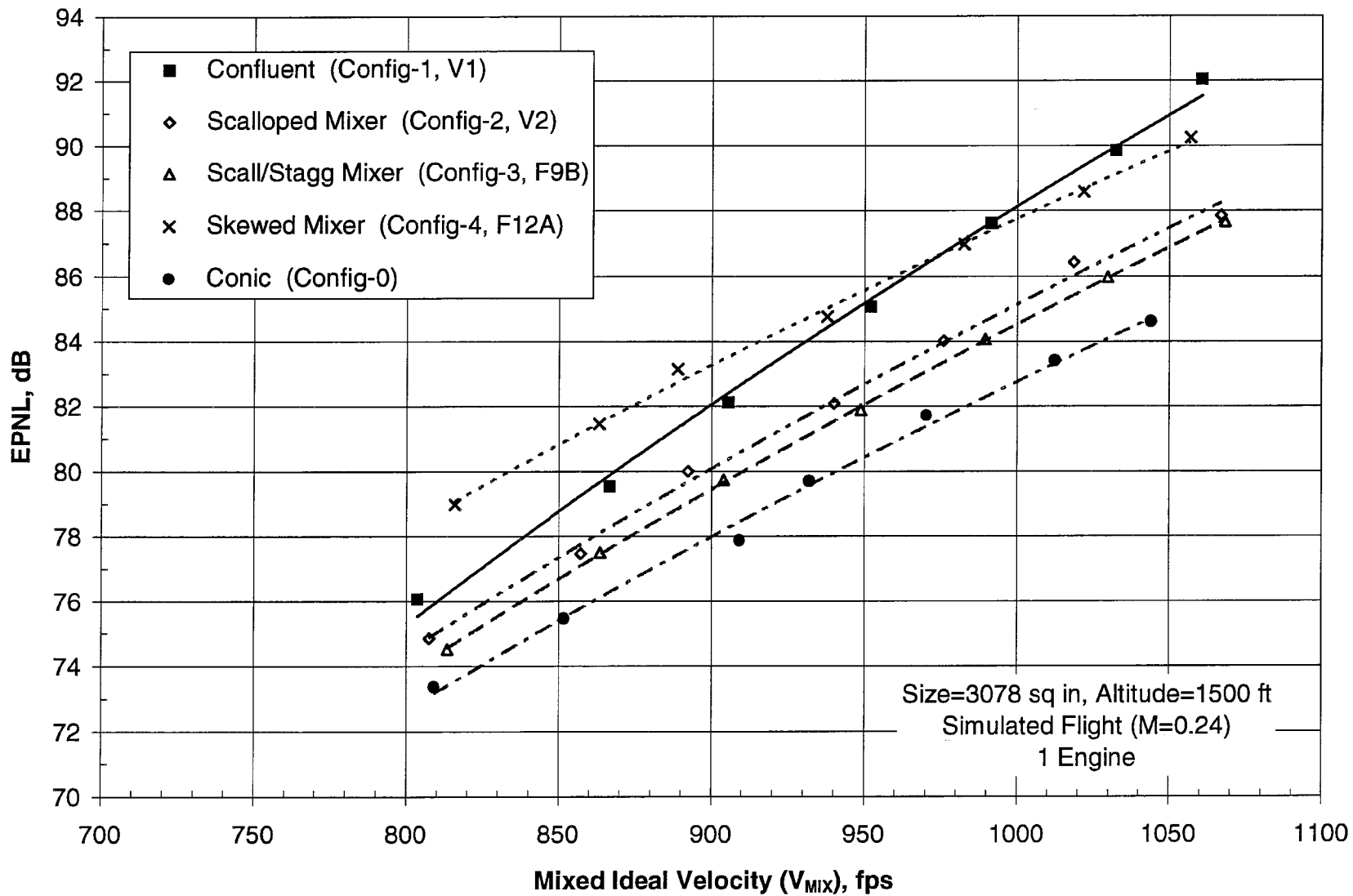


Figure 5.4 Comparison of confluent, 12-lobed mixers, and conic nozzle acoustic data, simulated flight M=0.24.

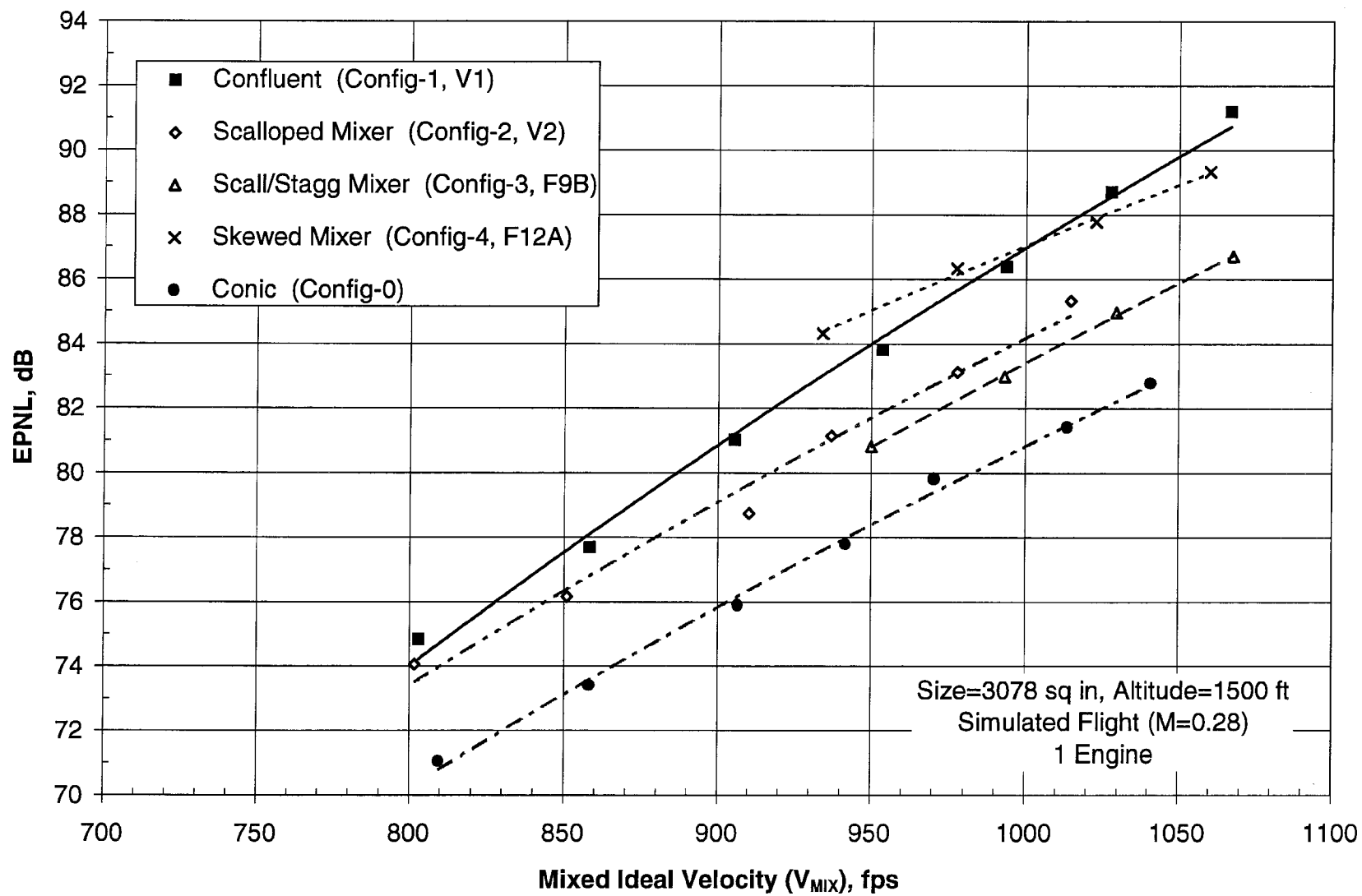


Figure 5.5 Comparison of confluent, 12-lobed mixers, and conic nozzle acoustic data, simulated flight M=0.28.

These figures indicate notable differences in the acoustic results of the three mixers. Under both static and simulated flight conditions, the scalloped/staggered mixer (config-3, F9B, 12 lobes, 48% penetration, 35.6° lobe spread angle) provides the lowest noise levels, and the skewed mixer (config-4, F12A, 12 lobes, 38% penetration, 31.2° lobe spread angle) the highest level. The differences, for a given  $V_{mix}$ , are close to 3 dB under static conditions and 4 dB under simulated flight conditions. The scalloped mixer (config-2, V2/ICLS, 12 alternating different radial lobes, 43% penetration, 38.9° lobe spread angle) provides levels that are slightly noisier than those of the scalloped/staggered mixer.

Figures 5.3 through 5.5 also show the mixer noise levels relative to the confluent and conic nozzles. The skewed mixer is noisier than the confluent flow nozzle at low mixed velocity conditions. And, it is slightly quieter than the confluent flow nozzle at higher velocities. The scalloped/staggered mixer provides the maximum noise benefit relative to the confluent flow nozzle. The conic nozzle with a fully-mixed uniform flow field at its exit, representing an ideal mixer, provides the lowest measured noise levels for a given  $V_{mix}$ . The acoustic benefits of the three mixers and the conic nozzle relative to the confluent flow configuration are summarized in Table 5.1 for selected  $V_{mix}$  of 900 and 1000 fps:

Table 5.1. Acoustic Benefits at Selected  $V_{mix}$  of 900 and 1000 fps.

Config Number (Desig.)	Nozzle Description	Acoustic Benefit of Mixer and Conic Nozzles Relative to Confluent Flow Nozzle					
		Static		Simulated Flight M=0.24		Simulated Flight M=0.28	
		PNL <sub>max</sub> ΔdB		EPNL ΔdB		EPNL ΔdB	
	$V_{mix} \rightarrow$	900 fps	1000 fps	900 fps	1000 fps	900 fps	1000 fps
Config-1 (V1)	Confluent Flow	Ref	Ref	Ref	Ref	Ref	Ref
Config-2 (V2)	Scalloped Mixer	0.5	1.8	2.0	3.0	1.8	2.8
Config-3 (F9B)	Scall/Stagg Mixer	1.7	3.4	2.6	3.6	2.7*	3.6
Config-4 (F12A)	Skewed Mixer	-1.0	1.0	-1.2	0.5	-2.0*	0
Config-0	Conic	3.5	5.0	4.0	5.4	5.0	6.2

(\* extrapolated from the plotted data)

The tabulated benefits, under simulated flight Mach number of 0.24, indicate that the scalloped and scalloped/staggered mixers provide 3 and 3.6 EPNdB reduction at typical takeoff  $V_{\text{mix}} = 1000$  fps relative to the confluent flow nozzle. This reduces to 2 and 2.6 EPNdB at  $V_{\text{mix}} = 900$  fps. The corresponding maximum benefits, at these two ideal mixed velocities, with the fully mixed conic nozzle are 5.4 and 4 EPNdB, respectively.

PNL-directivity, OASPL-directivity and typical forward and peak aft angle spectral comparisons at  $V_{\text{mix}}$  approximately equal to 1000 and 900 fps are provided in Figures 5.6 through 5.9 for the simulated flight condition ( $M=0.24$ ). These figures indicate:

- lower frequency jet noise benefit ( $< 400$  Hz 1/3-OB) with mixer and conic nozzles relative to confluent flow nozzle. This spectral benefit is significant in the aft quadrant. This benefit further contributes to the OASPL and PNL reductions noticed in the aft quadrant of the directivity plots. The three mixer configurations provide, more or less, equal spectral benefits in this range ( $\cong 6$ -8 dB in the aft quadrant microphone locations). The reduction in the noise levels in this frequency range is mainly due to decreased peak exhaust velocity achieved with mixer configurations.
- at most of the middle frequencies ( $500 \text{ Hz} < 1/3\text{-OB} < 4000 \text{ Hz}$ ), mixer sound pressure levels are higher than those of the confluent flow nozzle. Skewed mixer noise levels are highest in this frequency range and hence the higher PNL noted in the PNL-directivity plots. Only the fully mixed conic nozzle spectra is lower than those of the confluent nozzle levels and thus the conic nozzle provides the lowest levels in the PNL-directivity plots.
- At high frequencies ( $> 5000 \text{ Hz}$ ), the noise levels of the confluent and conic nozzles approach one another. The mixer levels also approach those of the confluent nozzle except those of skewed mixer. Skewed mixer data are generally greater than those of the other configurations.

Mixer acoustic data available in literature (Refs. 5 and 6) are all similar to those of the tested mixers as they all show significant benefits at lower frequencies and increased sound pressure levels at mid and higher frequency ranges relative to unmixed configurations. This increase in mid and higher frequency sound levels also increase the perceived noise level and thus offset some of the gain due to decreased levels at lower peak jet noise frequencies. The higher the increase in the mid and high frequency range, lower the overall PNL and EPNL benefit. This is clearly shown by the data of the skewed mixer (config-4). Mixer designs that will provide minimal sound pressure level increase in this frequency range will, therefore, provide increased overall noise benefit. The fully mixed conic nozzle is an ideal mixer with no increase in this frequency range and thus provides the maximum overall noise benefit relative to unmixed nozzles.

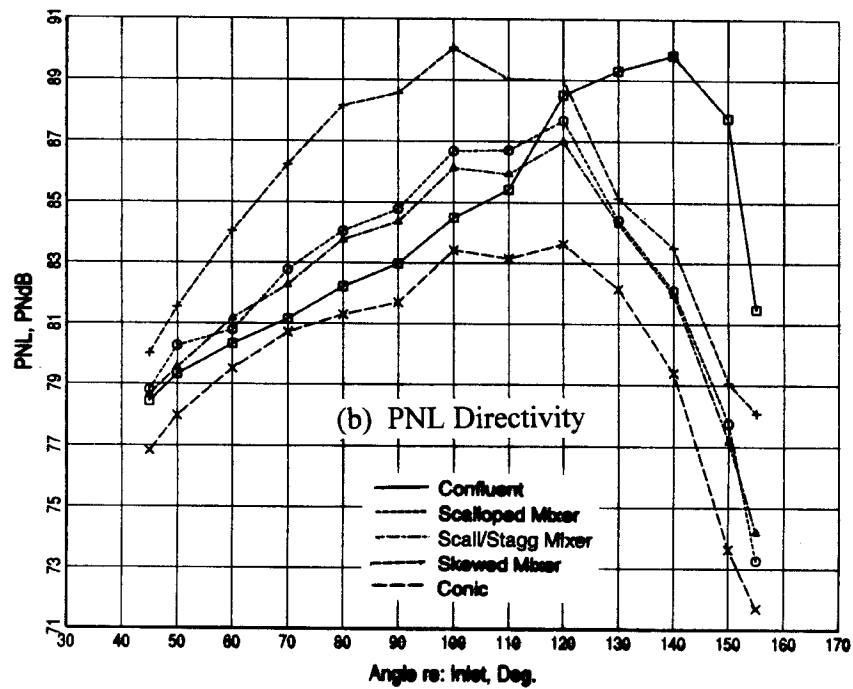
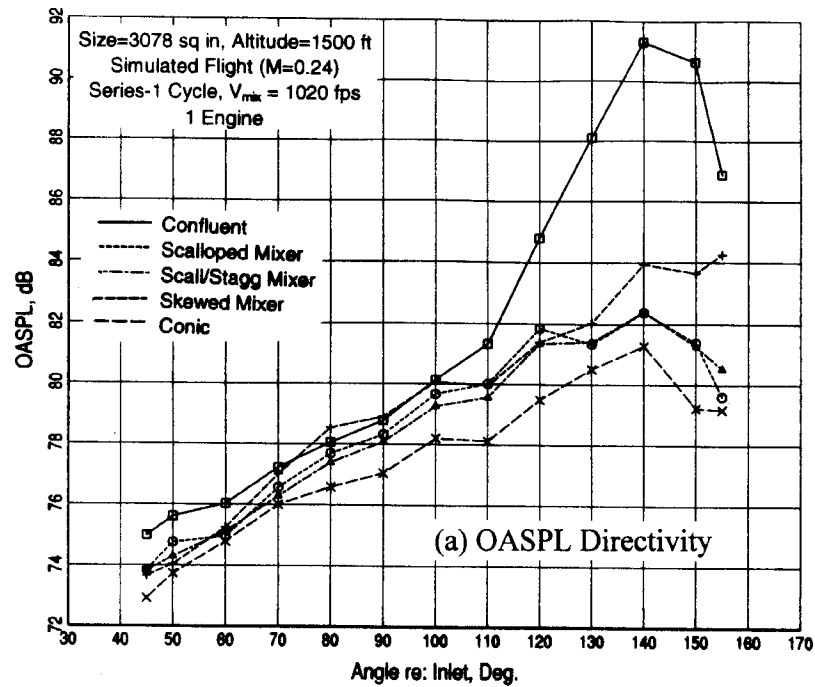


Figure 5.6 Comparison of confluent, 12-lobed mixers, and conic nozzle OASPL and PNL directivity; nominal  $V_{mix}=1020$  fps, simulated flight  $M=0.24$  (Test Point 6).



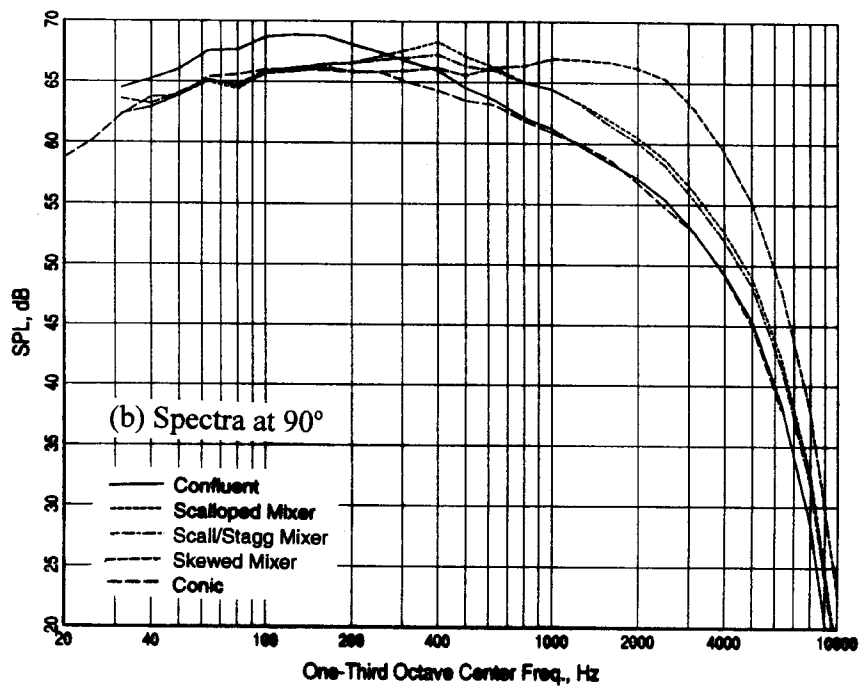
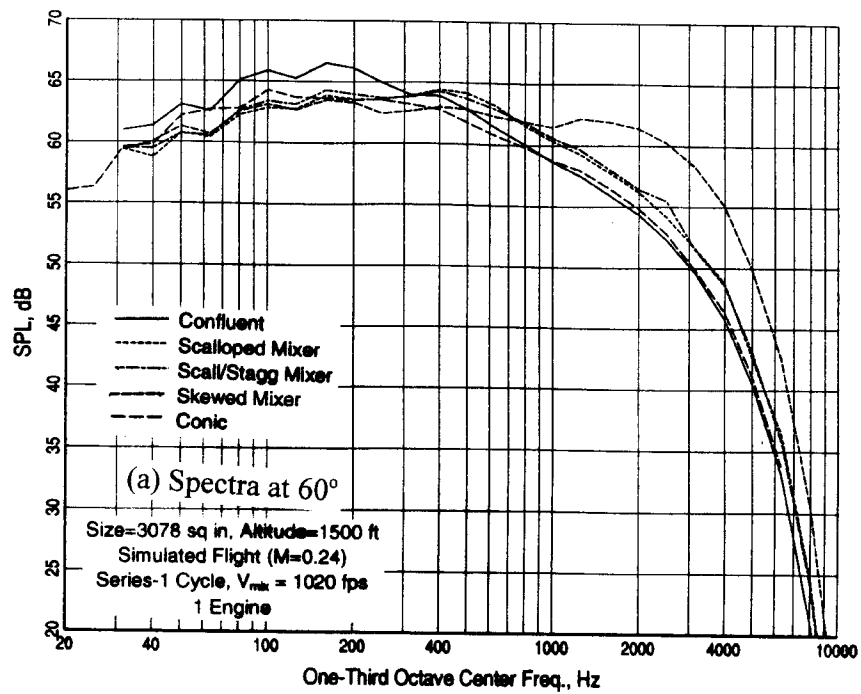


Figure 5.7 Comparison of confluent, 12-lobed mixers, and conic nozzle SPL spectra; nominal  $V_{mix}=1020$  fps, simulated flight  $M=0.24$  (Test Point 6).

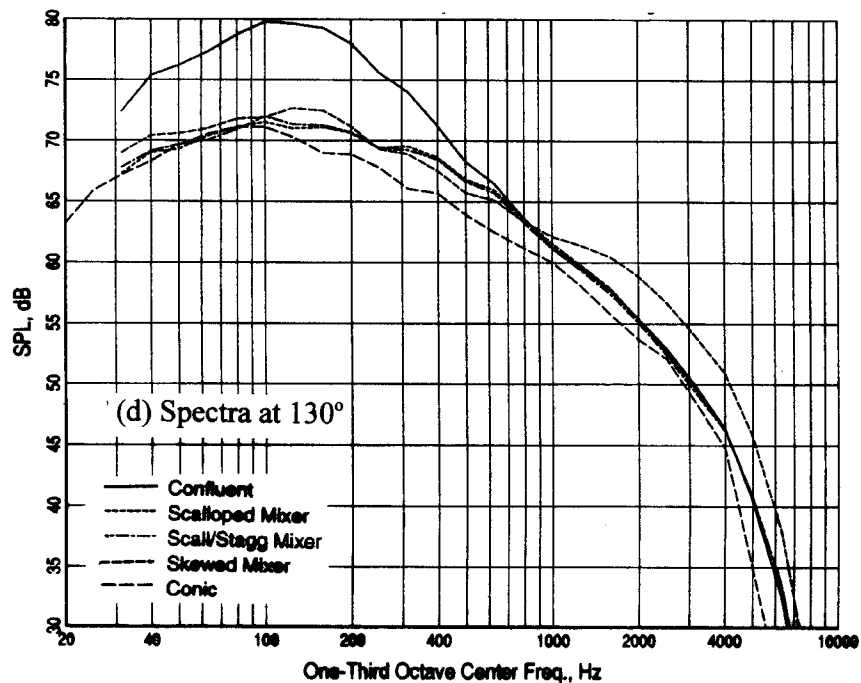
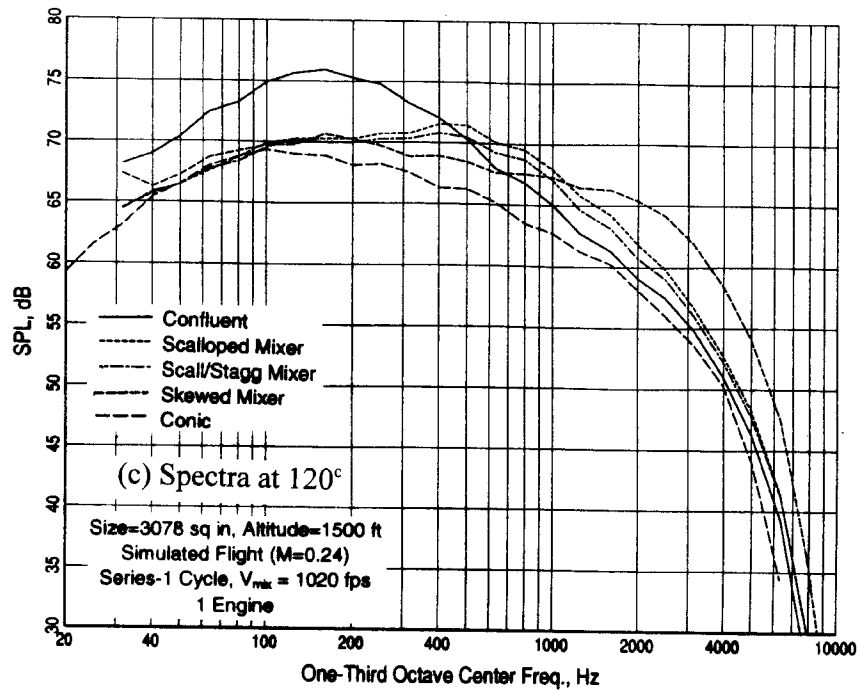


Figure 5.7 Comparison of confluent, 12-lobed mixers, and conic nozzle SPL spectra; nominal  $V_{mix}=1020$  fps, simulated flight M=0.24 (Test Point 6).

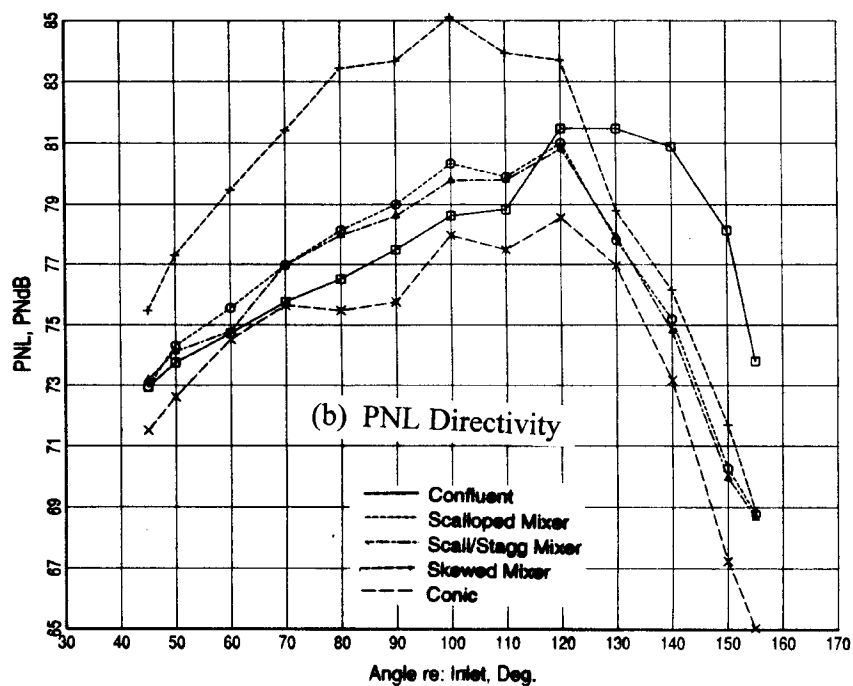
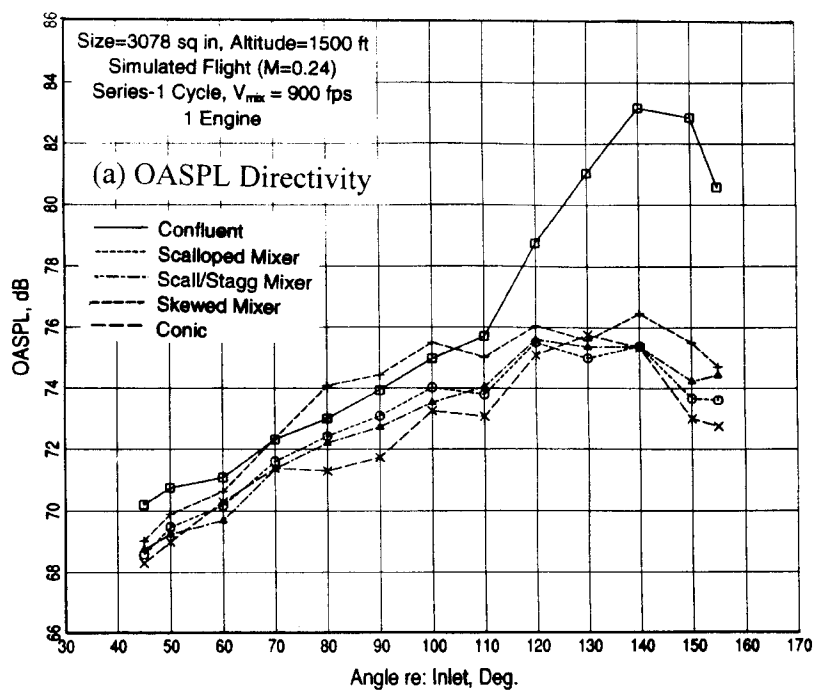


Figure 5.8 Comparison of confluent, 12-lobed mixers, and conic nozzle OASPL and PNL directivity; nominal  $V_{mix}=900$  fps, simulated flight  $M=0.24$  (Test Point 3).

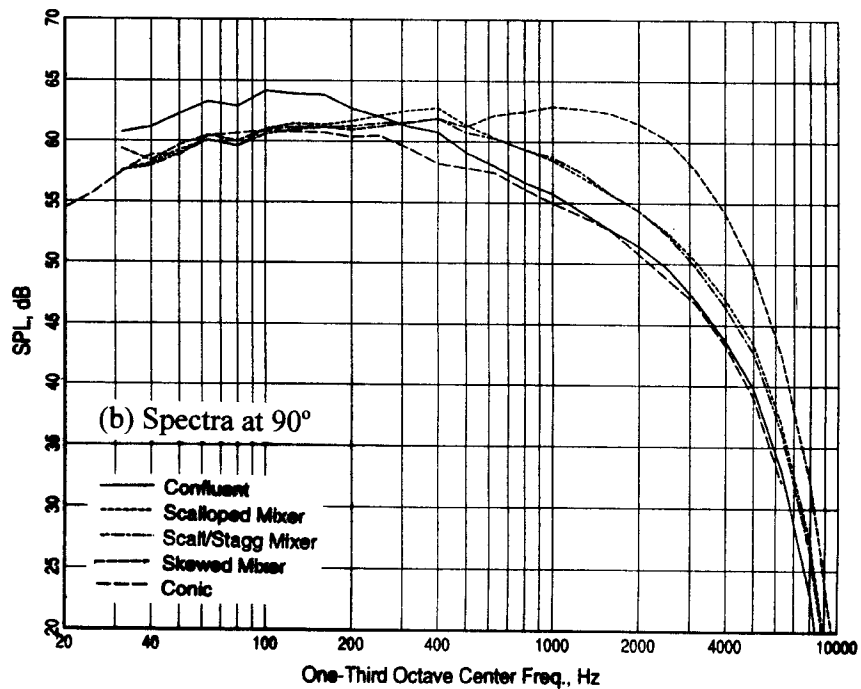
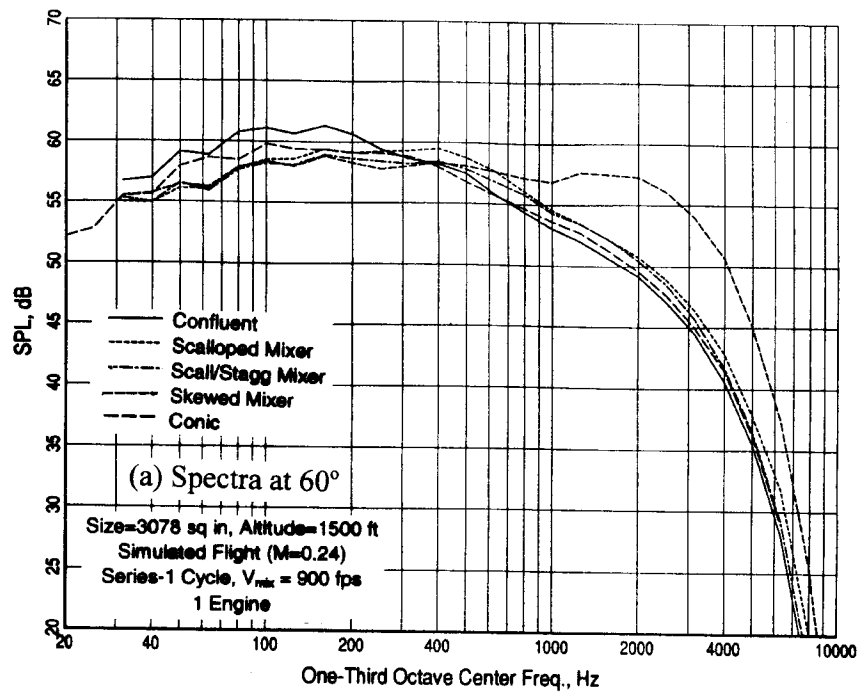


Figure 5.9 Comparison of confluent, 12-lobed mixers, and conic nozzle SPL spectra; nominal  $V_{mix}=900$  fps, simulated flight M=0.24 (Test Point 3).

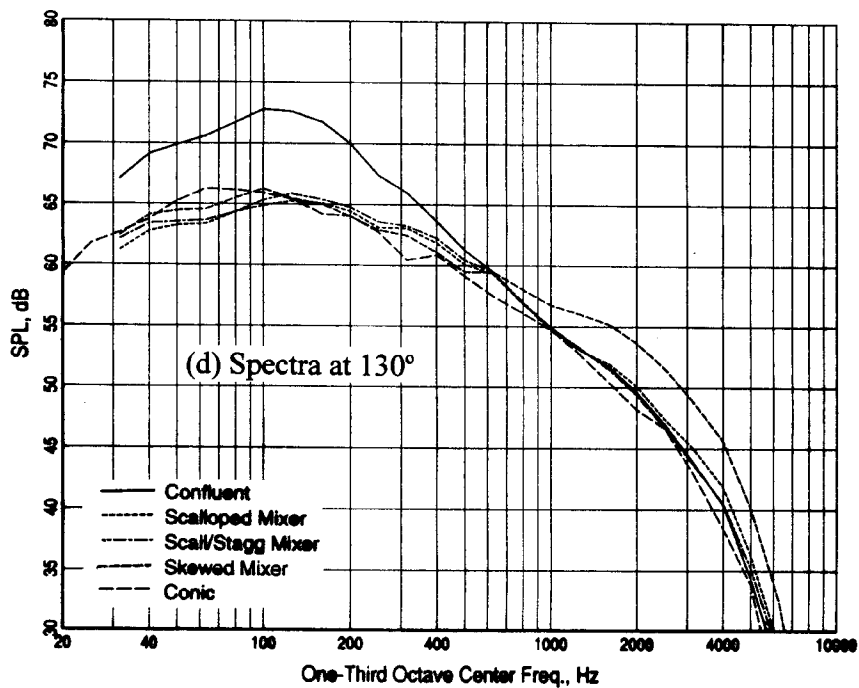
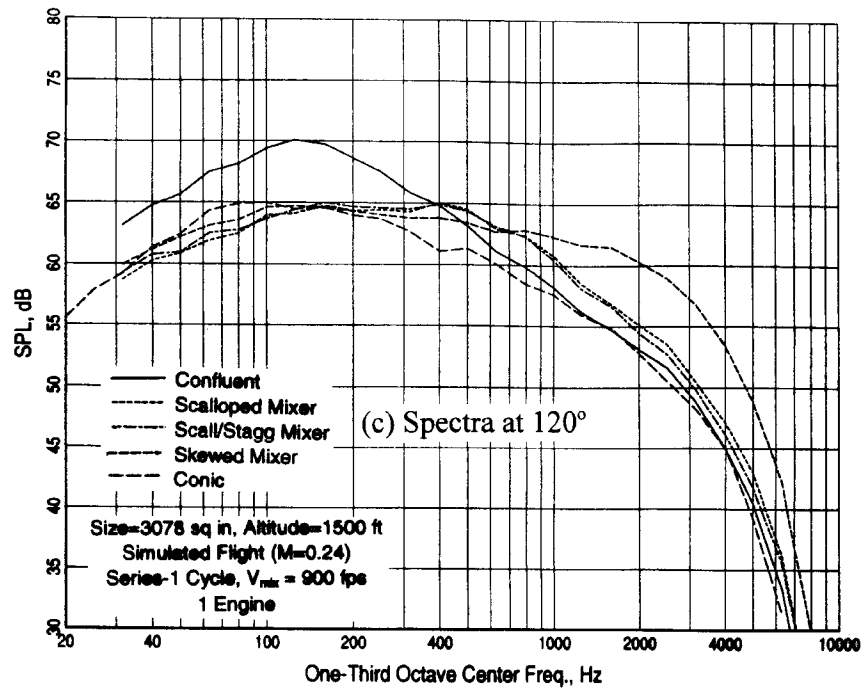


Figure 5.9 Comparison of confluent, 12-lobed mixers, and conic nozzle SPL spectra; nominal  $V_{mix}=900$  fps, simulated flight M=0.24 (Test Point 3).

The increase in mid and higher frequency noise levels observed with the mixers has generally been attributed to internally generated flow noise caused by flow over the lobes.

From the data provided in this section, it is therefore concluded that all the mixer and conic nozzles provided the low frequency jet noise reduction. The conic nozzle had no internal noise and provided maximum benefits at high frequencies. Thus the fully mixed conical nozzle provided the lowest PNL levels at all angles relative to confluent flow nozzle. The scalloped and scalloped/staggered mixers generated some internal noise. This reduced the overall PNL benefits relative to the confluent flow nozzle. The skewed mixer provided the highest internal noise levels and thus the overall PNL benefits were minimal or adverse relative to the confluent nozzle.

The jet noise improvement levels measured and reported to date have no installation representation associated with them. The installation effects of engine pylon(s) may significantly affect the mixing characteristics of a lobed mixer. This in turn, could have an impact on the "*installed*" jet noise reduction of a lobed mixer relative to a confluent mixer. Some of the planned activities under Subtask C of this task order should address this "*installation*" issue.

#### **5.4 Effect of Mixing Duct Length**

To determine the effect of the mixing duct length on acoustic data, scalloped mixer (config-2) was tested with both nominal length fan exhaust shroud and an extended shroud obtained by adding a 2 inch scale model tailpipe spacer (16.67 inches engine scale). The test points correspond to series-1 operating cycle. The simulated flight EPNL data at  $M = 0.24$  and  $0.28$  are provided in Figure 5.10. The data indicate noise reduction, of the order of 1 dB, with the longer duct exhaust shroud nozzle at all thrust conditions.

PNLmax directivity and typical aft angle spectral comparison at takeoff thrust ( $V_{\text{mix}} = 1020$  fps) is provided in Figure 5.11. A noise benefit with increased mixing length is seen at noise peak angles and over most of the mid and high frequencies. Figure 5.11a shows that while extending the tailpipe has no effect on the location of peak perceived noise it does, however, significantly reduce the noise in the forward quadrant and up to 130 degrees. The One-Third Octave Spectrum at 120 degrees (Figure 5.11b), shows that the mid-to-high frequency *mixing* noise has been reduced by extending the tailpipe.

References 1-4 show increase in mixing efficiency and thrust coefficient, as  $L/D_h$  is increased ( $L$  and  $D_h$  being the mixing length & average hydraulic diameter). Significant improvements are shown up to an  $L/D_h$  of 1.84 in reference 2. The mixing length of the tested mixer nozzle increased from  $L/D$  of 0.72 (nominal shroud,  $L=5.5''$  &  $D=7.62''$ , the nozzle exit diameter) to 0.985 (extended shroud,  $L=7.5''$ ). Hence, an improvement in the net thrust is also to be expected with the extended mixer configuration.

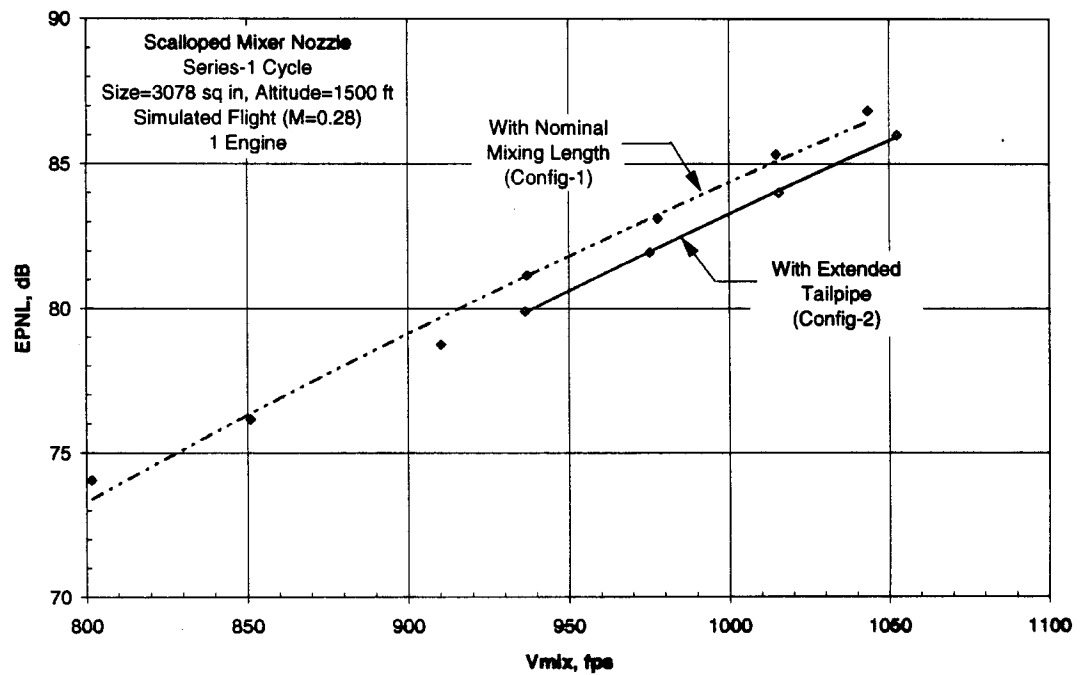
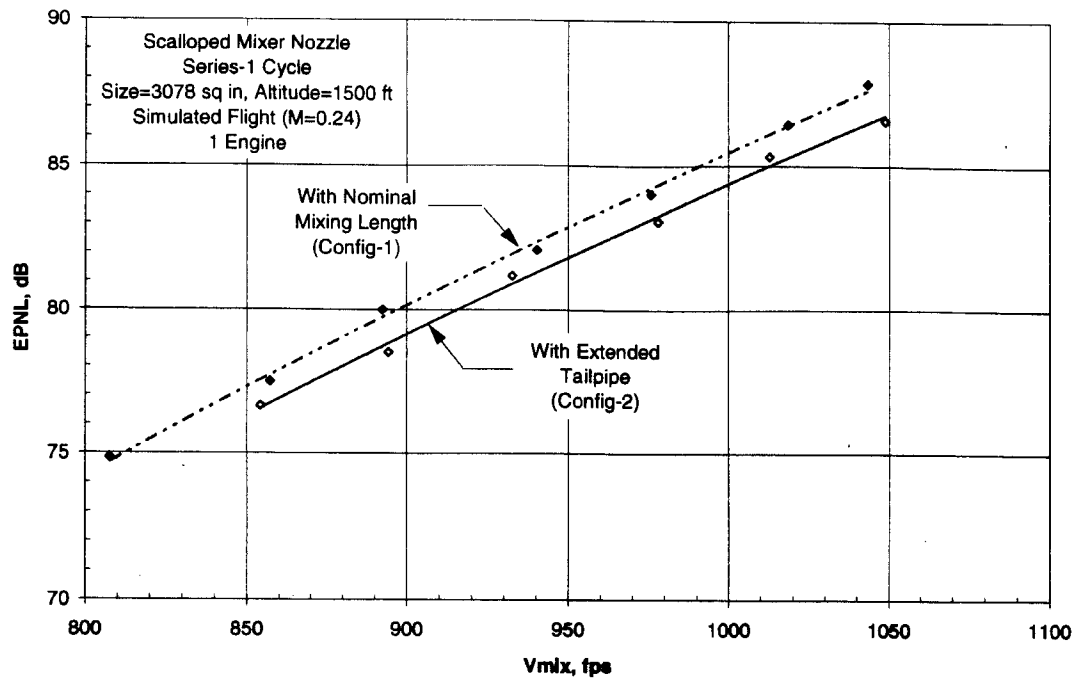


Figure 5.10. Effect of different mixing duct lengths on scalloped mixer acoustic data.

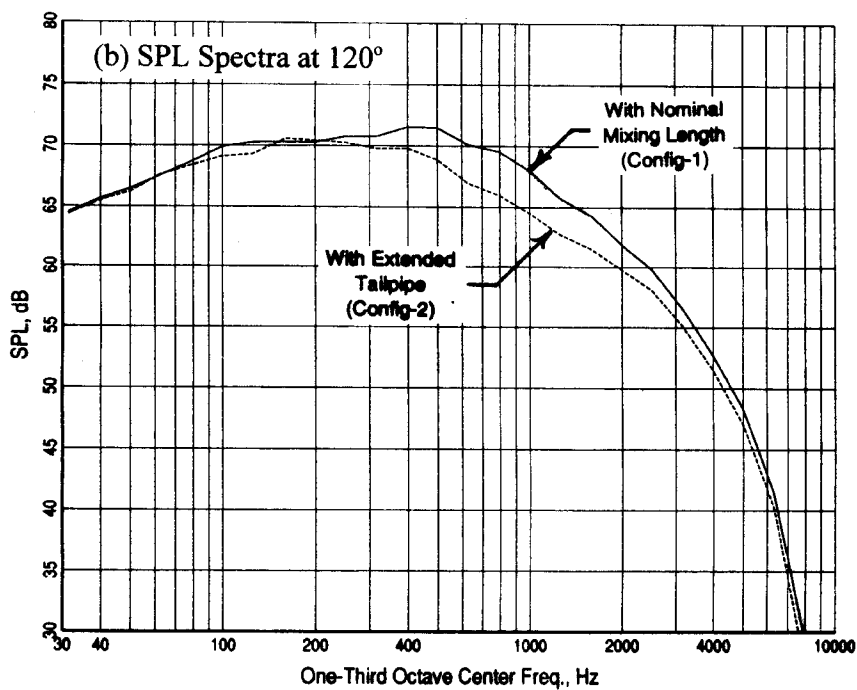
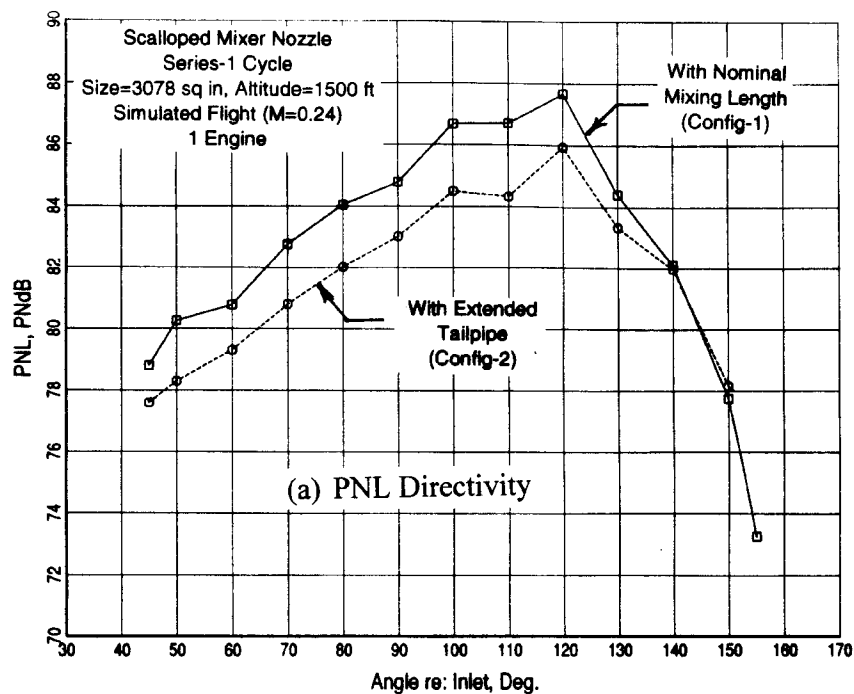


Figure 5.11. Effect of different mixing duct lengths on scalloped mixer PNL directivity and SPL spectra; nominal  $V_{\text{mix}}=1000$  fps, simulated flight M=0.24 (Test Point 6).



## 5.5 Effect of Variations from Engine Baseline Operating Cycle

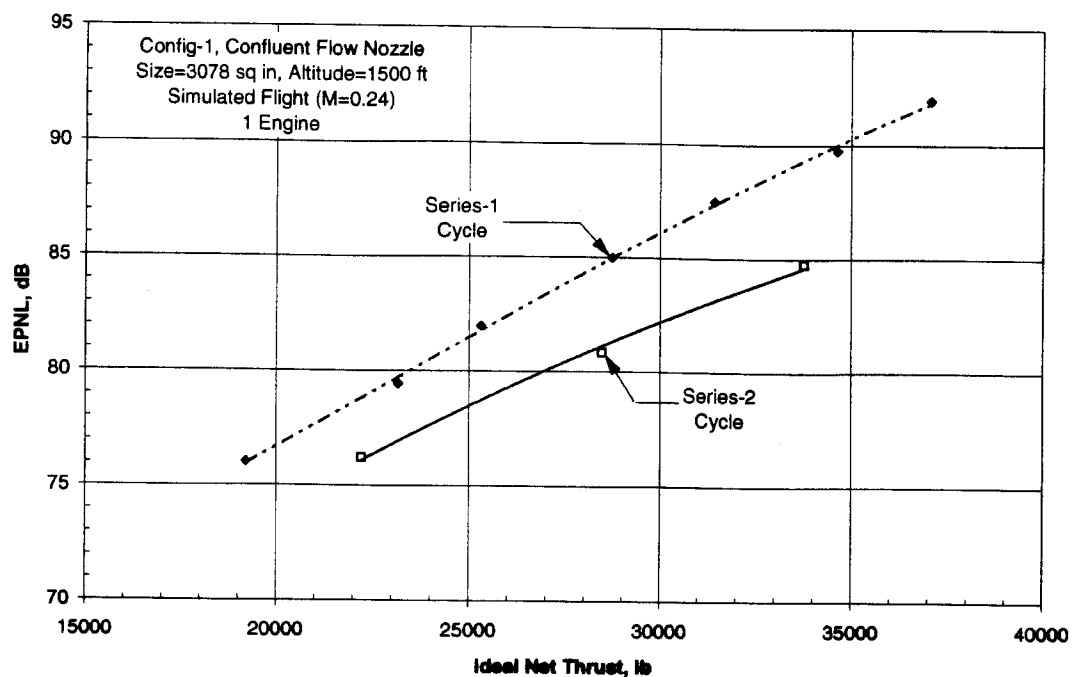
As shown in Figure 5.1, the scale model nozzle tests were conducted on two different cycle operating lines. Series-1 simulates ICLS engine cycle and is typical of engines with mixers or confluent nozzle. This baseline cycle is defined to provide an extraction ratio close to unity at the design point. Series-2 simulates typical separate flow engine cycle. This cycle provides a greater than one extraction ratio at the design point.

The impact of the operating cycle variations on the acoustics of confluent flow (config-1) and scalloped mixer (config-2) nozzles are shown in Figures 5.12 and 5.13. The EPNL data at simulated flight Mach number of  $M=0.24$  are plotted against ideal net thrust in Figure 5.12. The data indicate significant EPNL reduction with series-2 cycle relative to series-1 cycle. Reductions of 4.5 and 3 dB are noted with the confluent flow nozzle, and 4 and 2 dB with the scalloped mixer nozzle at the takeoff and cutback thrust conditions. This data is normalized with respect to 1000 lb thrust and plotted against  $V_{mix}$  in Figure 5.13.

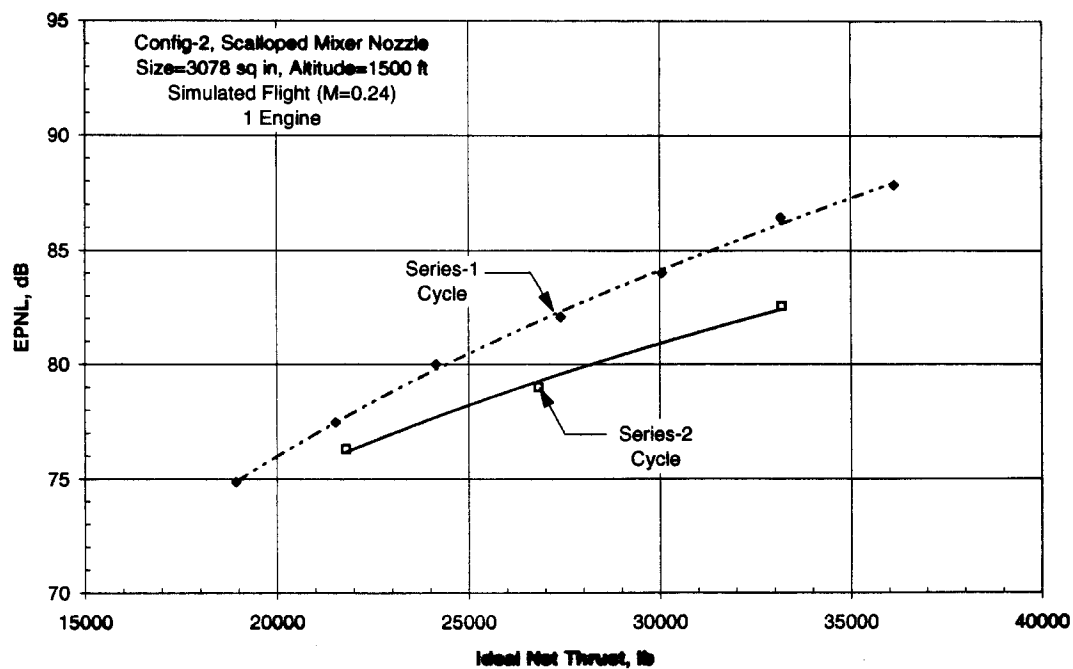
The following table summarizes the noise benefits noted in PNLmax for static cases and in EPNL for flight cases of the test nozzles with the series-2 cycle relative to series-1 cycle:

Config (Desig)	Nozzle	Cycle (Series)	Decrease in PNLmax/EPNL with Series-2 Cycle Rel. to Series-1 Engine Cycle, $\Delta$ dB			
			Static		Simulated Flight ( $M=0.24$ )	
			Takeoff	Cutback	Takeoff	Cutback
Config-1 (V1)	Confluent	Series-1 Series-2	Ref 5.0	Ref 2.0	Ref 4.5	Ref 3.0
Config-2 (V2)	Scalloped Mixer	Series-1 Series-2	Ref 3.0	Ref 2.2	Ref 4.0	Ref 2.0
Config-3 (F9B)	Scall/Stagg Mixer	Series-1 Series-2	Ref 2.8	Ref 1.8	Ref 3.4	Ref 2.2
Config-4 (F12A)	Skewed Mixer	Series-1 Series-2	Ref 4.7	Ref 4.1	Ref 3.0	Ref 2.5

PNL directivity and typical aft angle spectral data obtained with different operating lines are compared in Figures 5.14 through 5.16. They describe the confluent (config-1) and scalloped mixer (config-2) nozzles data at typical takeoff thrust. The data indicate significant jet noise reduction at all angles and over most of the frequencies with series-2 cycle condition relative to series-1 cycle condition. This is due to the reduction in both the core exhaust velocity and the mixed velocity  $V_{mix}$  for the series-2 condition relative to series-1 condition for a given thrust (see Figure 5.1). The cycle effects are significantly reduced when the acoustic data is normalized for constant thrust as shown in Figure 5.15 for confluent flow nozzle.

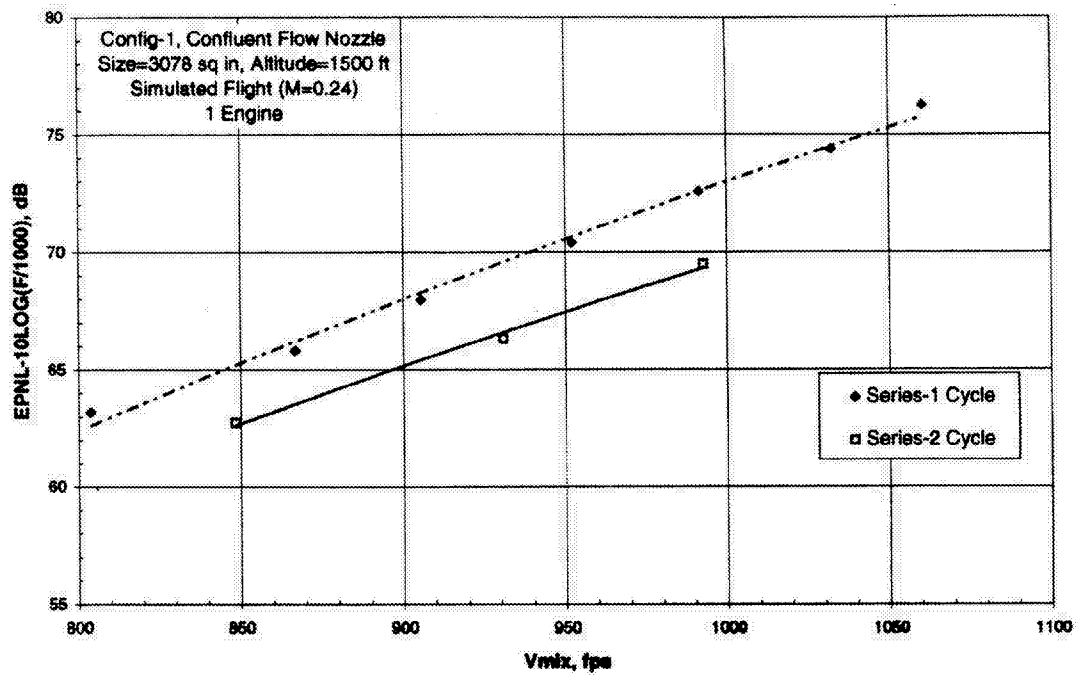


**a) Confluent Flow Nozzle (Config-1)**

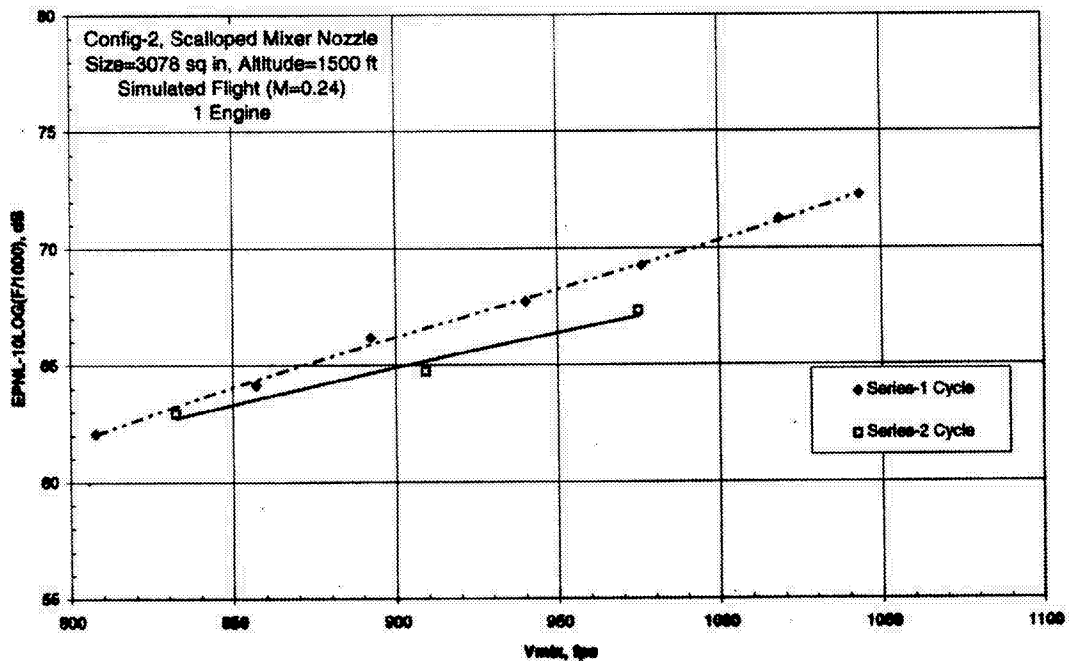


**b) Scalloped Mixer Nozzle (Config-2)**

Figure 5.12. Effect of operating cycle on confluent flow and scalloped mixer acoustic data with respect to ideal thrust.

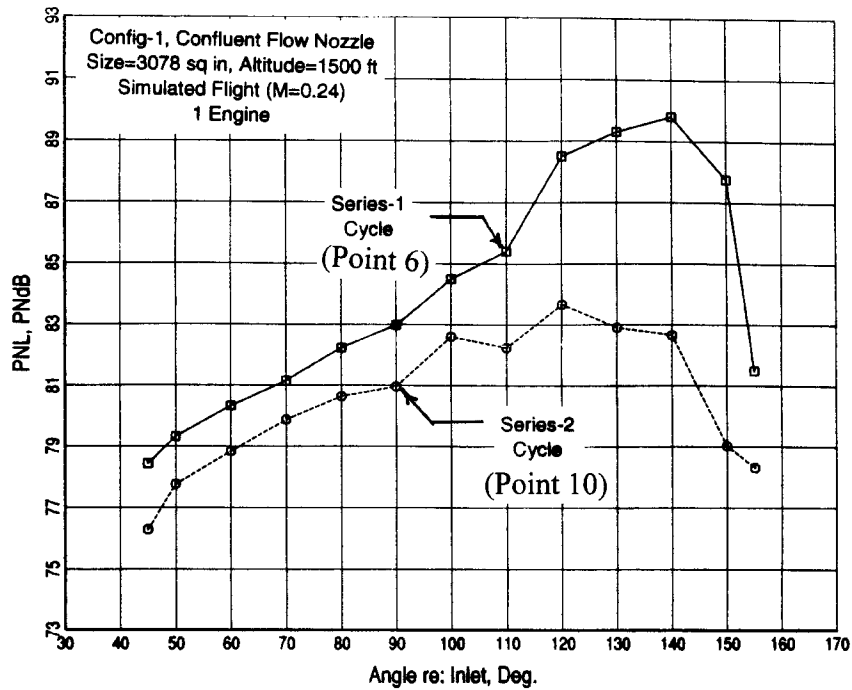


a) Confluent Flow Nozzle (Config-1)

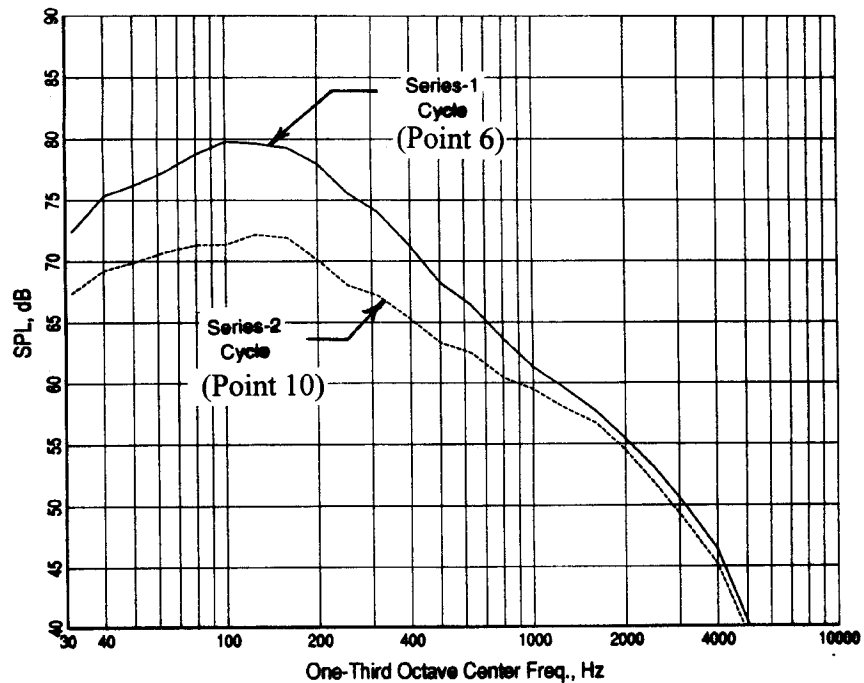


b) Scaloped Mixer Nozzle (Config-2)

Figure 5.13. Effect of operating cycle on confluent flow and scaloped mixer acoustic data with respect to mixed velocity.

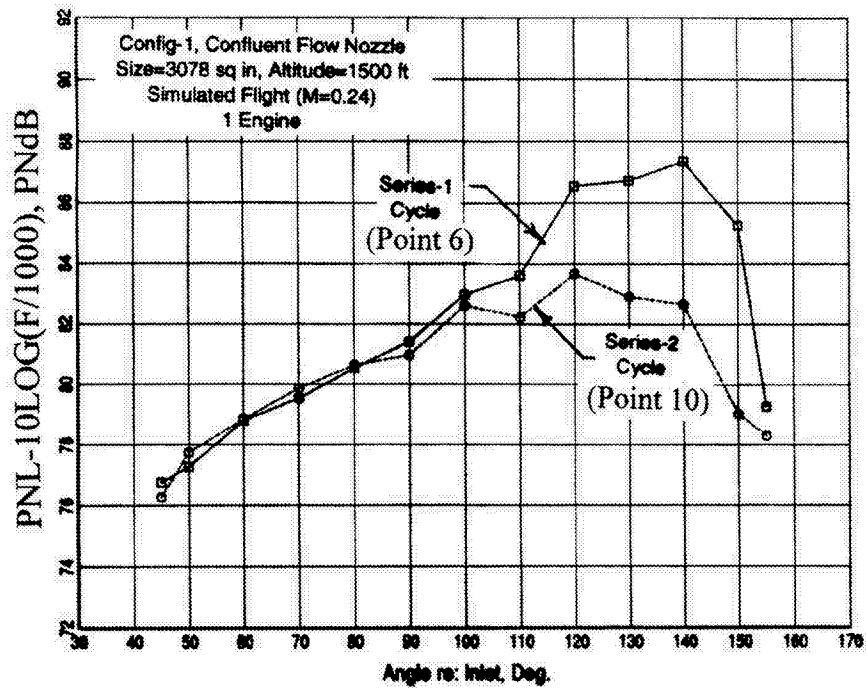


a) PNL-Directivity

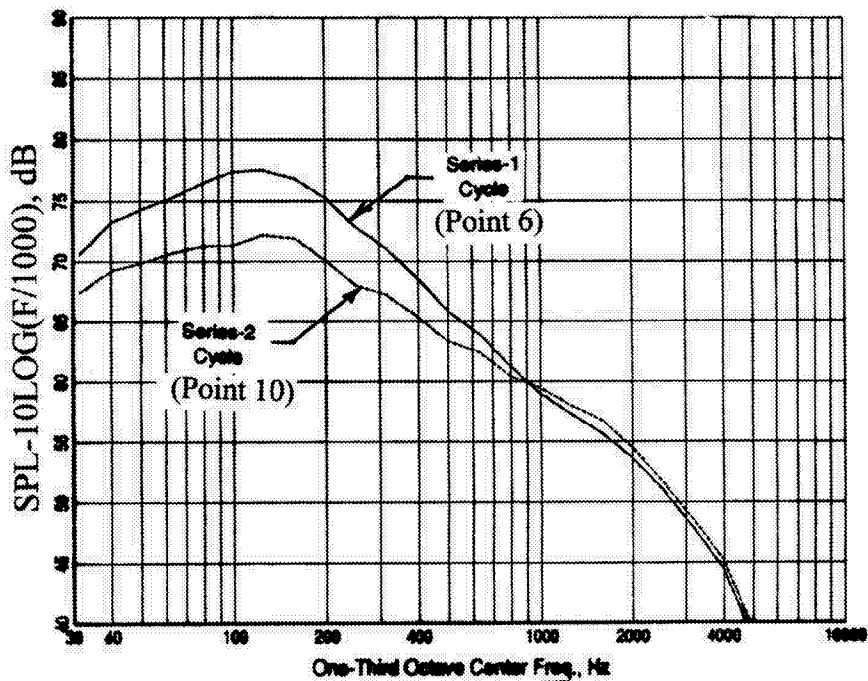


b) SPL-Spectra @ 130°

Figure 5.14. Effect of operating cycle on confluent flow nozzle PNL directivity and SPL spectra; nominal  $V_{mix}=1000$  fps, simulated flight M=0.24.



a) PNL-Directivity



b) SPL-Spectra @ 130°

Figure 5.15. Effect of operating cycle on confluent flow nozzle PNL directivity and SPL spectra on constant thrust basis; nominal  $V_{mix}=1000$  fps, simulated flight  $M=0.24$ .

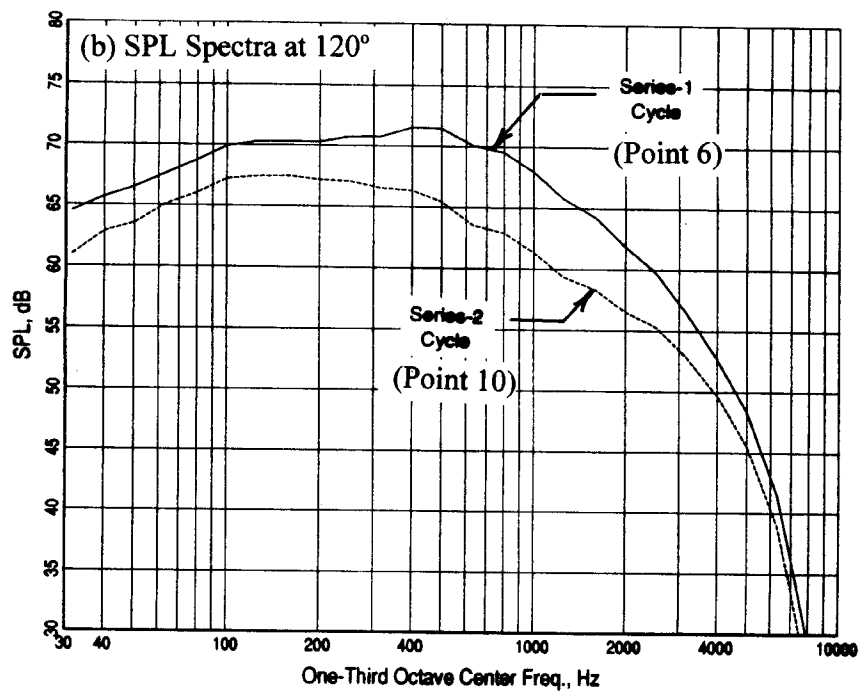
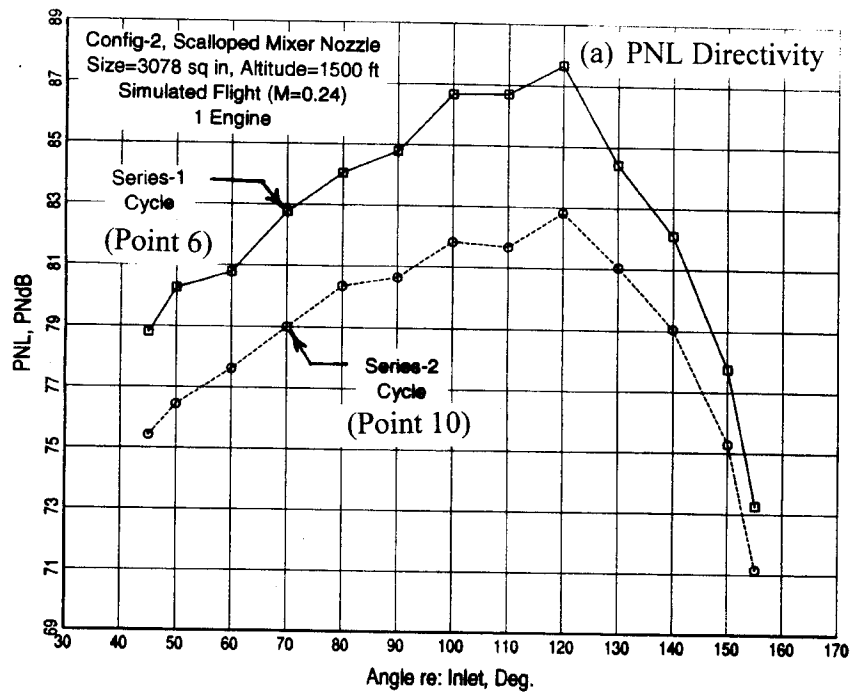


Figure 5.16. Effect of operating cycle on scalloped mixer PNL directivity and SPL spectra; nominal  $V_{mix}=1000$  fps, simulated flight  $M=0.24$ .

## 5.6 Effect of Flight Mach Number

As previously reported, acoustic measurements were performed at static conditions along with simulated flight conditions of Mach .24 and .28. The effect of flight Mach number on PNLT directivity and the one-third octave spectrum at a typical polar angle are shown for the *fully-mixed* Conic nozzle, the Confluent mixer, and the ICLS-V2 lobed mixer in Figures 5.17 through 5.19, respectively. Flight velocity yields significant source strength reduction for subsonic plumes at all frequencies at 90 degrees. Also, convective effects at other angles do significantly change the impact of forward flight velocity on source strength reduction.

## 5.7 Acoustic Conclusions

Acoustic tests were conducted to evaluate three lobe mixer designs that were developed during the Energy Efficient Engine (E<sup>3</sup>) program. Tests were also conducted on baseline confluent flow, an extended mixing region lobe mixer, and a conic nozzle configurations. Tests results were evaluated to determine effects of mixer designs relative to a confluent nozzle and a conical nozzle, variations from engine baseline operating cycle and mixing duct length. The acoustic tests were conducted at GEAE Cell-41 acoustic test facility. Analysis of the acoustic data provided the following conclusions:

- Under both static and simulated flight conditions and with reference to confluent nozzle, the scalloped/staggered mixer (config-3, F9B, 12 lobes, 48% penetration, 31.2° lobe spread angle) provided the lowest noise levels, and the skewed mixer (config-4, F12A, 12 lobes, 38% penetration, 35.6° lobe spread angle) the highest level. For a given  $V_{\text{mix}}$ , the differences were close to 3 dB under static conditions and 4 dB under simulated flight conditions. The scalloped mixer (config-2, V2/ICLS, 12 alternating different radial lobes, 43% penetration, 38.9° lobe spread angle) provided levels that were slightly noisier than those of the scalloped/staggered mixer.
- The skewed mixer was noisier than the confluent flow nozzle at low mixed velocity conditions and slightly quieter at higher velocities. The scalloped/staggered mixer provided the maximum noise benefit (3.6 EPNdB at  $V_{\text{mix}} = 1000$  fps) relative to the confluent flow nozzle. The conic nozzle provided the lowest measured noise levels for a given  $V_{\text{mix}}$ .
- Lower frequency jet noise benefit (< 400 Hz 1/3-OB) with mixer and conic nozzles were noted relative to confluent flow nozzle. The three mixer configurations provided, more or less, equal spectral benefits in this range ( $\cong$  6-8 dB in the aft quadrant microphone locations). The reduction in the noise levels in this frequency range is mainly due to decreased peak exhaust velocity achieved with mixer configurations.

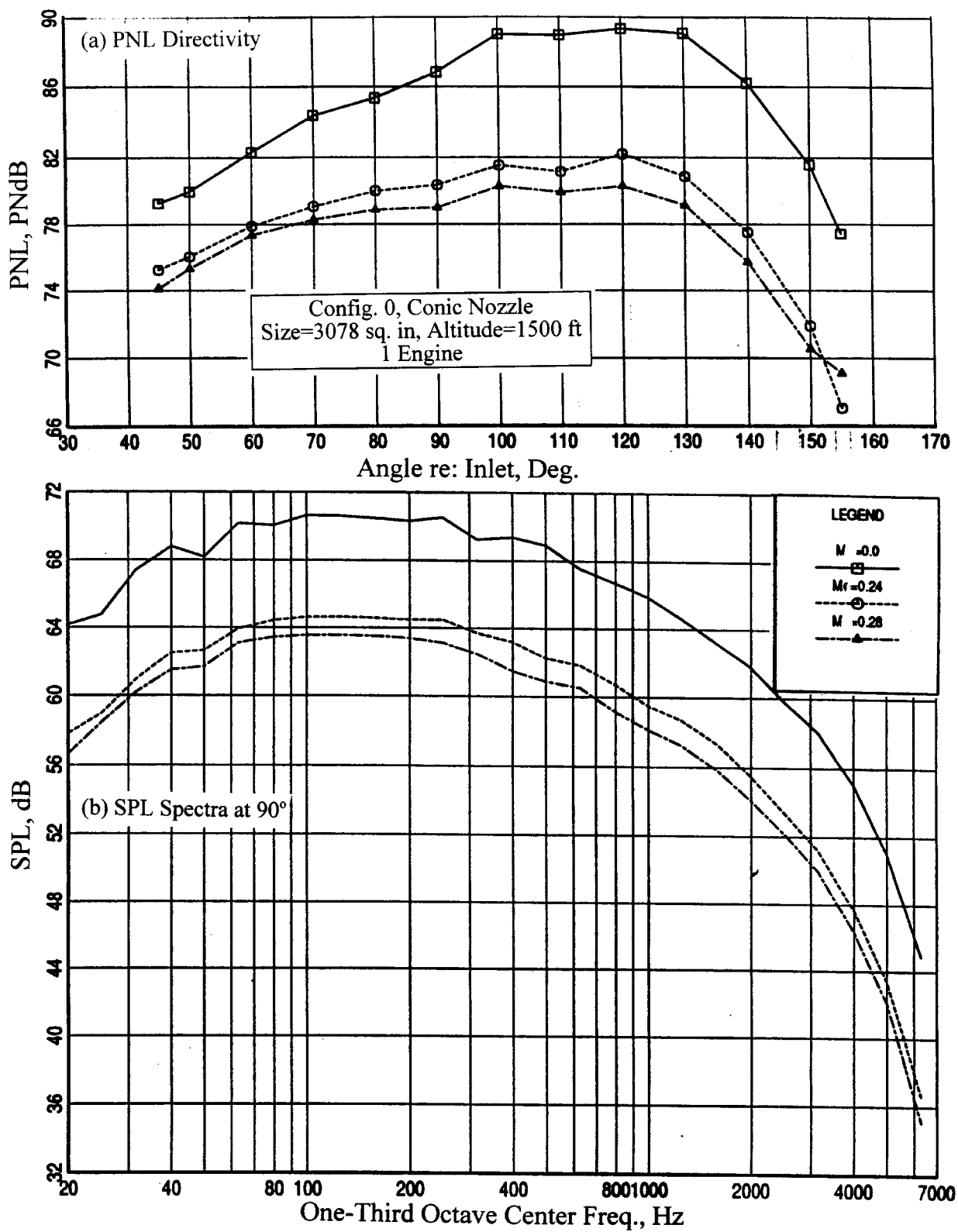
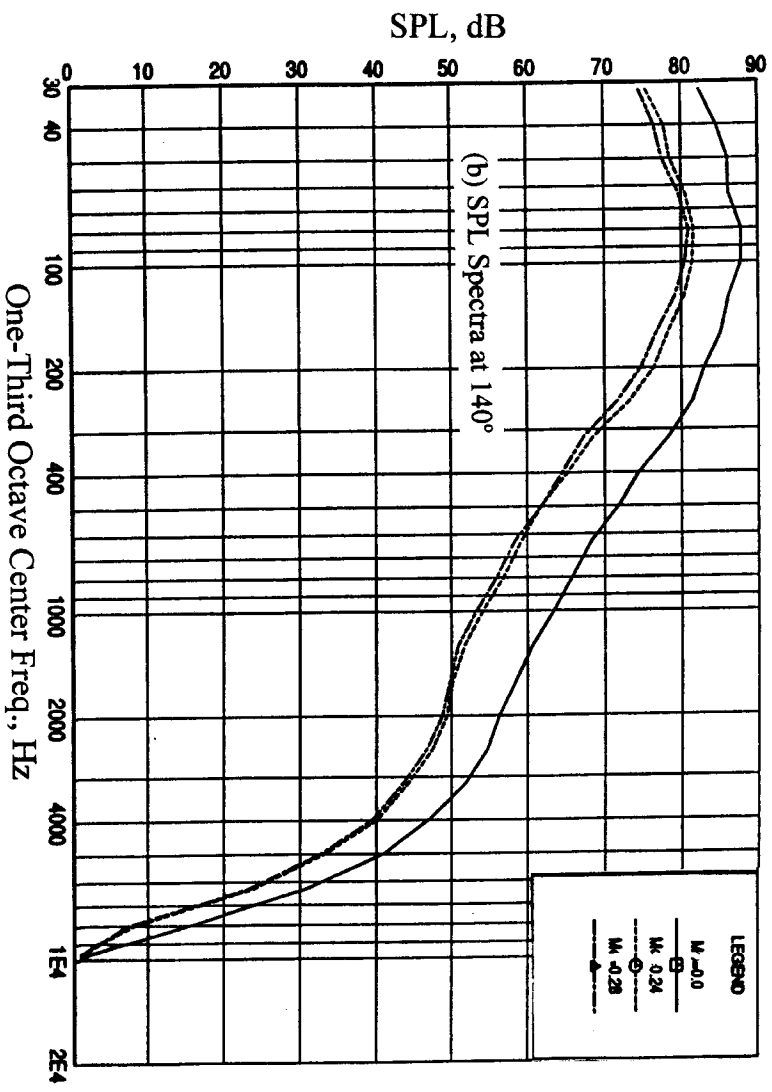
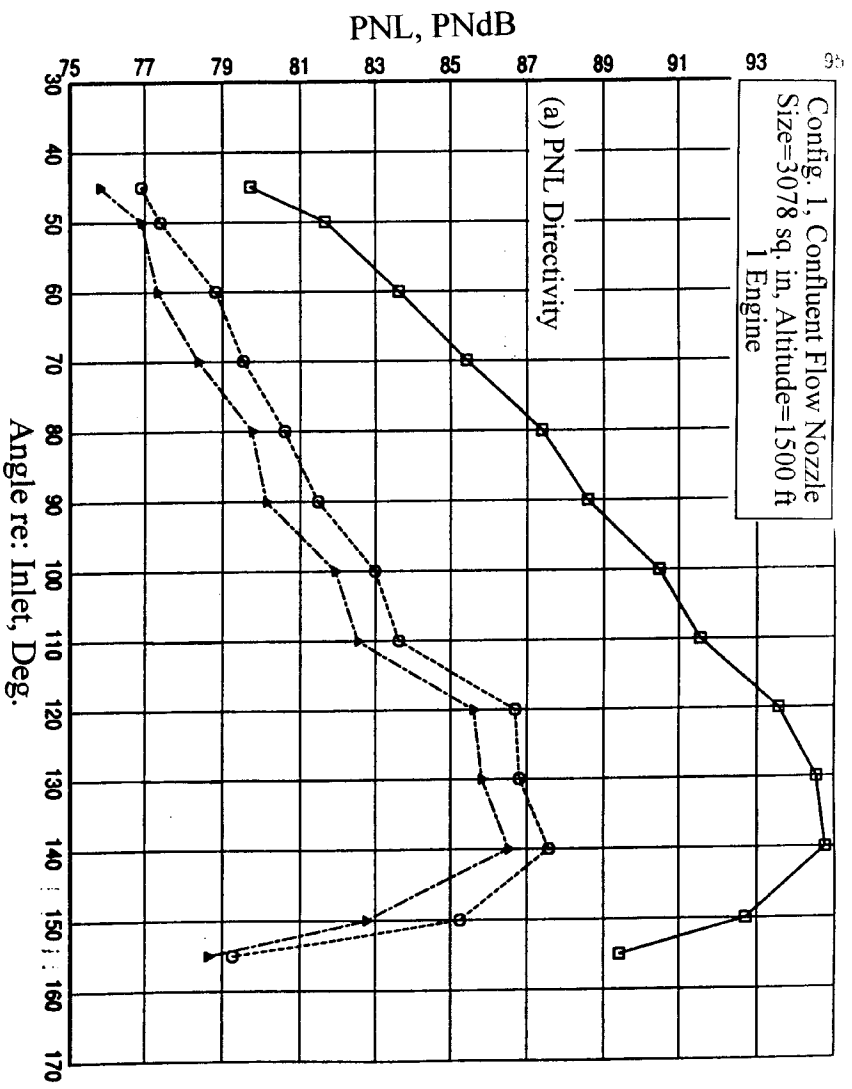


Figure 5.17. Effect of simulated flight on the conic nozzle PNL directivity and SPL spectra,  $V_{\text{mix}}=970$  fps (Test Point 5).





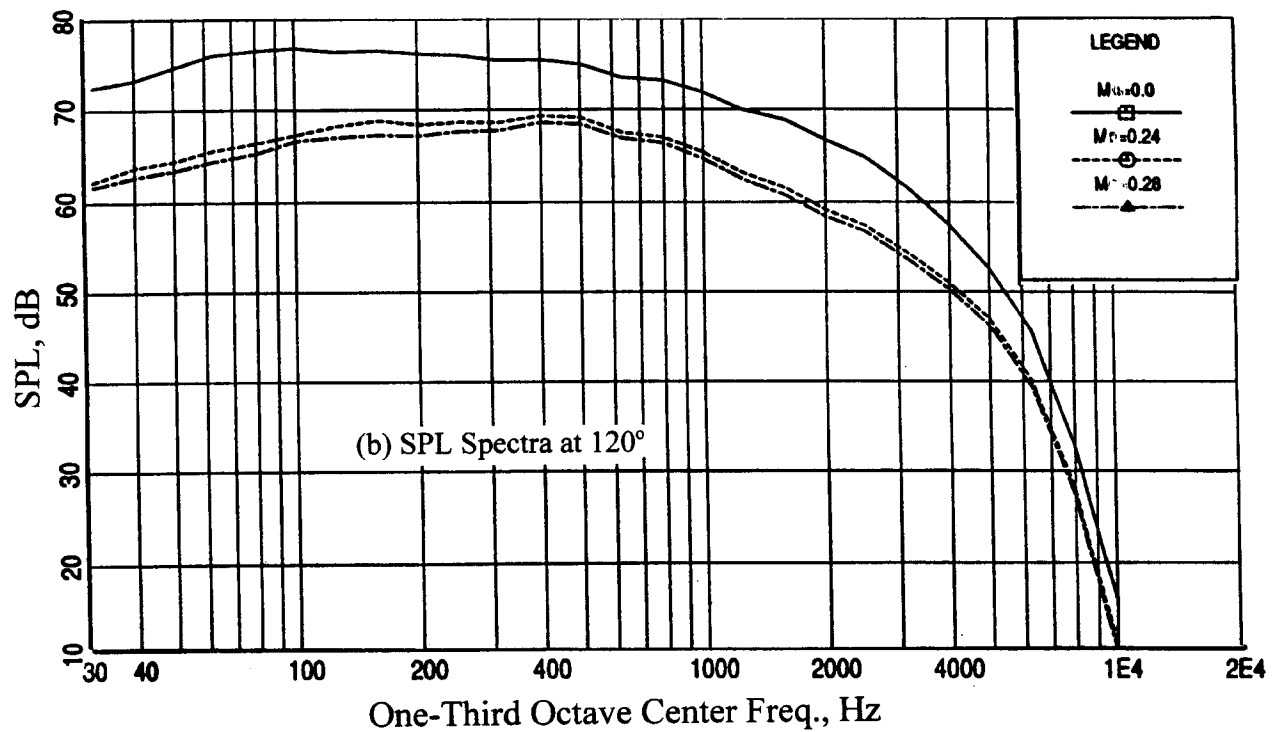
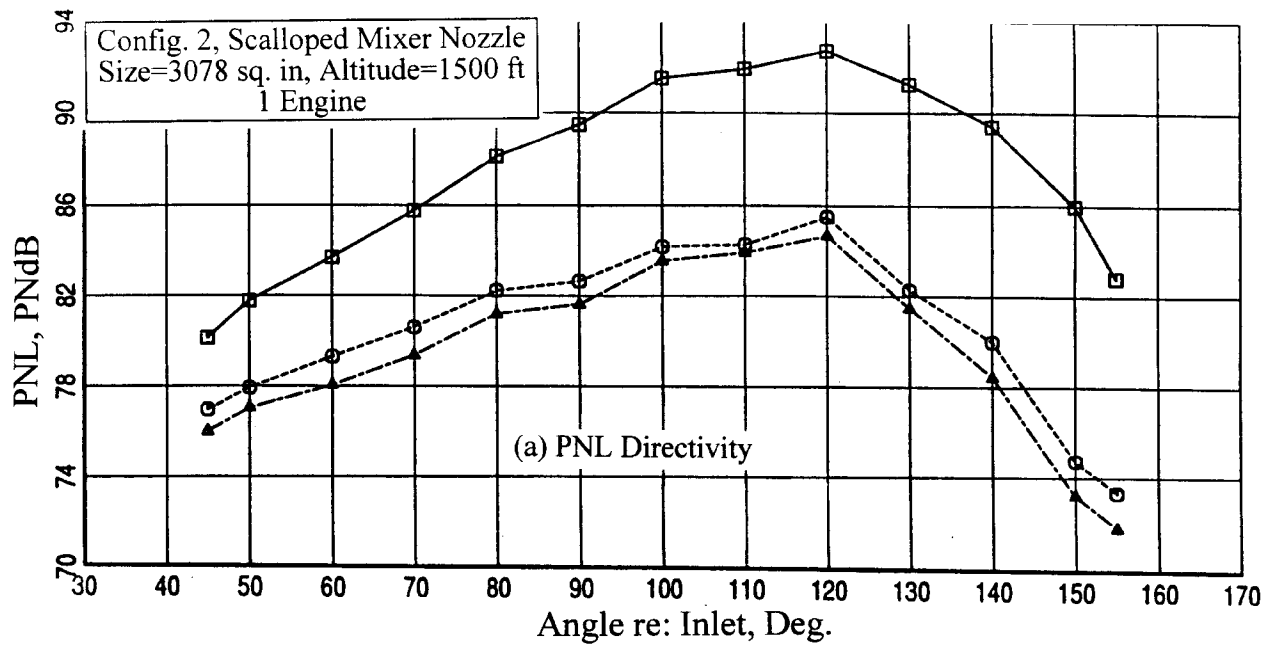


Figure 5.19. Effect of simulated flight on the scalloped mixer nozzle PNL directivity and SPL spectra,  $V_{mix}=975$  fps (Test Point 5).

- At most of the middle frequencies ( $500 \text{ Hz} < 1/3\text{-OB} < 4000 \text{ Hz}$ ) , mixer sound pressure levels were higher than those of the confluent flow nozzle. Skewed mixer noise levels were highest in this frequency range. Only the fully mixed conic nozzle spectra was lower than those of the confluent nozzle levels.
- At high frequencies ( $> 5000 \text{ Hz}$ ), the noise levels of the confluent and conic nozzles approached one another. The mixer levels also approached those of the confluent nozzle except those of skewed mixer. Skewed mixer data were generally greater than those of the other configurations.
- Increase in mixing duct length provided reduction in mid-to-high frequency mixing noise.
- Significant benefits at all aft angles and over most of the frequencies were noted with separate flow cycle conditions relative to typical mixer engine cycle.



## 6.0 AERO-FLOWFIELD DATA

The objective of the study was to provide detailed velocity, turbulence and thermodynamic state variable data for use in evaluating the acoustic characteristics of mixed flow exhaust systems, and for assessing the accuracy and assisting the further development of computational fluid dynamics (CFD) codes for aero-flowfield and acoustic predictions. Aero flow field measurements were performed with surface static pressure taps, along with a Laser Doppler Anemometer (LDA) system to measure velocity. Nozzle exit total pressure and temperature mapping was performed with a Kiel probe. This study presents the results of internal to and external of the nozzle aero-flowfield measurements.

Test conditions for the aero flow field measurements are summarized in the table below. For all mixer configurations, test point 5 was established for both LDA and nozzle exit total pressure and temperature measurements. In addition, nozzle exit total pressure and temperature measurements were made for mixer configuration V1 at test point 10 conditions and at test point 7 for all other mixer configurations.

Test Point	NPRfan	NPRcore	Ttfan (°R)	Ttcore (°R)
5	1.6	1.631	540	1454
7	1.7	1.776	540	1502
10	1.698	1.505	540	1327

### 6.1 Nozzle Exit Total Pressure and Total Temperature Survey.

Nozzle exit total pressure and temperature were obtained on four mixer configurations, V1-confluent, V2, V2A (ICLS), and F12A-skewed mixers. The nozzle exit measurements were conducted using a single Kiel-temperature probe mounted to a two-dimensional actuation system as illustrated in Figures 6.1 and 6.2. The approximate survey sampling region is illustrated in Figure 6.3. The sampling grid is comprised of 325 pressure and temperature measurements.

The pressure measurements have been normalized by the core charging station averaged total pressure ( $p_{\text{measured}} / p_{\text{tcore}}$ ). The temperature measurements have also been normalized, but in a different manner. Fan charging station average total temperature was subtracted from the measured temperatures and this was then normalized by the temperature difference between the core charging station average total temperature and the fan charging station average total temperature  $(T_{\text{Tmeasured}} - T_{\text{Tfan}}) / (T_{\text{Tcore}} - T_{\text{Tfan}})$ .

The non-dimensional temperature and total pressure contours for a confluent mixer, V1, at test condition 5 and 10 are shown in Figure 6.4. The rings in this plot (and also subsequent plots) correspond to the radii of the core plug (1.9"), the core nozzle exit lip (2.6"), at the mixing plane and the fan cowl lip (3.8") at the nozzle exit respectively.

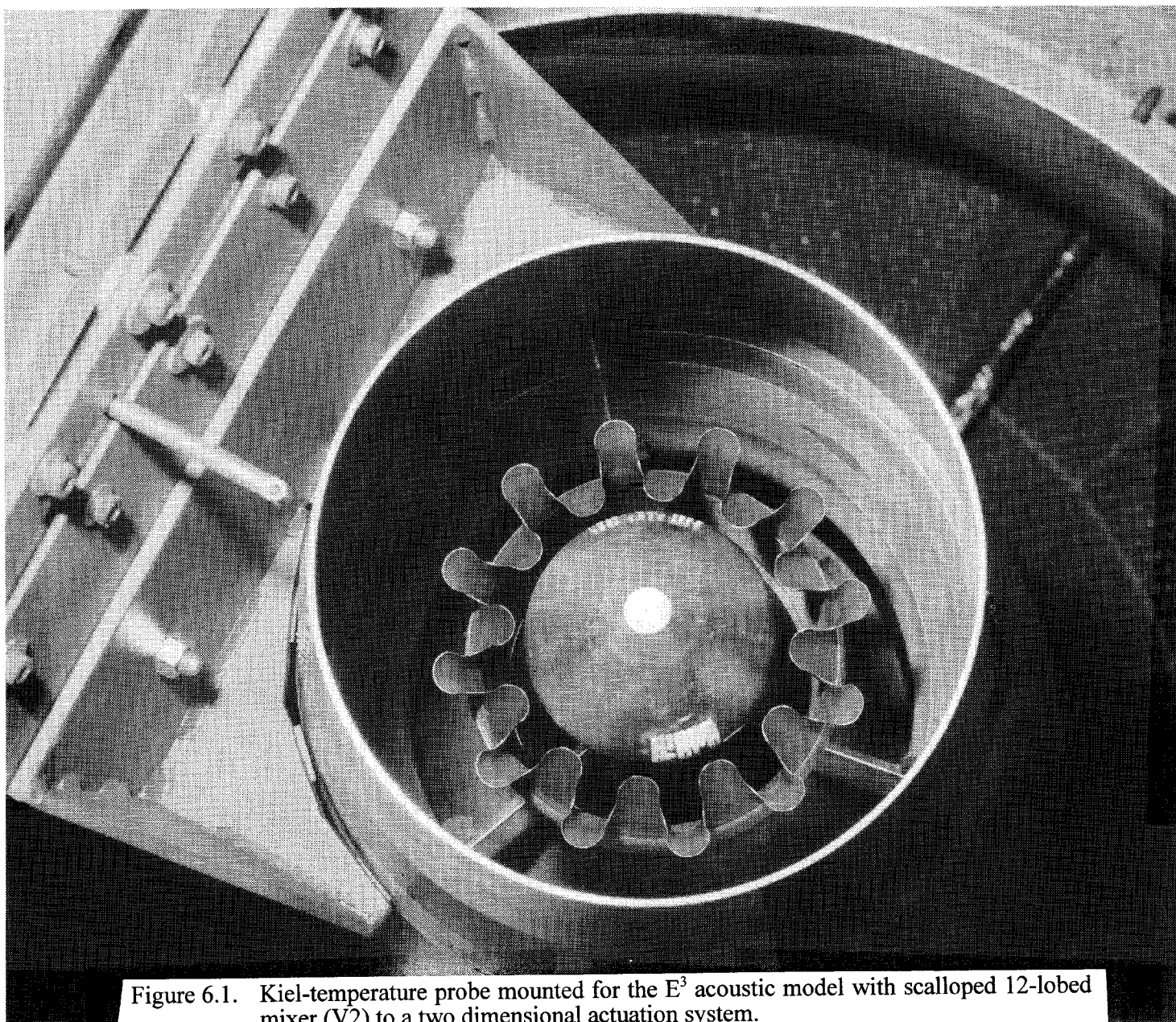


Figure 6.1. Kiel-temperature probe mounted for the E<sup>3</sup> acoustic model with scalloped 12-lobed mixer (V2) to a two dimensional actuation system.

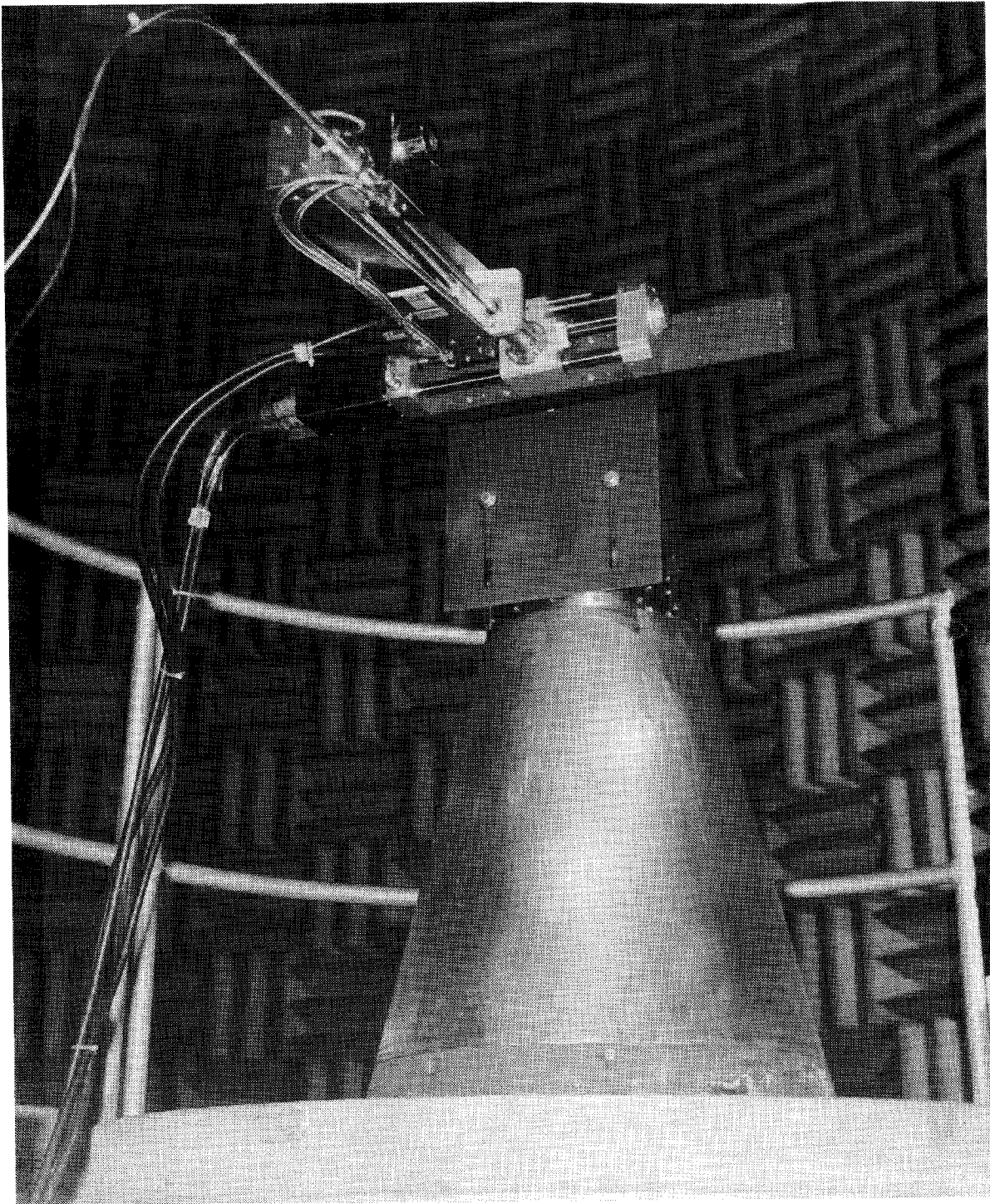


Figure 6.2. Kiel-temperature probe mounted for the  $E^3$  acoustic model to a two dimensional actuation system.

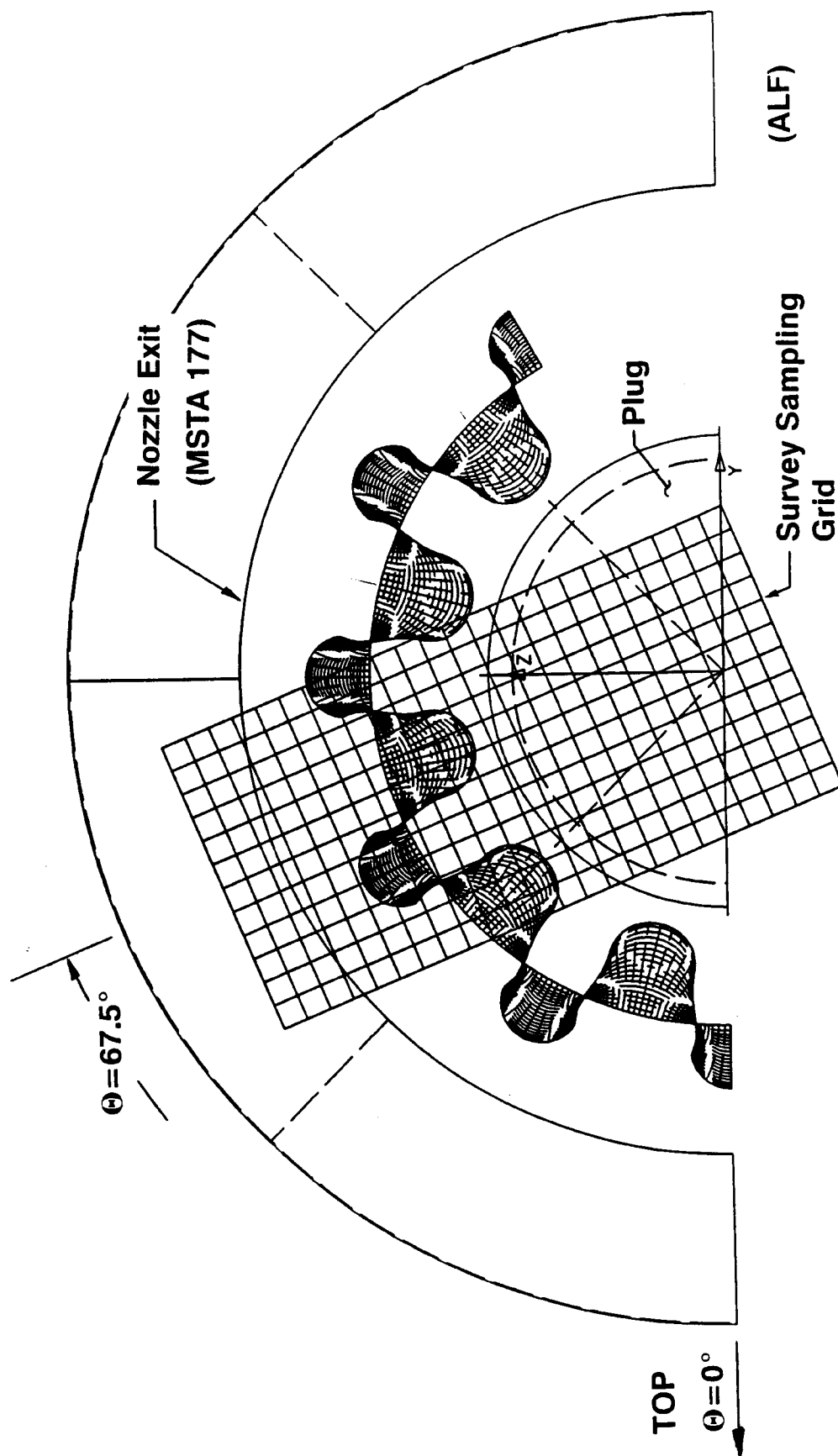


Figure 6.3. Survey sampling region for the Kiel-temperature probe.



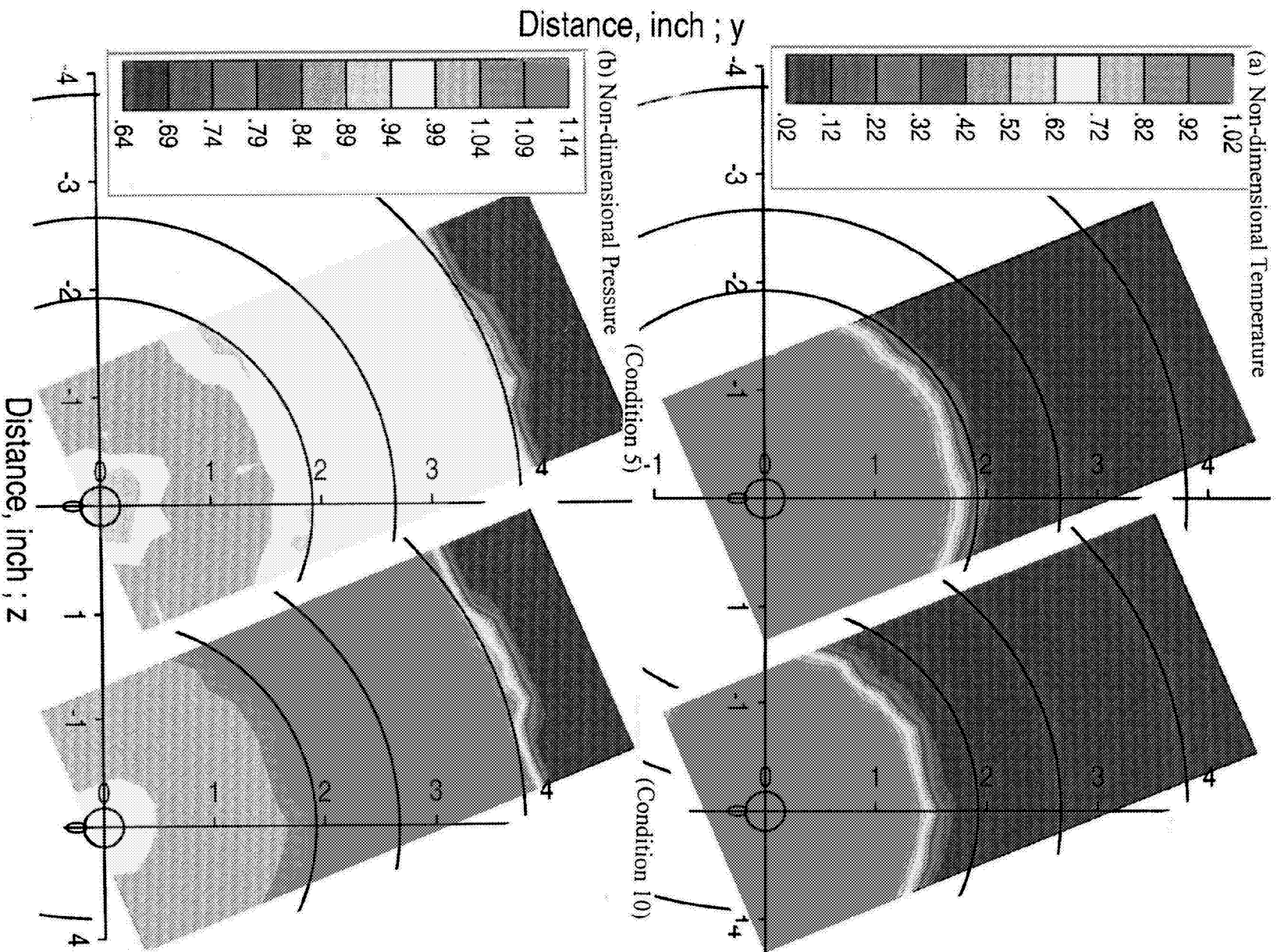


Figure 6.4. Non dimensional temperature and pressure profiles at the confluent mixer (VI) exit plane for a nominal  $V_{\text{mix}}=1000$  fps at two different cycle conditions, 5 and 10,  $M=0$ .

These temperature contours clearly illustrate the hot core jet, the thermal shear layer between the core and fan streams, and the cold fan flow. The core jet region is smaller for the condition 10 compared to condition 5 because the fan-to-core bypass ratio is higher (therefore, less relative core flow). For the V1 configuration, the nozzle exit survey sampling was intentionally performed behind one of the three exhaust upstream system support struts. The strut wake appears to be relatively small. Acoustic measurements also did not indicate discrete tones indicating of significant structure shedding or separation.

The non-dimensional temperature and total pressure contours for the two ICLS configurations, nominal-V2 and tailpipe extension-V2A, are shown in Figures 6.5 and 6.6, respectively. The temperature profiles for these configurations display a temperature inversion with the hot core flow projected radially outward and the cold fan flow radially inward. There is a low total pressure region exhibited downstream of the center plug. The tailpipe extension ICLS, V2A, shows diffused temperature and pressure profiles both in the radial and circumferential direction because of the additional mixing length (see Figure 6.6).

Similar results for the skewed F12A mixer are shown in Figure 6.7. The temperature profile does not display the temperature inversion characteristics of the ICLS configurations. Rather, the temperature profile is hotter at the centerline and decreases radially outward. Mixing levels based on past hot-to-cold thrust performance measurements suggest that the Skewed-F12A mixer with this type of temperature profile, offers very high mixing relative to the more conventional lobe mixers but at a very high pressure loss penalty. The pressure contours for the Skewed-F12A mixer show large regions of lower total pressure substantiating the higher pressure loss relative to the ICLS mixer configurations.

The standard deviation of temperature normalized by average temperature within the sampling domain was applied to the nozzle exit plane data. This value can be used as a mixedness parameter for relative comparison between mixers. This measure of mixedness is given by  $M_{sd}$ , and in this case the best mixed state is given by  $M_{sd} = 0$ . Figure 6.8 shows the mixedness parameter for the mixers at two different conditions. For the lobe mixers, the temperature distributions appear very similar between the two test conditions, (5 and 7). Condition 7 however shows slightly better mixing than condition 5. Among the mixers examined in this section V2A seems to show slightly better mixing.

## 6.2 Velocity Measurements

Two-dimensional, four-beam, two-color, LDA measurements of axial mean velocity ( $u$ ), horizontal mean velocity ( $v$ ) which is perpendicular to axial velocity and parallel to horizontal centerline, and the axial and horizontal component of turbulence velocities ( $u'$ ,  $v'$ ) were performed on five engine exhaust configurations. Table 2.1 summarizes the test configurations. The measured axial and tangential velocities are presented in units of feet/second. Figures 3.5 and 6.9 illustrate the LDA measurement set-up. A sketch of the

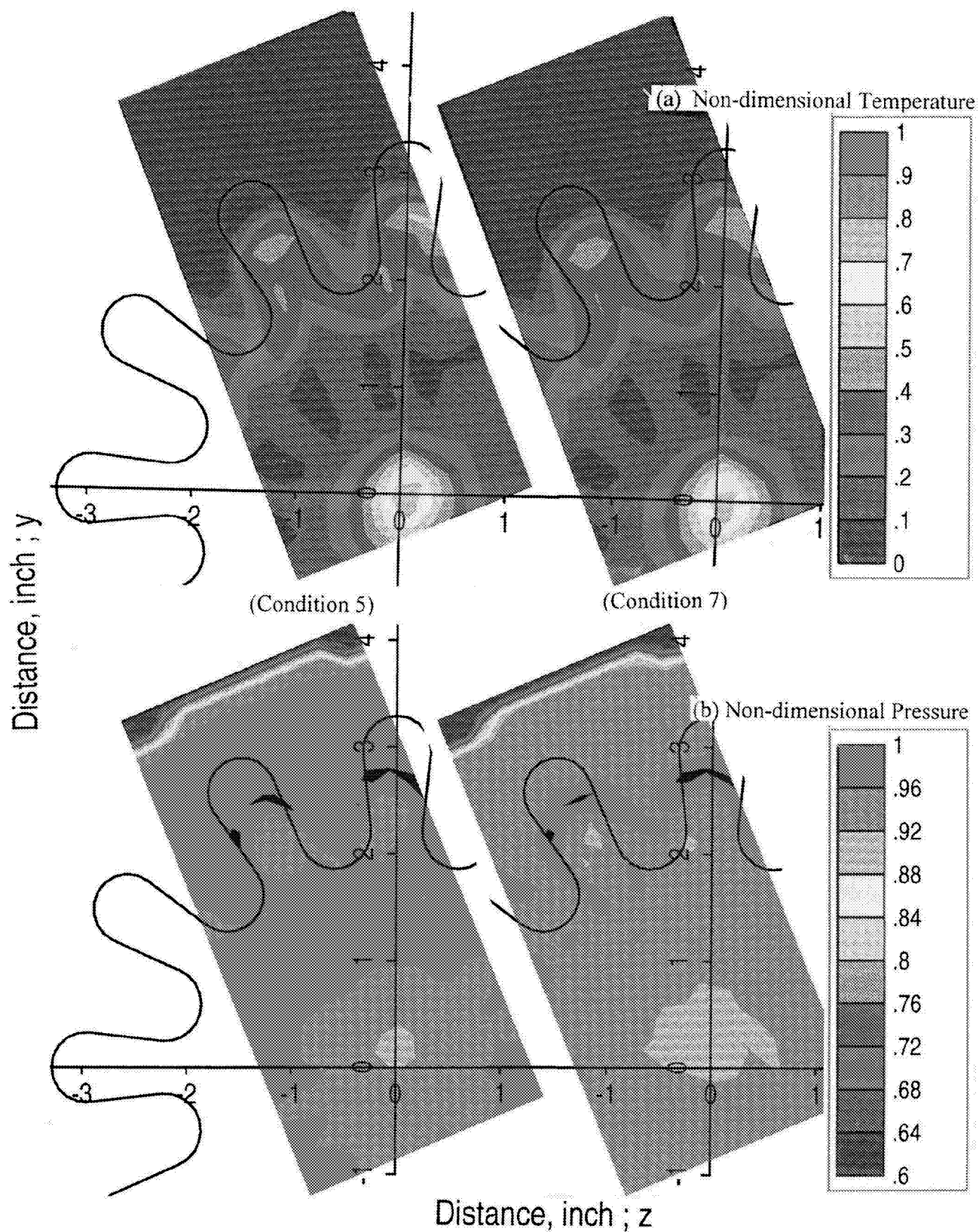


Figure 6.5. Non dimensional temperature and pressure profiles at the 12-lobed scalloped mixer (V2) exit plane at two different cycle conditions, 5 ( $V_{\text{mix}}=1000$  fps) and 7 ( $V_{\text{mix}}=1041$  fps),  $M=0$ .

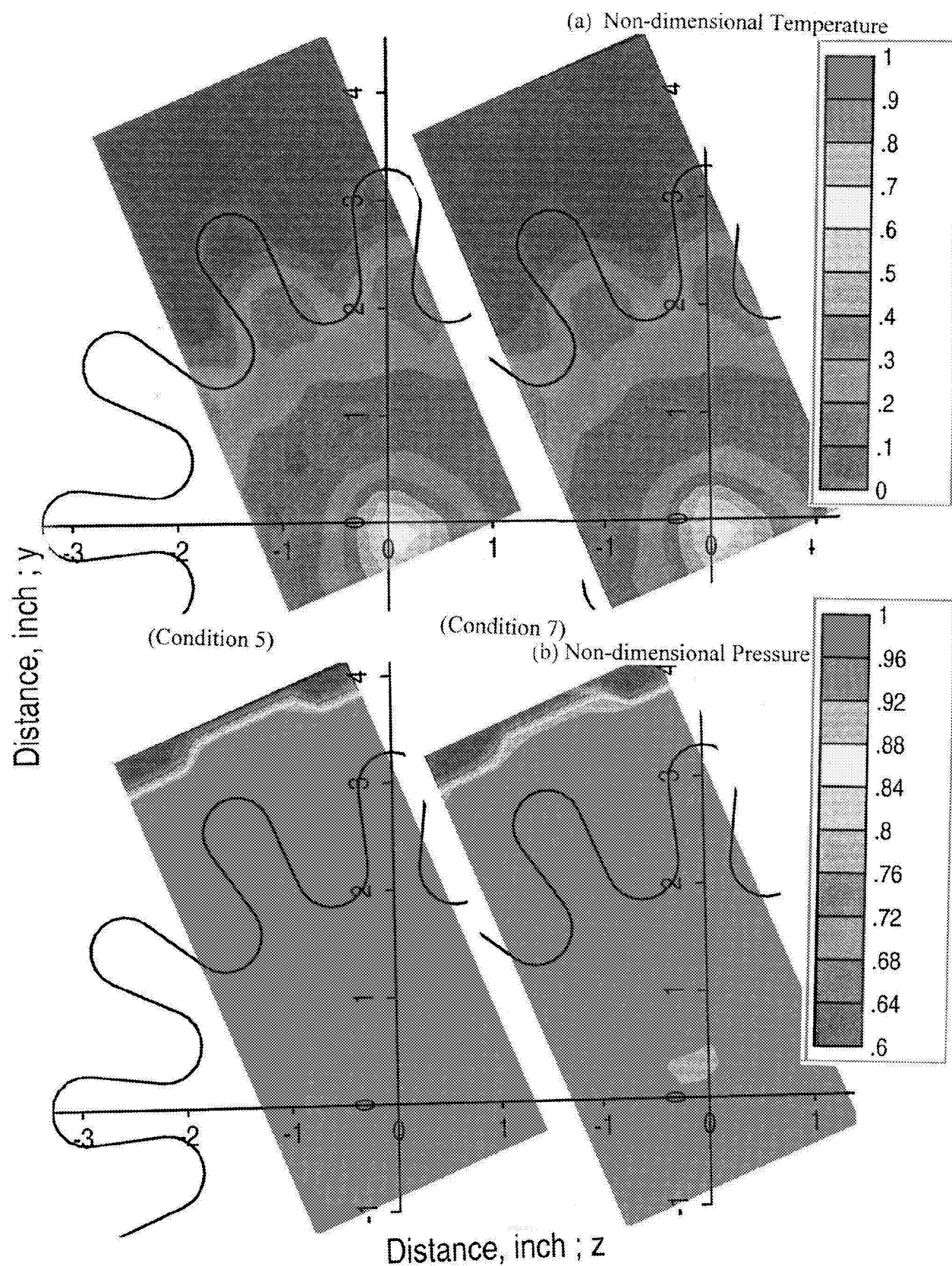


Figure 6.6. Non dimensional temperature and pressure profiles at the exit plane for the 12-lobed scalloped mixer with 2" extension (V2A) at two different cycle conditions, 5 ( $V_{mix}=1000$  fps) and 7 ( $V_{mix}=1041$  fps),  $M=0$ .

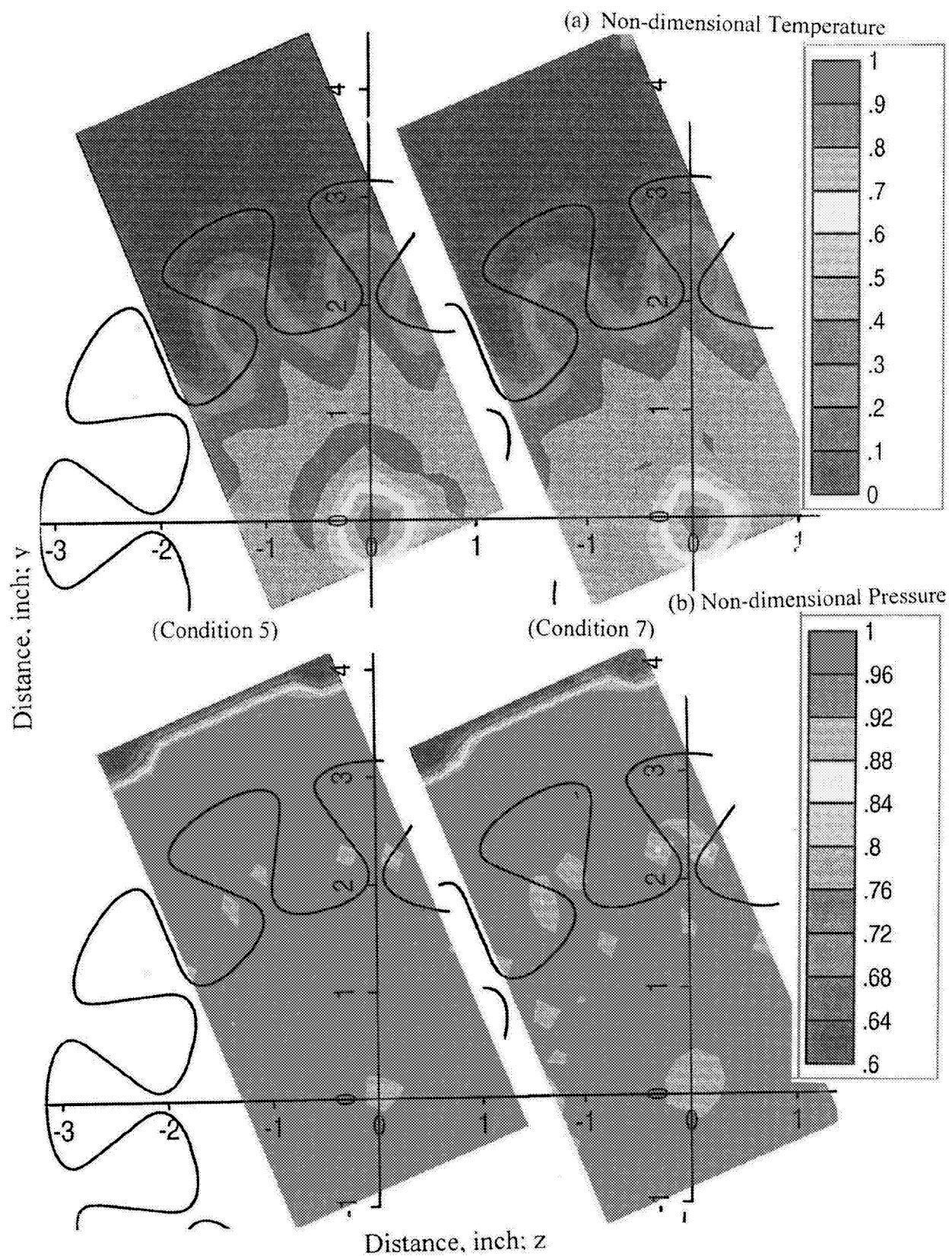


Figure 6.7. Non dimensional temperature and pressure profiles at the 12-lobed skewed mixer (F12A) exit plane at two different cycle conditions, 5 ( $V_{\text{mix}}=1000$  fps) and 7 ( $V_{\text{mix}}=1041$  fps),  $M=0$ .

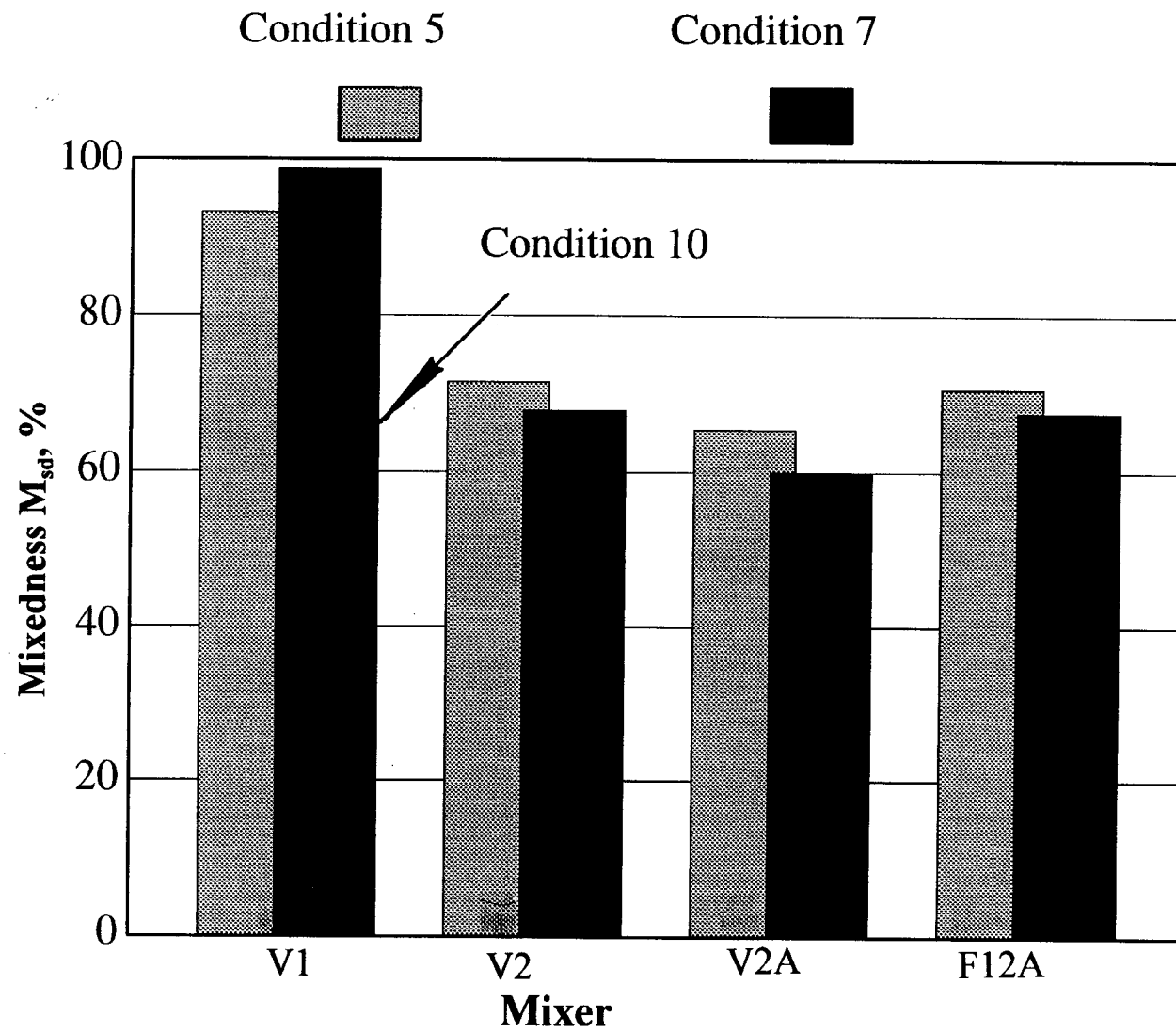


Figure 6.8. Temperature mixedness ( $M_{sd}$ ) comparison between mixers.



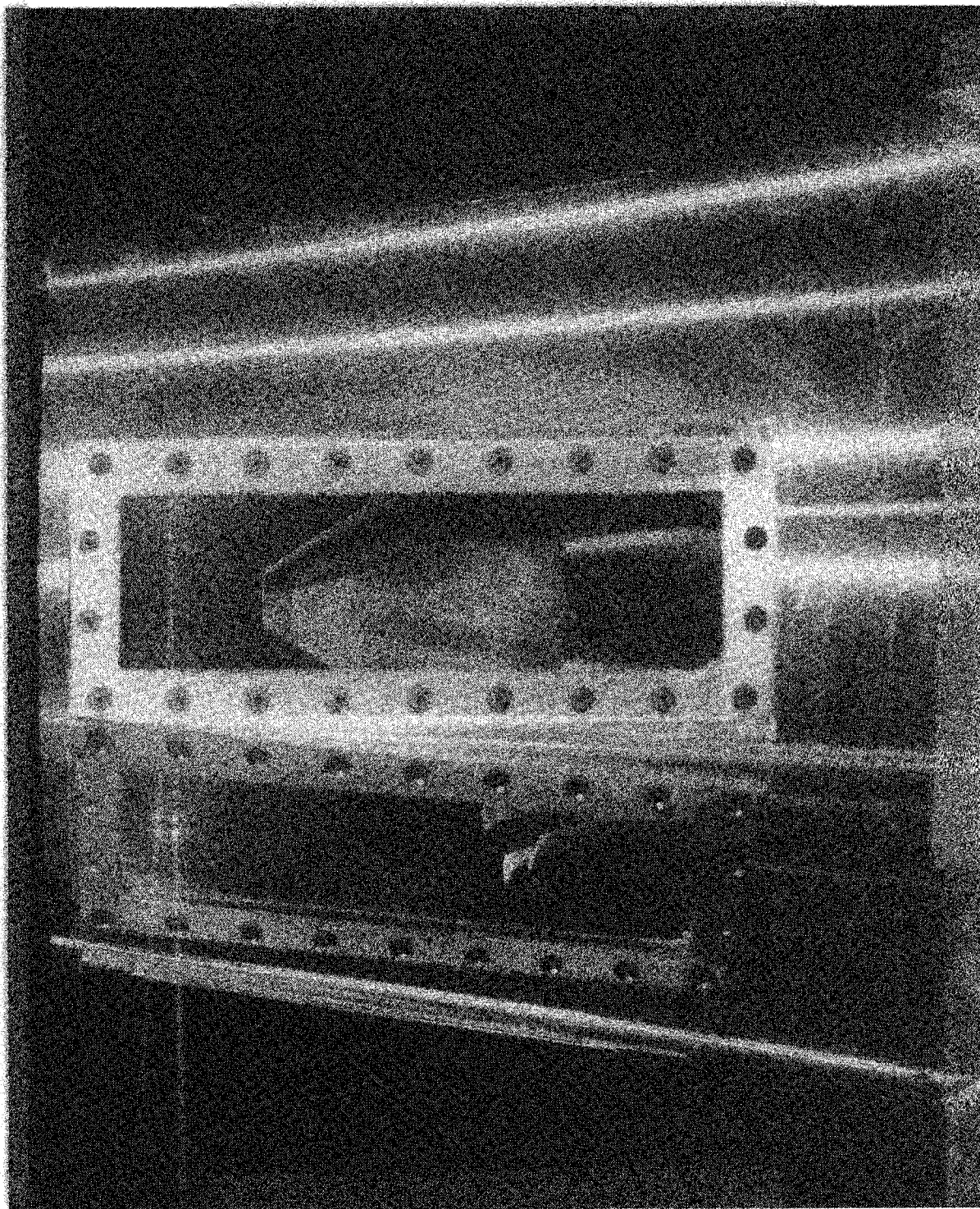


Figure 6.9. LDA window in the exhaust nozzle.

nozzle external and nozzle internal measurement location grids used in surveying the velocity profiles for the mixer/nozzles is shown in Figure 6.10.

### **6.2.1 Velocity Measurements of V1 (Confluent Mixer)**

The confluent mixed flow exhaust system is essentially an internal mixer with an axisymmetric core nozzle. It allows internal, ducted mixing of the fan and core streams upstream of the fan nozzle exit plane; but the mixing is not *forced* by directed penetration of one stream into the other.

#### ***External Velocity Measurements of V1 (Confluent Mixer)***

The axial and transverse velocity color contour plots at 0.5 inch down stream of the nozzle exit are shown in Figure 6.11. Two distinct levels of velocity are shown corresponding to the cool fan stream and hot core stream. The y-component velocity contour plot indicates a swirl flow near the nozzle lip. Figure 6.12 illustrates data comparison between on-line data and histogram data obtained at 0.5 inch downstream of the nozzle exit and along the center line. It shows very good agreement between the two methods of measuring velocity. The nozzle exit velocity distribution, as also shown in Figure 6.12, demonstrates the effect of a center body on the velocity distribution.

Histogram data were obtained at five downstream positions (0.5", 0.5D, 1.5D, 3D, and 5D) from the nozzle exit. The histogram data at 0.5 inches is shown in Figure 6.13. The open square symbol represents axial velocity and the open circle symbol represents horizontal velocity. Turbulence intensities were plotted as closed symbols. Turbulence intensity increased through the mixing layer then leveled off in the fan flow stream. Higher turbulence intensities were obtained from the free stream mixing layer at the nozzle lip because of a zero free stream velocity. The RMS values are shown in this figure for actual disturbance indication (turbulence intensity was normalized by local velocity). Figure 6.14 to 6.17 show the velocity distribution and turbulence intensity at four different locations downstream of the nozzle exit (.5Diam, 1.5D, 3D, & 5D downstream of the nozzle exit). The velocity distribution plots shown in Figure 6.18 illustrate the gradual mixing process downstream of the nozzle exit.

#### ***Internal Velocity Measurements of V1 (Confluent Mixer)***

The velocity distributions were measured at seven different positions within the nozzle ranging from the confluent mixer exit to the nozzle exit. Figure 6.19 shows the velocity, turbulence intensity, and rms velocity distributions at one inch upstream from the nozzle exit for the V1 mixer configuration. The center body effect on the velocity distribution is clearly indicated in this figure. The velocity defect due to the center body, however, is recovered quickly as observed in the external plume (ref. Figure 6.12). The core and fan turbulence intensities are about 4% and 9% respectively. However, the absolute level of turbulence intensity are nearly the same for the core and fan streams.



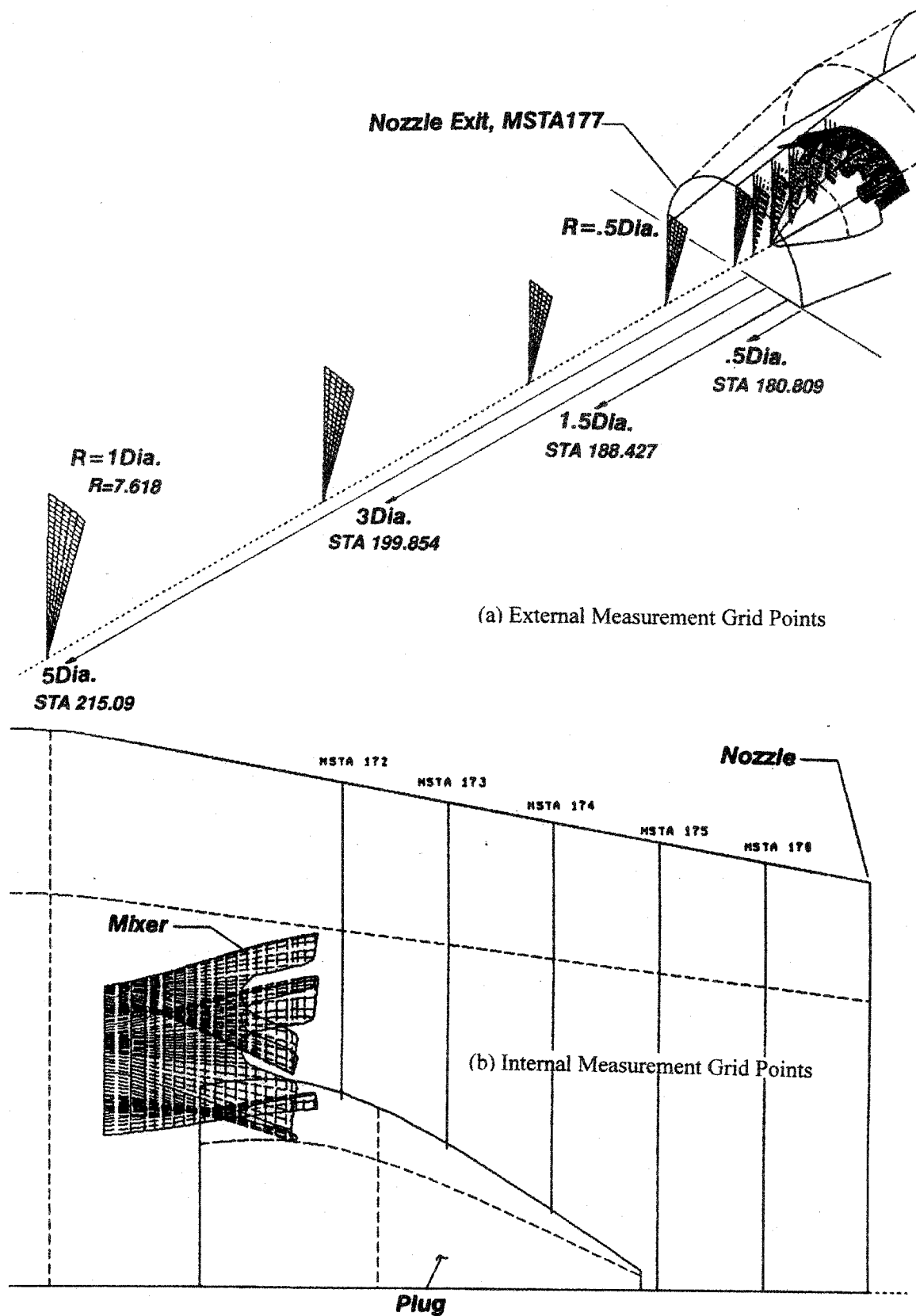
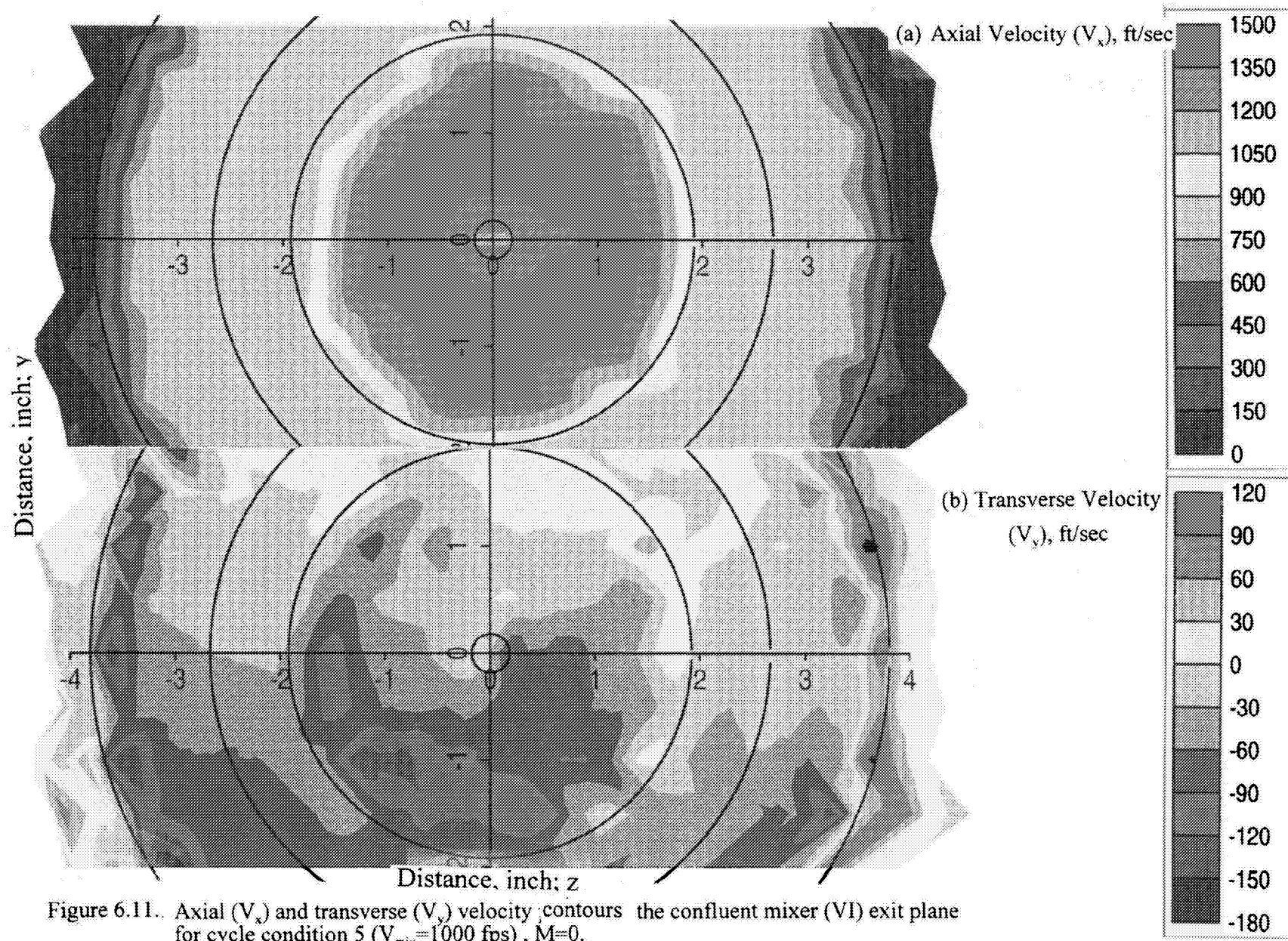


Figure 6.10. External and internal LDA survey data grid point matrix.



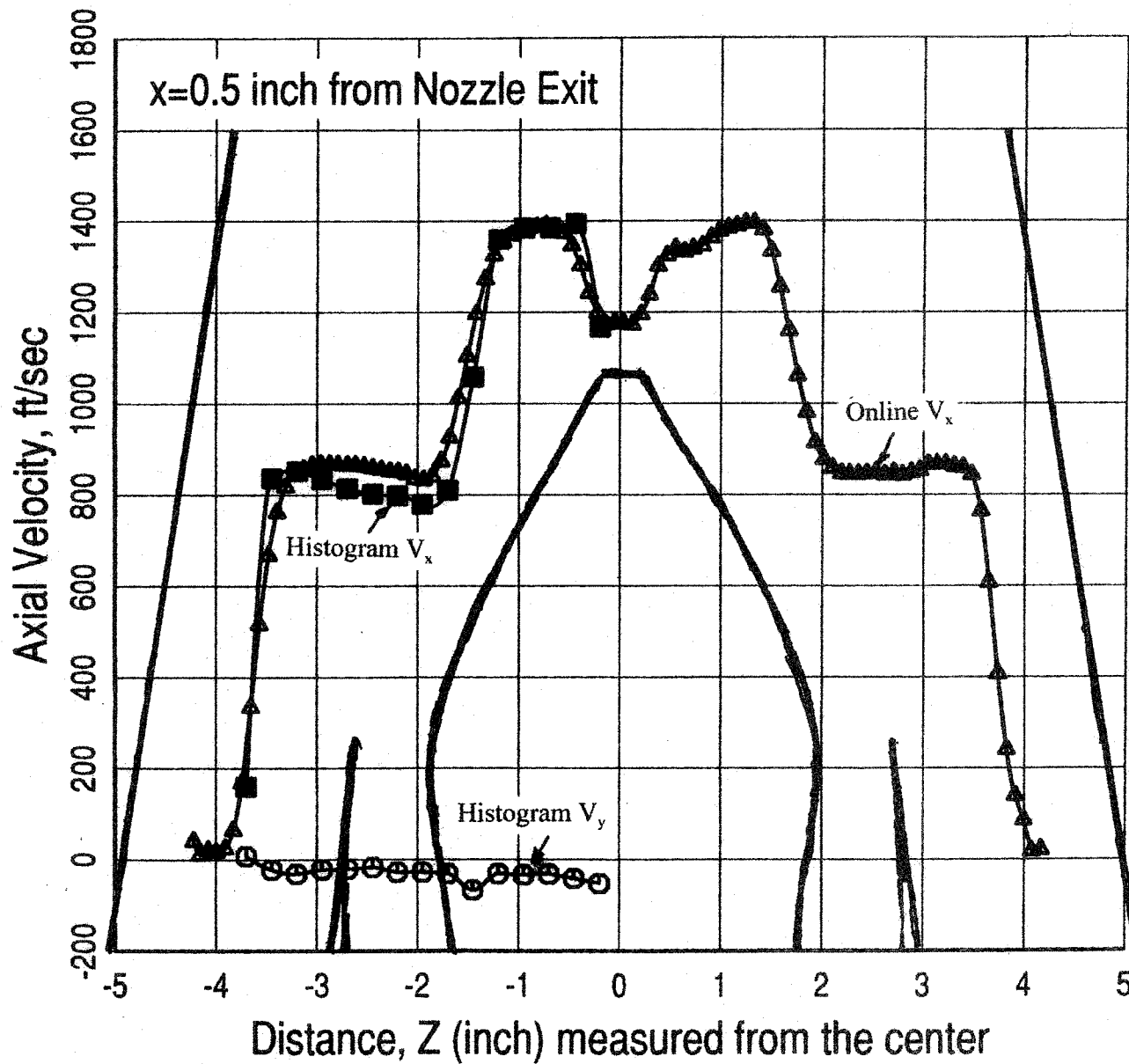


Figure 6.12. Axial velocity comparison between online and histogram data for confluent (V1) mixer at  $x=0.5$ " for condition 5,  $M=0$ .

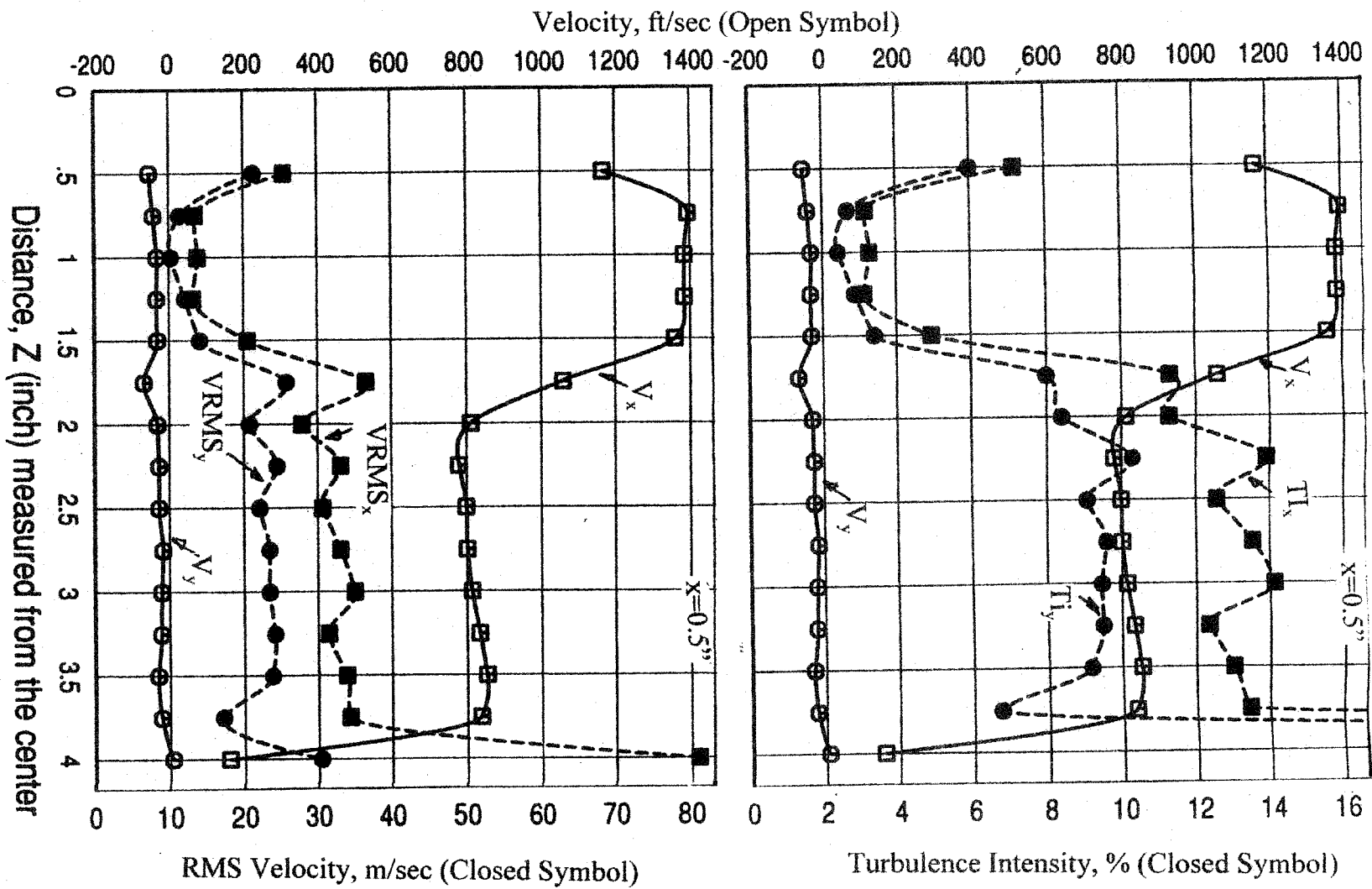


Figure 6.13. Velocity, turbulence intensity, and rms velocity distributions at  $x=0.5''$  for confluent mixer ( $V1$ ) for condition 5,  $M=0$ .

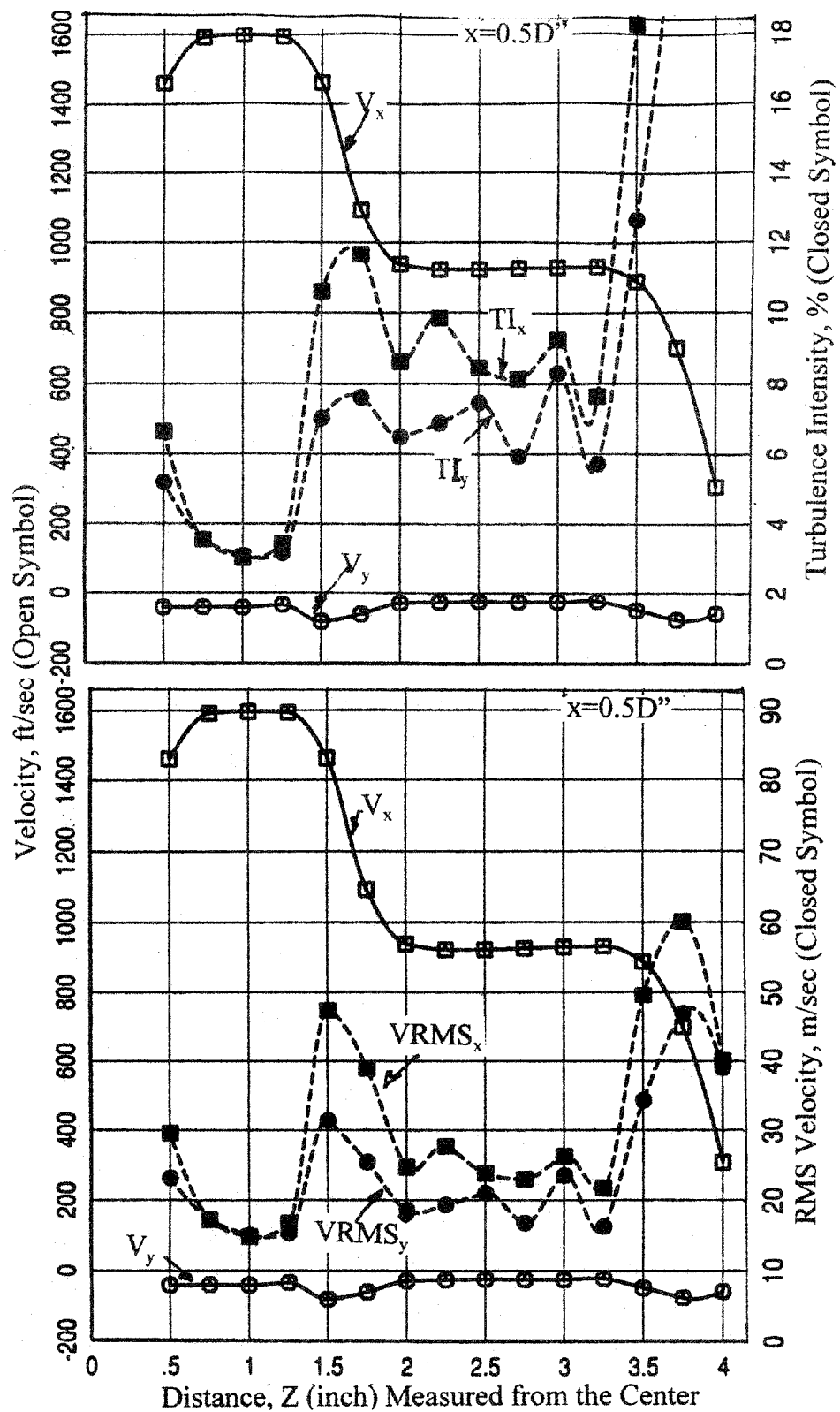


Figure 6.14. Velocity, turbulence intensity, and rms velocity distributions at  $x=0.5D''$  for confluent mixer (V1) for condition 5,  $M=0$ .

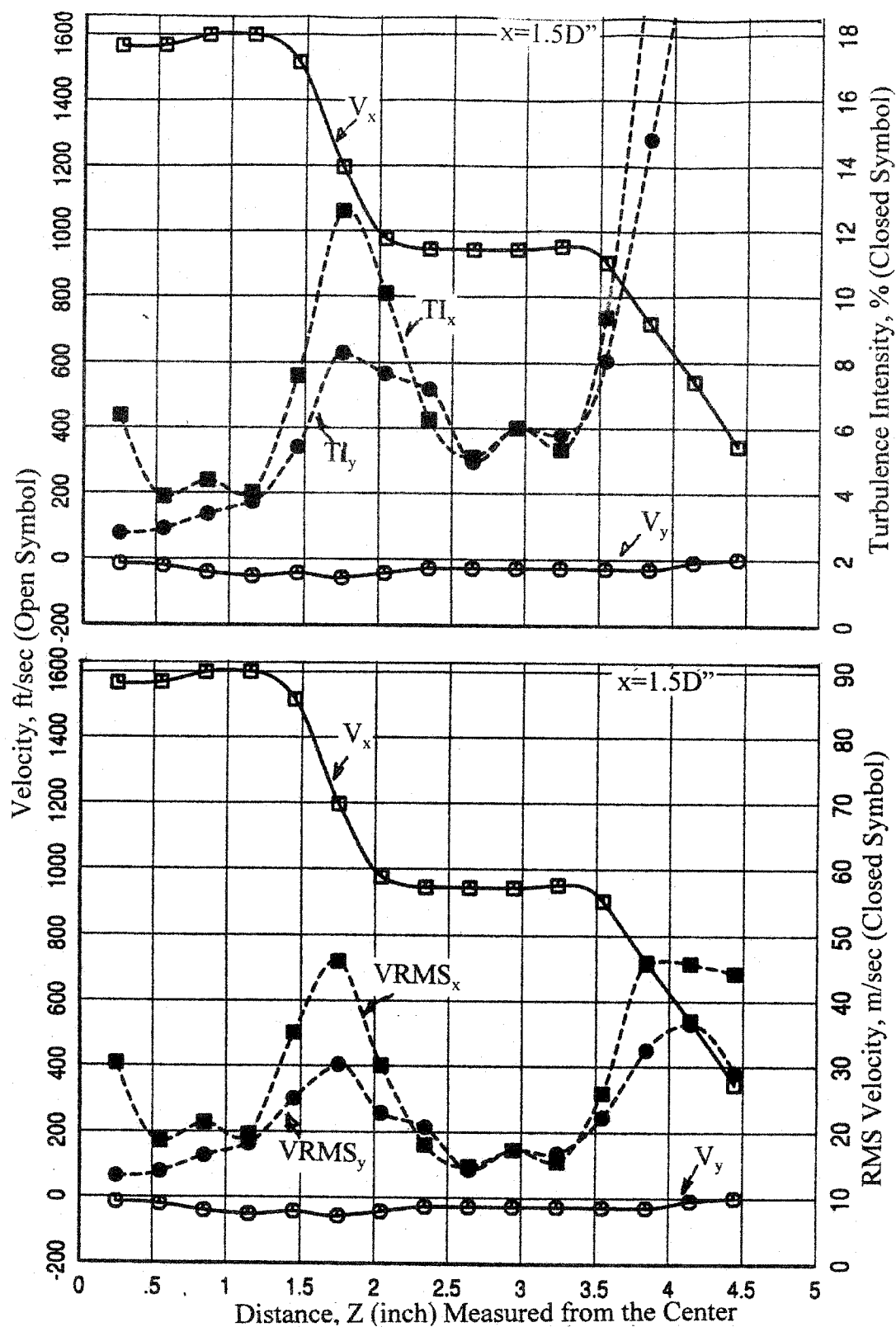


Figure 6.15. Velocity, turbulence intensity, and rms velocity distributions at  $x=1.5D''$  for confluent mixer (V1) for condition 5,  $M=0$ .

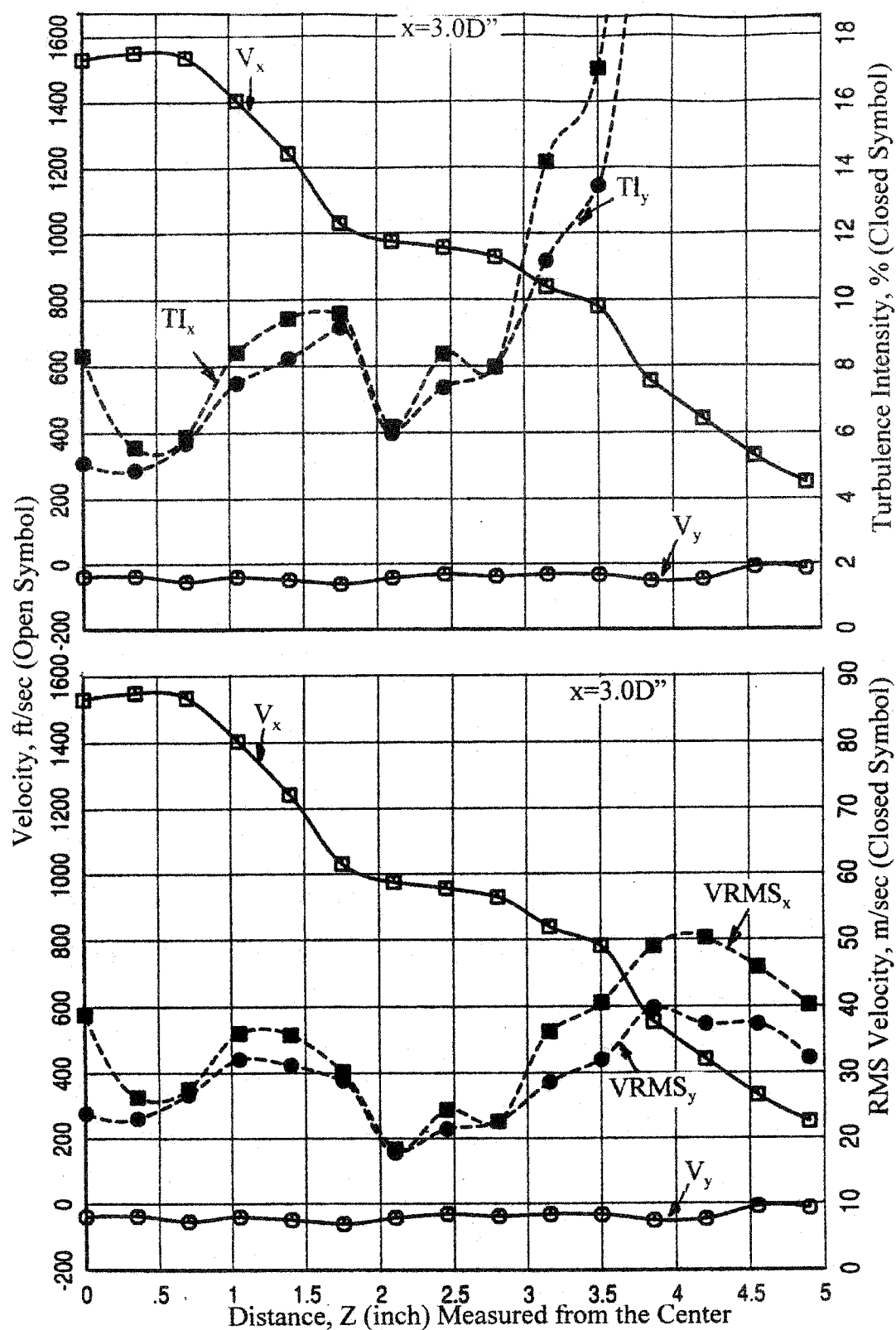


Figure 6.16. Velocity, turbulence intensity, and rms velocity distributions at  $x=3D''$  for confluent mixer (V1) for condition 5,  $M=0$ .

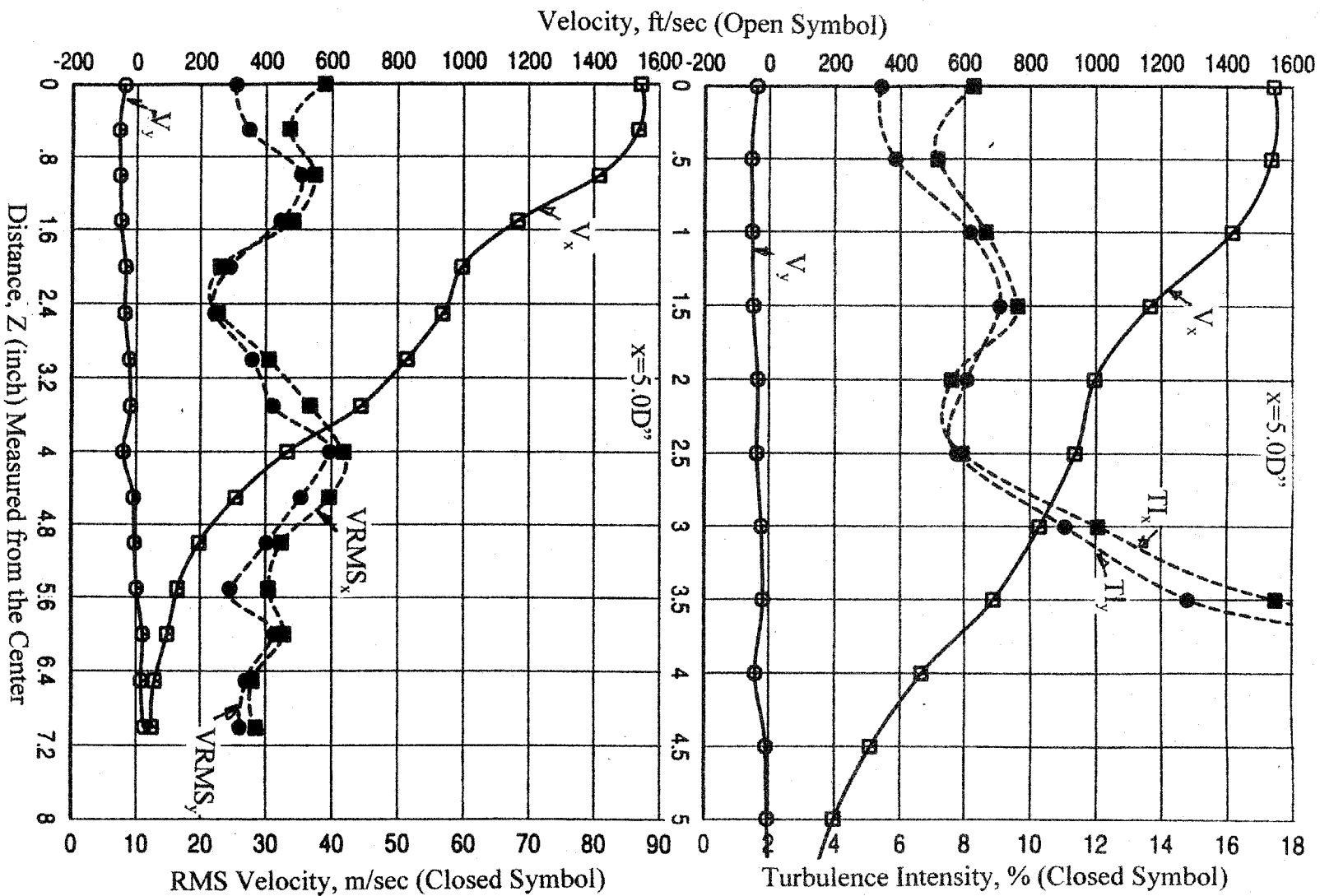


Figure 6.17. Velocity, turbulence intensity, and rms velocity distributions at  $x=5D$  for confluent mixer (V1) for condition 5,  $M=0$ .



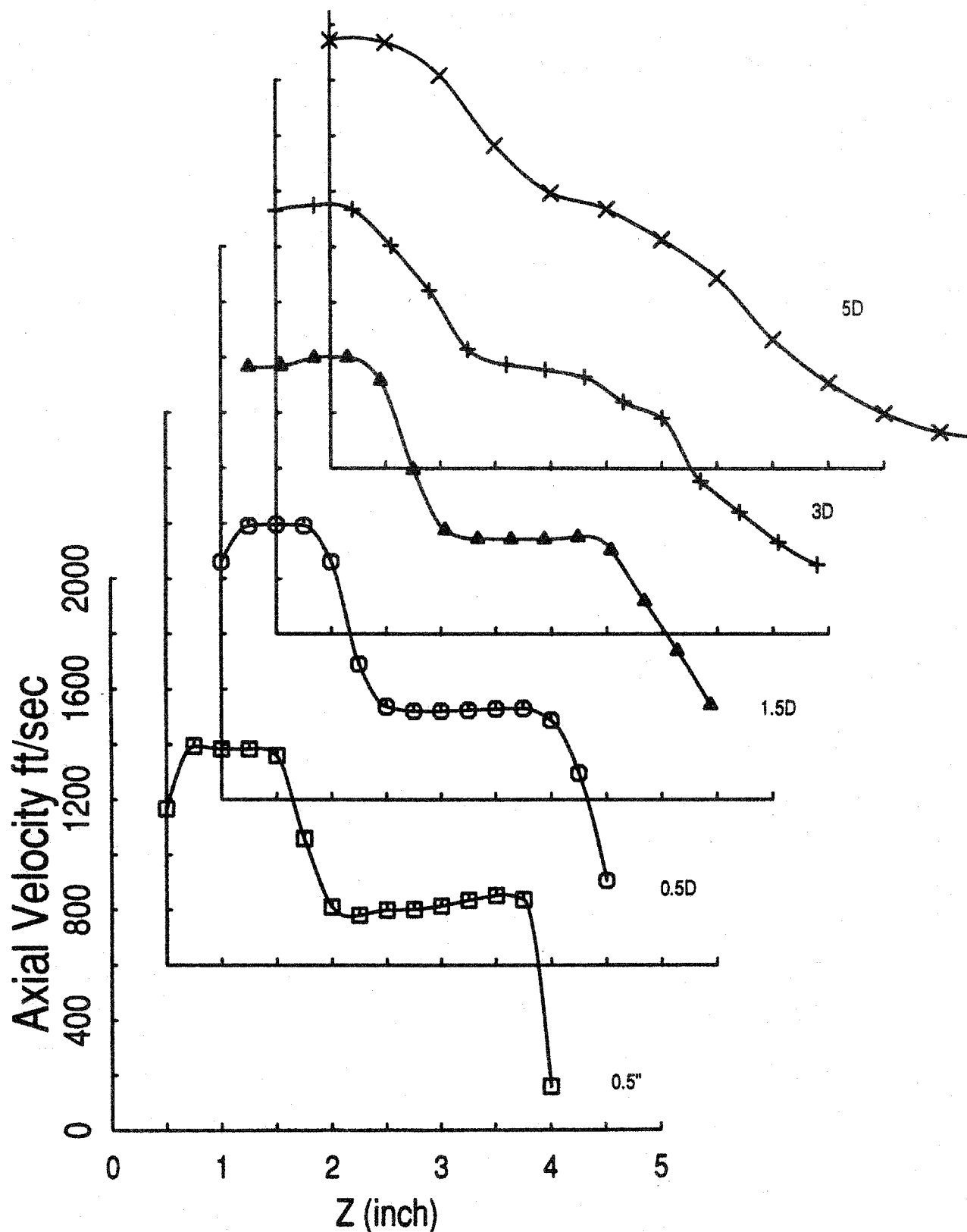


Figure 6.18. Axial velocity distributions at various axial locations for confluent mixer (V1) for condition 5,  $M=0$ .

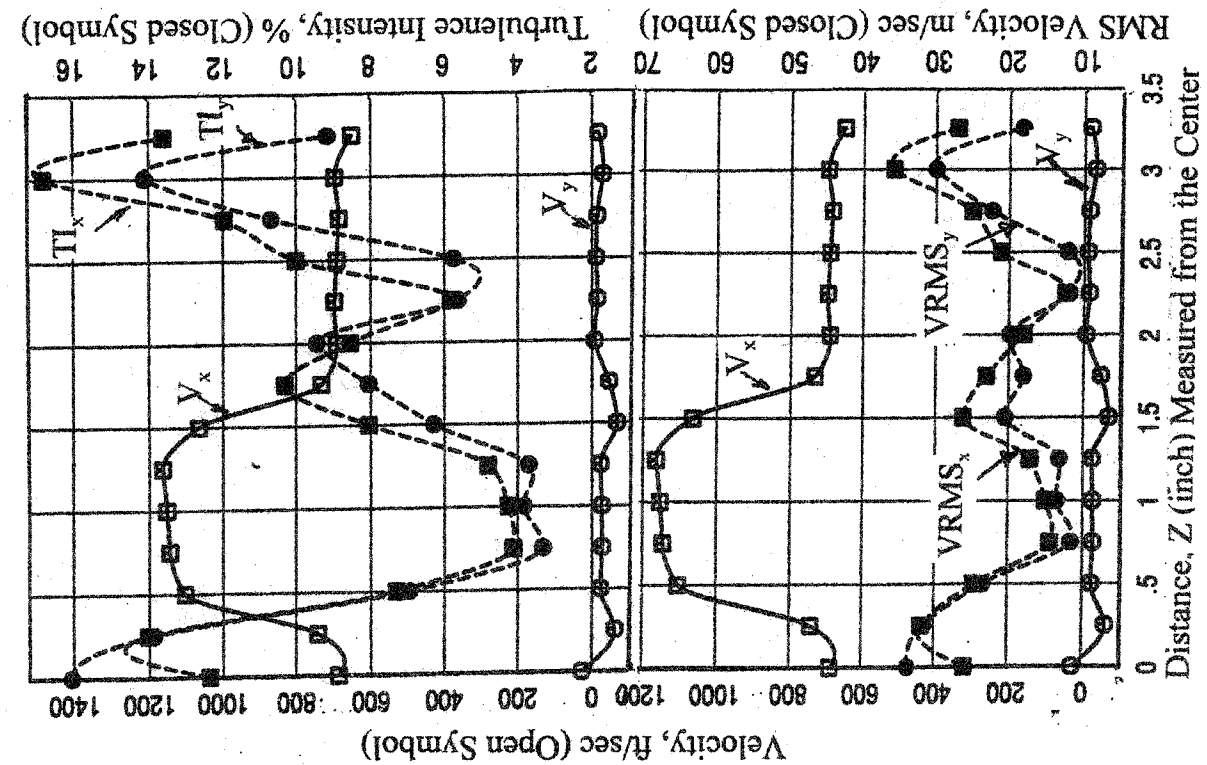
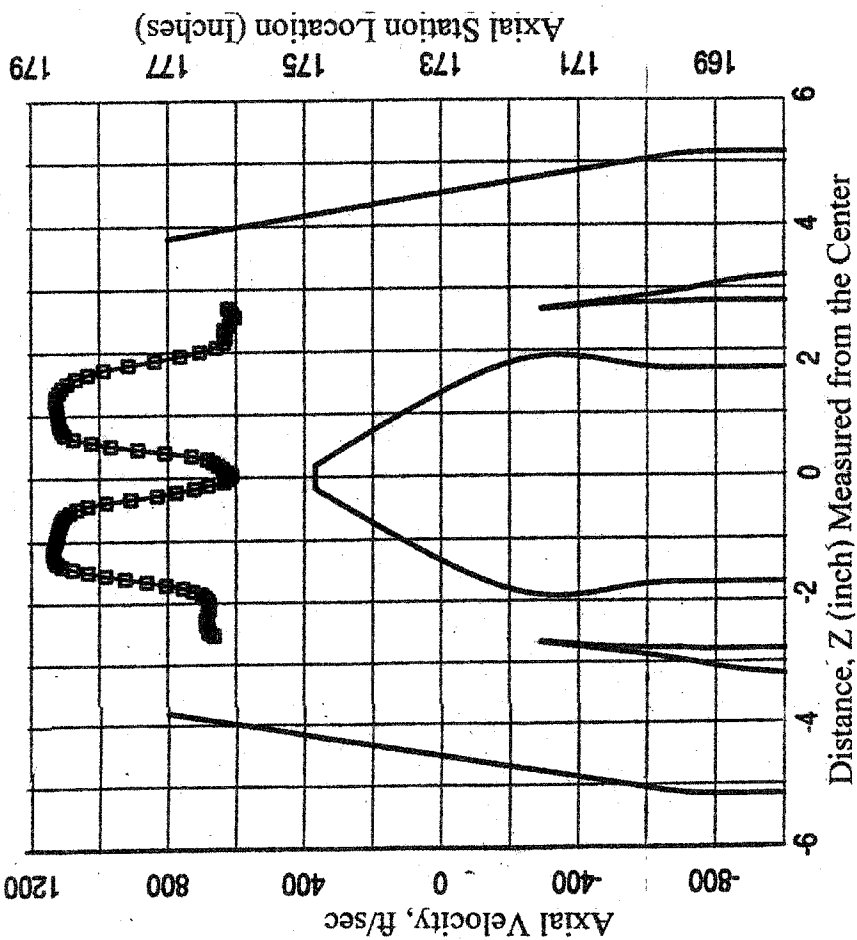


Figure 6.19. Velocity, turbulence intensity, and rms velocity distributions at  $x=-1.0''$  (internal to the nozzle) for confluent mixer (V1) for condition 5,  $M=0$ .

Figure 6.20 shows the velocity and turbulence intensity distributions at 2 inches inside the nozzle exit. At this location, the effect of center body on the flow is more pronounced since the distance between the center body and the LDA measurement location is reduced (less than 0.5 inches). The turbulence intensity at the center of the nozzle was very high due to the lower mean velocity.

Figures 6.21 to 6.23 show the velocity and turbulence intensity distributions at 3, 4, and 5 inches upstream of the nozzle exit, respectively. The LDA traversed about 1 inch radially to investigate the wake of the core cowl nozzle. There is no indication of the confluent mixer wake until 0.14 inch downstream of the core nozzle lip. Therefore the core nozzle produces only a small velocity defect. The turbulence intensities of the fan flow near the wake of the core nozzle at  $x=-4.0$  inches reaches a maximum value of 20% (Figure 6.22), and then decreases quickly to the level of 9% at the  $x=-3.0$  inches.

## **6.2.2 Velocity Measurements of V2 (Scalloped Mixer)**

### ***External Velocity Measurements of V2 (Scalloped Mixer)***

The axial and transverse velocity color contour plots at 0.5 inch downstream of the nozzle exit is shown in Figure 6.24. The core flow is replaced periodically circumferentially by fan flow because mixing was “forced” by direct penetration of the fan stream into the core. The static pressure in the core is lower than the fan static pressure. This is the reason the core flow did not penetrate into the fan flow area. The circumferential lobe areas have high velocity distribution (shown as the red area in Figure 6.24) due to the penetration of one stream into the other as shown in the transverse velocity contour plot at  $y=-2.0$ ,  $-2 < z < 2$ .

The axial velocity contours at 0.5” downstream of the exit plane between the confluent (V1) and scalloped (V2) mixers are shown in Figure 6.25. Clearly, the mixing is significantly enhanced due to the lobed mixer. The uniformity of the axial velocity at this plane is further demonstrated in Figure 6.26. The mixing between the core and the fan flows were well processed but the high velocity level was remained at the outer lobe diameter due to the lobe vortex which could be seen later.

The color contours for the axial velocities in Figure 6.27 were constructed at four downstream location (0.5”, 0.5D, 1.5D and 5D) by using histogram data in order to visualize the mixing process. The high velocity islands can be found at 0.5” downstream of the nozzle exit in this figure. These islands expanded and connected with neighborhood island to become the donut shape at 0.5D. The high velocity in the area of the center and the donut island diminished with downstream distance. A uniform velocity distribution at the core area was obtained at 5D downstream from the nozzle exit. There was a very rapid mixing process between the nozzle flow and ambient air ( $M = 0.0$ ) as observed from this figure.

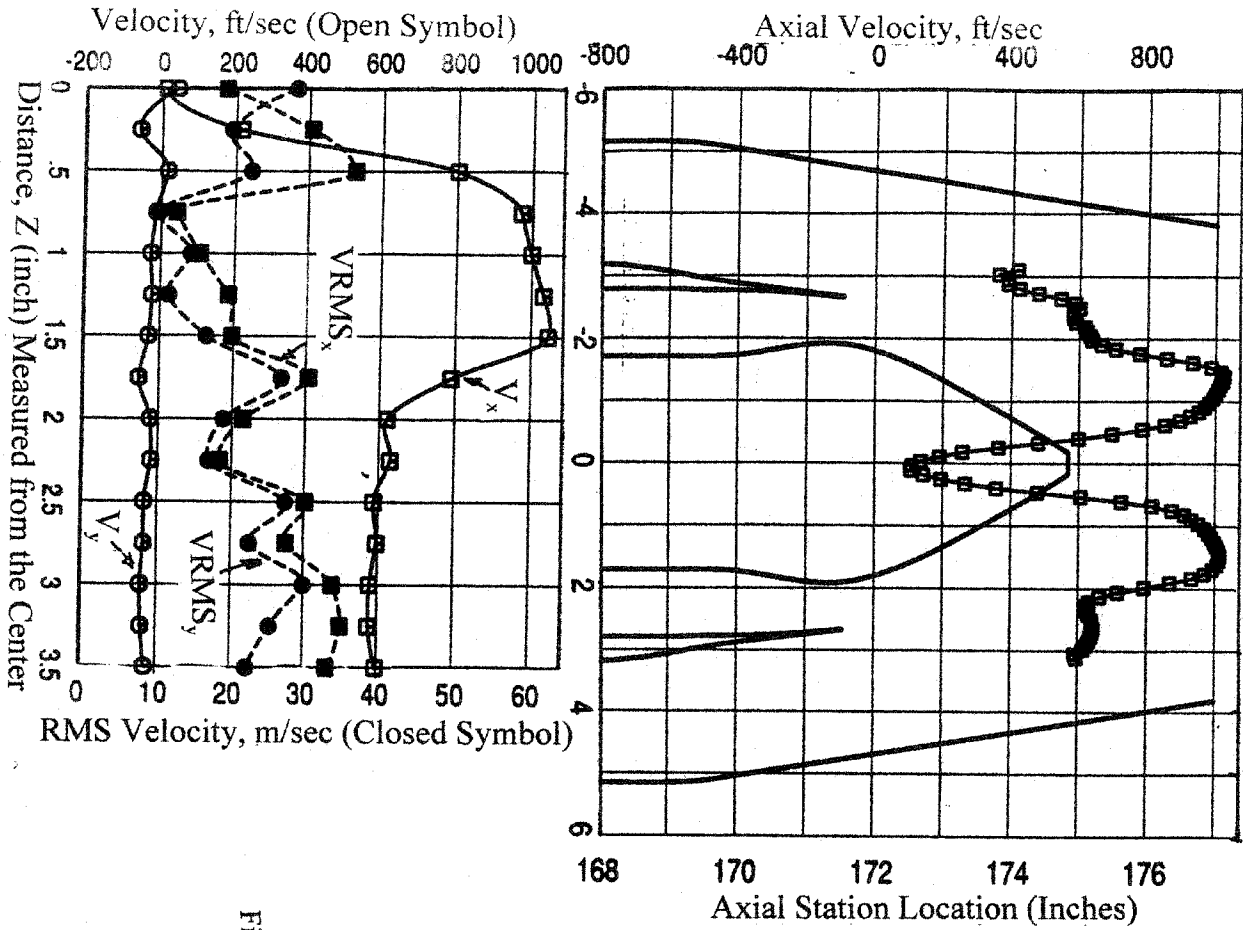
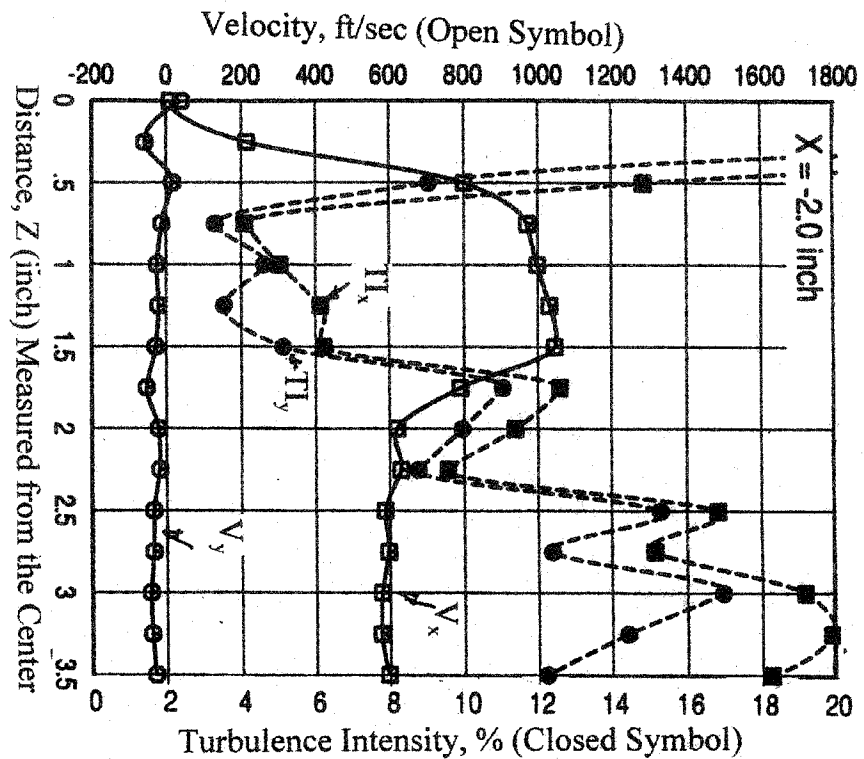


Figure 6.20. Velocity, turbulence intensity, and rms velocity distributions at  $x=-2.0$ " (internal to the nozzle) for confluent mixer (V1) for condition 5,  $M=0$ .



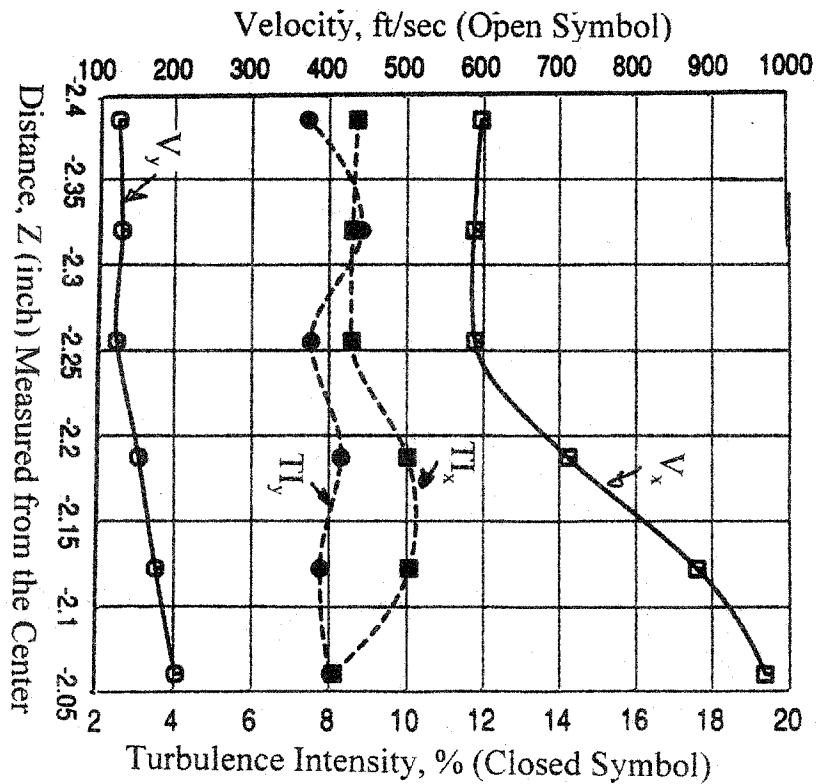
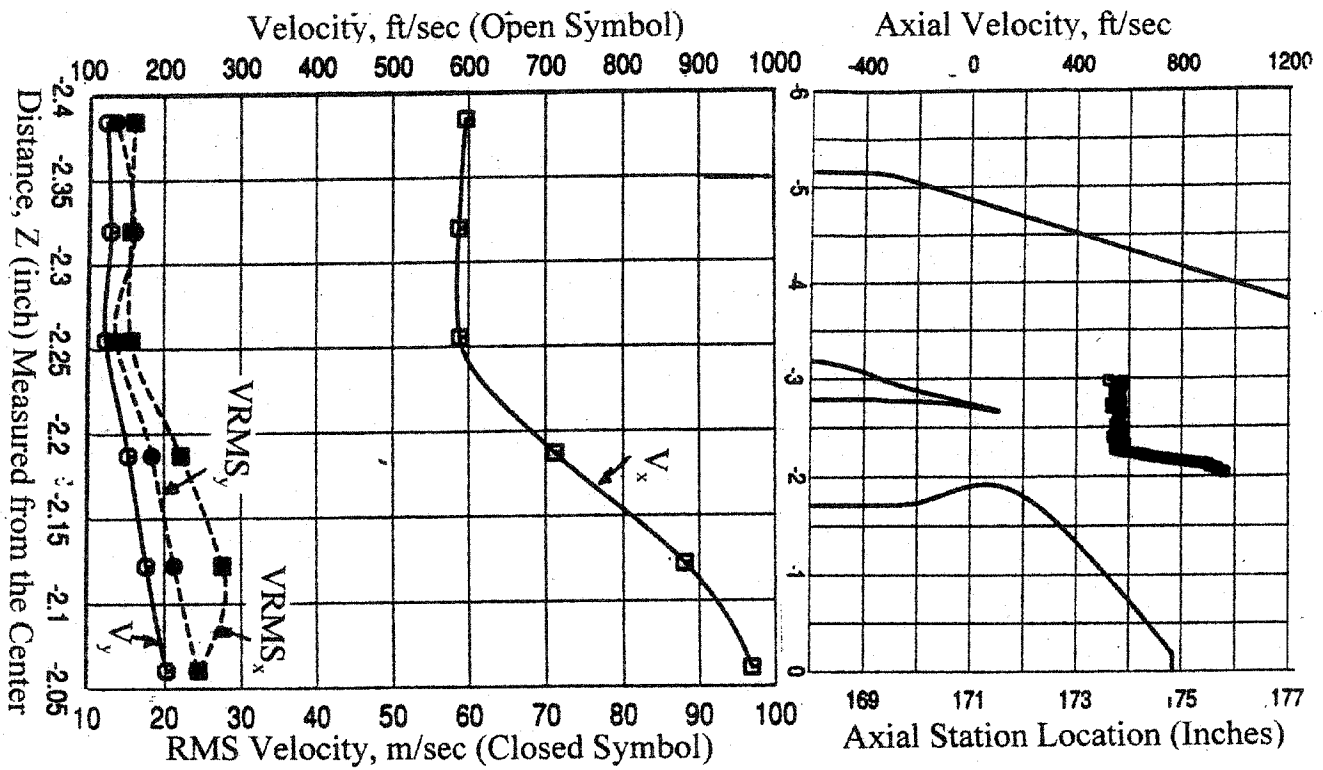


Figure 6.21. Velocity, turbulence intensity, and rms velocity distributions at  $x=-3.0''$  (internal to the nozzle) for confluent mixer (V1) for condition 5,  $M=0$ .

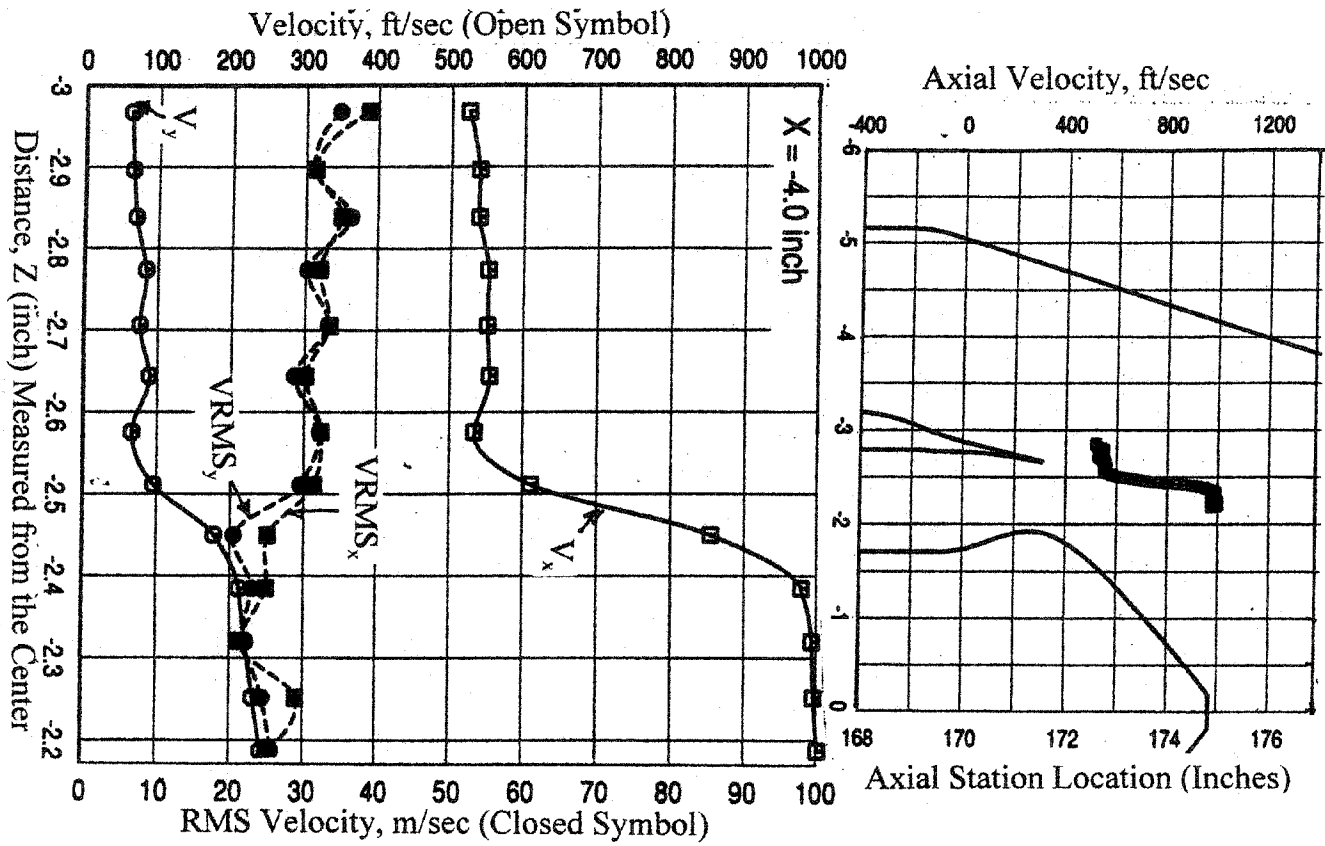


Figure 6.22. Velocity, turbulence intensity, and rms velocity distributions at  $x=-4.0$ " (internal to the nozzle) for confluent mixer (V1) for condition 5,  $M=0$ .

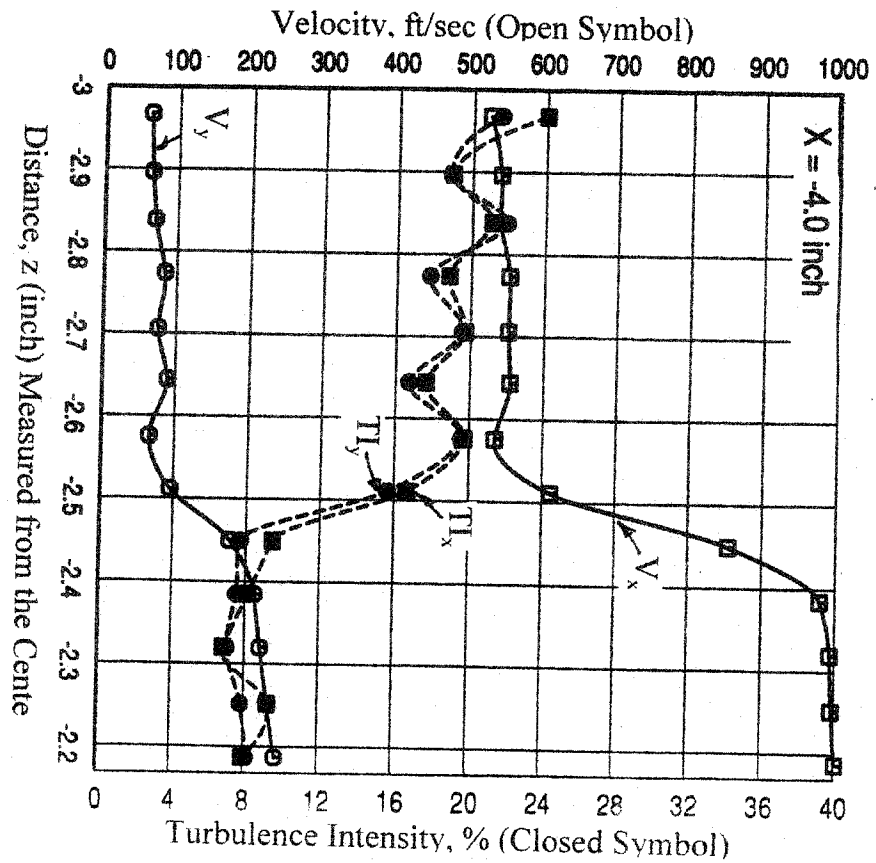
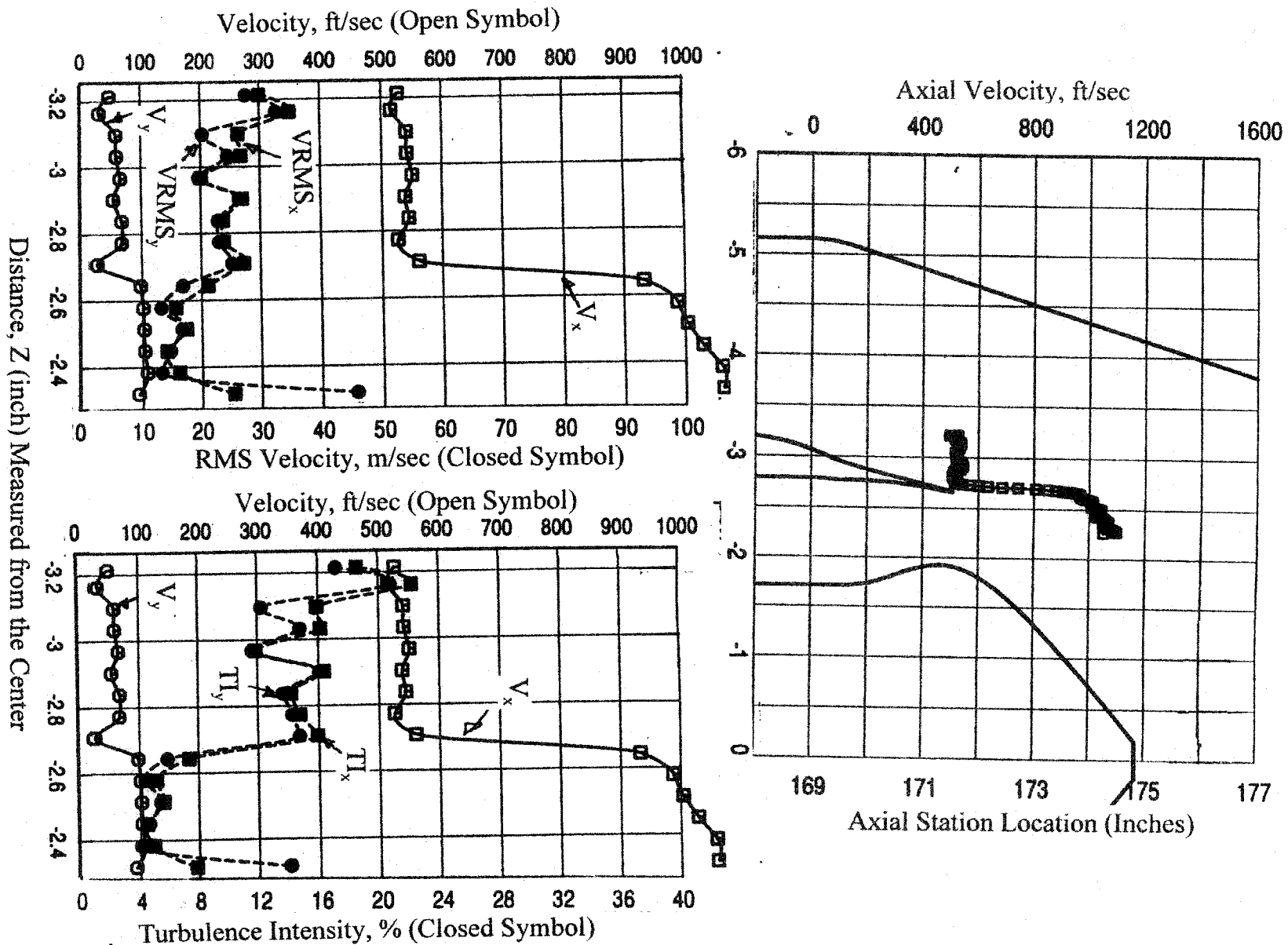


Figure 6.23. Velocity, turbulence intensity, and rms velocity distributions at  $x=5.0''$  (internal to the nozzle) for confluent mixer (V1) for condition 5,  $M=0$ .



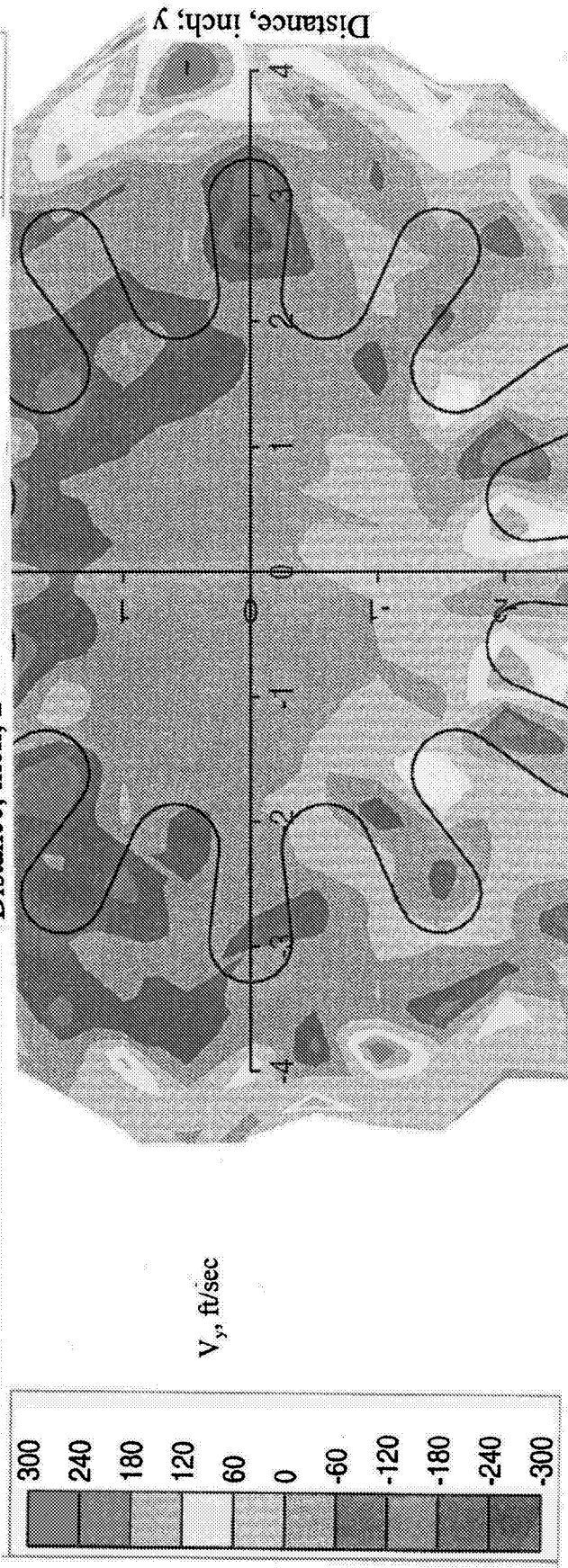
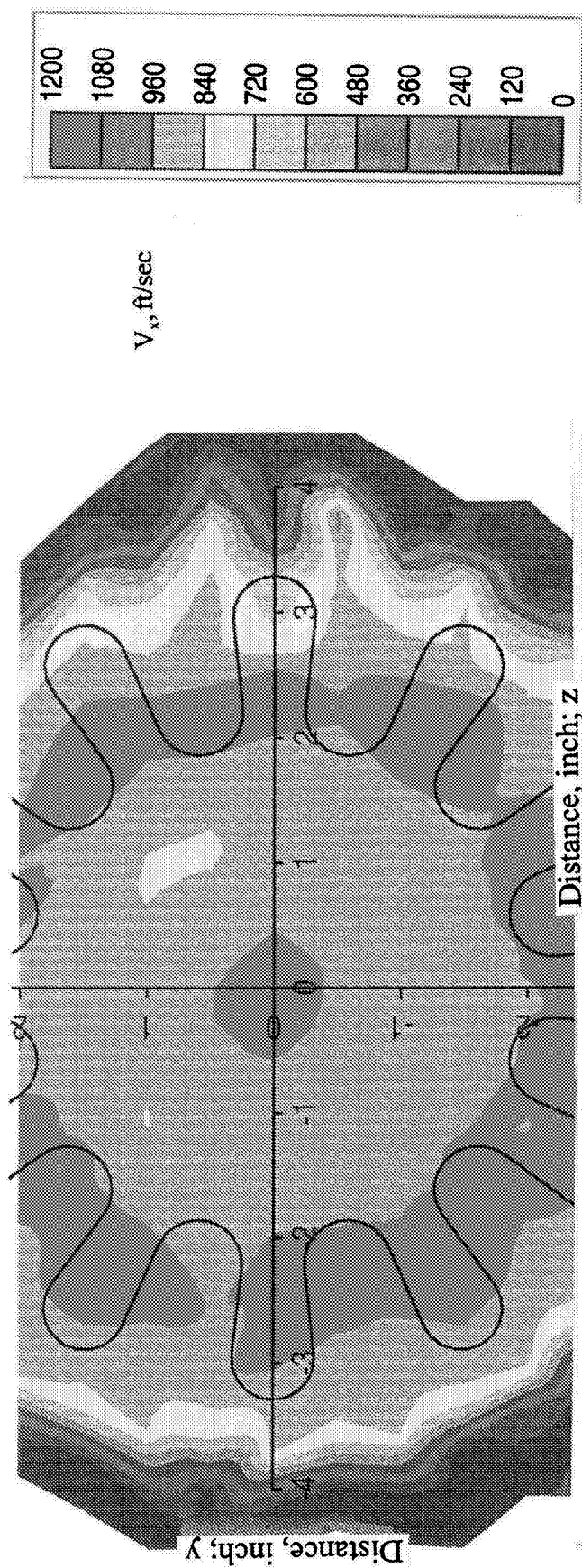


Figure 6.24. Axial ( $V_x$ ) and transverse ( $V_y$ ) velocity contours at the nozzle exit plane at  $x=0.5$ " for scalloped mixer ( $V_2$ ) for cycle condition 5 ( $V_{\text{mix}}=1000$  fps),  $M=0$ .



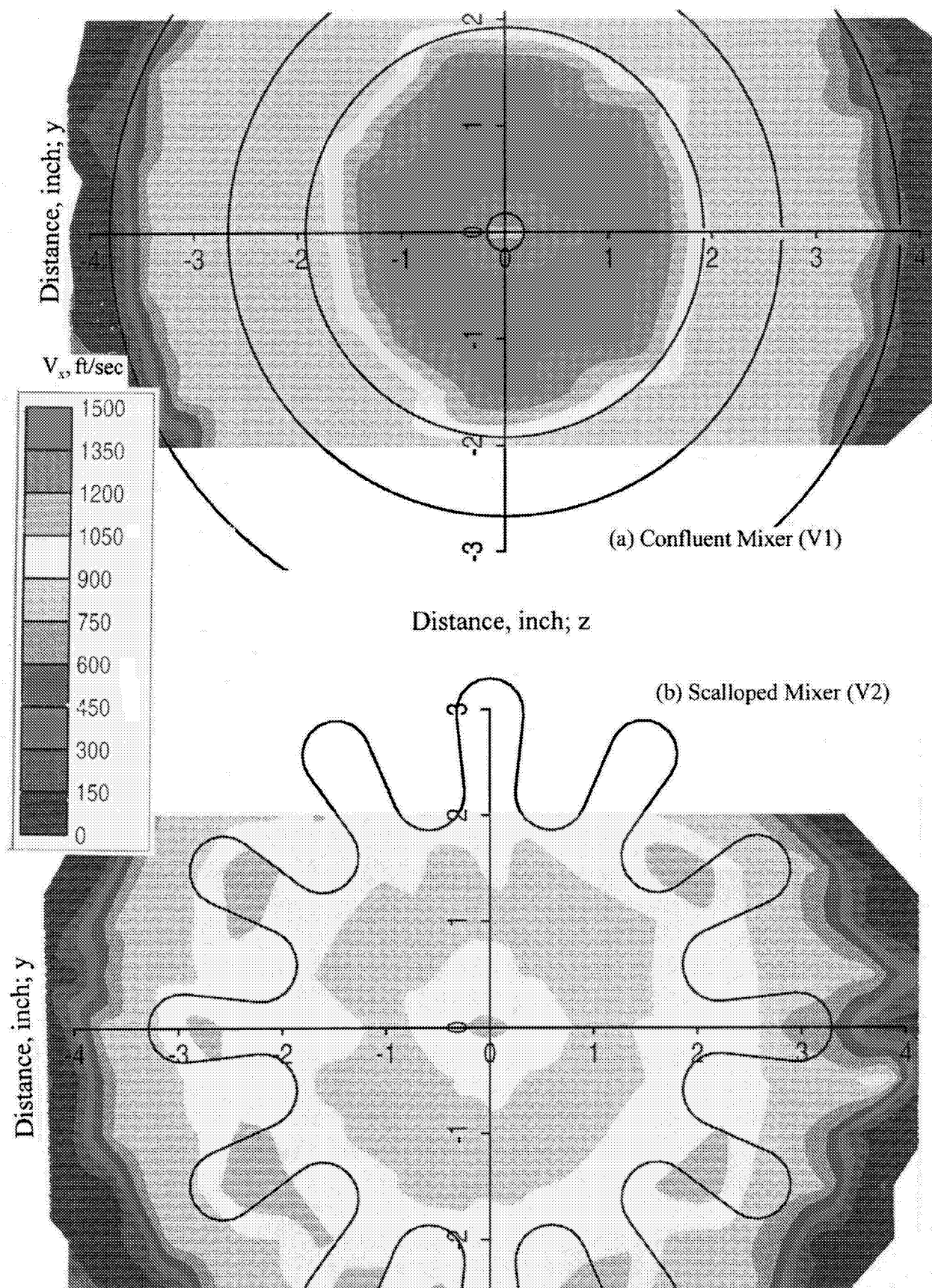


Figure 6.25. Comparison of axial velocity ( $V_x$ ) contours at 0.5" downstream of the nozzle exit plane between confluent (V1) and scalloped (V2) mixers for cycle condition 5 ( $V_{mix}=1000$  fps),  $M=0$ .

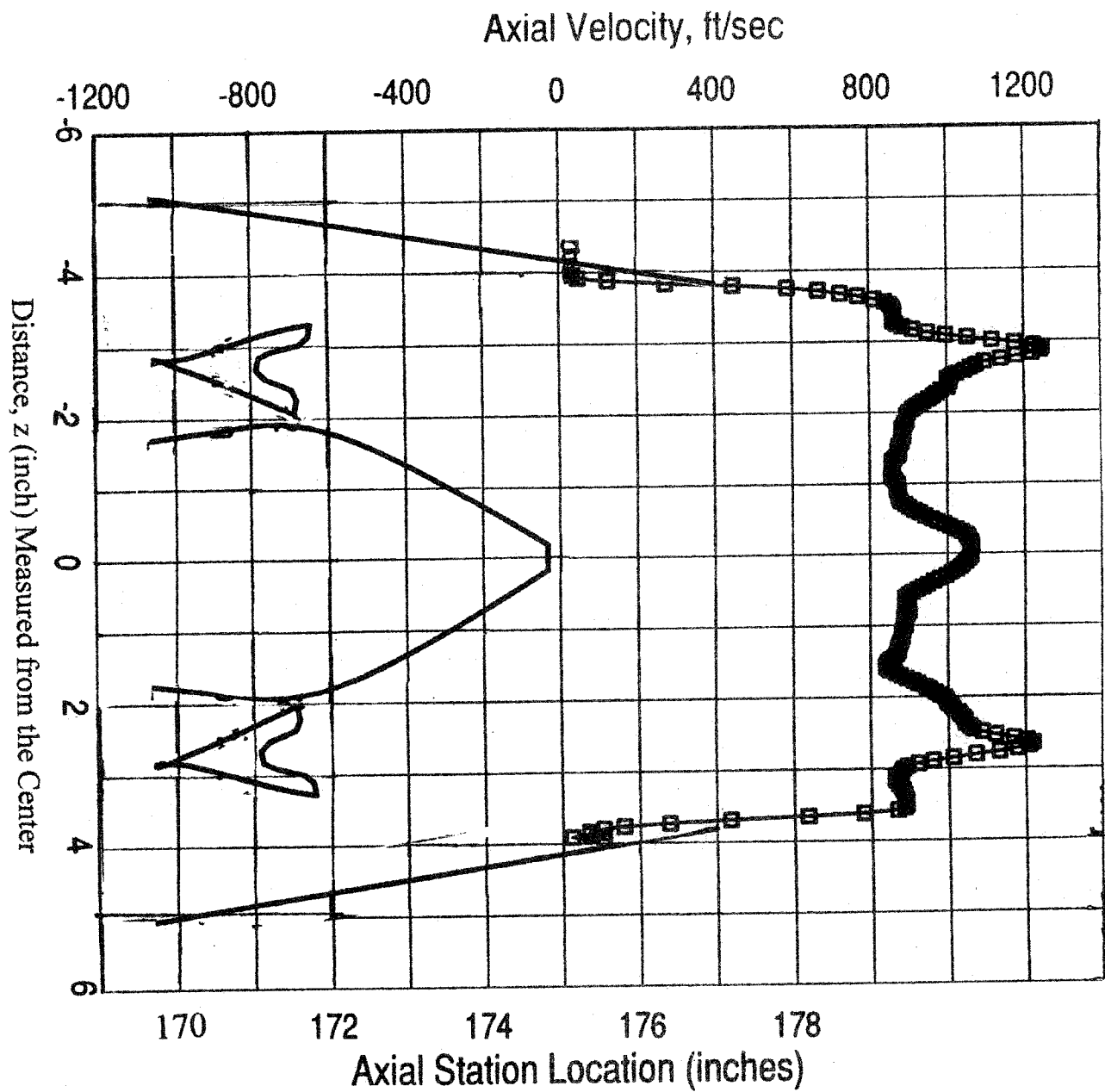


Figure 6.26. Axial velocity ( $V_x$ ) distribution for the scalloped mixer ( $V_2$ ) at 0.5" downstream of the nozzle exit plane for cycle condition 5 ( $V_{mix}=1000$  fps),  $M=0$ .

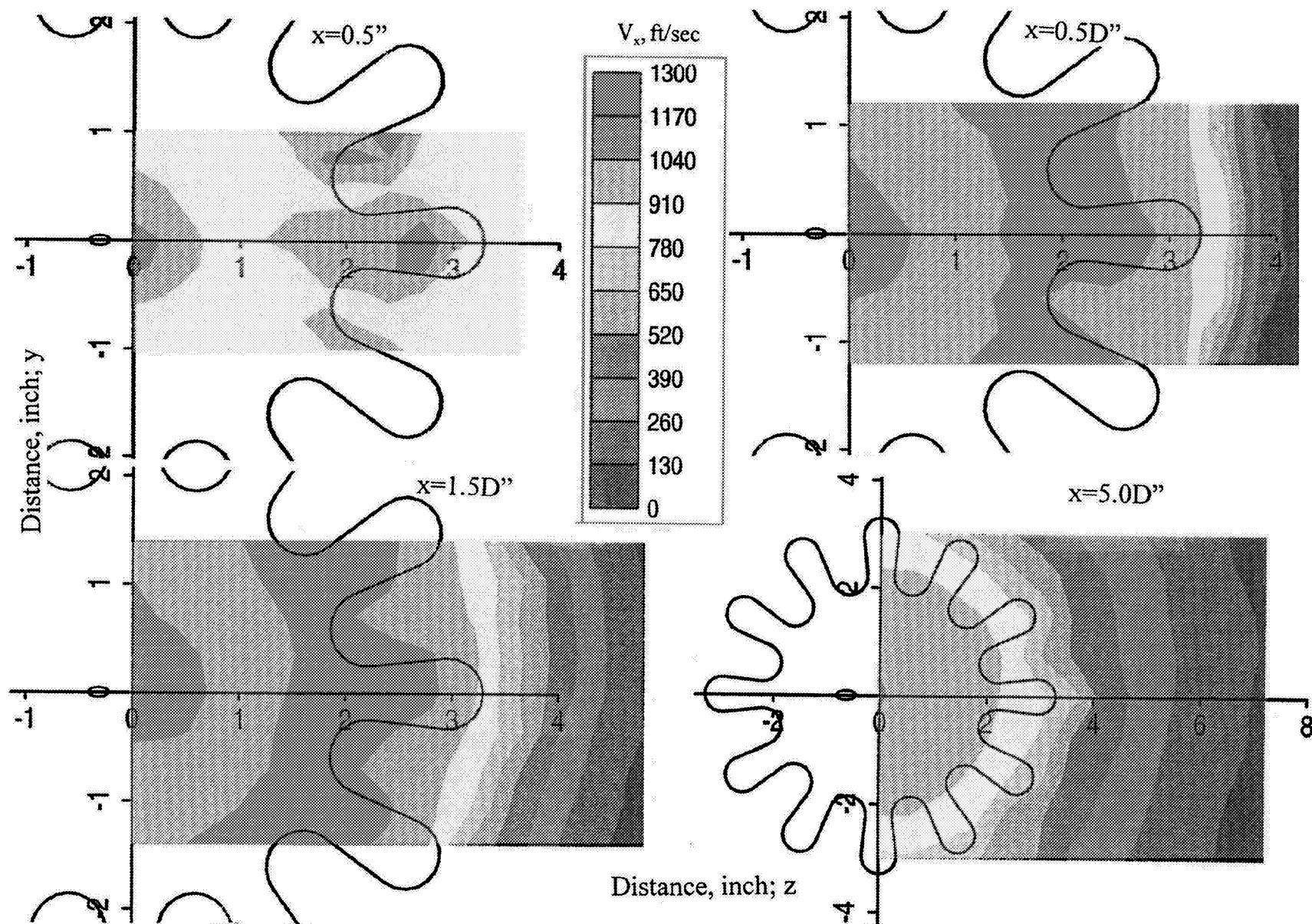


Figure 6.27. Axial velocity ( $V_x$ ) profiles for the scalloped mixer (V2) at various axial locations from the nozzle exit plane for cycle condition 5 ( $V_{mix}=1000$  fps),  $M=0$ .

### ***Internal Velocity Measurements of V2 (Scalloped Mixer)***

Internal velocity measurements were made at three locations. The velocity and turbulence intensity distributions at 0.47" downstream from the mixer lobe lip are shown in the Figure 6.28. Figure 6.28 indicates the distinct axial mean velocity level between the core and the fan flows. The  $V_y$  component of velocity shows that the mixer created a radially outward and inward flow. The opposing directions of velocity between the core and the fan flows create a vortex.

The velocity distributions at 1.47" (i.e.,  $x=-4$ ") downstream from the mixer lobe lip are shown in Figure 6.29. The color contour plot for axial mean velocity indicates that the core flow merged to the top of lobe while the fan flow started to migrate toward the middle of the lobe. The yellow line between the core and fan flows rotated clockwise compared to Figure 6.28 indicating a vortex generated by the lobe. A similar feature can be seen from  $V_y$  contours of Figures 6.28 and 6.29.

The velocity distributions at 4.47" downstream from the lobe lip or 1.0" upstream from the nozzle exit (i.e.,  $x=-1$ ") are shown in the Figure 6.30. The high velocity flow remained locally inside the lobe head area due to the vortex generated by the lobe but the core flow was well mixed with the fan flow at the center body area. Because of the absence of a center body at this axial location, the static pressure was lower and the lobes were able to guide sufficient fan flow to penetrate this region.

### ***Jet Plume Survey Measurements of V2 Mixer Configuration***

The effect of free jet on the axial velocity distributions at various axial locations, shown in Figure 6.31(a), was minimal. The jet plume decay comparison between  $M=0$  and 0.28, shown in Figure 6.31(b), indicates insignificant effect of free jet on the axial distribution of axial mean velocity distribution along the center of the nozzle up to 50 inches downstream from the nozzle exit. The difference in  $x=5-22$  inch could be due to a lack of seeding materials because Figure 6.31(a) shows essentially no velocity differences between  $M=0.0$  and  $M=0.28$  at the center of the mixer nozzle.

### **6.2.3 Velocity Measurements of V2A (Scalloped Mixer with Extended Tailpipe)**

The mean velocity and turbulence intensity color contour plot at 0.5 inch downstream of the nozzle exit for mixer configuration V2A are shown in Figure 6.32. One can see the effect of the extension piece on the velocity distribution by comparing Figure 6.32 with Figure 6.24. The peak velocity in the core lobe for the V2A mixer was reduced and flattened, and turbulence intensity was also reduced compared to V2. The axial velocity distribution for V2A, shown in Figure 6.33 can be compared with similar result for V2 of Figure 6.26. The figures show reduced peak velocity in the lobe area due to the 2.0" extension tailpipe but slightly increased center velocities for the V2A mixer configuration.

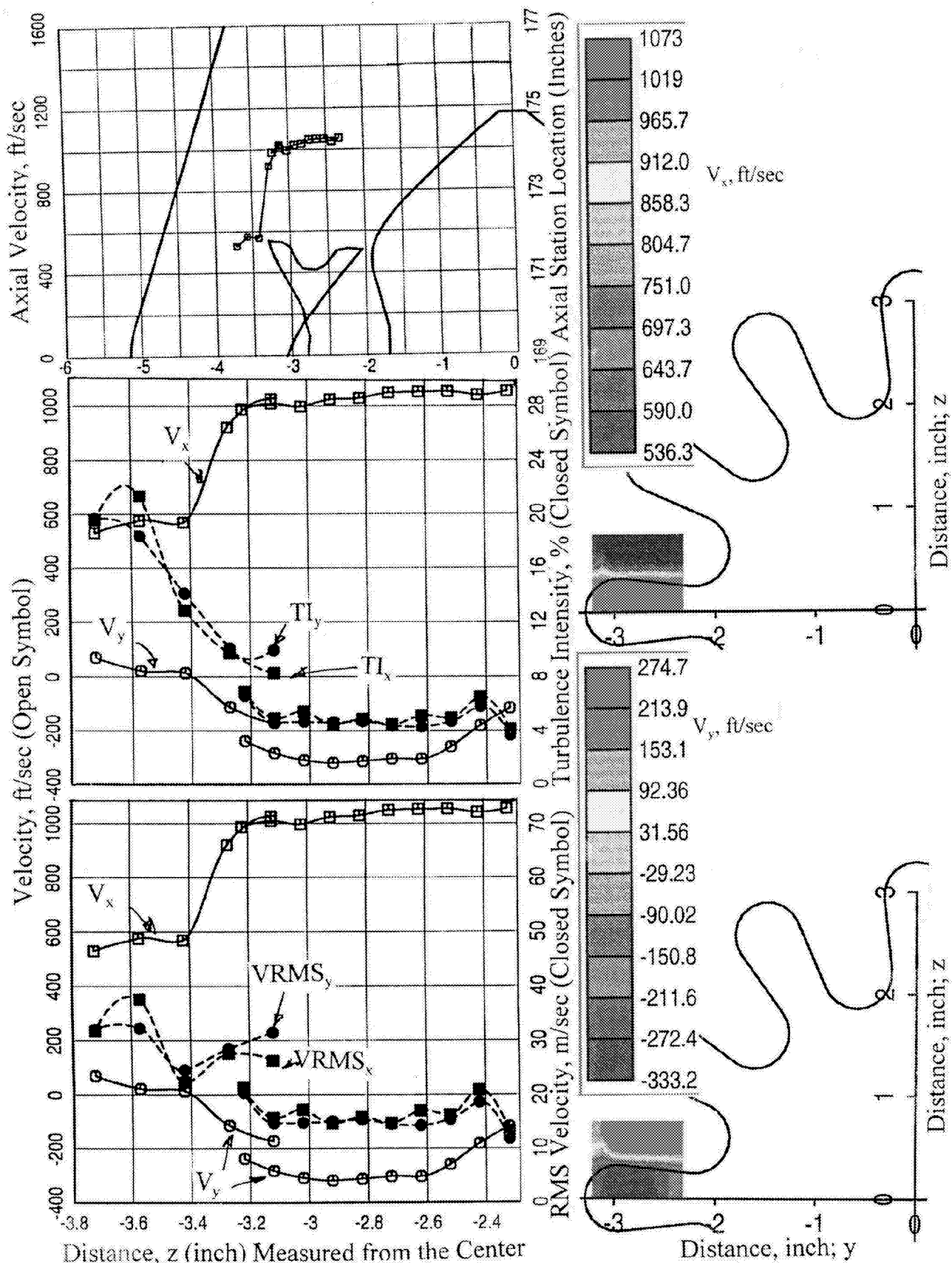


Figure 6.28. Velocity, turbulence intensity, & rms velocity distributions and axial & transverse velocity contours at  $x=-5.0$ " (internal to the nozzle at station 172) for scalloped mixer (V2) for condition 5,  $M=0$ .

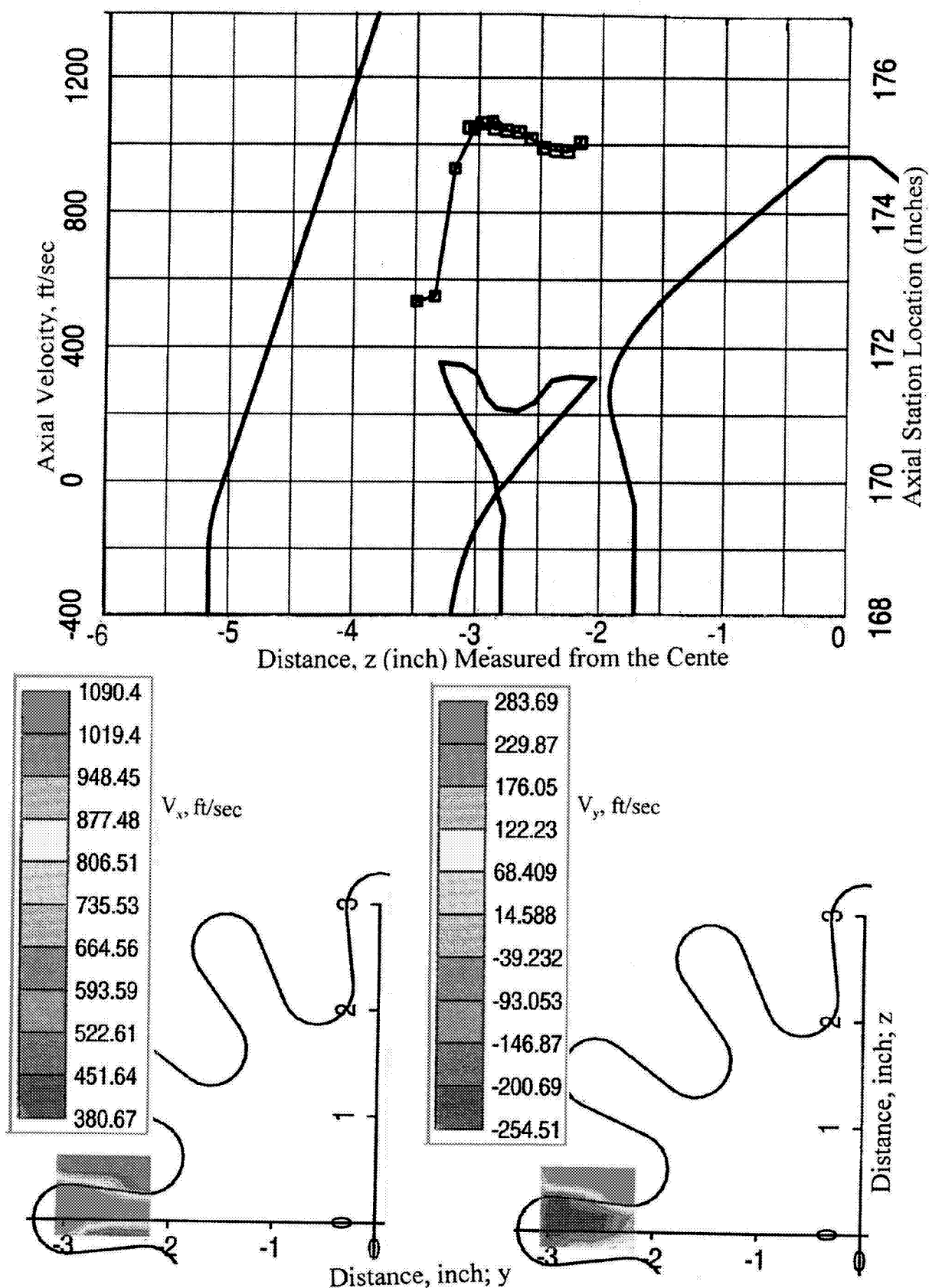


Figure 6.29. Axial velocity distribution and axial & transverse velocity contours at  $x=-4.0''$  (internal to the nozzle at station 173) for scalloped mixer (V2) for condition 5,  $M=0$ .

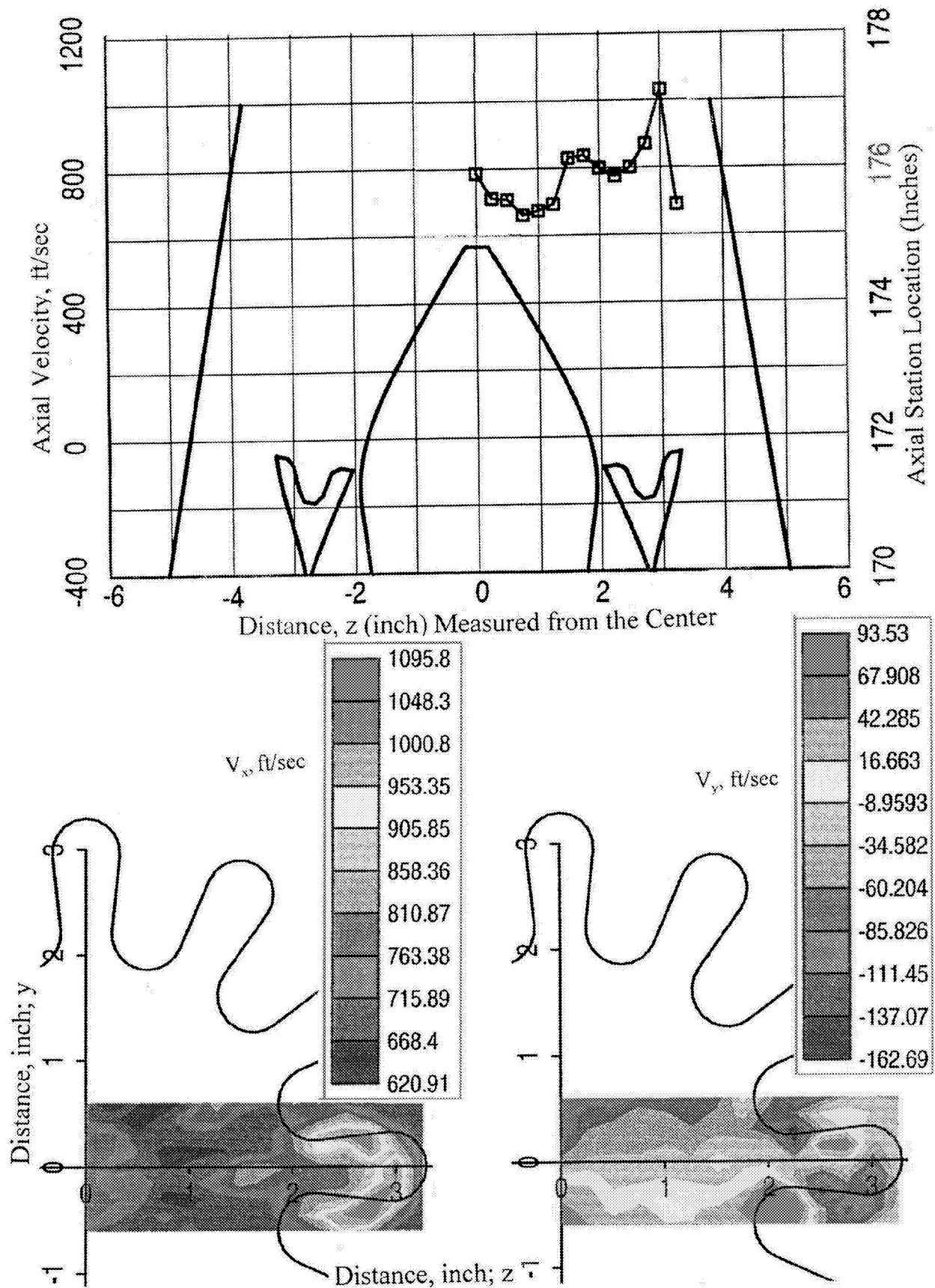


Figure 6.30. Axial velocity distribution and axial & transverse velocity contours at  $x=-1.0''$  (internal to the nozzle at station 176) for scalloped mixer (V2) for condition 5,  $M=0$ .

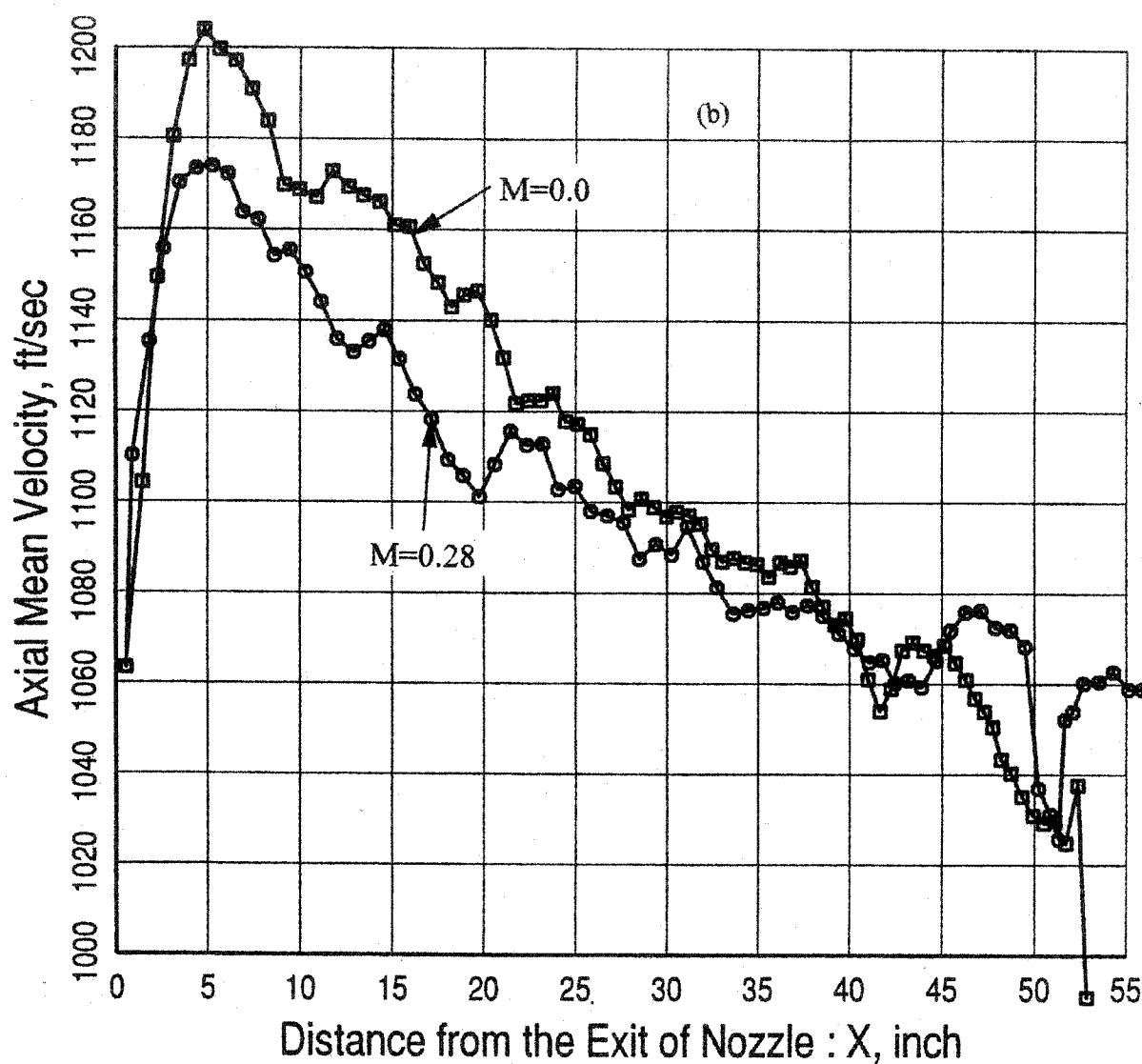
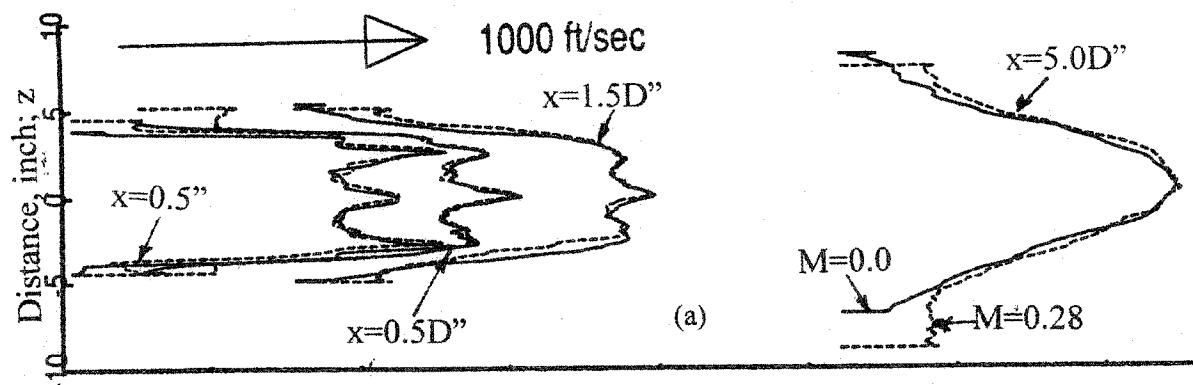


Figure 6.31. Effect of simulated flight on axial velocity distributions, (a) along  $z$  at several axial locations and (b) along  $x$  at the nozzle centerline, external to the nozzle exit for the scalloped mixer (V2) for cycle condition 5.



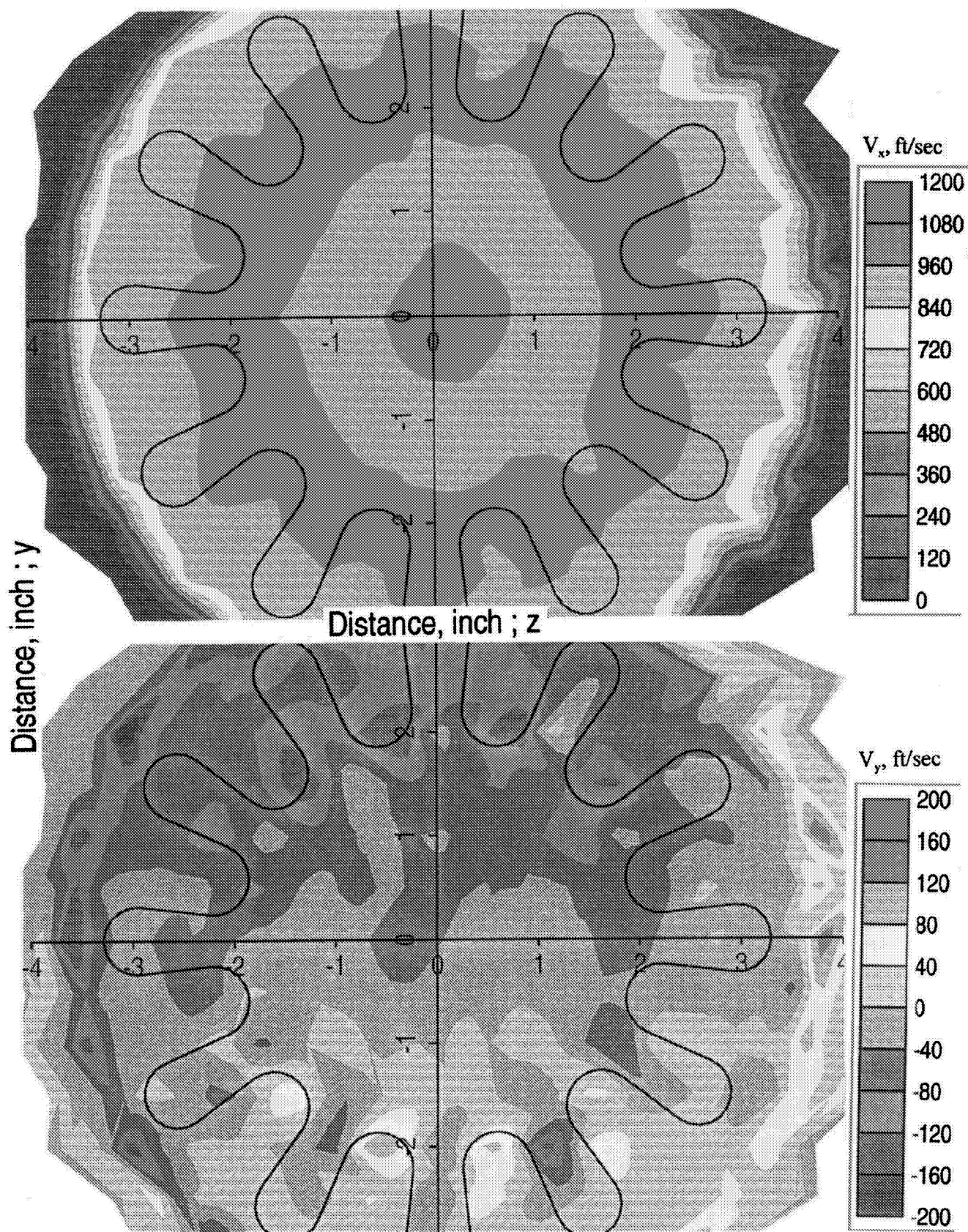
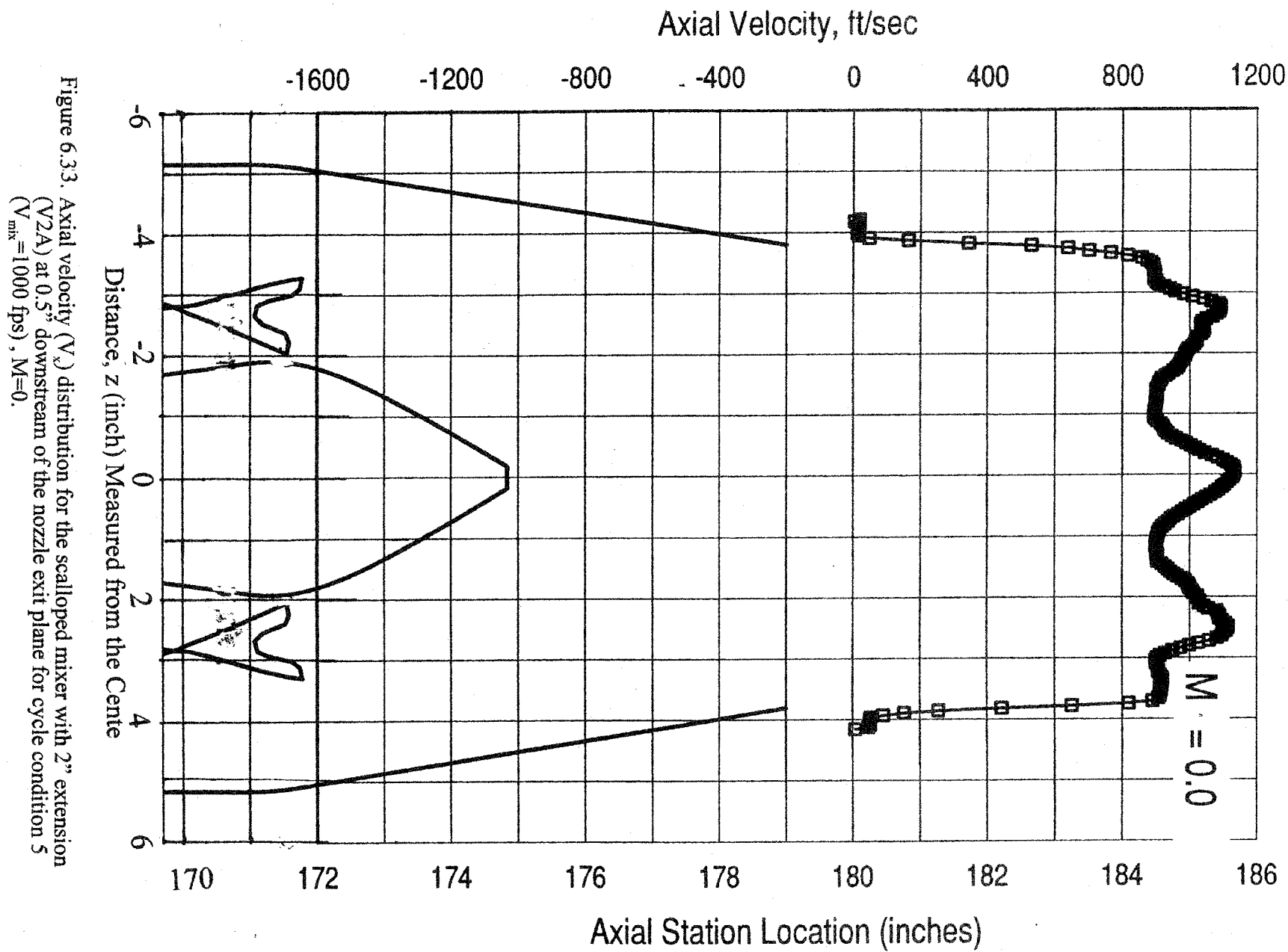


Figure 6.32. Axial ( $V_x$ ) and transverse ( $V_y$ ) velocity contours at the nozzle exit plane for the scalloped mixer with 2" extension (V2A) for cycle condition 5 ( $V_{mix}=1000$  fps),  $M=0$ .



The effect of free jet on the axial velocity distributions at various axial locations downstream of the nozzle exit, shown in Figure 6.34(a), was minimal. Figure 6.34(b) shows a jet plume decay comparison between  $M = 0$  and 0.28. There is no significant effect of free jet on the axial distribution of axial mean velocity distribution along the center of the nozzle up to 40 inches downstream from the nozzle exit.

#### **6.2.4 Velocity Measurements of F12A (Skewed Mixer)**

The F12A mixer configuration mean velocities color contour plot at 0.5 inch downstream of the nozzle exit are shown in Figure 6.35. This mixer does not exhibit the fan/core temperature inversion flow characteristics of the V2 or V2A mixers. Rather, a more uniform relatively high velocity level in the core area persists. The region for radial inward component apparently is not sufficient to allow fan flow to penetrate into the core area. Because of that, the radial component of velocity was larger than that of the V2 mixer. The turbulence intensity levels are similar or even lower than for the V2 model. Nozzle exit plane turbulence level may not be a suitable correlating parameter in determining the noise characteristics for these configurations.

The effect of free jet on the axial velocity distributions at various axial locations downstream of the nozzle exit, shown in Figure 6.36(a), was minimal. Figure 6.36(b) shows the jet plume decay comparison between  $M = 0$  and 0.28. The difference of axial velocity distribution along axial distance between  $M = 0$  and 0.28 shown in Figure 6.36(b) for the axial distance range  $x=5-30$  inches could be due again to a lack of Laser seeding materials. Figure 6.36(a) indicates virtually no difference between  $M=0.0$  and  $M=0.28$  velocity distributions. These results are consistent with the V2 and V2A lobe mixers.

#### **6.2.5 Velocity Measurements of F9B (Scalloped and staggered Mixer)**

The F9B mixer mean velocity color contour plots at 0.5 inch downstream of the nozzle exit are shown in Figure 6.37. This mixer scattered the core flow in sections. The on-set of the mixing might occur sooner than with the other mixers as evidenced by the spotted velocity pattern. The  $V_y$  contour plot indicates deeper penetration of the fan flow than for the V2 mixer.

The effect of free jet on the axial velocity distributions at various axial locations downstream of the nozzle exit, shown in Figure 6.38(a), was minimal but show an earlier velocity decay than seen for other mixer models. Figure 6.38(b) shows a jet plume decay comparison between  $M = 0$  and 0.28. No difference in velocity distribution is exhibited until  $x=32$  inches.

Figure 6.39 shows a comparison of axial velocity contour plots between the confluent (V1) and the scalloped & staggered (F9B) mixers. The uniformity of velocity distributions at the exit plane for the F9B mixer is significantly better compared to the

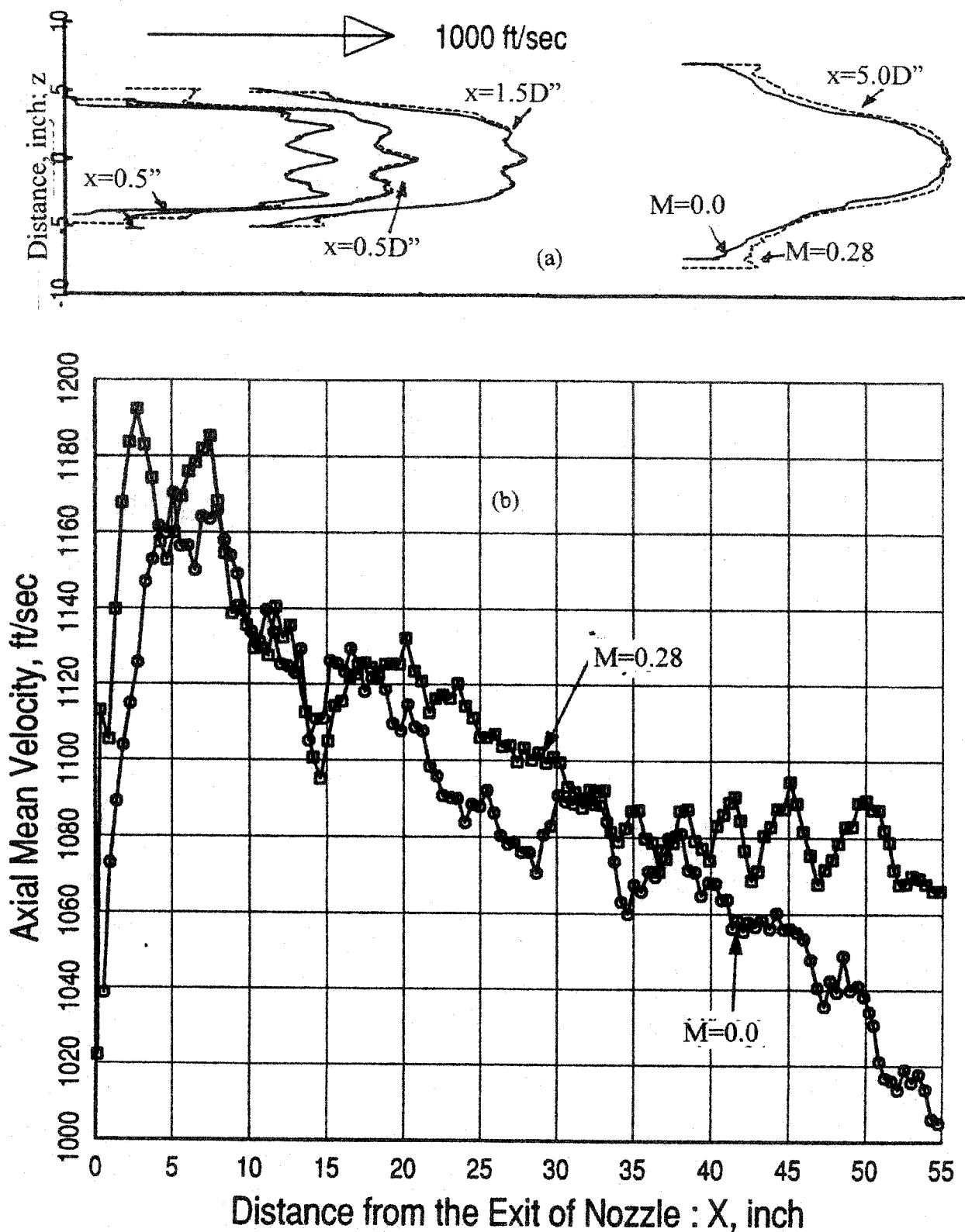


Figure 6.34. Effect of simulated flight on axial velocity distributions, (a) along  $z$  at several axial locations and (b) along  $x$  at the nozzle centerline, external to the nozzle exit for the scalloped mixer with 2" extension (V2A) for cycle condition 5.

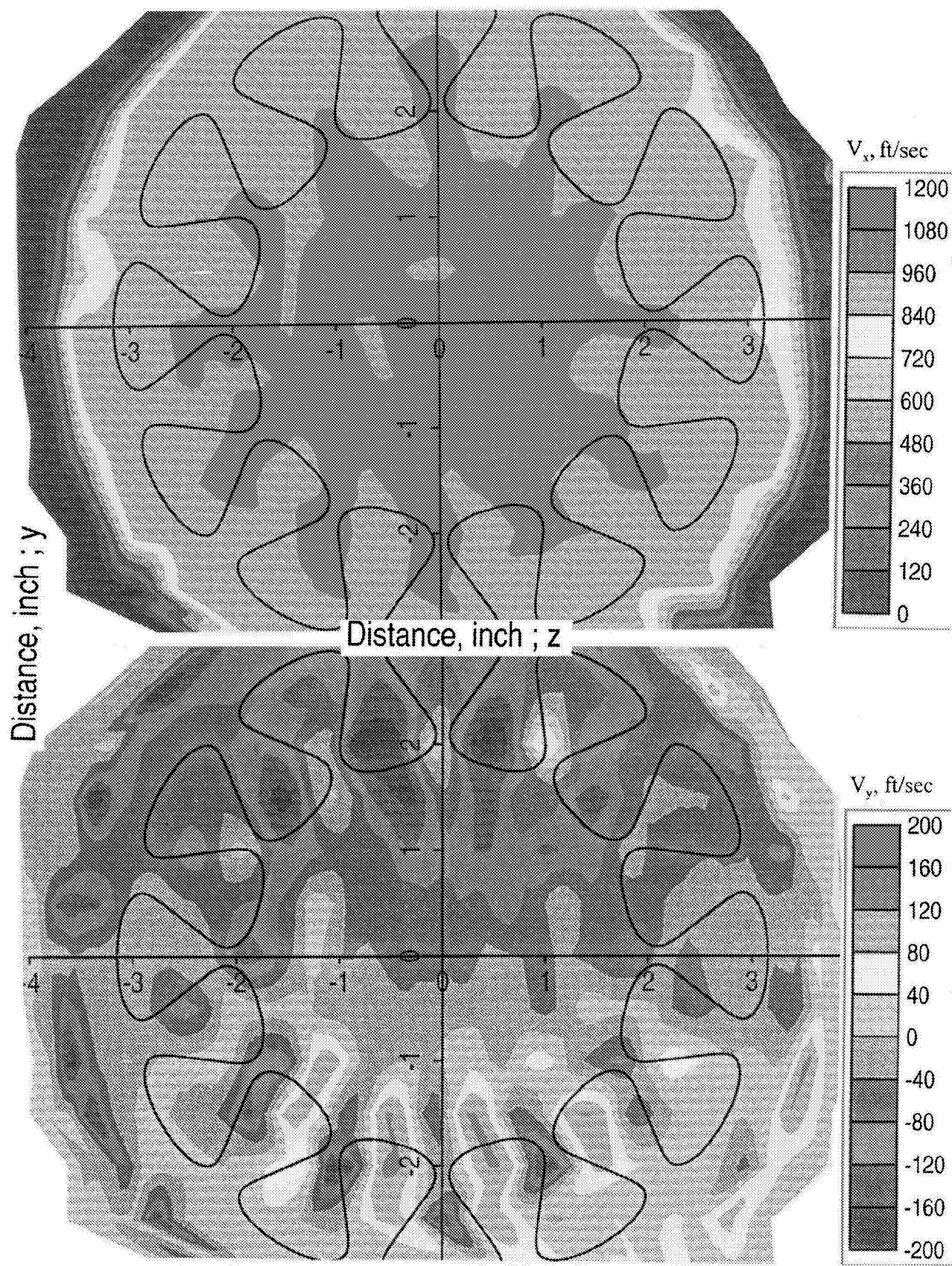


Figure 6.35. Axial ( $V_x$ ) and transverse ( $V_y$ ) velocity contours at the nozzle exit plane for the skewed (F12A) for cycle condition 5 ( $V_{\text{mix}}=1000$  fps),  $M=0$ .

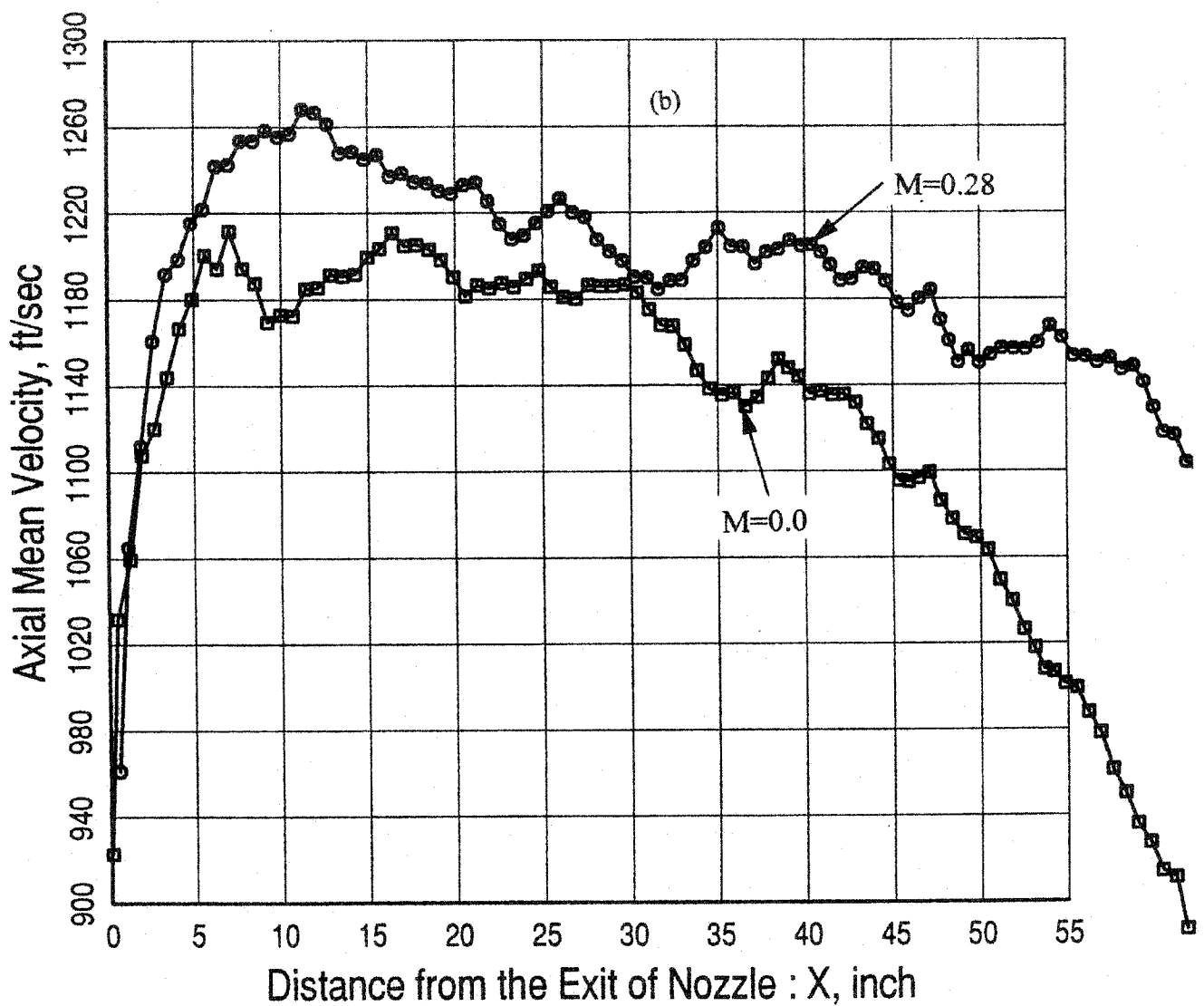
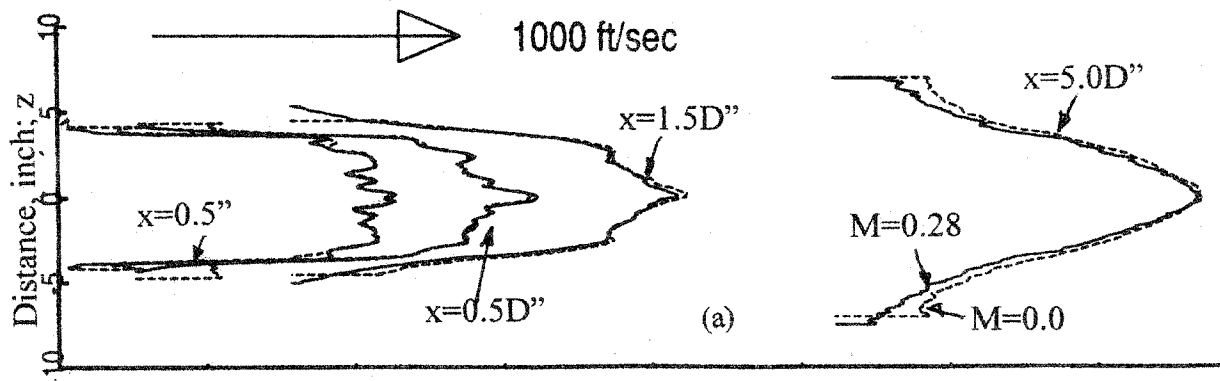


Figure 6.36. Effect of simulated flight on axial velocity distributions, (a) along  $z$  at several axial locations and (b) along  $x$  at the nozzle centerline, external to the nozzle exit for the skewed (F12A) for cycle condition 5.



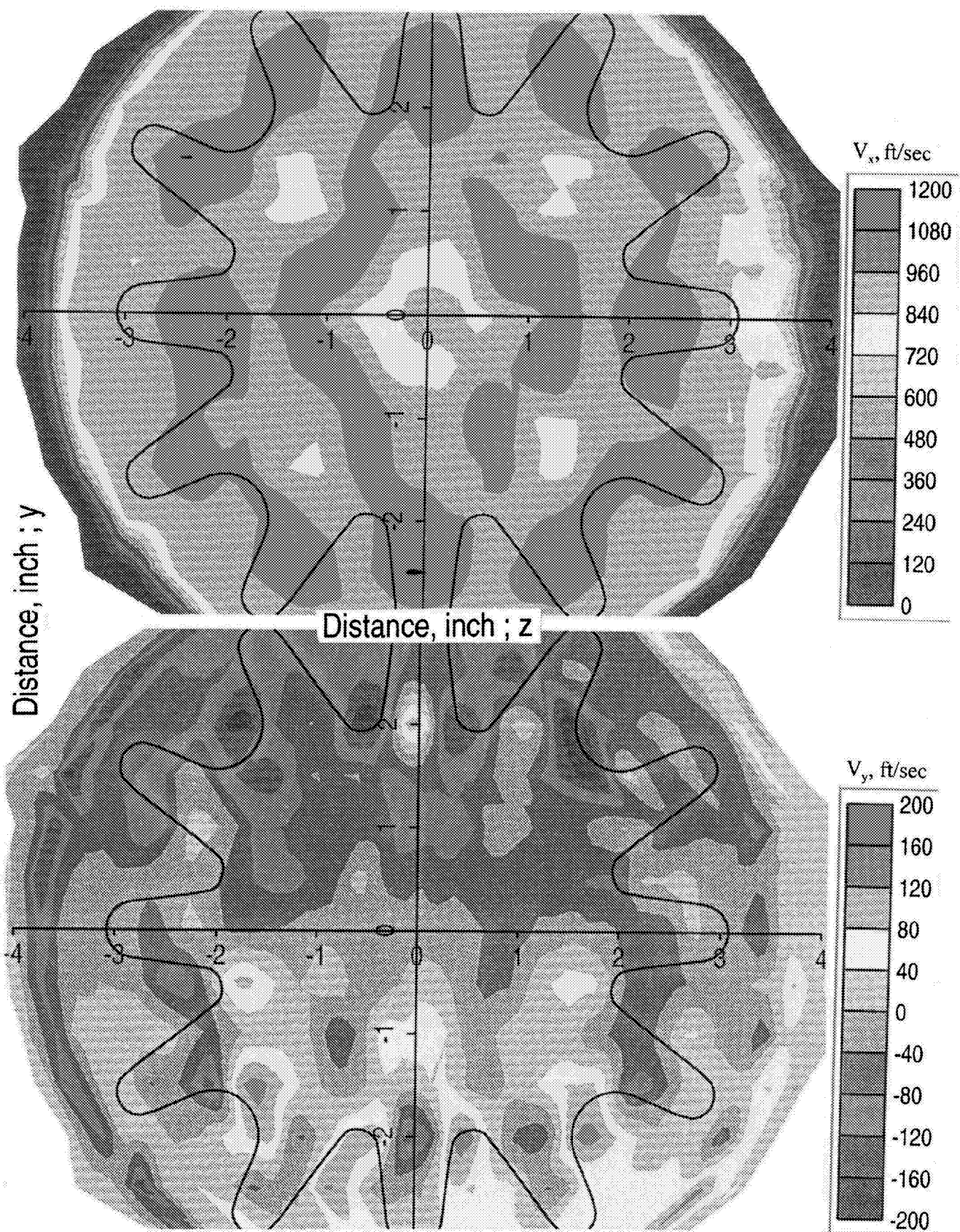


Figure 6.37. Axial ( $V_x$ ) and transverse ( $V_y$ ) velocity contours at the nozzle exit plane for the scalloped & staggered (F9B) for cycle condition 5 ( $V_{mix}=1000$  fps),  $M=0$ .

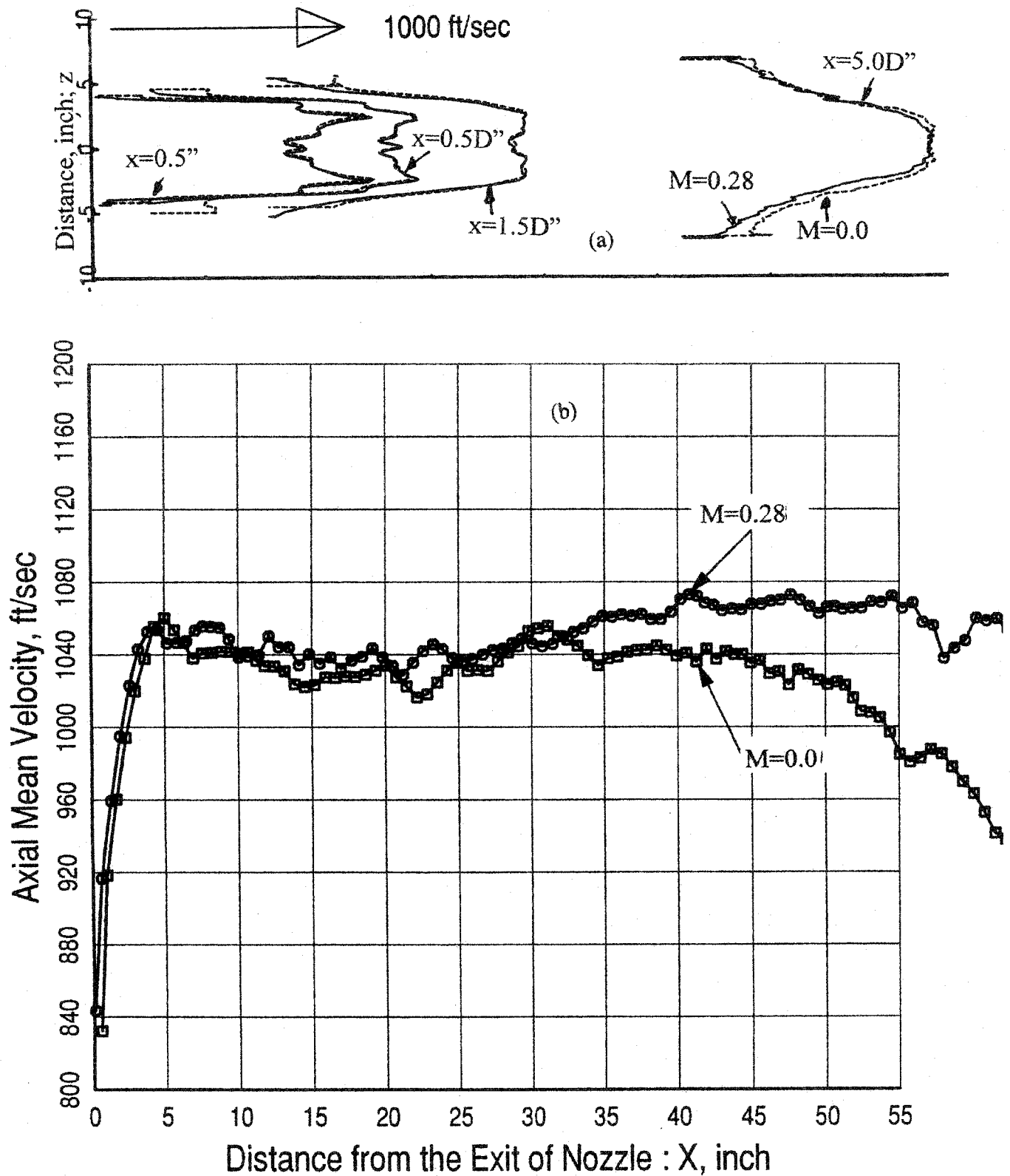


Figure 6.38. Effect of simulated flight on axial velocity distributions, (a) along z at several axial locations and (b) along x at the nozzle centerline, external to the nozzle exit for the scalloped & staggered (F9B) for cycle condition 5.



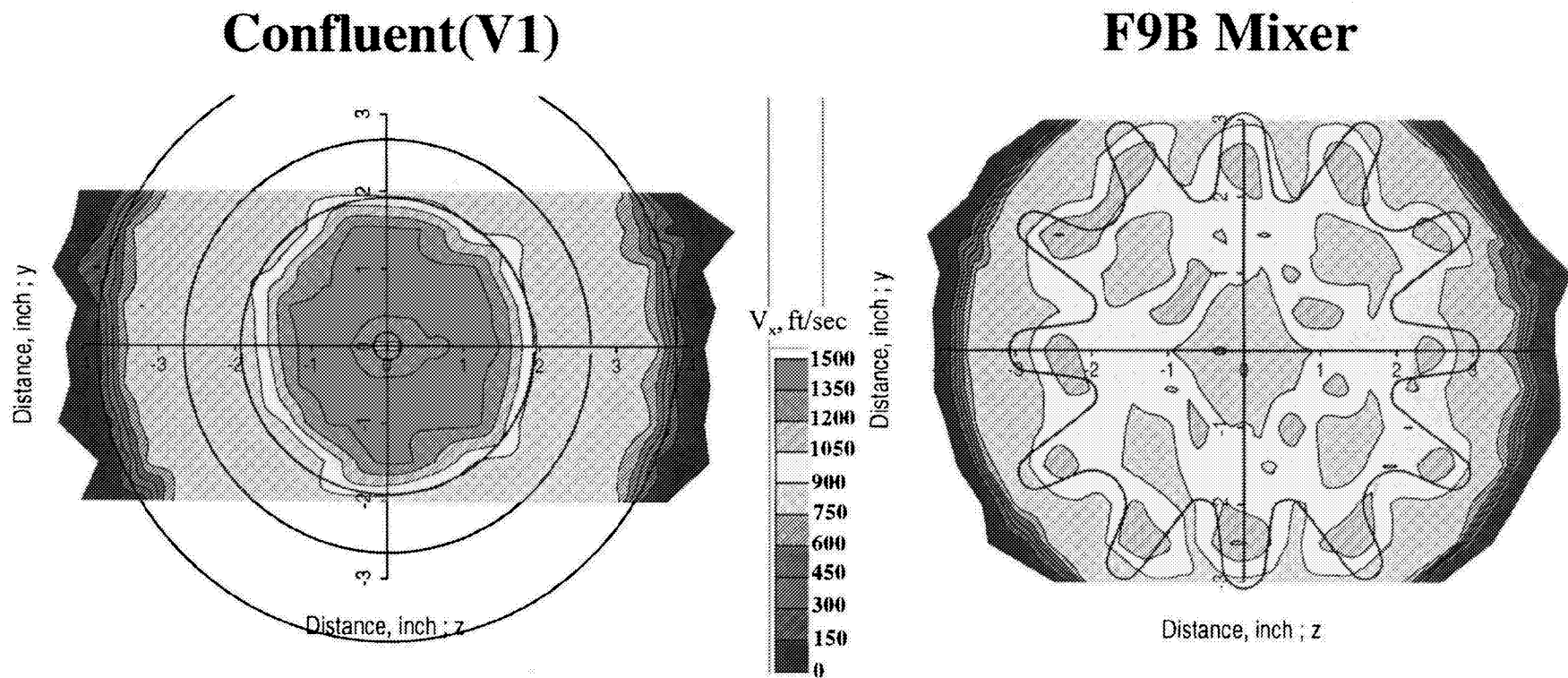


Figure 6.39. Comparison of axial ( $V_x$ ) velocity contours at 0.5" downstream of the nozzle exit plane between confluent (V1) and scalloped & staggered (F9B) mixers for cycle condition 5 ( $V_{mix}=1000$  fps),  $M=0$ .

confluent mixer. Thus, the mixing due to lobed mixer resulted in a more uniform and lower velocity, which, in turn resulted in a lower noise level.

### 6.3 Nozzle Exit Plane Velocity Comparison

Figures were made to plot measured velocities at a given axial distance vs. radial distance ( $r$ ) from the nozzle centerline. With this type of display, the vertical spread in data points is qualitatively indicative of the lobe-to-lobe variation in exit plane properties and the velocity distribution comparison between mixers can be made in one-dimensional space. Figure 6.40(a) shows the V1 mixer velocity distribution along the radial location with a Fourier curve fit. It can be seen that the data collapses fairly well as a curve  $V$  vs  $R$ , except in the range  $1.2 < r < 1.8$ , where considerable spread in the data is observed. This range corresponds to the axial projection of the separation region between the core and fan flows.

The velocity comparisons between the V1 mixer and other mixers are shown in Figures 6.40(b) through 6.40(e). For the V2 mixer considerable spread in the data is observed in the range  $2 < r < 3$ , which, corresponds to the axial projection of the lobe inner and outer diameters onto the exit plane. The corresponding velocities in this range shown in Figure 6.40(c) for V2A were lower than those of V2 due to the extended tailpipe. The F12A mixer has a higher velocity distribution than V2 or V2A in the radial range  $0 < r < 2$  due to the poor performance as a forced mixer (see Figure 6.40(d)). A considerable spread in the data ranging  $0.75 < r < 3.25$  is observed in the F9B mixer data as shown in Figure 6.40(e). This range corresponds to more than the axial projection of the lobe inner and outer diameters onto the exit plane.

### 6.4 Conclusions

Data have been presented to define the two dimensional flowfield generated by exhaust system mixers. In addition, the Laser Doppler Anemometer measurement technique has been successfully developed and adopted to acquire the present set of data from a scale model Energy Efficiency Engine (E<sup>3</sup>) Long Duct Mixed Flow (LDMF) exhaust system. The following observations can be made from the data presented here;

- The effects of the forced mixing and the tailpipe extension on the total temperature and pressure distributions are clearly captured.
- The internal velocity profiles show the effects of center plug on the velocity profiles and the process of vortex creation by lobes.
- These experimental data are being used to calibrate on-going CFD code development.

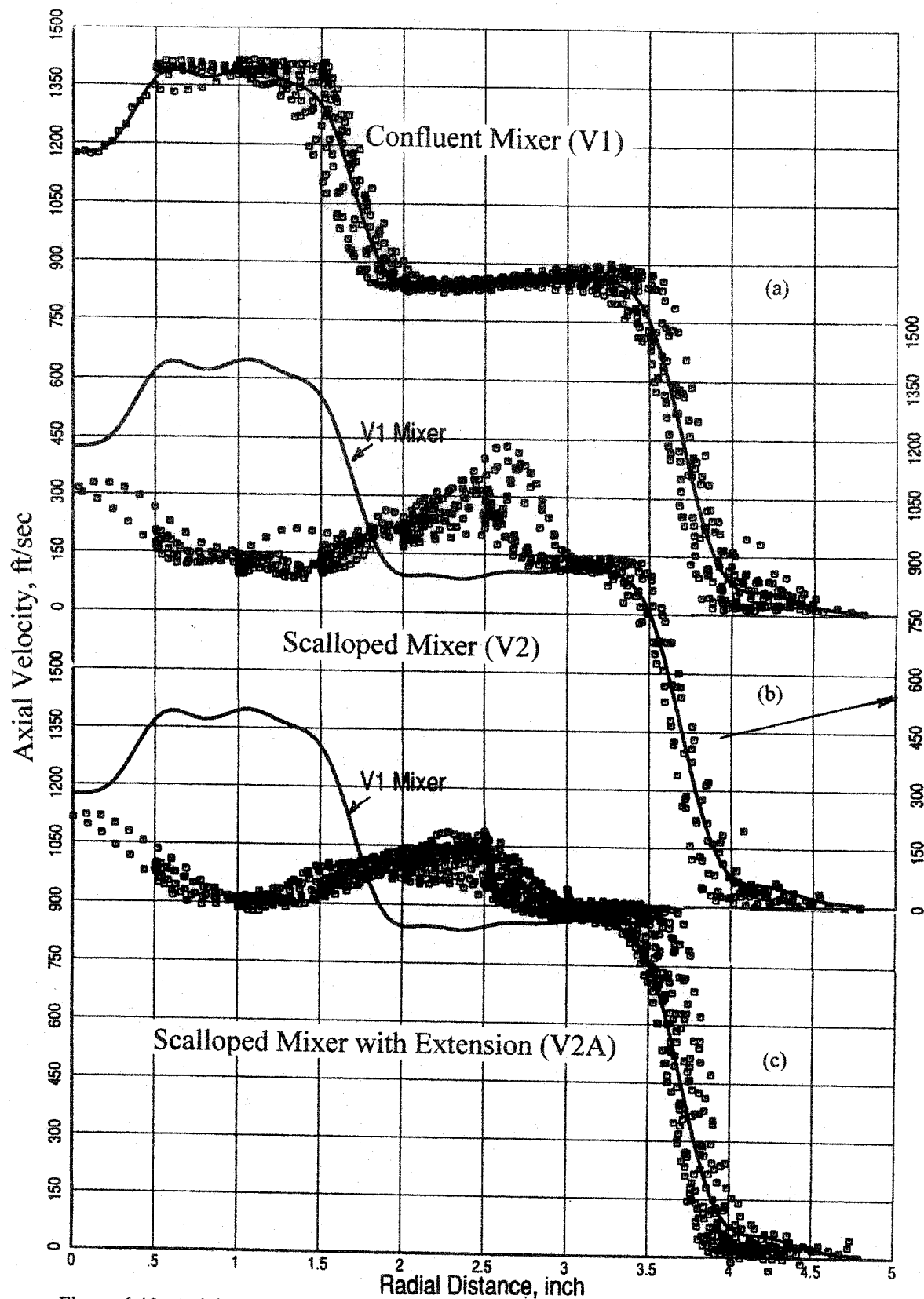


Figure 6.40. Axial velocity ( $V_x$ ) distribution along radial direction at different azimuthal angles for various mixer models for cycle condition 5 ( $V_{mix}=1000$  fps),  $M=0$ .

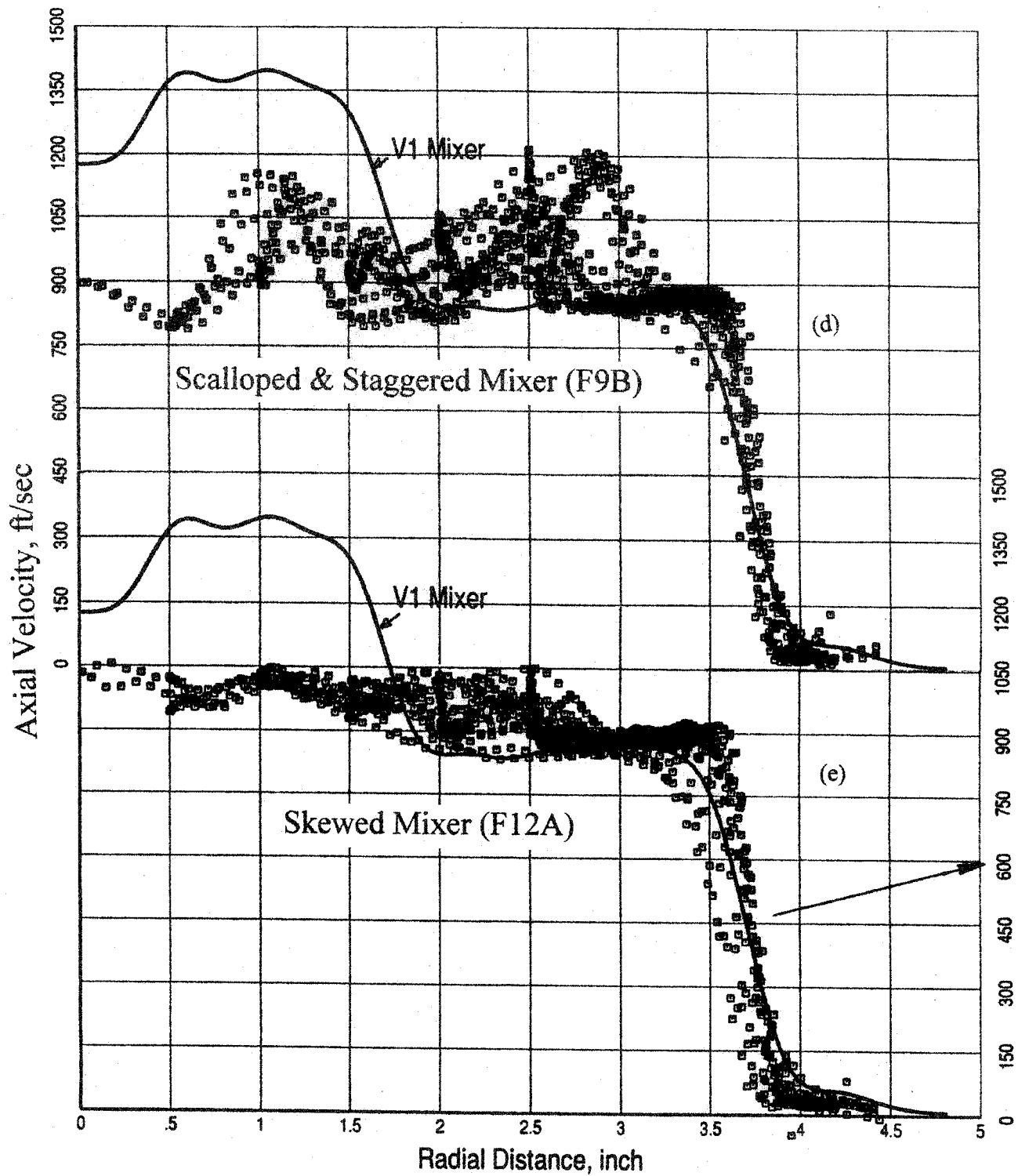


Figure 6.40. Axial velocity ( $V_x$ ) distribution along radial direction at different azimuthal angles for various mixer models for cycle condition 5 ( $V_{mix}=1000$  fps),  $M=0$  (concluded).

## 7.0 ANALYSIS COMPARED TO DATA

The jet noise prediction code for exhaust nozzles is called MGB. The CFD analysis code is PAB3D version 12. PAB3D is a fully three-dimensional Navier-Stokes code. The validation of PAB3D for exhaust system CFD analysis, both at GEAE and elsewhere, has been well documented. The PAB3D analysis algorithm is illustrated in Figure 7.1. The data base created from the mixer aero-acoustic testing will be used to refine the PAB3D multi-zone two-equation turbulence modeling scheme. The aerodynamic data will be used to develop and assess a general blending function that combines low and high Reynold's number forms of the two-equation linear turbulence model. The low Reynold's number form is to be applied close to the walls, the high Reynold's Number form in the mixing region. Also, an algebraic (non-linear) turbulence model shows promise and will be evaluated. Accurately capturing the mixing process analytically is key to providing reasonable boundary conditions to the MGB noise prediction program.

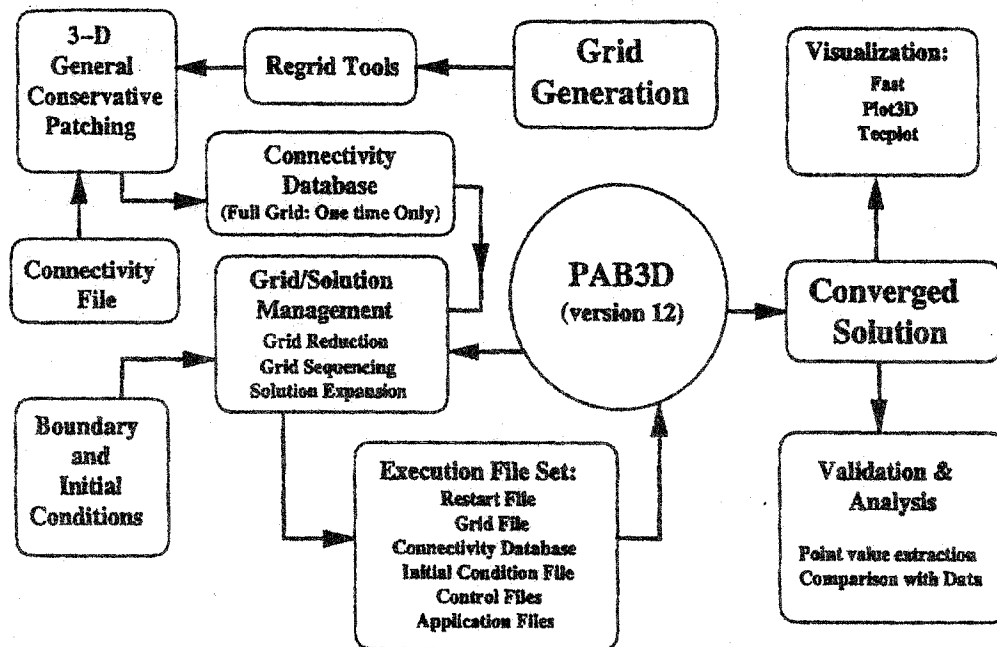
The MGB Noise prediction program, originally developed by GEAE, has been modified by NASA LeRC to accept flowfield data predicted by a CFD code. GEAE has further modified the MGB code to integrate it with the CFD-PAB3D flow solver. This aero-acoustic model is called, *MGB/PAB3D Integrated aero & acoustic Analysis (MPIA)*. The process flow chart of the MPIA prediction model is shown in Figure 7.2. The flow fields obtained from the PAB3D analysis are the inputs for the MGB jet noise analysis.

The noise modeling is performed in two steps. The first step adapts PAB3D predicted velocity, temperature, and turbulence intensity profiles at the exit plane of the mixer as starting conditions for the MGB aeroacoustic computations. By coupling the PAB3D flow fields with the MGB code, the noise generated by the internal mixing can be assessed. The second step adapts the PAB3D predicted external jet plume aerodynamics as well, rather than using the MGB aerodynamic mixing algorithms (based on Reichardt's momentum and enthalpy transport theory).

The first step provides the capability for studying mixer exit profile shape effects on the noise generation, and can provide some guidance on possible new mixer designs that may provide lower noise. The second step provides a more accurate simulation of the jet plume mixing characteristics. This two step approach, the PAB3D-MGB integrated model, will provide a useful design tool for developing low noise nozzle designs. The MGB model has been shown to predict external plume noise for a conic nozzle. The validity and applicability of the MGB model to predicting internal jet (mixing) noise, and the extent to which the internal noise is significant, remains to be demonstrated.

Pretest aero-flowfield predictions were completed in October of 1994. PAB3D, a computational fluid dynamic code developed by Analytic Service and Materials, Inc., was used to perform the analyses. Four configurations were analyzed; a confluent mixer, V1, two scalloped lobed mixers, ICLS / V2 & F8, and a "skewed" lobed mixer, F12A. These

## PAB3D (version 12): System Flow Chart



- **Navier–Stokes Upwind Schemes Up to Third–Order in Accuracy, Space Marching.**
- **Multi–Block and Multi–Zone Capabilities. Each Block Can be Solved Using Individually Specifiable Options.**
- **Turbulence Models Including Four Algebraic Formulations, Four  $k-\epsilon$  Models, and a Nonlinear Reynold’s Stress Model.**

Figure 7.1 CFD analysis process for exhaust nozzles with mixer using PAB3D.

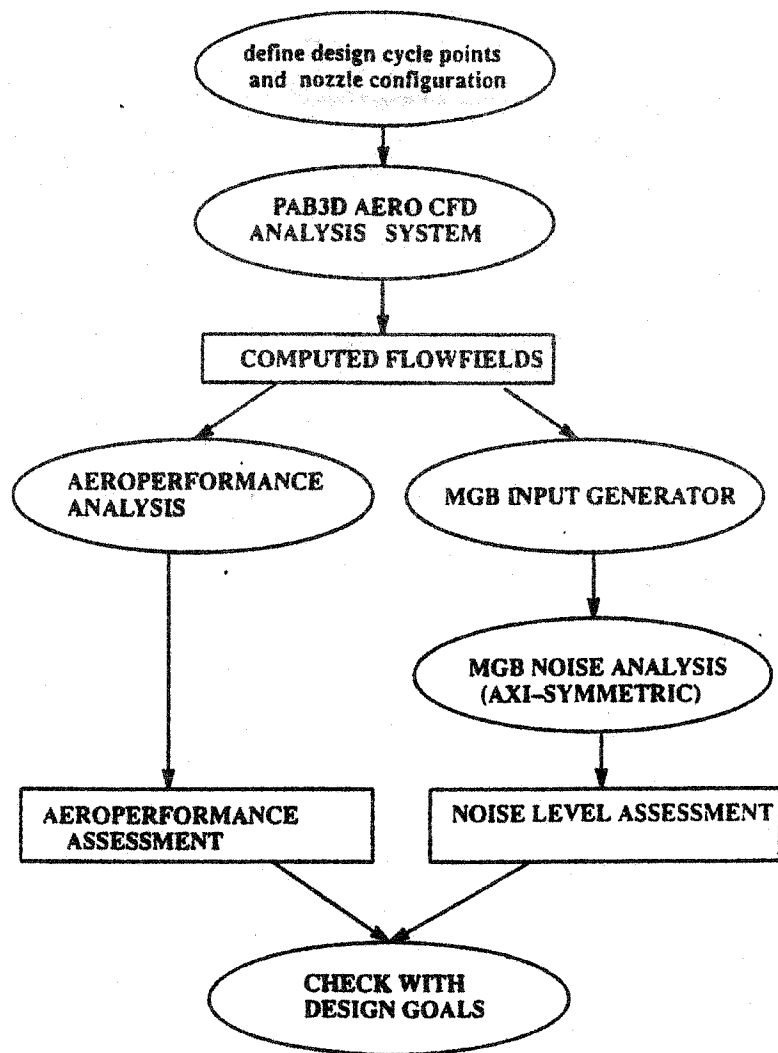


Figure 7.2. Unified aero & acoustic analysis model scheme for exhaust nozzles with mixer.

configurations were tested in the GE Cell 41 anechoic test facility for jet acoustics, flowfield velocities and turbulence intensities, surface pressures, and nozzle exit total pressure and temperature measurements. Acoustic and LDV results are presented in sections 5 and 6 of this report. The aero results are compared with the PAB3D pretest predictions and some of the comparisons are presented in this section..

Substantial amount of prediction and implementation work with the use of CFD tools, especially PAB3D, has been done by Khaled S. Abdol-Hamid of AS&M, a subcontractor to GEAE, with respect to pre-test and post-test of various mixer configurations. The outcome of this effort is presented in an informal report, "Implementation & Evaluation of Enhanced Multi-Zone Two-Equation Turbulence Model for PAB3D, Viscous Coupling Analysis for Three-Dimensional Square Duct & Scalloped (V2) Mixer, and Navier-Stokes Simulation of Three-Dimensional Mixer Flows."

### 7.1 CFD - PAB3D (Ps-Distribution)

Wall static pressure distributions have been compared to the PAB3D pretest predictions for the confluent and two scalloped lobed mixer configurations. Figure 7.3 displays results for the confluent and the ICLS / V2 lobed mixer configurations. Wall static pressures are presented along the fan outer diameter, cowl (fan side), and plug. Figure 7.3(a) shows good agreement between the test data and PAB3D analysis. The analysis, however, does tend to deviate from the test data downstream of axial station 172. It has been determined that the gridding of the plug tip was incorrect. This has been revised for subsequent analyses. For the ICLS / V2 lobed mixer configuration the PAB3D pretest predictions compare very well with the Cell 41 test data. It is apparent in Figure 7.3(b) that the core stream test conditions are not consistent with the pretest predictions, however, the trends match very well. It should also be noted that there are two separate analysis lines designated "Plug". One line is along a mixer crown plane while the other line is along a mixer keel plane, as are the plug pressure measurements.

The final wall static pressure comparisons are for the scalloped lobed mixer configuration, F8. The F8 configuration is instrumented along the mixer crown and keel in addition to the fan outer diameter, cowl, and plug. Figure 7.4(a) shows pretest predictions compared to Cell 41 test data along the fan outer diameter, cowl (fan side), plug, and along the mixer lobes. Once again, there is excellent agreement between the test data and analysis. For clarity, the data along the mixer lobe crown and keel cuts have been isolated and compared to the PAB3D analysis in Figure 7.4(b). The agreement is extremely good considering the complexity of the geometry being modeled.

### 7.2 CFD - PAB3D (Exit PT & TT Profiles)

Exit *total pressure* and *total temperature* measurements have been compared to the PAB3D predictions for the confluent configuration, V1, the ICLS-V2 and -V2A scalloped lobed mixer configurations (nominal tailpipe and tailpipe extension), and the "skewed" mixer, F12A. Figure 7.5 compares the normalized *radial* total temperature



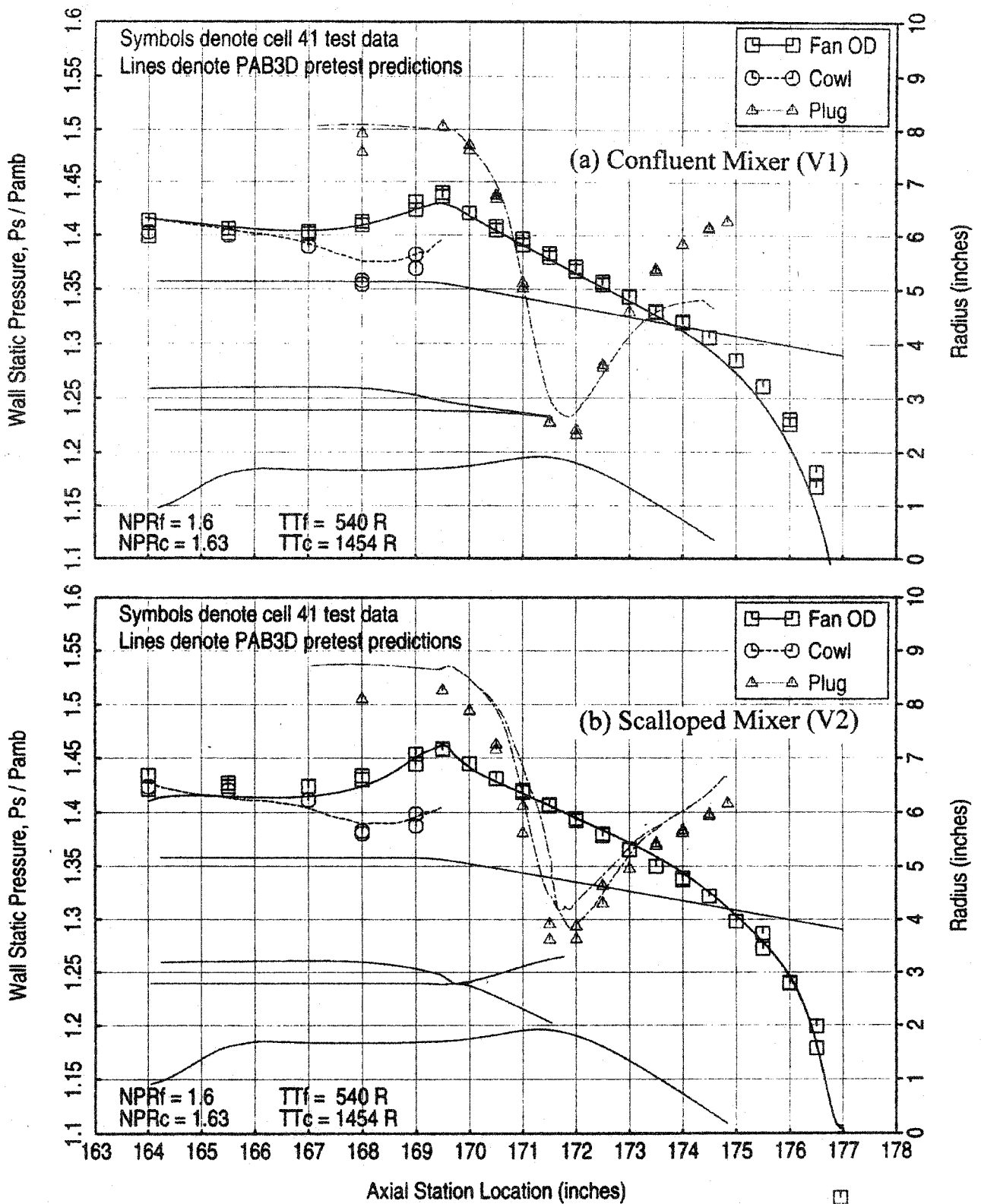


Figure 7.3. Wall static pressure comparisons between measured data and prediction for exhaust system with (a) confluent (V1) and (b) scalloped (V2) mixers for cycle condition 5 ( $V_{mix}=1000 \text{ fps}$ ),  $M=0$ .

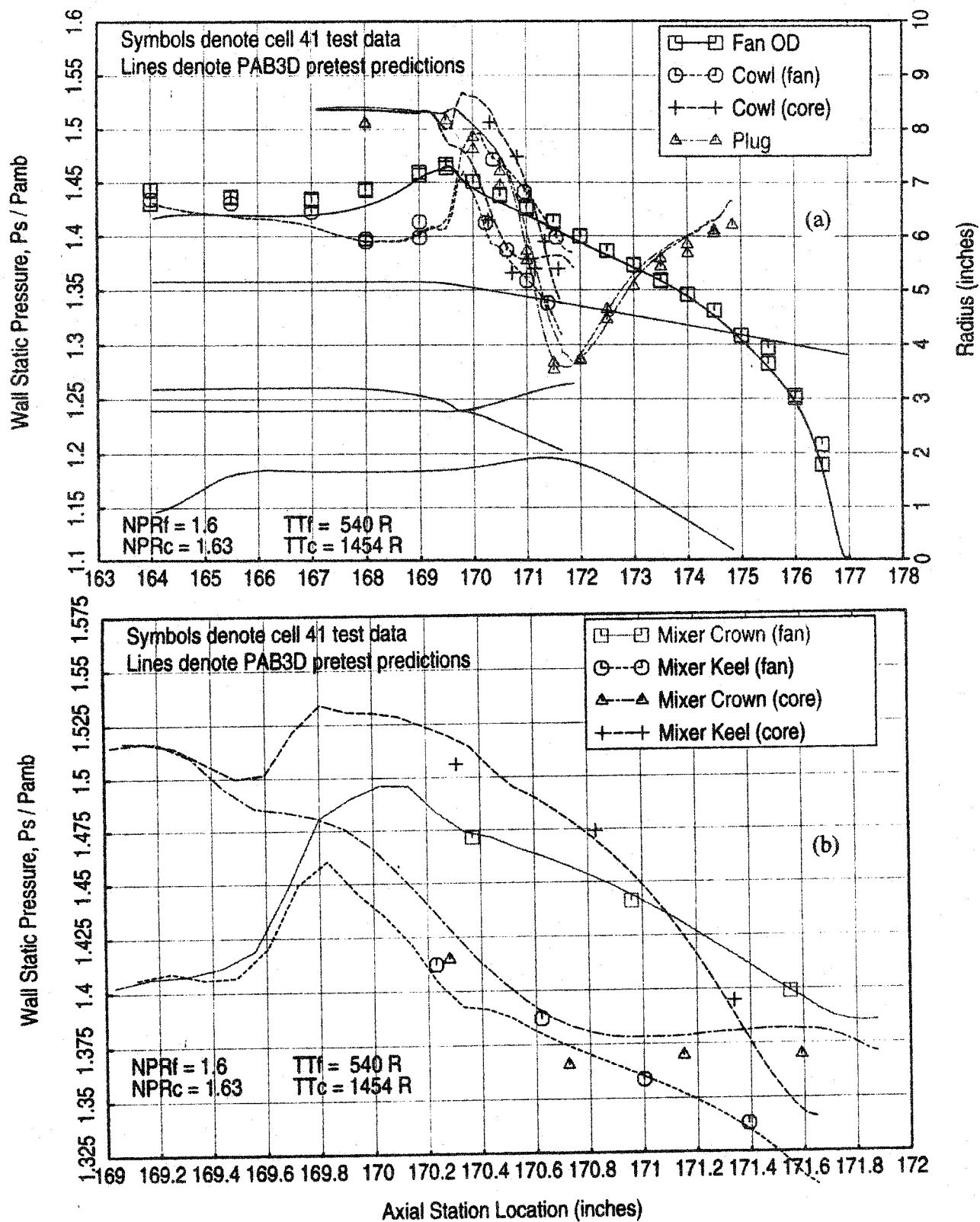


Figure 7.4. Wall static pressure comparisons between measured data and prediction for exhaust system with the scalloped mixer (F8) for cycle condition 5 ( $V_{mix} = 1000 \text{ fps}$ ),  $M = 0$ .

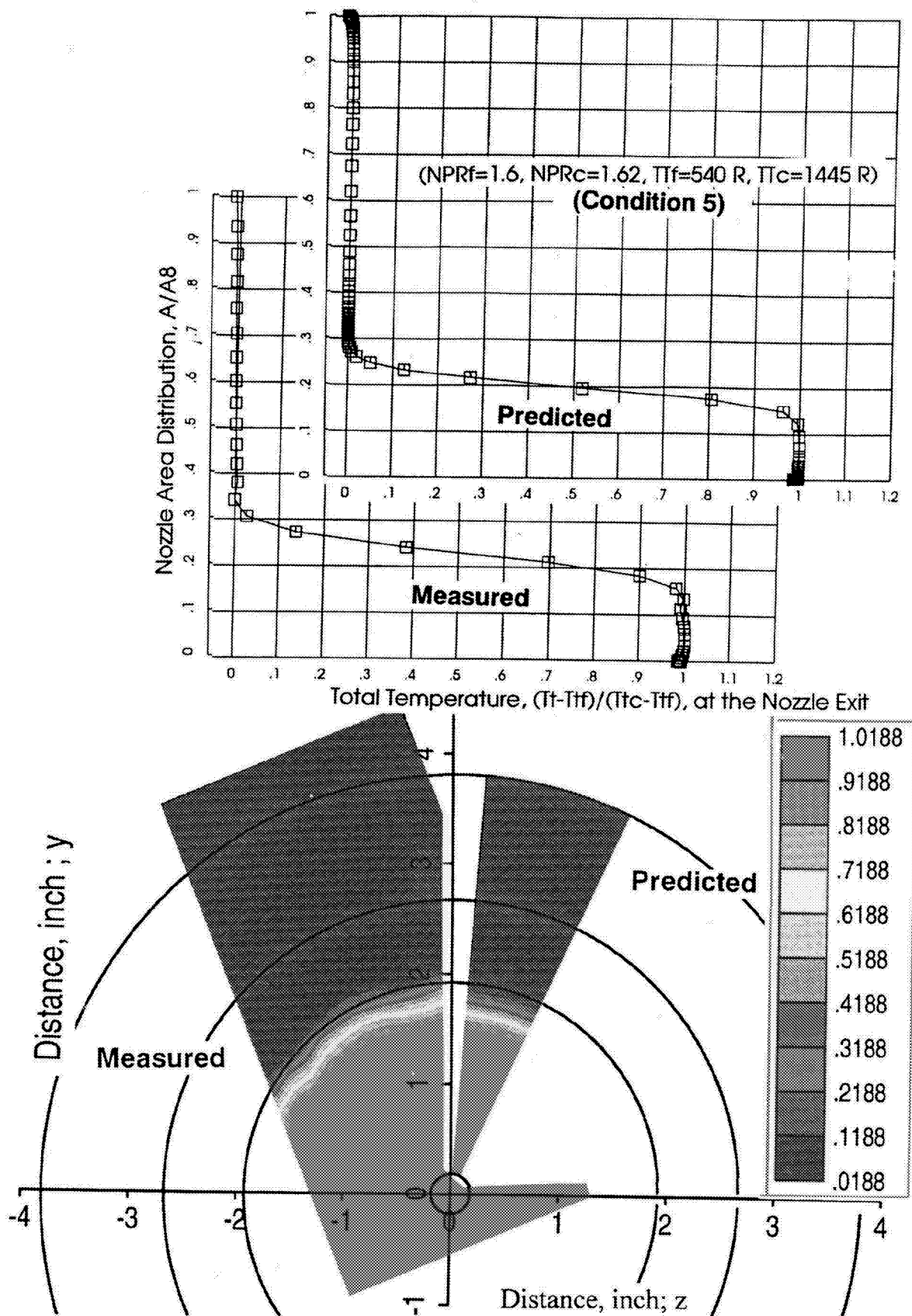


Figure 7.5. Comparisons of non dimensional total temperature distribution and contours between measured data and prediction at the exit plane for the confluent mixer (V1) for cycle condition 5 ( $V_{mix}=1000$  fps),  $M=0$ .

profiles and contour plots for the V1-confluent configuration. Corresponding normalized pressure results are plotted in Figure 7.6. The PAB3D predictions agree reasonably well with the measured test data.

Exit survey comparisons for the ICLS-V2 nominal tailpipe lobed mixer configuration are shown in Figures 7.7 and 7.8. The comparison of normalized total pressure is in reasonable agreement. The comparison of normalized total temperature, however, displays large discrepancies between the analysis and test data. The analysis predicts less mixing in comparison to the test data.

The ICLS-V2 tailpipe extension configuration shows similar analysis to data comparison. Normalized total temperature and total pressure data are compared to analysis in Figures 7.9 and 7.10, respectively. Once again, the analysis under predicts mixing.

Data and analysis exit survey comparisons for configuration F12A are shown in Figures 7.11 and 7.12. In general, the total pressure data is in good agreement with the pretest predictions. The trend of under predicting mixing, however, persists.

These data will be combined with the LV data of measured mean velocities and turbulence intensities and used to improve the turbulence modeling routines in the CFD mixed-flow modeling.

### **7.3 Flowfield Mean and Turbulent Velocities**

Axial velocity component measurements have been compared to the PAB3D predictions for the confluent configuration (V1), the ICLS scalloped lobe mixer configurations (V2 and V2A), and the skewed mixer configuration (F12A). The axial velocity contour comparisons are made by drawing CFD results in the first quadrant only and LDA data in the remaining three quadrants.

#### **7.3.1 Confluent Mixer (V1) Velocity Data Comparison.**

The axial velocity comparison between CFD results and LDA data for the V1 configuration is shown in Figure 7.13. The figure shows reasonable agreement between them. The velocity distribution comparisons along the radial direction at various locations downstream of the nozzle are shown in Figure 7.14. Again, the comparisons indicate reasonable agreement.

#### **7.3.2 ICLS Scalloped Lobe Mixer (V2) Velocity Data Comparison.**

The axial velocity comparison between CFD results and LDA data for the V2 configuration is shown in Figure 7.15. The comparison of color contour of axial velocity displays discrepancies between the analysis and test data. The analysis predicts less mixing in comparison to test data. However, the size and location of the mushroom where

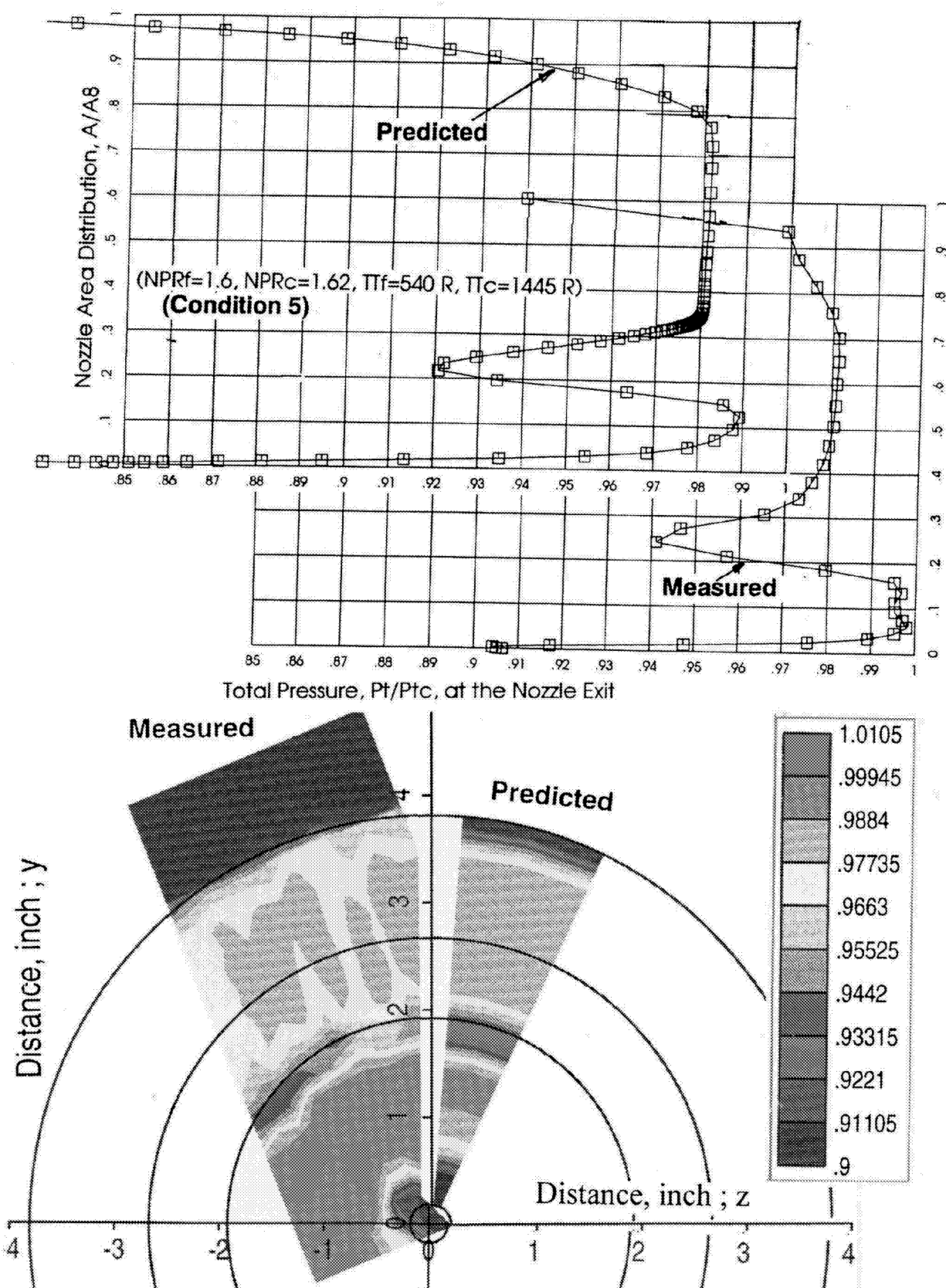


Figure 7.6. Comparisons of non dimensional total pressure distribution and contours between measured data and prediction at the exit plane for the confluent mixer (V1) for cycle condition 5 ( $V_{mix}=1000$  fps),  $M=0$ .

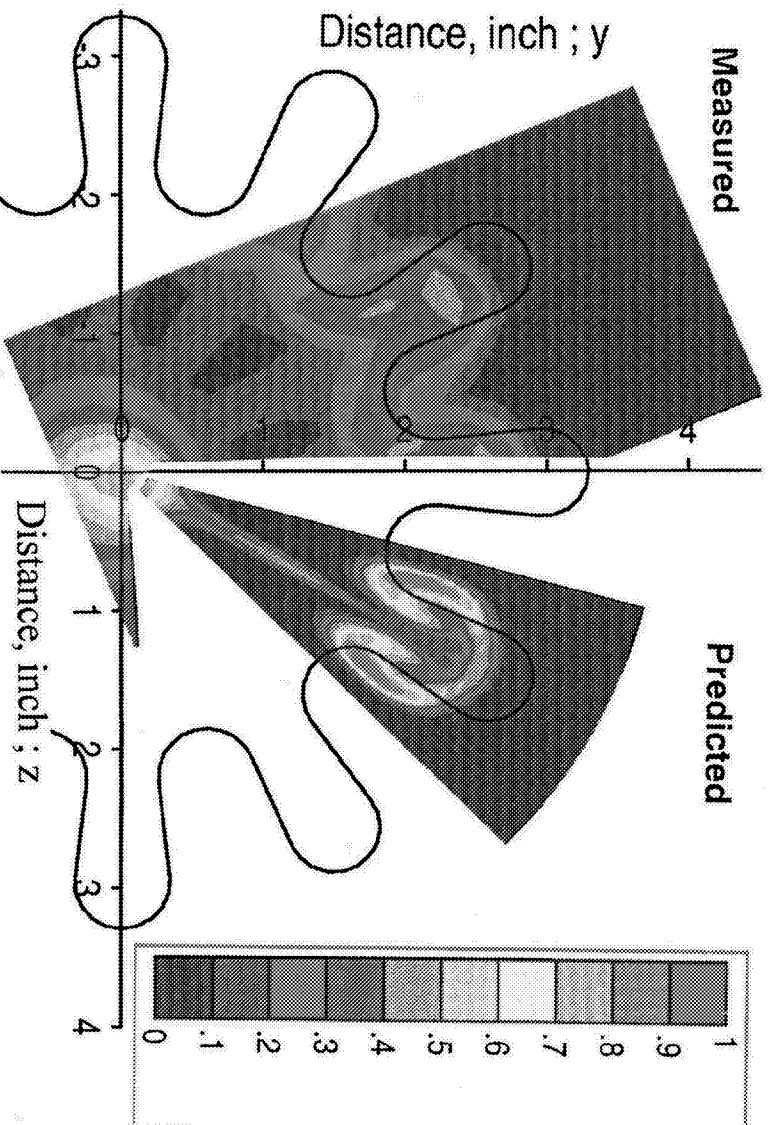
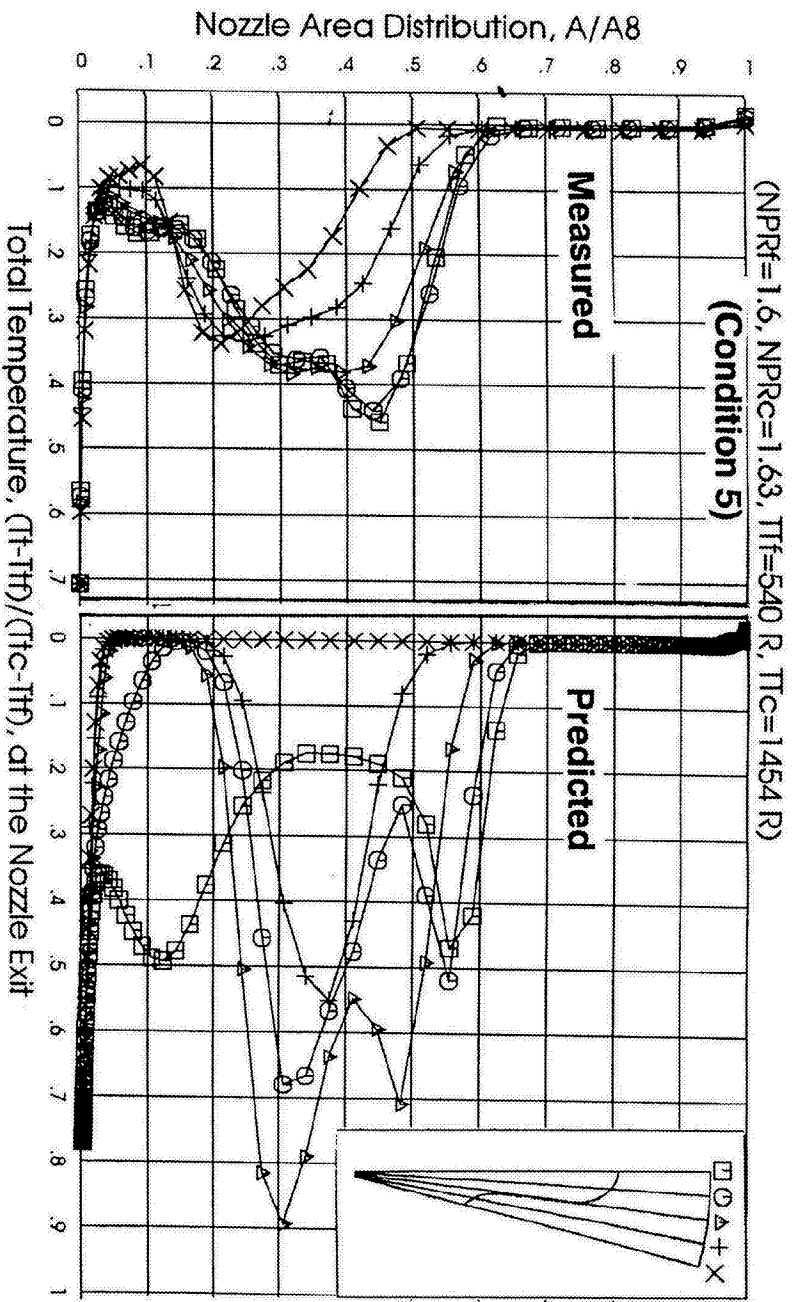


Figure 7.7. Comparisons of non dimensional total temperature distribution and contours between measured data and prediction at the exit plane for the scalloped mixer (V2) for cycle condition 5 ( $V_{mix}=1000$  fps),  $M=0$ .

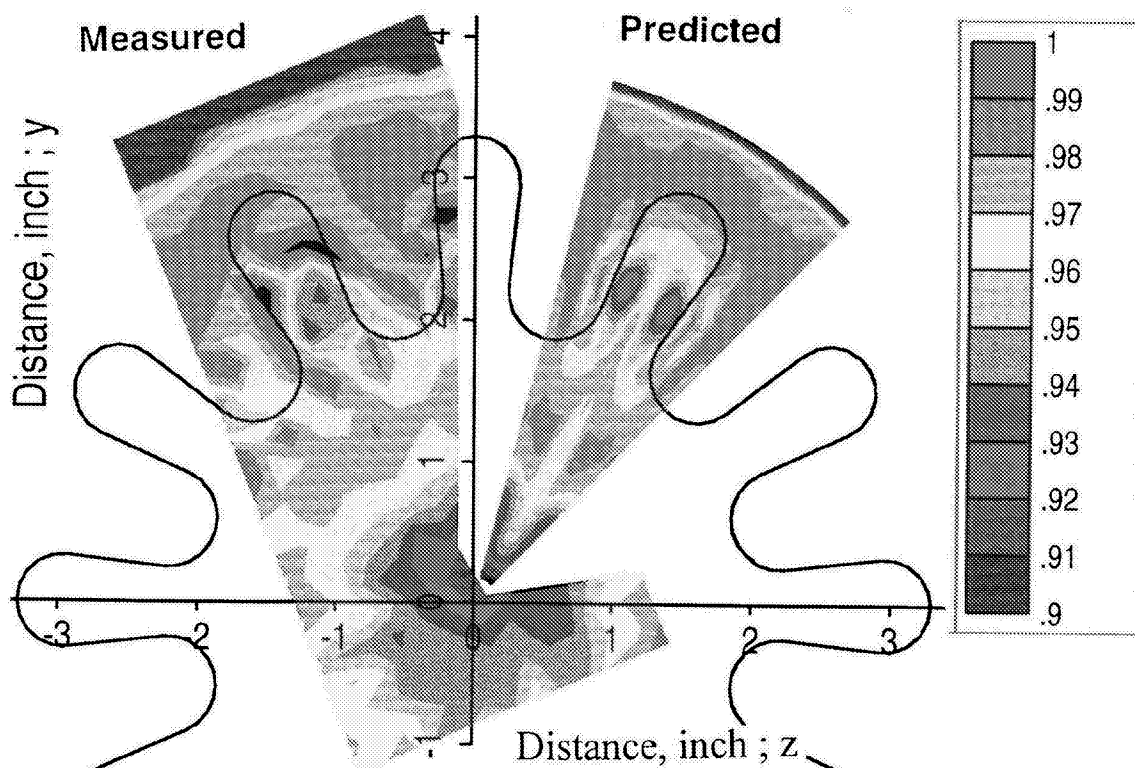
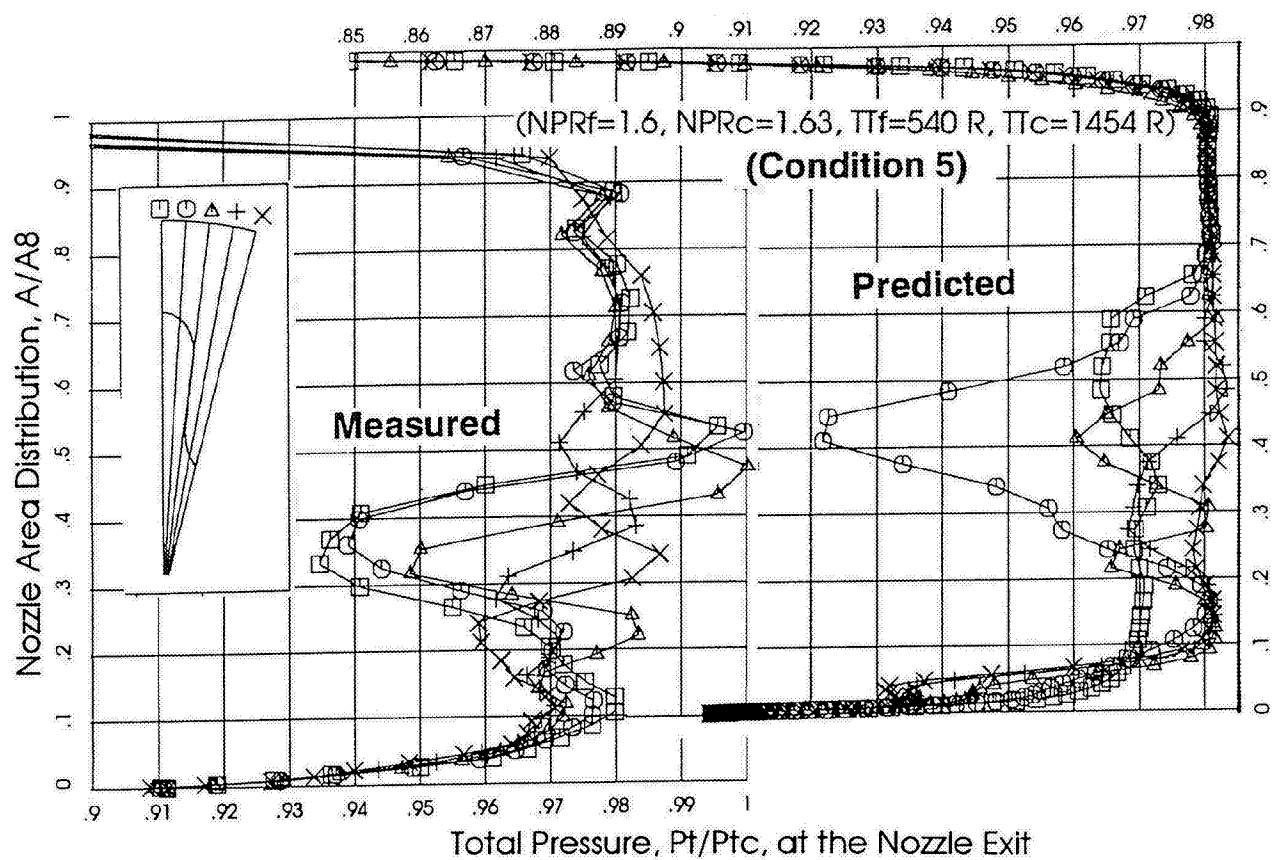


Figure 7.8. Comparisons of non dimensional total pressure distribution and contours between measured data and prediction at the exit plane for the scalloped mixer (V2) for cycle condition 5 ( $V_{mix}=1000 \text{ fps}$ ),  $M=0$ .

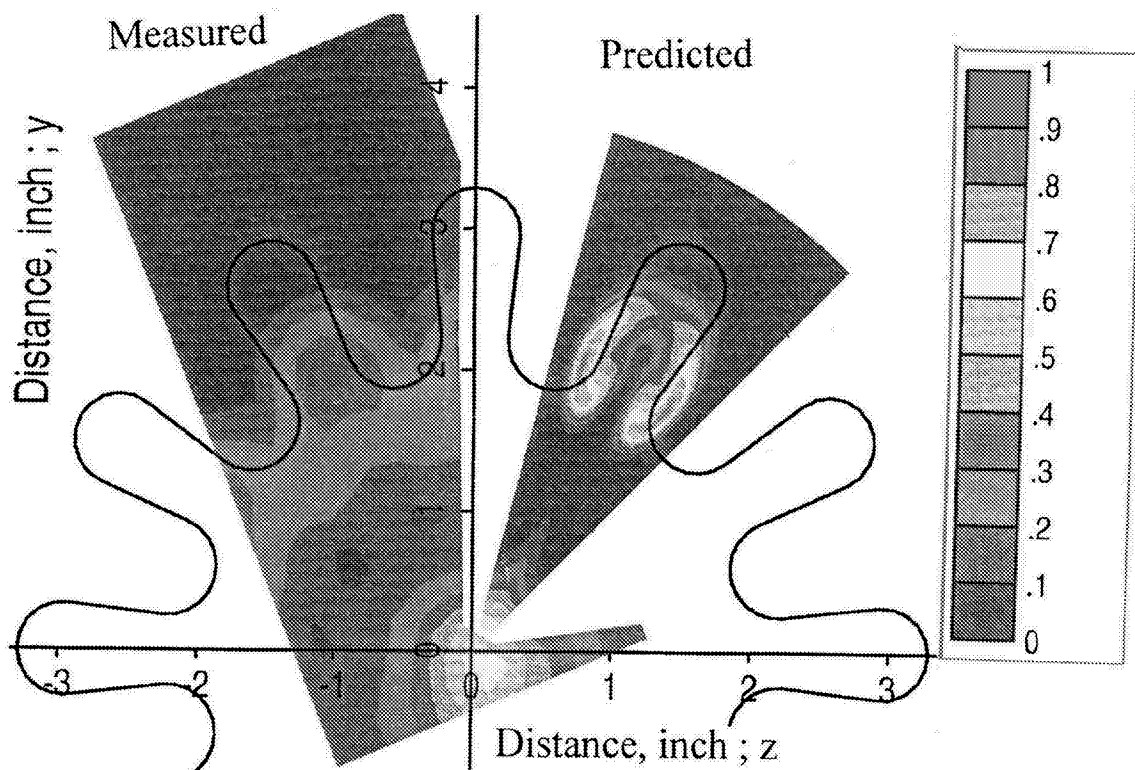
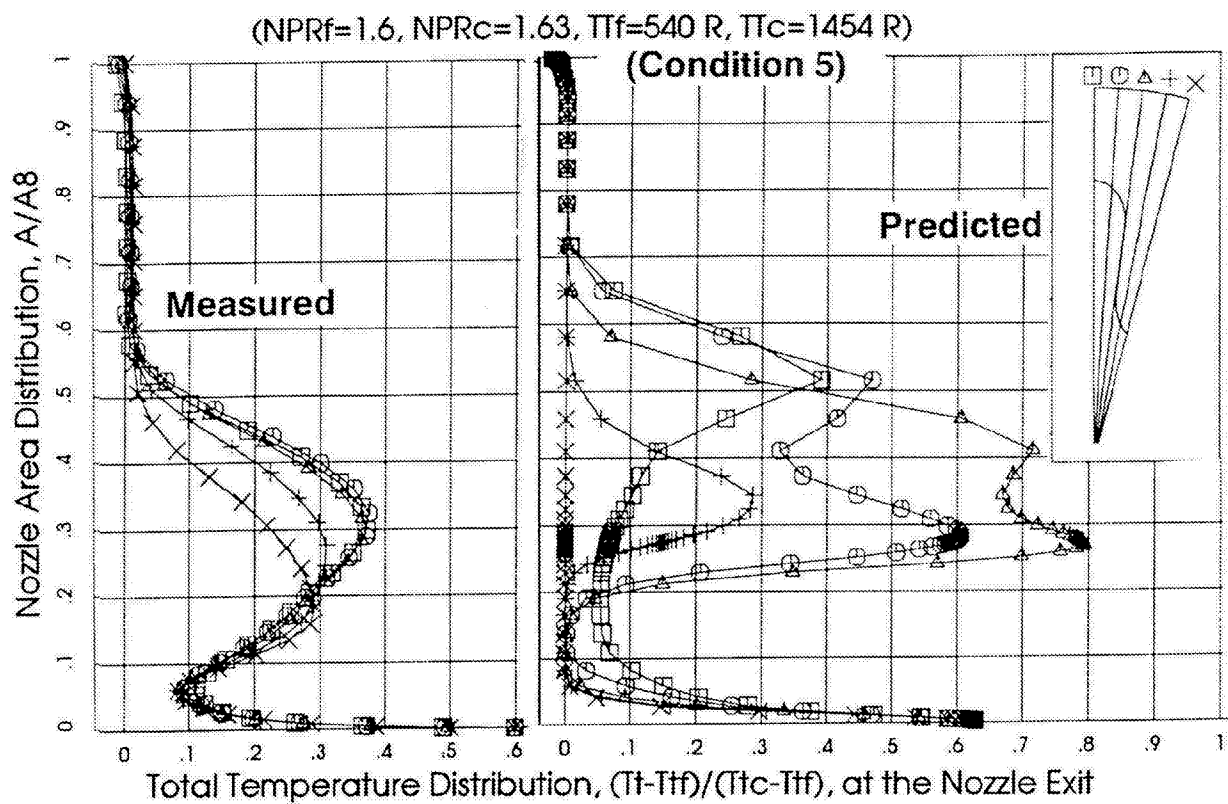


Figure 7.9. Comparisons of non dimensional total temperature distribution and contours between measured data and prediction at the exit plane for the scalloped mixer with extension (V2A) for cycle condition 5 ( $V_{mix}=1000$  fps),  $M=0$ .



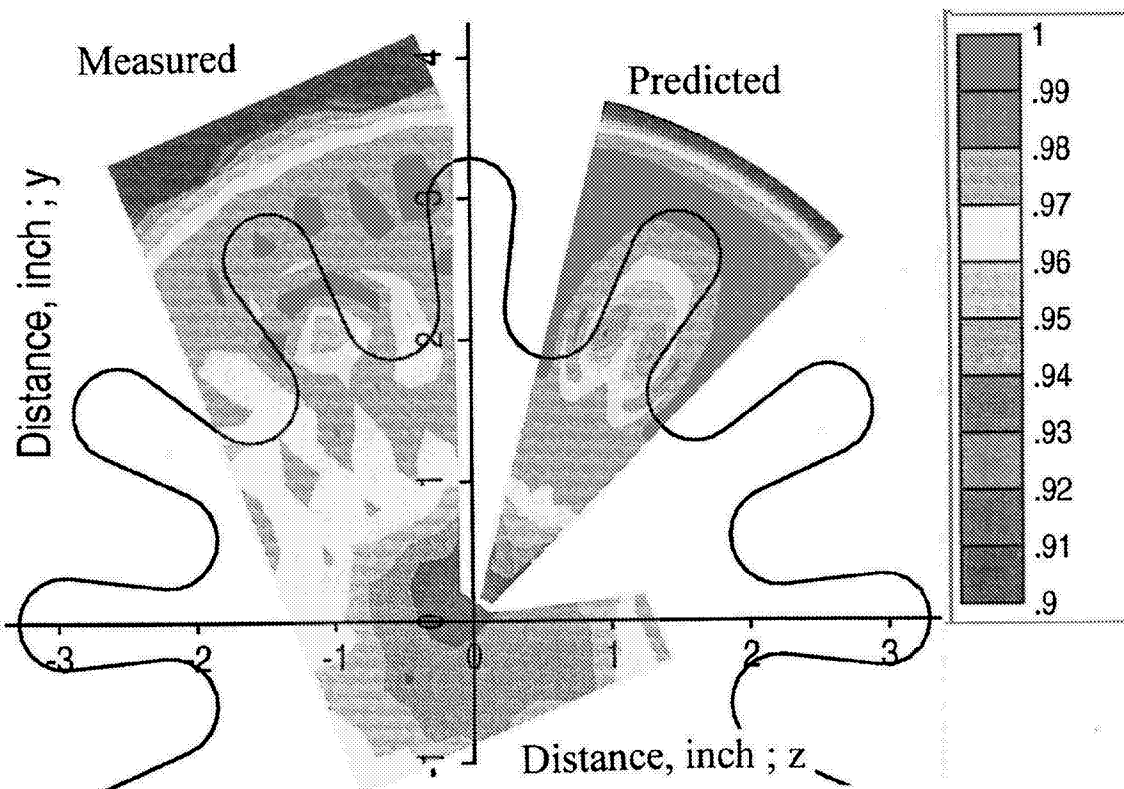
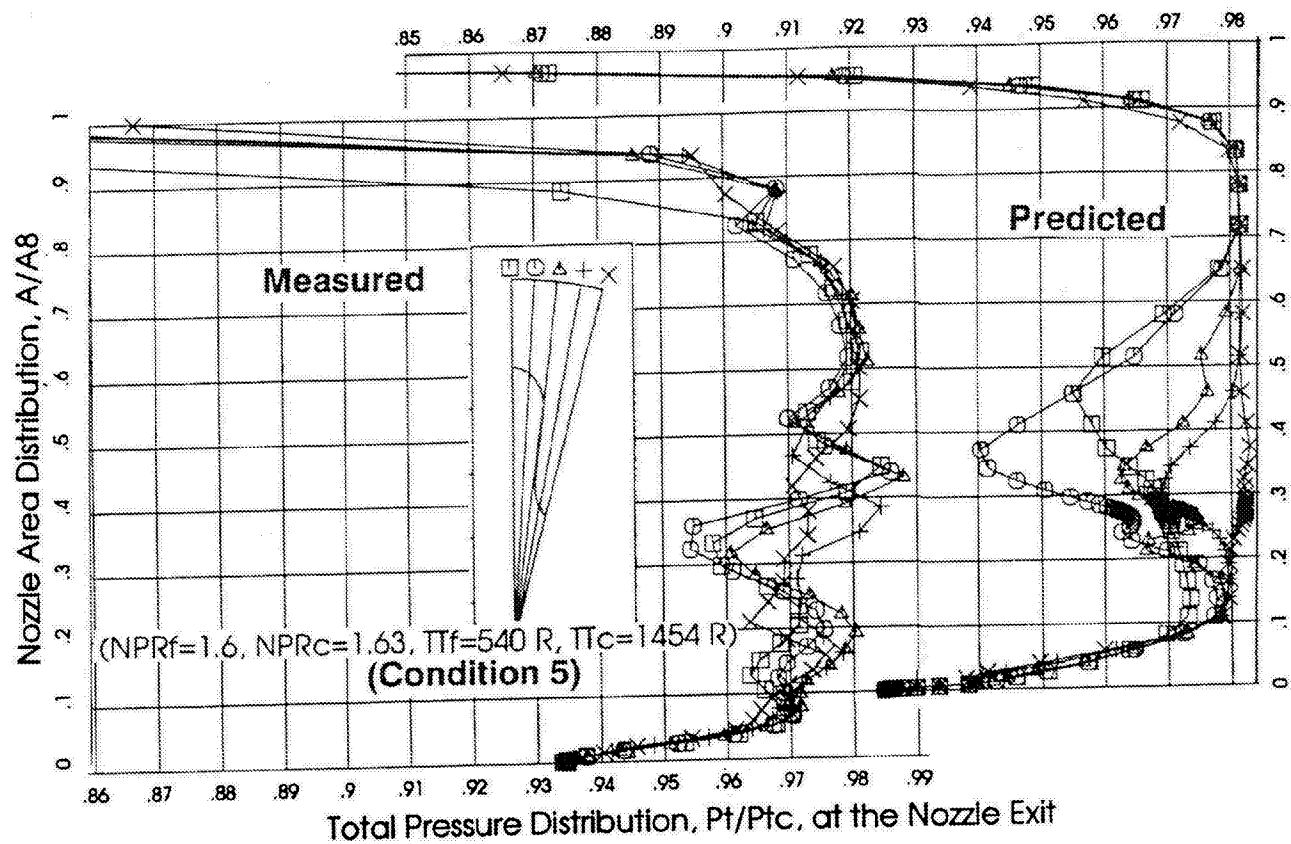


Figure 7.10. Comparisons of non dimensional total pressure distribution and contours between measured data and prediction at the exit plane for the scalloped mixer with extension (V2A) for cycle condition 5 ( $V_{mix}=1000$  fps),  $M=0$ .

(NPR=1.6, NPRc=1.63,  $Tf=540\text{ R}$ ,  $Tc=1454\text{ R}$ )  
(Condition 5)

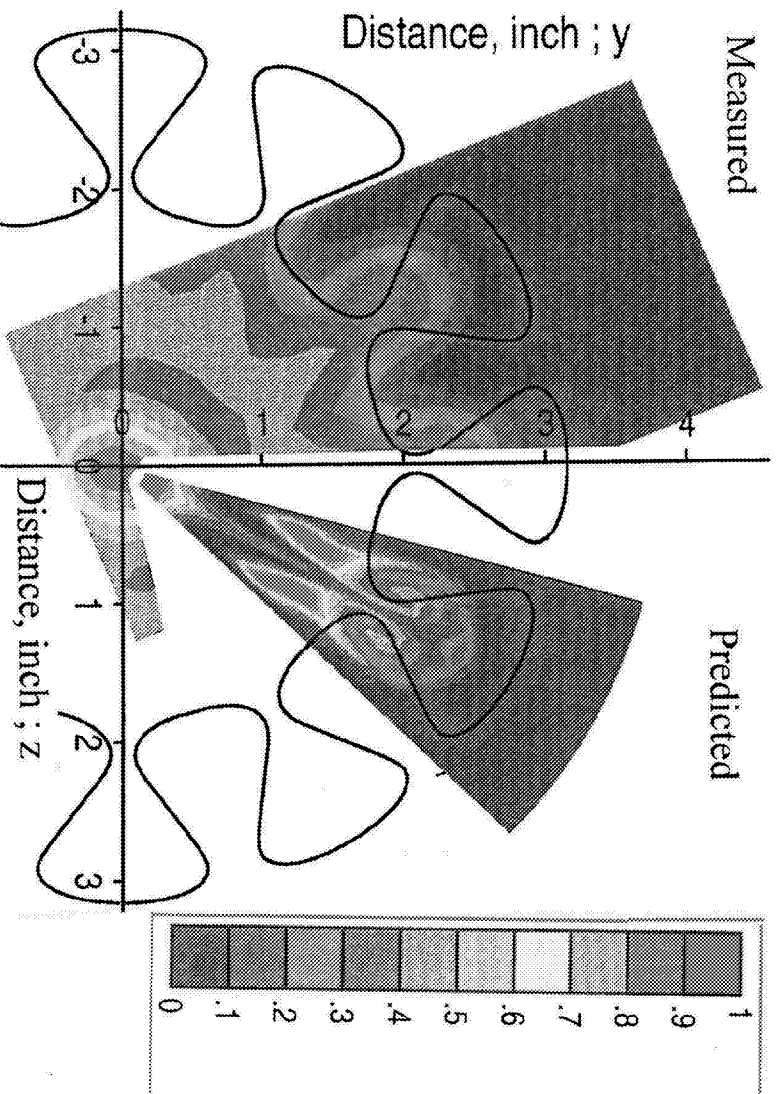
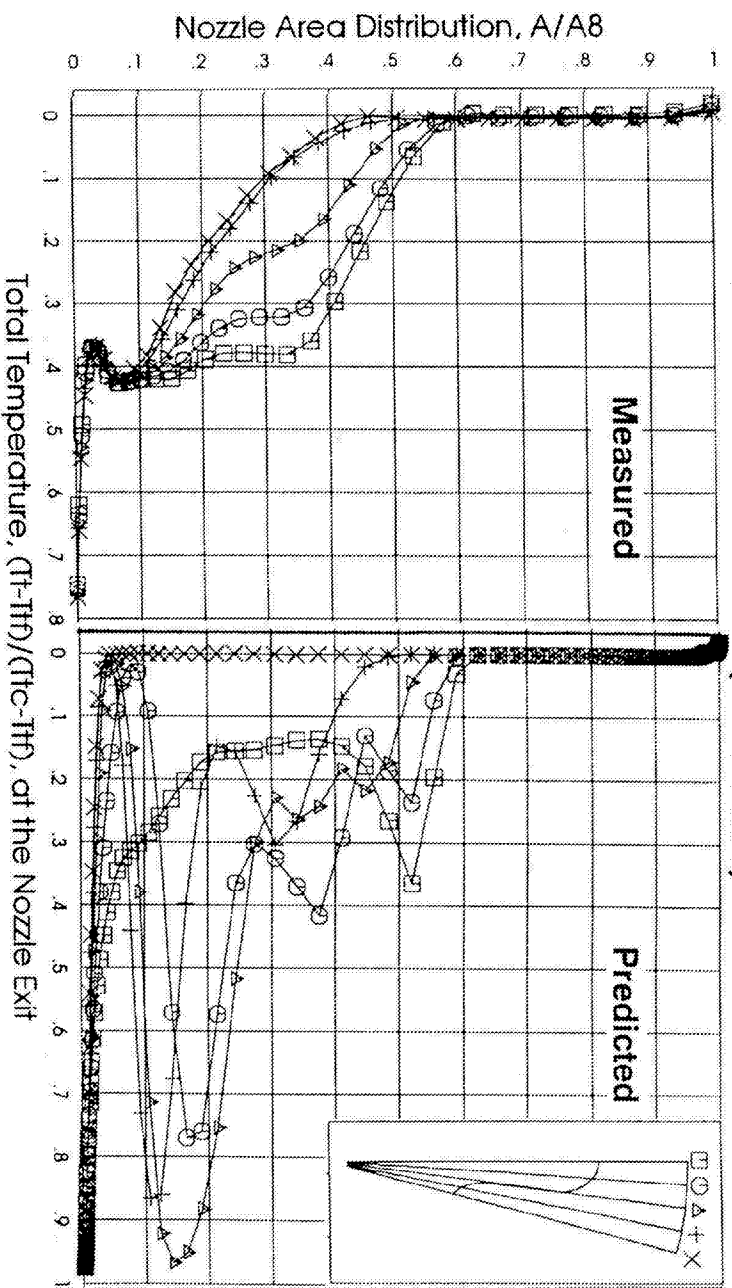


Figure 7.11. Comparisons of non dimensional total temperature distribution and contours between measured data and prediction at the exit plane for the skewed lobed mixer (F12A) for cycle condition 5 ( $V_{mix}=1000\text{ fps}$ ),  $M=0$ .

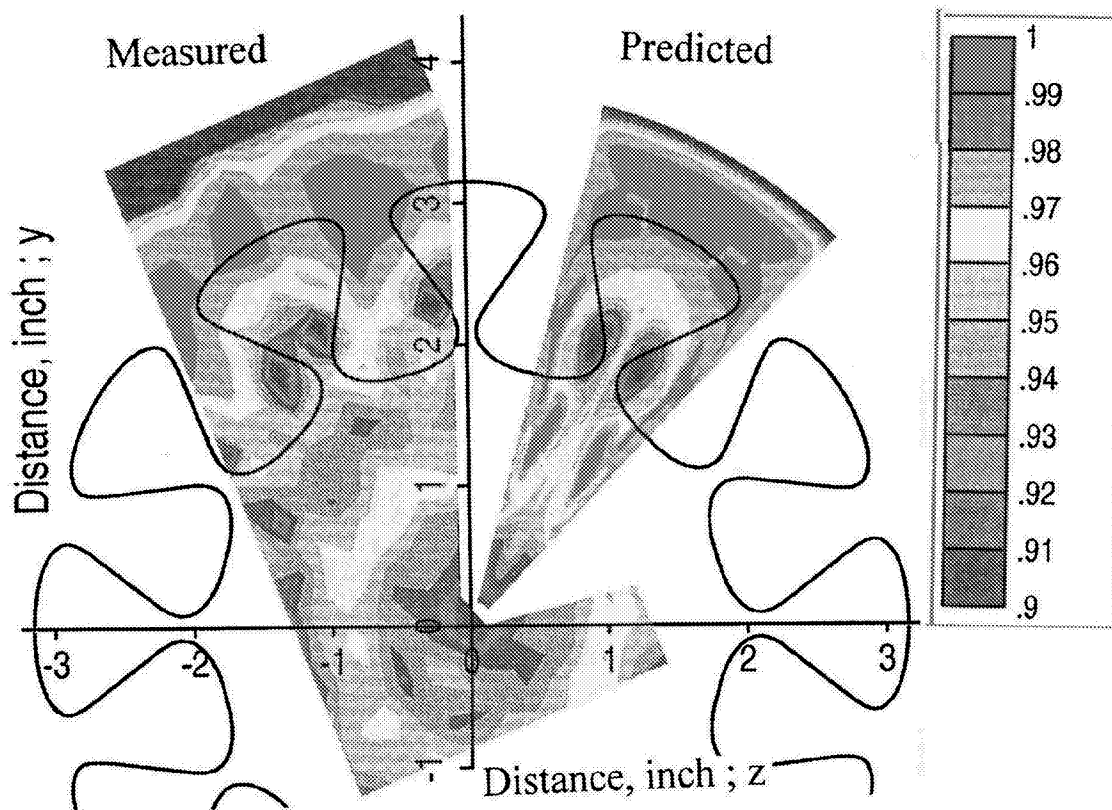
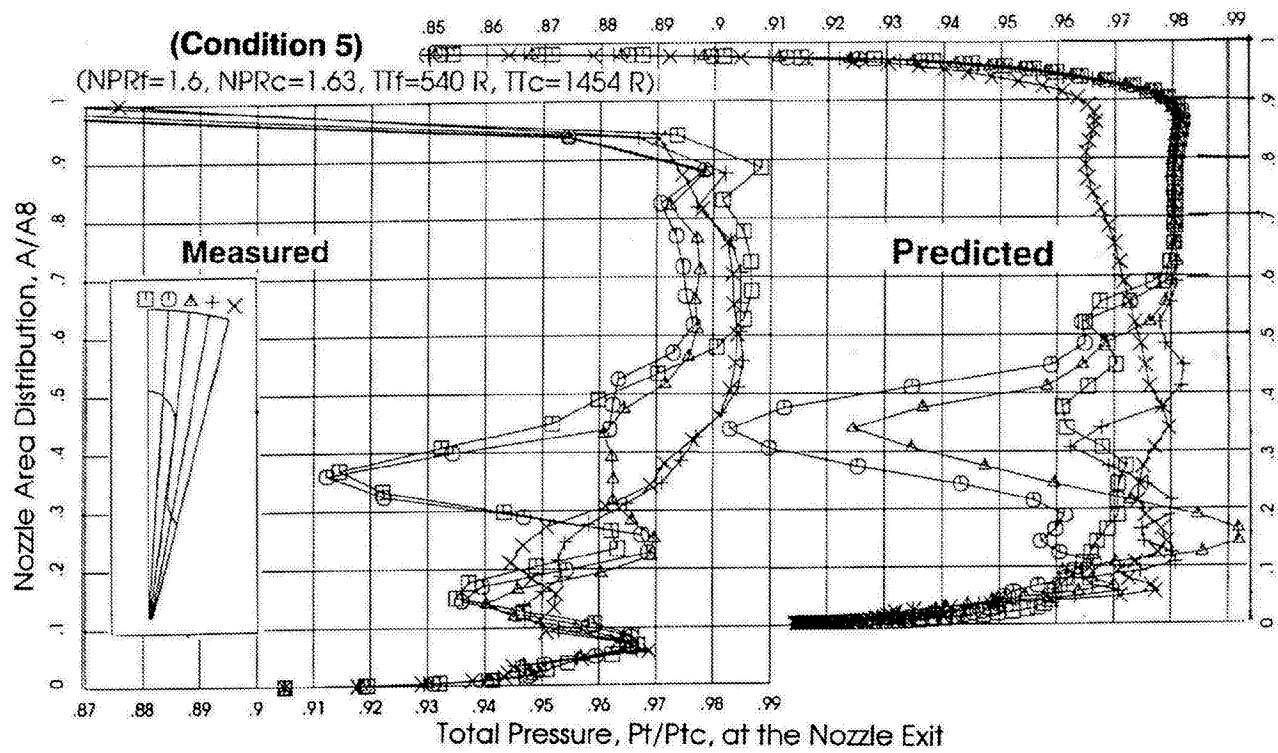


Figure 7.12. Comparisons of non dimensional total pressure distribution and contours between measured data and prediction at the exit plane for the skewed lobed mixer (F12A) for cycle condition 5 ( $V_{mix}=1000$  fps),  $M=0$ .

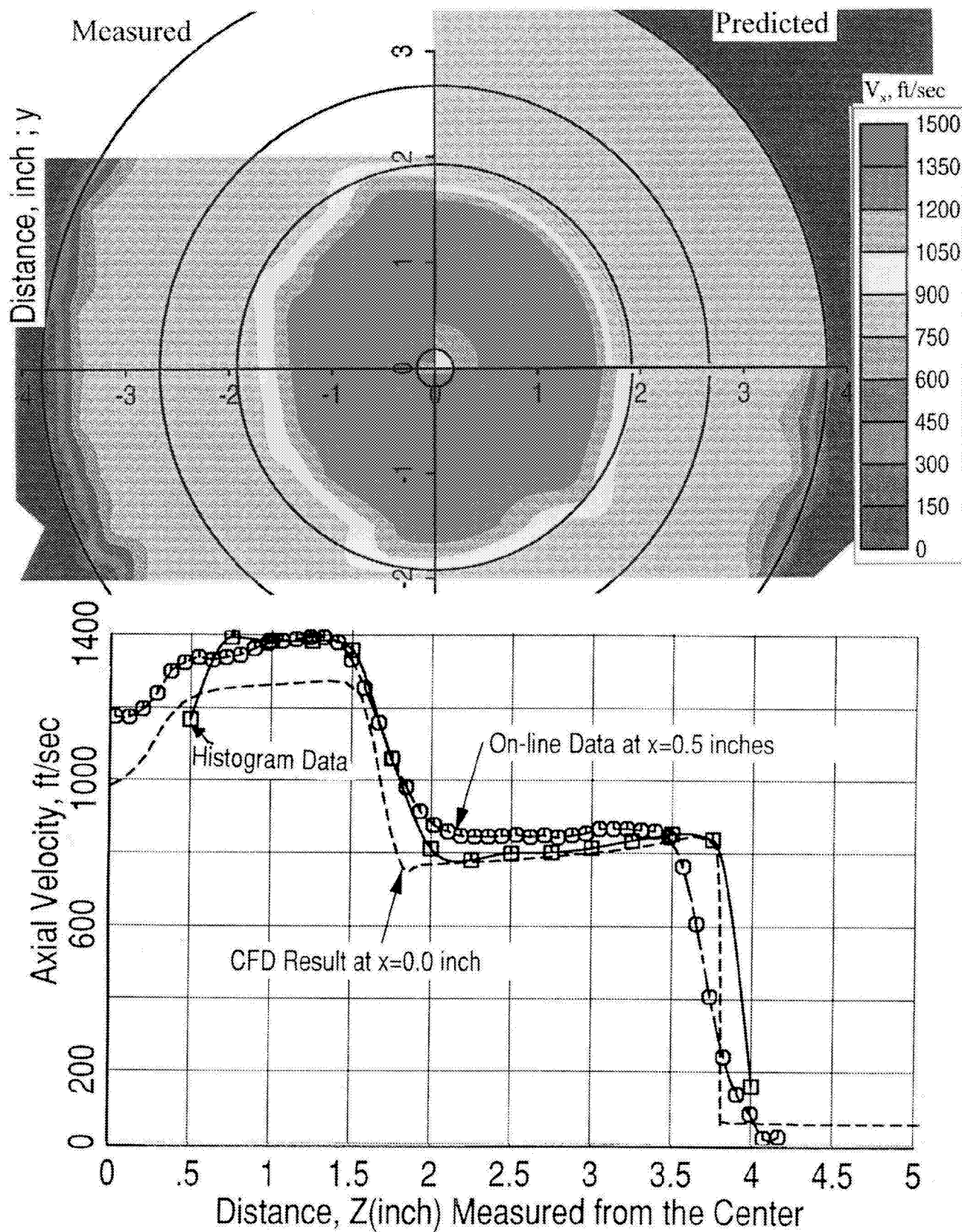


Figure 7.13. Comparisons of axial velocity distribution and contours between measured LDA data and CFD prediction at the exit plane for the confluent mixer (V1) for cycle condition 5 ( $V_{\max}=1000$  fps),  $M=0$ .

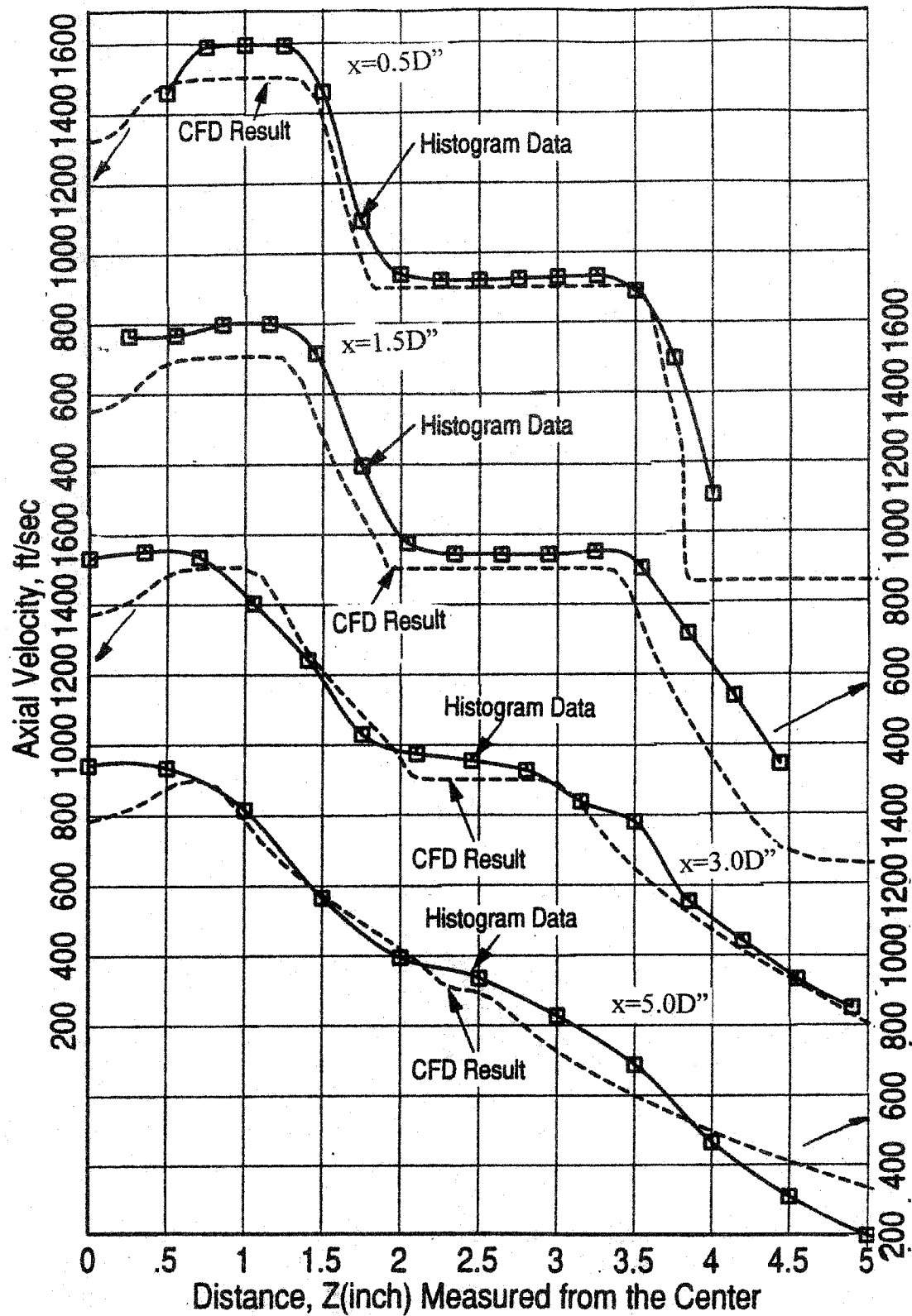


Figure 7.14. Comparisons of axial velocity distributions between measured LDA data and CFD prediction at various axial locations from the nozzle exit plane for the confluent mixer (V1) for cycle condition 5 ( $V_{mix}=1000$  fps),  $M=0$ .

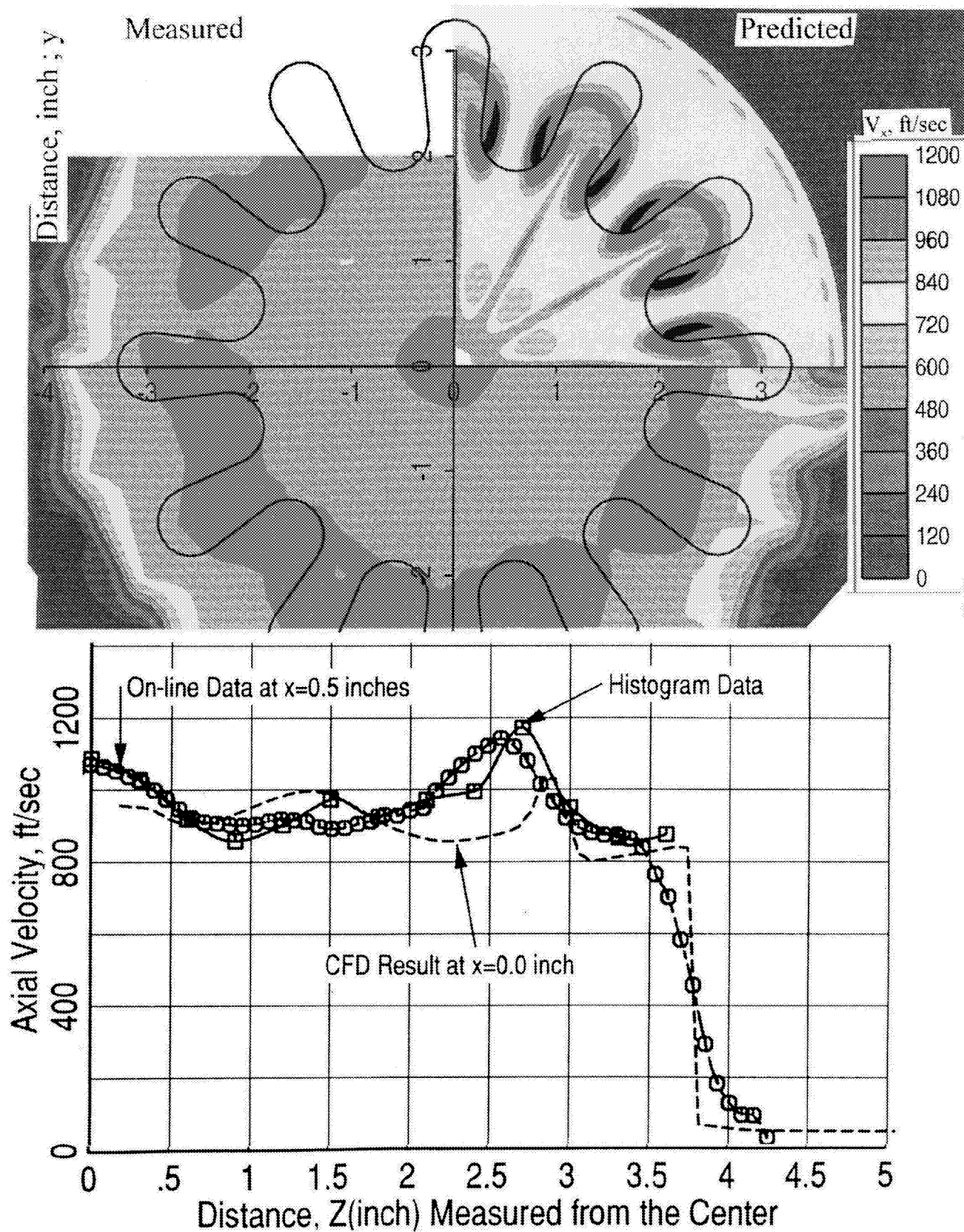


Figure 7.15. Comparisons of axial velocity distribution and contours between measured LDA data and CFD prediction at the exit plane for the scalloped mixer (V2) for cycle condition 5 ( $V_{mix}=1000$  fps),  $M=0$ .

high velocity resides are categorically predicted. The velocity distribution comparisons along radial direction at various locations downstream of the nozzle are shown in Figure 7.16. The velocity peaks near  $z=2.5$  for  $x=0.5''$  and  $x=0.5D''$  were predicted by CFD. This could possibly be due to the lack of diffusion out of the chutes and consequently less effective mixing. The velocity decay at  $z=3.5$  for  $x=1.5D''$  and  $x=3.0D''$  was under predicted compared to LDA data. However, the velocity distributions at  $x=5D$  are in reasonable agreement.

### **7.3.3 ICLS Scalloped Lobe Mixer (V2A) Velocity Data Comparison.**

The axial velocity comparison between CFD results and LDA data for the V2A configuration is shown in Figure 7.17. The ICLS-V2 tailpipe extension configuration shows analysis/data comparison trends similar to those exhibited for the V2 configuration. The velocity distribution comparisons along radial direction at various locations downstream of the nozzle are shown in Figure 7.18. The velocity distributions show reasonable agreement except at  $x=1.5D$  where less mixing occurs between the fan stream and the surrounding ambient air as.

### **7.3.4 Skewed Lobe Mixer (F12A) Velocity Data Comparison.**

The axial velocity comparison between CFD result and LDA data for the F12A configuration is shown in Figure 7.19. The comparison of color contour of axial velocity displays discrepancies between the analysis and test data. The analysis predicts less mixing in comparison to test data. However, the location where high velocity resides are categorically predicted. The velocity distribution comparisons along radial direction at various locations downstream of the nozzle are shown in Figure 7.20. The velocities in the mid-region are over predicted.

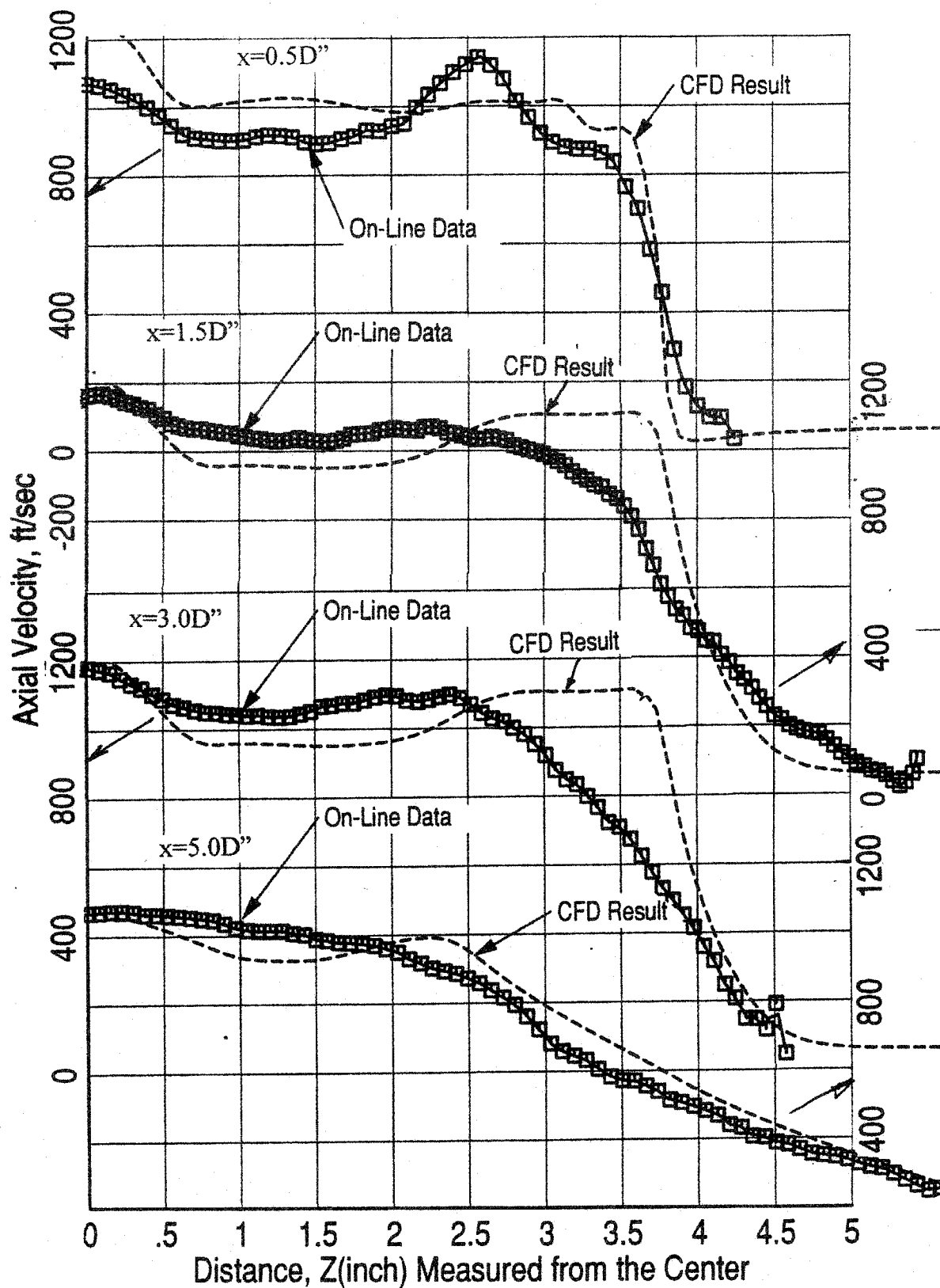


Figure 7.16. Comparisons of axial velocity distributions between measured LDA data and CFD prediction at various axial locations from the nozzle exit plane for the scalloped mixer (V2) for cycle condition 5 ( $V_{mix}=1000$  fps),  $M=0$ .



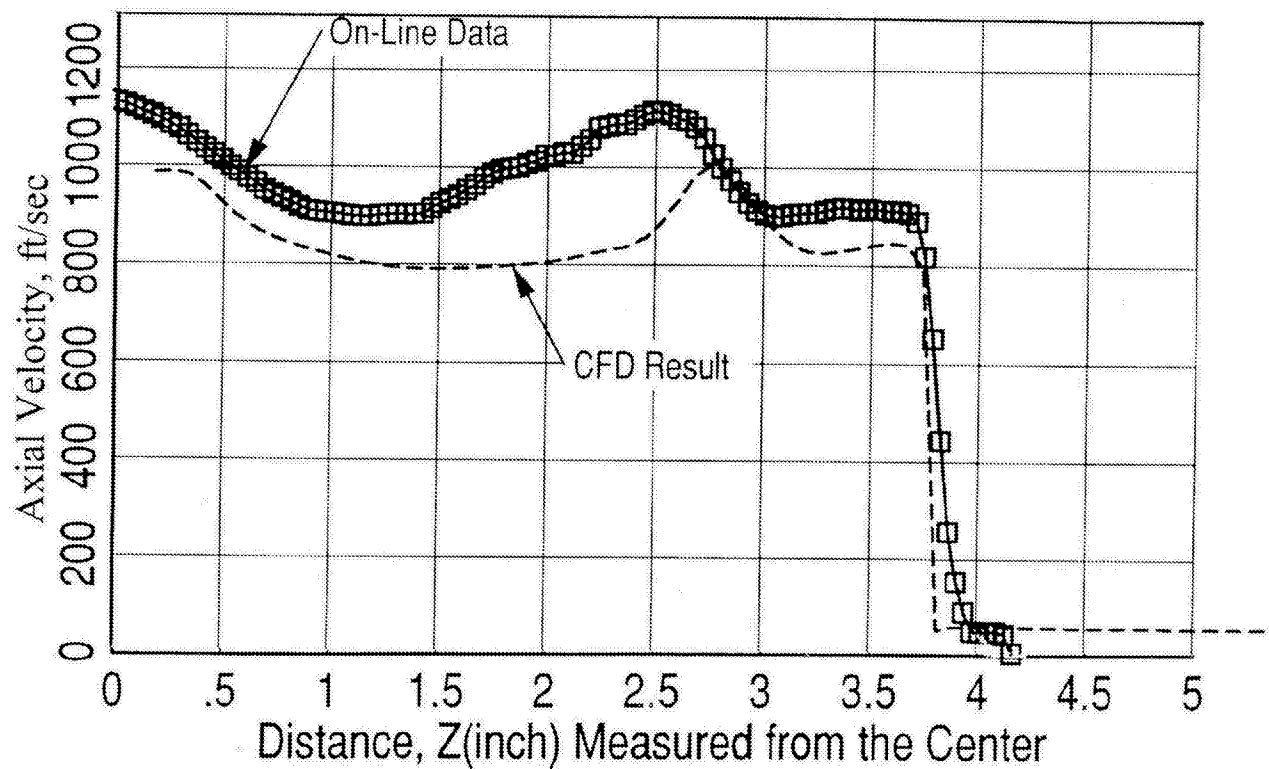
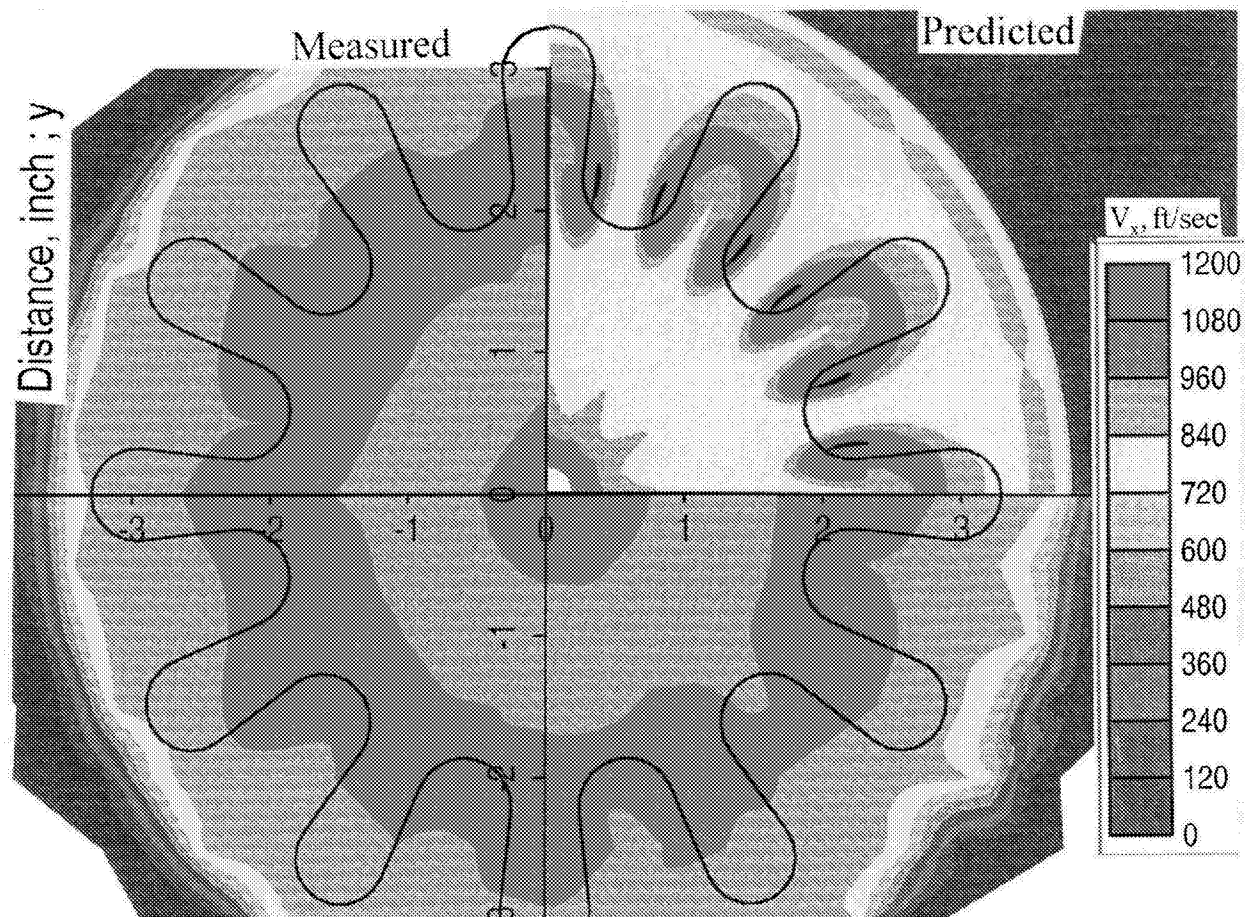


Figure 7.17. Comparisons of axial velocity distribution and contours between measured LDA data and CFD prediction at the exit plane for the scalloped mixer with extension (V2A) for cycle condition 5 ( $V_{mix}=1000$  fps),  $M=0$ .

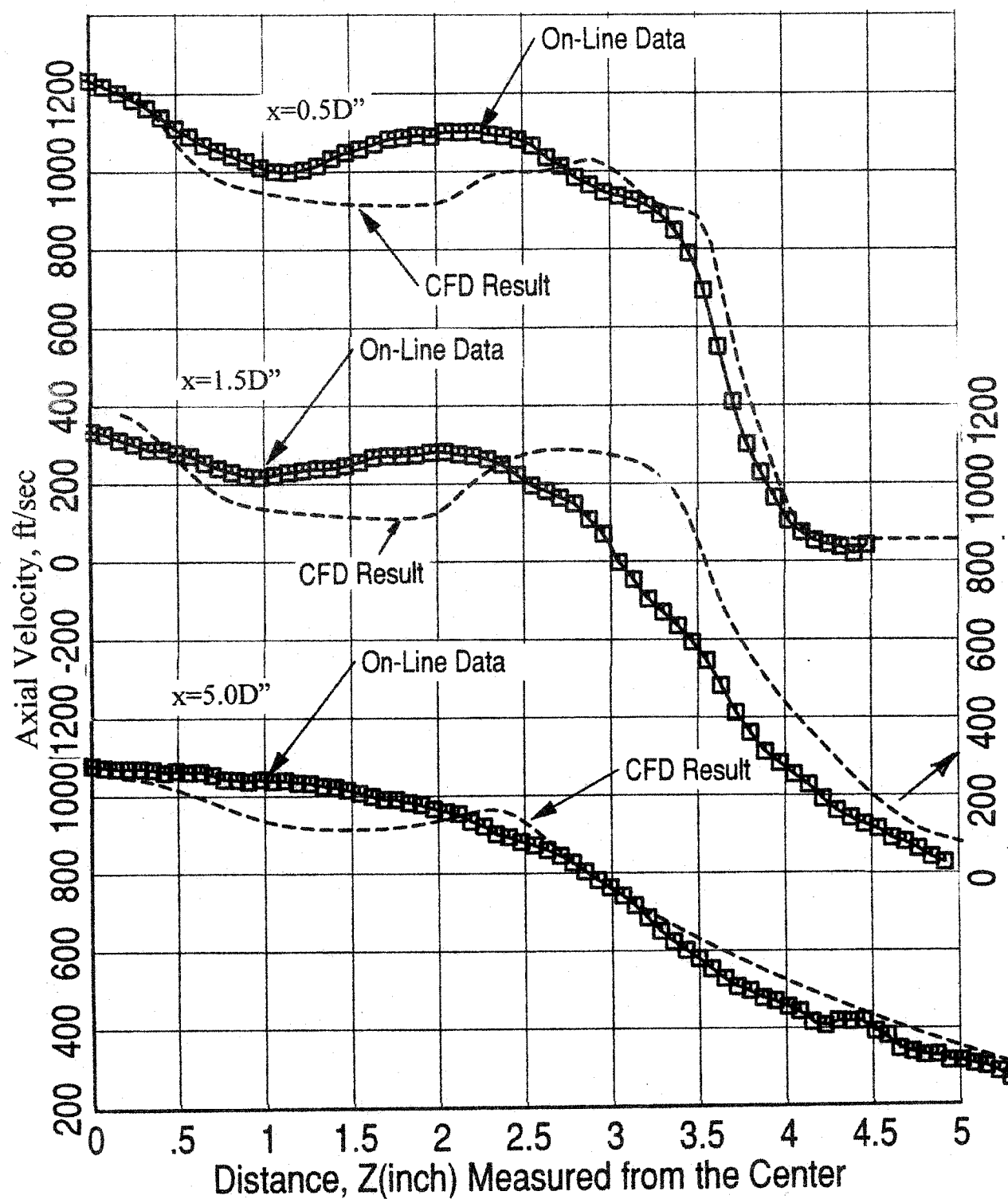


Figure 7.18. Comparisons of axial velocity distributions between measured LDA data and CFD prediction at various axial locations from the nozzle exit plane for the scalloped mixer with extension (V2A) for cycle condition 5 ( $V_{mix}=1000$  fps),  $M=0$ .

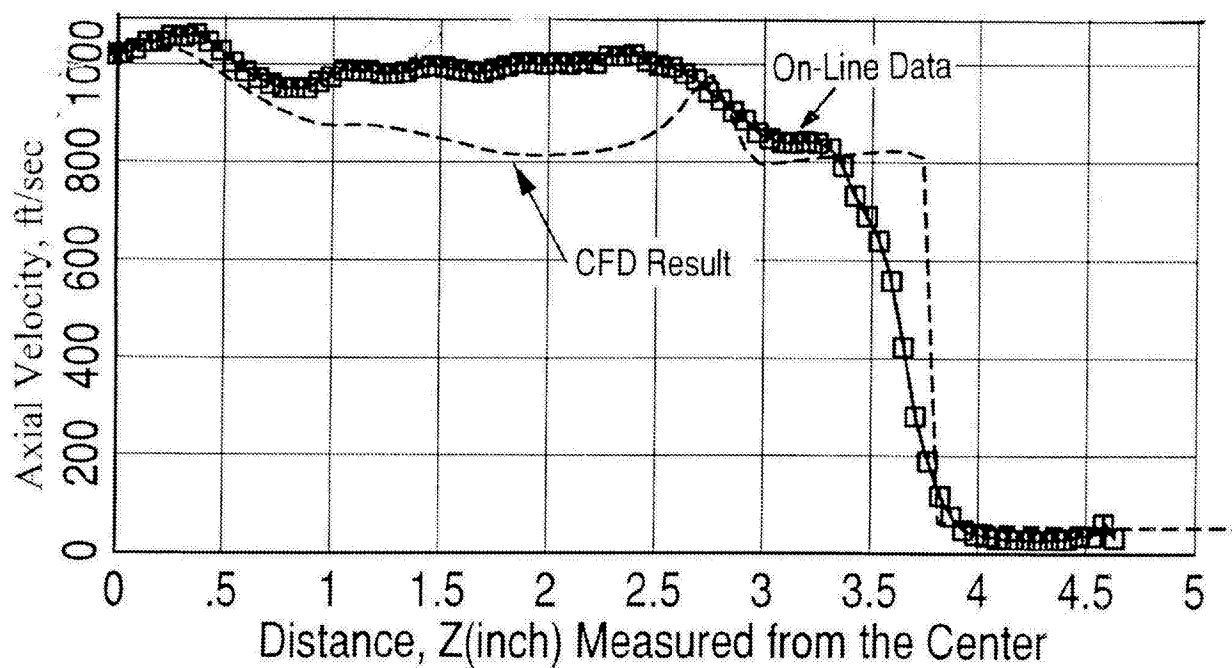
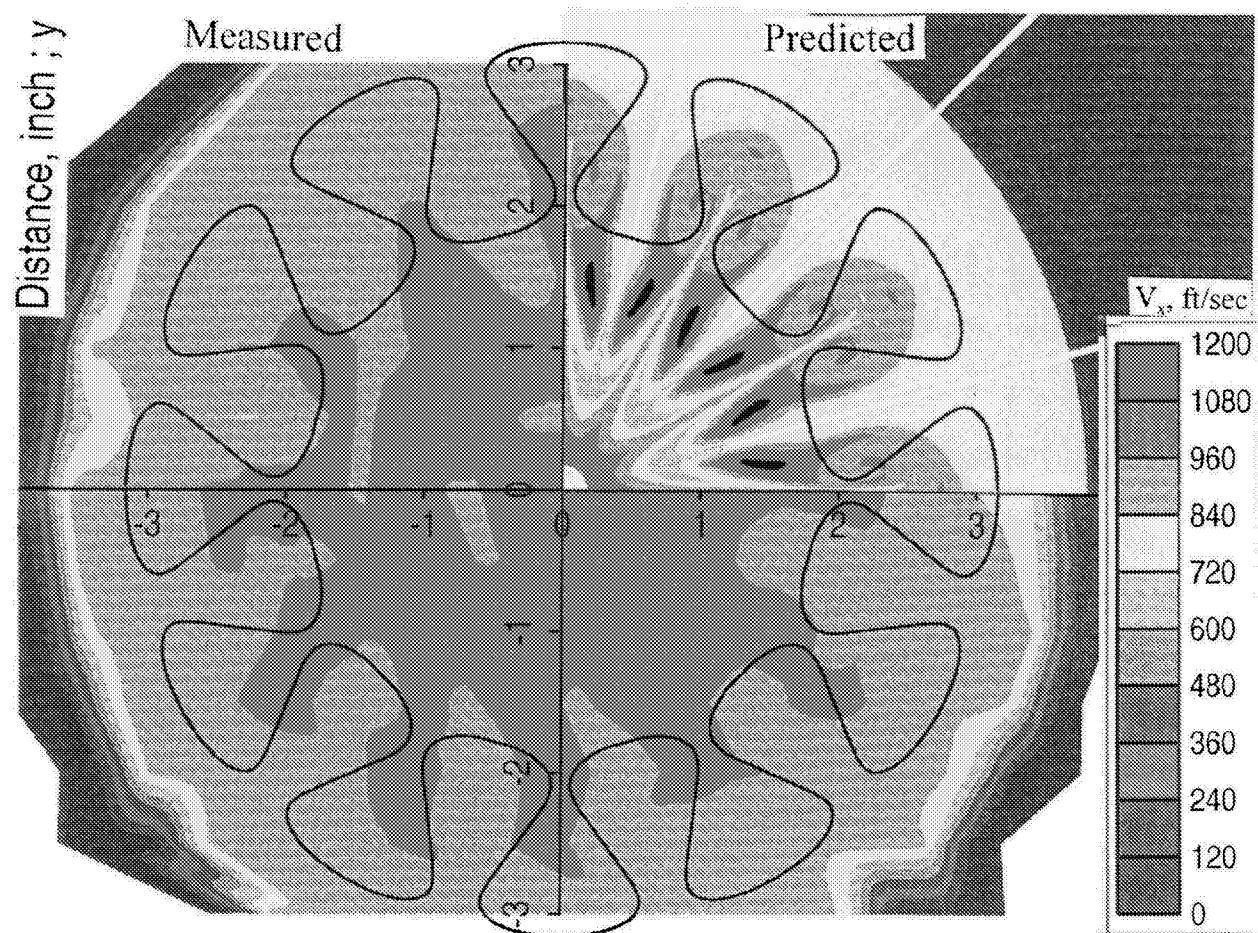


Figure 7.19. Comparisons of axial velocity distribution and contours between measured LDA data and CFD prediction at the exit plane for the skewed mixer (F12A) for cycle condition 5 ( $V_{mix}=1000$  fps),  $M=0$ .

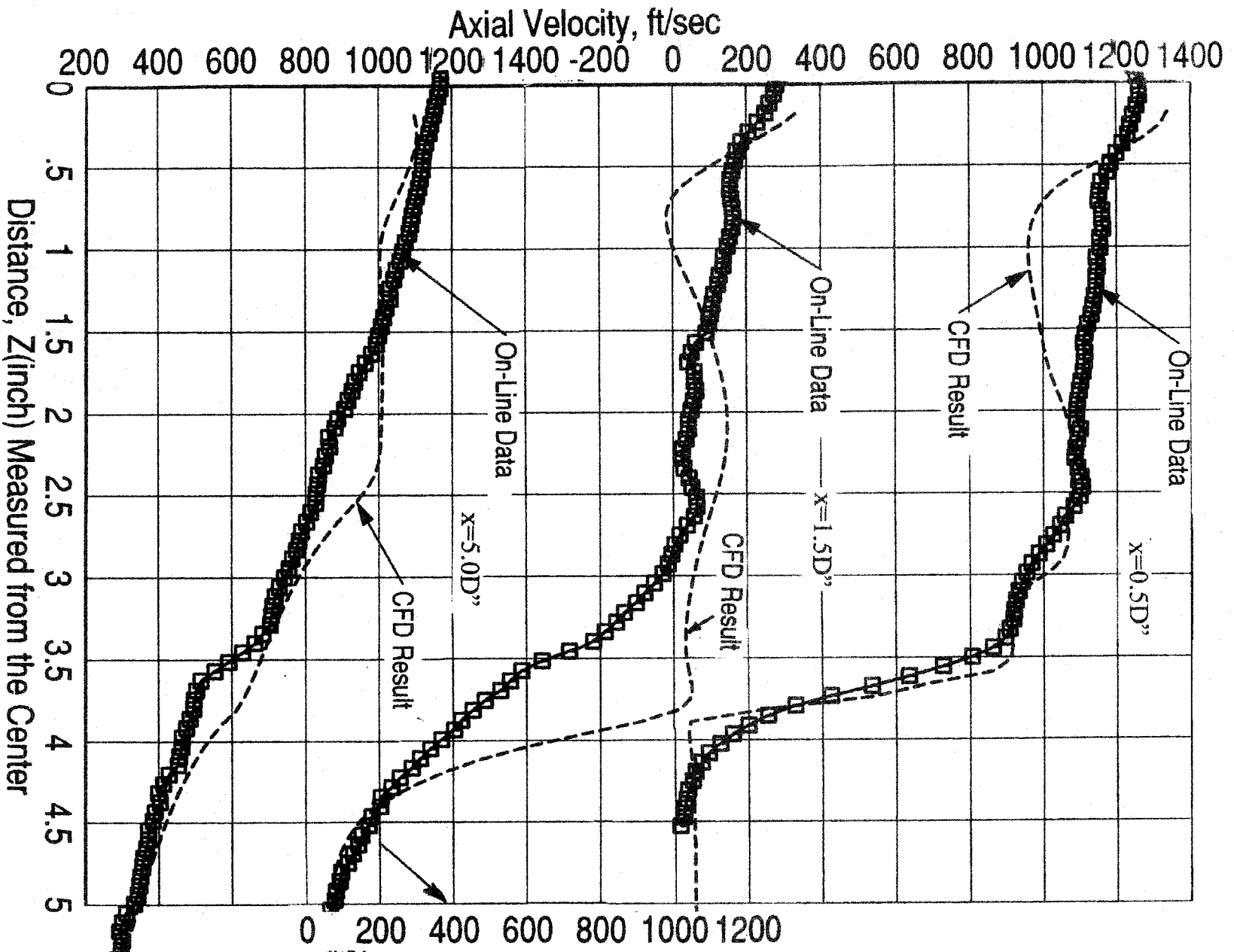


Figure 7.20. Comparisons of axial velocity distributions between measured LDA data and CFD prediction at various axial locations from the nozzle exit plane for the skewed mixer (F12A) for cycle condition 5 ( $V_{mix}=1000$  fps),  $M=0$ .

## 8.0 REFERENCES

1. Pennock, A.P., "Mixer Nozzle Noise Characteristics", AIAA 80-0166, 1980.
2. Shumpert, P.K., "An Experimental Investigation of Turbofan Engine Internal Exhaust Gas Mixer Configurations", AIAA 80-0228, 1980.
3. Kuchar, A.P. and Chamberlin, R., "Scale Model Performance Investigation of Mixed Flow Exhaust Systems for an Energy Efficient Engine (E<sup>3</sup>) Propulsion System, AIAA 80-0229, 1980.
4. Abolfadl, M.A. and Sehra, A.K., "Experimental Investigation of Exhaust System Mixers for a High Bypass Turbofan Engine", AIAA 93-0022, 1993.
5. Gliebe, P.R., Sandusky, G.T. and Chamberlin, R., "Mixer Nozzle Aeroacoustic Characteristics for the Energy Efficient Engine", AIAA 81-1994, 1981.
6. Goodykoontz, J.H., "Experiments of High Bypass Internal Mixer Nozzle Jet Noise", NASA TM 83020, 1982.



## **Appendix A-Acoustic Data**





A1 - Aeroacoustic Data Summary of E<sup>3</sup> Nozzles

Test Date: Jan-95  
 Test Site: Cell 41  
 Config. No.: 0  
 Nozzle: Conical

Model Size, sq.in.: 20.38  
 Engine Size, sq.in.: 3078  
 Distance, ft.: 1500

Definition			Test Cell			Freejet	Model Total					Engine Total				
Operating Line	Point No.	Reading No.	Relative Humidity	Ambient Pressure, (Pamb, psi)	Ambient Temp., (Tamb, °F)	Mach No. (Ma)	Pressure Ratio (PR)	Total Temp (TT, °R)	Weight Flow (W)	Fan Velocity (V)	Mach No. (M)	Model Thrust	Ideal Thrust	Ideal Net Thrust FN/6	PNL <sub>max</sub> dB	EPNL dB
			RELHUM	PSB105	TTCHA1	TERMAC	FANRAV	TTFVAV	FLOW	FVELAV	FANMAV					
Mix	1	42	41.3	14.143	57.9	0	1.375	641.3	7.56	819	0.69	192	29039	30174	82.52	82.10
Mix	2	43	42.0	14.112	57.8	0	1.431	644.7	8.05	868	0.73	217	32751	34107	83.87	83.75
Mix	3	44	42.4	14.105	58.2	0	1.484	647.1	8.50	910	0.77	240	36281	37800	86.39	86.02
Mix	4	45	42.1	14.102	58.2	0	1.531	649.5	8.87	945	0.80	260	39320	40975	87.80	87.68
Mix	5	46	42.2	14.096	58.3	0	1.575	654.6	9.17	978	0.83	279	42095	43886	89.32	88.96
Mix	6	47	45.6	14.099	58.1	0	1.641	658.5	9.63	1021	0.87	306	46148	48104	90.44	90.36
Mix	7	96	88.3	14.495	22.8	0	1.677	661.1	10.15	1044	0.89	329	49734	50425	93.73	93.32
Sep	8	51	56.0	14.064	55.3	0	1.431	615.5	8.21	848	0.73	216	32661	34129	83.94	83.55
Sep	9	50	59.9	14.064	54.8	0	1.523	620.2	8.98	919	0.80	256	38709	40449	86.86	86.52
Sep	10	49	62.7	14.083	54.2	0	1.633	626.1	9.81	992	0.87	302	45640	47627	89.93	89.96
Mix	1	78	45.6	14.552	35.4	0.24	1.365	641.4	7.67	809	0.68	193	29126	19644	73.94	73.35
Mix	2	79	49.7	14.547	34.0	0.24	1.410	646.7	8.08	852	0.72	214	32304	22398	75.62	75.45
Mix	3	82	50.0	14.539	34.2	0.24	1.479	651.0	8.68	909	0.77	245	37037	26368	78.57	77.87
Mix	4	83	50.1	14.535	33.9	0.24	1.509	653.7	8.91	932	0.79	258	38975	28042	80.34	79.69
Mix	5	87	87.0	14.481	22.9	0.24	1.562	655.5	9.31	970	0.82	281	42391	31104	82.19	81.72
Mix	6	75	45.9	14.558	35.9	0.24	1.621	661.9	9.78	1013	0.86	308	46443	34437	83.63	83.40
Mix	7	74	50.5	14.558	35.0	0.24	1.676	661.7	10.18	1044	0.89	330	49961	37976	85.06	84.60
Sep	8	95	91.2	14.495	22.6	0.24	1.410	615.5	8.26	831	0.72	213	32187	22079	75.82	75.25
Sep	9	92	93.1	14.494	22.8	0.24	1.516	620.3	9.20	914	0.79	261	39451	28238	79.79	79.18
Sep	10	91	89.6	14.492	22.6	0.24	1.624	627.4	10.02	987	0.86	307	46372	34221	83.32	82.68
Mix	1	77	47.7	14.551	34.5	0.28	1.364	642.4	7.67	810	0.68	193	29104	18007	71.76	71.04
Mix	2	80	48.7	14.545	33.8	0.28	1.418	645.8	8.17	858	0.72	218	32669	21088	73.99	73.39
Mix	3	81	47.3	14.542	34.4	0.28	1.476	650.1	8.67	907	0.77	244	36868	24371	77.42	75.88
Mix	4	84	50.6	14.533	33.7	0.28	1.522	653.3	9.03	942	0.80	264	39912	26921	78.67	77.78
Mix	5	89	88.3	14.481	22.8	0.28	1.562	655.3	9.32	970	0.82	281	42415	29136	80.28	79.80
Mix	6	76	48.8	14.555	34.7	0.28	1.624	661.5	9.80	1014	0.86	308	46582	32483	82.20	81.40
Mix	7	73	50.9	14.555	35.2	0.28	1.670	662.1	10.13	1041	0.89	327	49453	34888	83.74	82.77
Sep	8	94	91.6	14.492	22.4	0.28	1.418	616.5	8.31	837	0.72	216	32597	20665	73.91	72.96
Sep	9	93	91.6	14.496	22.7	0.28	1.521	622.8	9.23	919	0.80	263	39785	26577	78.21	77.43
Sep	10	90	91.2	14.486	22.8	0.28	1.626	628.2	10.02	989	0.86	308	46476	32198	81.43	80.81

A2 - Aeroacoustic Data Summary of E<sup>3</sup> Nozzles

Test Date: Feb-95  
 Test Site: Cell 41  
 Config. No.: 1  
 Nozzle: Confluent (V1)

Model Size, sq.in.: 45.7  
 Engine Size, sq.in.: 3078  
 Distance, ft.: 1500

Definition			Test Cell			Freejet	Model Core					Model Fan					Model Total				Engine Total			
Operating Line	Point No.	Reading No.	Relative Humidity	Ambient Pressure (Pamb, psi)	Ambient Temp. (Tamb, °F)	Mach No. (Mc)	Pressure Ratio (PR)	Total Temp (TTc, °R)	Weight Flow (Wc)	Velocity (Vc)	Mach No. (Mc)	Pressure Ratio (PRf)	Total Temp (TTf, °R)	Weight Flow (Wf)	Fan Velocity (Vf)	Mach No. (Mf)	Weight Flow (Wt)	Thrust	Mixed Velocity (Vmix)	Bypass Ratio	Ideal Thrust	Ideal Net Thrust FN/6	PNL <sub>max</sub> dB	EPNL dB
			RELHUM	PSB105	TTCHA1	TERMAC	CORRAV	TTCAVG	QFLOW	QVELAV	CORMAV	FANRAV	TTFAVG	FFLOW	FVELAV	FANMAV	TOTFLO	FGITOT	Vmix	BPR				
Mix	1	143	45.8	14.603	43.9	0	1.376	1333.6	2.19	1184	0.70	1.414	544.9	14.93	785	0.72	17.12	444.9	836	6.83	29965	30157	85.87	86.43
Mix	2	144	45.7	14.599	44.1	0	1.440	1359.5	2.41	1273	0.75	1.456	546.5	15.58	817	0.75	17.99	491.0	878	6.48	33072	33291	86.06	86.70
Mix	3	145	43.4	14.607	45.1	0	1.498	1401.4	2.60	1358	0.79	1.498	547.7	16.20	847	0.78	18.80	536.1	917	6.23	36107	36328	90.53	91.36
Mix	4	146	43.9	14.608	44.3	0	1.582	1411.2	2.74	1427	0.83	1.553	548.9	17.11	882	0.82	19.85	590.7	958	6.24	39788	40028	92.62	93.52
Mix	5	147	44.5	14.606	44.7	0	1.628	1452.7	2.89	1509	0.87	1.606	550.1	17.99	914	0.85	20.78	644.2	997	6.19	43387	43854	94.69	95.42
Mix	6	148	45.1	14.604	44.4	0	1.702	1471.2	3.08	1582	0.92	1.658	551.0	18.84	943	0.88	21.71	697.8	1034	6.06	46999	47293	97.21	97.22
Mix	7	142	45.5	14.615	43.3	0	1.782	1498.7	3.26	1660	0.96	1.711	549.3	19.33	989	0.91	22.60	750.4	1068	5.93	50538	50920	99.79	99.07
Sep	8	139	47.8	14.624	43.3	0	1.296	1249.0	1.51	1037	0.63	1.478	545.3	16.85	832	0.77	18.36	484.2	849	11.15	32609	32769	86.00	85.99
Sep	9	140	48.9	14.630	43.3	0	1.386	1299.3	1.66	1180	0.71	1.605	545.1	19.11	910	0.85	20.79	602.0	932	11.38	40549	40734	89.44	89.85
Sep	10	141	46.4	14.623	43.3	0	1.502	1332.3	2.10	1328	0.79	1.702	545.3	20.35	961	0.91	22.45	694.3	995	9.70	46763	46998	92.39	93.38
Mix	1	120	65.2	14.665	38.5	0.24	1.369	1330.8	2.22	1173	0.69	1.393	516.8	14.89	749	0.70	17.11	427.4	804	6.70	28789	19208	75.56	76.06
Mix	2	121	61.6	14.664	37.8	0.24	1.429	1379.3	2.33	1270	0.74	1.466	525.5	16.13	809	0.76	18.46	497.4	867	6.92	33498	23169	78.34	79.54
Mix	3	124	58.8	14.679	39.4	0.24	1.486	1401.5	2.52	1345	0.78	1.497	536.9	16.43	838	0.78	18.95	533.5	906	6.51	35930	25302	81.48	82.12
Mix	4	125	54.1	14.674	39.7	0.24	1.562	1424.3	2.79	1434	0.83	1.550	540.6	17.26	874	0.82	20.05	593.4	952	6.18	39964	28734	84.61	85.07
Mix	5	127	51.8	14.660	39.8	0.24	1.630	1447.6	2.86	1509	0.86	1.601	546.5	17.86	909	0.85	20.73	636.7	991	6.24	43016	31440	87.35	87.60
Mix	6	130	51.5	14.649	41.6	0.24	1.699	1471.2	3.06	1580	0.91	1.656	550.3	18.53	942	0.88	21.59	682.8	1032	6.05	46664	34636	89.81	89.84
Mix	7	131	49.6	14.645	41.2	0.24	1.784	1496.8	3.18	1645	0.95	1.696	552.4	19.12	984	0.90	22.28	734.6	1061	6.04	49476	37076	92.90	92.03
Sep	8	138	48.7	14.620	42.6	0.24	1.297	1250.8	1.46	1038	0.63	1.478	545.8	16.74	832	0.77	18.21	480.1	848	11.44	32336	22215	76.18	76.31
Sep	9	135	48.0	14.633	42.8	0.24	1.402	1286.1	1.75	1193	0.72	1.597	546.6	18.69	906	0.85	20.44	591.4	931	10.66	39833	28463	80.27	80.91
Sep	10	134	48.1	14.637	43.1	0.24	1.507	1321.5	2.17	1327	0.80	1.689	547.8	20.02	957	0.90	22.19	684.7	993	9.23	46115	33774	83.67	84.90
Mix	1	119	66.7	14.670	35.5	0.28	1.372	1349.3	2.16	1185	0.70	1.394	513.4	14.91	747	0.71	17.09	426.5	803	6.83	28724	17545	75.22	74.83
Mix	2	122	61.3	14.665	38.0	0.28	1.424	1356.5	2.32	1253	0.74	1.448	530.0	15.73	800	0.76	18.05	481.6	858	6.78	32437	20641	77.17	77.69
Mix	3	123	58.4	14.671	39.1	0.28	1.493	1388.0	2.57	1345	0.79	1.498	534.7	16.53	837	0.78	19.10	537.5	905	6.42	36202	23714	80.32	81.01
Mix	4	126	50.7	14.670	40.5	0.28	1.584	1424.2	2.77	1435	0.83	1.550	541.8	17.07	875	0.82	19.84	588.0	954	6.15	39602	26636	83.38	83.80
Mix	5	128	52.2	14.656	40.5	0.28	1.632	1456.0	2.93	1515	0.88	1.598	547.2	17.79	908	0.85	20.72	639.9	994	6.07	43102	29590	86.30	86.38
Mix	6	129	50.5	14.657	41.3	0.28	1.694	1471.6	2.98	1576	0.91	1.654	549.1	18.81	940	0.88	21.59	689.7	1028	6.25	46456	32376	89.40	88.70
Mix	7	132	49.9	14.648	41.2	0.28	1.774	1505.5	3.29	1658	0.95	1.695	553.3	18.99	964	0.90	22.28	738.5	1067	5.77	48741	35243	92.27	91.19
Sep	8	137	49.3	14.622	42.4	0.28	1.298	1257.4	1.44	1043	0.63	1.492	546.4	17.04	842	0.78	18.49	492.8	857	11.80	33181	21161	75.01	75.06
Sep	9	136	47.7	14.626	43.1	0.28	1.406	1291.0	1.80	1201	0.72	1.593	546.3	18.59	904	0.84	20.39	589.7	930	10.30	38715	26464	79.21	79.69
Sep	10	133	48.1	14.636	42.4	0.28	1.510	1321.3	2.16	1330	0.80	1.686	548.2	19.90	955	0.90	22.06	680.0	992	9.22	45801	31459	82.88	83.82

A3 - Aeroacoustic Data Summary of E<sup>3</sup> Nozzles

Test Date: Feb-95  
 Test Site: Cell 41  
 Config. No.: 2A  
 Nozzle: Scaloped mixer with Extended Tailpipe (V2)

Model Size, sq.in.: 45.7  
 Engine Size, sq.in.: 3078  
 Distance, ft.: 1500

Definition			Test Cell			Fresjet	Model Core					Model Fan					Model Total				Engine Total			
Operating Line	Point No.	Reading No.	Relative Humidity	Ambient Pressure (Pamb, psi)	Ambient Temp. (Tamb, °F)	Mach No. (Mc)	Pressure Ratio (PR)	Total Temp (TTc, °R)	Weight Flow (Wc)	Velocity (Vc)	Mach No. (Mc)	Pressure Ratio (PRf)	Total Temp (TTf, °R)	Weight Flow (Wf)	Fan Velocity (Vf)	Mach No. (Mf)	Weight Flow (Wt)	Thrust (F)	Mixed Velocity (Vmix)	Bypass Ratio	Ideal Thrust	Ideal Net Thrust FN/8	PNLmax dB	EPNL dB
			RELHUM	PSB105	TTCHA1	TERMAC	CORRAV	TYCAVG	CFLOW	CVELAV	CORMAV	FANRAV	TTFVAV	FFLOW	FVELAV	FANMAV	TOTRLO	FB/TOT	Vmix	BPR				
Mix	2	190	38.8	14.410	46.0	0	1.439	1368.6	1.94	1277	0.75	1.458	527.5	16.05	804	0.75	17.99	478.2	855	8.27	32206	32846	85.50	85.22
Mix	3	205	30.1	14.288	55.9	0	1.514	1394.6	2.13	1371	0.80	1.506	547.4	16.27	852	0.79	18.40	521.5	912	7.63	35123	36127	87.75	87.39
Mix	4	204	30.8	14.294	54.5	0	1.576	1408.5	2.33	1439	0.84	1.547	548.1	18.83	878	0.81	19.16	563.7	946	7.23	37965	39033	89.13	89.09
Mix	5	203	30.6	14.302	54.5	0	1.647	1436.8	2.52	1518	0.88	1.608	548.5	17.78	914	0.85	20.30	624.2	989	7.05	42042	43201	91.19	90.98
Mix	6	202	31.0	14.310	54.1	0	1.715	1466.7	2.60	1590	0.92	1.653	550.3	18.28	940	0.88	20.89	662.9	1021	7.03	44645	45851	92.46	92.56
Mix	7	201	30.0	14.318	54.2	0	1.785	1487.8	2.74	1656	0.96	1.702	549.5	18.91	965	0.91	21.85	707.9	1052	6.90	47681	48940	94.01	94.26
Mix	2	191	37.6	14.394	46.9	0.24	1.435	1362.1	1.93	1269	0.75	1.453	531.8	15.83	804	0.75	17.76	471.5	854	8.22	31754	32226	77.20	76.62
Mix	3	192	38.6	14.384	47.2	0.24	1.504	1399.2	2.12	1363	0.80	1.493	534.4	16.23	833	0.78	18.35	510.0	894	7.66	34349	34552	78.40	78.50
Mix	4	193	35.4	14.370	48.5	0.24	1.557	1417.9	2.19	1426	0.83	1.548	536.8	17.15	870	0.82	19.34	560.7	933	7.84	37762	37497	81.70	81.19
Mix	5	196	33.6	14.346	50.9	0.24	1.642	1436.3	2.47	1513	0.88	1.597	542.8	17.63	903	0.85	20.10	611.2	978	7.13	41165	30581	83.60	83.08
Mix	6	197	33.1	14.340	51.4	0.24	1.703	1462.4	2.61	1578	0.92	1.647	545.0	18.39	933	0.88	21.00	661.2	1013	7.05	44532	33534	85.80	85.33
Mix	7	200	30.0	14.324	54.0	0.24	1.771	1497.4	2.70	1651	0.95	1.698	549.5	18.69	963	0.90	21.59	703.9	1049	6.89	47408	36184	87.10	86.57
Mix	4	194	35.6	14.363	48.6	0.28	1.558	1416.5	2.21	1426	0.83	1.553	538.3	17.23	874	0.82	19.43	565.7	937	7.80	38102	25942	80.69	79.90
Mix	5	195	32.5	14.352	51.4	0.28	1.637	1440.5	2.43	1511	0.88	1.595	541.6	17.81	901	0.84	20.04	607.4	975	7.25	40908	28432	82.74	81.96
Mix	6	198	32.1	14.337	52.5	0.28	1.704	1465.6	2.52	1581	0.92	1.656	546.4	18.49	939	0.88	21.01	663.2	1016	7.33	44670	31661	84.59	84.00
Mix	7	199	30.4	14.330	53.5	0.28	1.783	1492.4	2.80	1657	0.96	1.701	548.6	18.89	963	0.91	21.69	709.5	1053	6.76	47788	34418	86.70	86.00

A4 - Aeroacoustic Data Summary of E<sup>3</sup> Nozzles

Test Date: Feb-95  
 Test Site: Cell 41  
 Config. No.: 2 & 2R  
 Nozzle: Scalloped Mixer (V2)

Model Size, sq.in.: 45.7  
 Engine Size, sq.in.: 3078  
 Distance, ft.: 1500

Definition			Test Cell			Freejet	Model Core					Model Fan					Model Total				Engine Total			
Oper- ating Line	Point No.	Reading No.	Relative Humidity	Ambient Pressure (Pamb, psi)	Ambient Temp. (Tamb, °F)	Mach No. (M <sub>0</sub> )	Pressure Ratio (PR)	Total Temp (T <sub>0</sub> , °R)	Weight Flow (W <sub>0</sub> )	Velocity (V <sub>0</sub> )	Mach No. (M <sub>0</sub> )	Pressure Ratio (PR <sub>F</sub> )	Total Temp (T <sub>0F</sub> , °R)	Weight Flow (W <sub>F</sub> )	Fan Velocity (V <sub>F</sub> )	Mach No. (M <sub>F</sub> )	Weight Flow (W <sub>T</sub> )	Thrust (F)	Mixed Velocity (V <sub>mix</sub> )	Bypass Ratio	Ideal Thrust	Ideal Net Thrust FN/s	PNL <sub>max</sub> dB	EPNL dB
			RELHUM	PSB105	TTOHA1	TERMAC	CORRAV	TTCGVG	CFLOW	CVELAV	CORMAV	FANRAV	TTFVAVG	FFLOW	FVELAV	FANMAV	TOTFLO	FGITOT	Vmix	BPR				
Mix	1	152	65.5	14.350	42.2	0	1.381	1361.7	2.06	1202	0.70	1.399	520.3	14.29	756	0.71	16.35	412.7	812	6.93	27799	28469	84.41	83.46
Mix	2	178	51.3	14.553	39.6	0	1.397	1363.3	2.04	1223	0.72	1.441	515.2	15.54	783	0.74	17.58	455.8	834	7.62	30700	31002	86.02	85.49
Mix	3	179	54.2	14.557	39.5	0	1.483	1390.1	2.33	1336	0.78	1.497	518.0	16.40	823	0.78	18.73	516.3	857	7.04	34773	35106	88.61	88.01
Mix	4	180	54.9	14.559	39.4	0	1.559	1411.6	2.53	1424	0.83	1.555	522.4	17.18	862	0.82	19.71	572.3	934	6.80	38543	38905	90.91	90.13
Mix	5	181	52.3	14.565	39.5	0	1.619	1441.1	2.85	1495	0.87	1.607	525.3	17.89	894	0.85	20.55	620.5	972	6.75	41789	42166	92.55	91.83
Mix	6	182	51.9	14.570	39.6	0	1.690	1470.9	2.81	1572	0.91	1.656	528.1	18.49	923	0.88	21.30	667.6	1008	6.58	44965	45354	94.02	93.60
Mix	7	183	54.0	14.572	39.9	0	1.763	1489.4	2.96	1640	0.95	1.707	531.8	19.13	951	0.91	22.09	716.4	1043	6.46	48253	48662	95.23	94.89
Sep	8	185	51.7	14.571	35.6	0	1.291	1263.0	1.45	1034	0.62	1.475	529.3	16.90	817	0.77	18.35	476.0	834	11.62	32060	32335	85.08	84.93
Sep	9	174	43.6	14.236	54.3	0	1.402	1283.3	1.77	1193	0.72	1.577	534.1	17.85	885	0.83	18.82	556.5	912	10.06	37479	38690	87.79	87.59
Sep	10	184	49.1	14.569	34.9	0	1.497	1322.3	2.01	1317	0.79	1.690	529.4	20.24	941	0.90	22.25	674.2	975	10.06	45410	45807	91.39	91.55
Mix	1	153	64.0	14.353	43.9	0.24	1.363	1358.7	1.95	1176	0.69	1.400	521.3	14.43	758	0.71	16.39	411.3	807	7.38	27700	18929	76.2	74.95
Mix	2	158	49.6	14.345	50.5	0.24	1.423	1363.9	2.16	1255	0.74	1.447	531.5	14.90	800	0.75	17.06	454.4	857	6.91	30607	21530	78.66	77.47
Mix	3	159	49.0	14.338	51.2	0.24	1.471	1391.6	2.26	1319	0.77	1.493	531.4	15.78	831	0.78	18.04	500.4	882	6.97	33704	24148	81	80.00
Mix	4	163	50.9	14.320	50.8	0.24	1.551	1414.8	2.47	1418	0.83	1.549	535.1	16.53	869	0.82	18.99	555.0	940	6.70	37388	27404	83.45	82.08
Mix	5	164	50.3	14.316	51.3	0.24	1.615	1437.7	2.81	1490	0.87	1.597	536.0	17.16	898	0.85	19.77	599.6	976	6.57	40985	30049	85.38	84.02
Mix	6	167	50.8	14.293	50.9	0.24	1.704	1465.7	2.82	1581	0.92	1.651	538.8	17.73	929	0.88	20.55	650.5	1019	6.28	43810	33166	87.68	86.43
Mix	7	168	54.0	14.572	39.9	0.24	1.763	1489.4	2.96	1640	0.95	1.707	531.8	19.13	951	0.91	22.09	716.4	1043	6.46	48253	36136	89	87.85
Sep	8	186	50.7	14.566	35.2	0.24	1.281	1253.9	1.38	1015	0.61	1.475	529.1	16.92	817	0.77	18.30	473.4	832	12.28	31887	21791	76.56	76.31
Sep	9	172	46.2	14.248	53.0	0.24	1.399	1288.5	1.77	1191	0.72	1.568	535.7	17.62	881	0.83	19.40	546.0	909	9.95	36912	26826	79.28	78.99
Sep	10	171	49.1	14.569	34.9	0.24	1.497	1322.3	2.01	1317	0.79	1.690	529.4	20.24	941	0.90	22.25	674.2	975	10.06	45410	33168	82.82	82.54
Mix	1	155	58.0	14.355	46.1	0.28	1.359	1339.8	1.95	1163	0.68	1.390	523.9	14.17	752	0.70	16.13	401.8	802	7.25	27064	16877	75.2	74.04
Mix	2	157	51.8	14.349	49.6	0.28	1.410	1381.9	2.07	1248	0.73	1.444	529.4	14.92	796	0.74	17.00	449.7	851	7.19	30286	19599	77.84	76.15
Mix	3	160	50.2	14.337	50.6	0.28	1.481	1408.1	2.19	1343	0.78	1.526	532.2	16.38	852	0.80	18.57	525.5	910	7.48	35390	23788	80.21	78.74
Mix	4	162	48.3	14.321	51.7	0.28	1.551	1415.9	2.48	1419	0.83	1.540	535.1	16.20	863	0.81	18.88	543.9	937	6.53	36633	25021	82.79	81.14
Mix	5	165	50.0	14.305	51.7	0.28	1.621	1439.0	2.62	1496	0.87	1.598	536.0	17.06	898	0.85	19.68	598.2	978	6.51	40288	28126	84.55	83.12
Mix	6	166	51.0	14.301	51.4	0.28	1.700	1460.3	2.83	1575	0.91	1.643	537.8	17.56	924	0.87	20.39	643.2	1015	6.20	43319	30769	86.66	85.32
Mix	7	169	54.0	14.572	39.9	0.28	1.763	1489.4	2.96	1640	0.95	1.707	531.8	19.13	951	0.91	22.09	716.4	1043	6.46	48253	34049	88.29	86.83
Sep	8	187	50.3	14.562	36.1	0.28	1.283	1260.8	1.36	1022	0.61	1.483	528.1	17.08	822	0.77	18.44	479.2	836	12.58	32277	20369	75.33	74.85
Sep	9	173	45.6	14.243	53.0	0.28	1.404	1288.4	1.81	1198	0.72	1.560	535.4	17.35	876	0.82	19.16	539.7	906	9.80	36349	24538	78.03	77.57
Sep	10	170	49.1	14.569	34.9	0.28	1.497	1322.3	2.01	1317	0.79	1.690	529.4	20.24	941	0.90	22.25	674.2	975	10.06	45410	31085	81.92	81.42

## 2 Repeat

Oper- ating Line	Point No.	Reading No.	Relative Humidity	Ambient Pressure (Pamb, psi)	Ambient Temp. (Tamb, °F)	Mach No. (M <sub>0</sub> )	Pressure Ratio (PR)	Total Temp (T <sub>0</sub> , °R)	Weight Flow (W <sub>0</sub> )	Velocity (V <sub>0</sub> )	Mach No. (M <sub>0</sub> )	Pressure Ratio (PR <sub>F</sub> )	Total Temp (T <sub>0F</sub> , °R)	Weight Flow (W <sub>F</sub> )	Fan Velocity (V <sub>F</sub> )	Mach No. (M <sub>F</sub> )	Weight Flow (W <sub>T</sub> )	Thrust (F)	Mixed Velocity (V <sub>mix</sub> )	Bypass Ratio	Ideal Thrust	Ideal Net Thrust FN/s	PNL <sub>max</sub> dB	EPNL dB
Mix	4	317	79.2	14.358	61.7	0	1.570	1424.8	2.52	1442	0.84	1.545	532.4	16.60	864	0.81	19.12	558.9	941	6.58	37641	38527		
Mix	5	318	78.2	14.358	62.3	0	1.629	1439.4	2.68	1503	0.87	1.593	534.0	17.24	893	0.84	19.91	603.7	975	6.44	40662	41619		
Mix	6	319	77.6	14.354	62.6	0	1.696	1466.2	2.92	1575	0.91	1.648	542.0	17.94	930	0.88	20.77	657.0	1018	6.35	44249	45305		
Mix	7	320	77.2	14.353	62.8	0	1.776	1489.5	2.95	1650	0.95	1.707	547.6	18.59	965	0.91	21.54	709.1	1059	6.30	47757	48898		
Mix	4	325	75.5	14.346	64.7	0.24	1.561	1410.7	2.50	1426	0.83	1.548	535.7	16.30	885	0.82	18.80	559.1	957	6.51	37658	27748		
Mix	5	324	75.4	14.349	64.6	0.24	1.626	1439.1	2.58	1501	0.87	1.604	536.2	17.08	918	0.85	19.66	607.8	995	6.62	40938	30607		
Mix	6	323	76.9	14.347	64.0	0.24	1.700	1461.2	2.79	1576	0.91	1.658	536.4	17.83	948	0.88	20.62	661.9	1033	6.40	44583	33792		
Mix	7	322	77.8	14.347	63.5	0.24	1.772	1490.8	2.96	1648	0.95	1.707	536.8	18.43	973	0.91	21.39	709.2	1067	6.22	47768	38610		87.85

A5 - Aeroacoustic Data Summary of E<sup>3</sup> Nozzles

Test Date: Feb-95  
 Test Site: Cell 41  
 Config. No.: 3  
 Nozzle: Scalloped/Staggered Mixer (F9B)

Model Size, sq.in.: 45.7  
 Engine Size, sq.in.: 3078  
 Distance, ft.: 1500

Definition			Test Cell			Freejet	Model Core					Model Fan					Model Total				Engine Total			
Operating Line	Point No.	Reading No.	Relative Humidity	Ambient Pressure (Pamb, psi)	Ambient Temp. (Tamb, °F)	Mach No. (Ma)	Pressure Ratio (PR)	Total Temp (TTC, °R)	Weight Flow (Wc)	Velocity (Vc)	Mach No. (Mc)	Pressure Ratio (PRc)	Total Temp (TTC, °R)	Weight Flow (Wc)	Fan Velocity (Vf)	Mach No. (Mf)	Weight Flow (Wf)	Thrust (F)	Mixed Velocity (Vmix)	Bypass Ratio	Ideal Thrust	Ideal Net Thrust FN/5	PNLmax dB	EPNL dB
			RELHUM	PSB105	TTCHA1	TERMAC	CORRAY	TTCVAG	CFLOW	CVELAV	CORMAV	FANRAV	TTFVAG	FFLOW	FVELAV	FANMAV	TOTFLO	FGTOT	Vmix	BPR				
Mix	1	242	59.5	14.474	56.2	0	1.365	1344.7	1.98	1174	0.89	1.406	520.6	14.74	762	0.72	16.72	421.1	811	7.45	28362	28796	84.02	83.35
Mix	2	266	75.4	14.434	56.5	0	1.438	1367.8	2.26	1274	0.75	1.453	553.1	14.92	820	0.75	17.18	470.0	880	6.59	31653	32228	86.73	86.18
Mix	3	265	78.1	14.441	56.5	0	1.505	1397.0	2.43	1363	0.80	1.509	554.3	15.76	859	0.79	18.18	523.6	926	6.50	35265	35889	88.60	88.10
Mix	4	264	77.7	14.445	56.1	0	1.565	1419.5	2.59	1434	0.84	1.550	566.5	16.28	887	0.82	18.86	564.1	962	6.29	37890	38652	90.39	89.88
Mix	5	263	77.1	14.448	56.1	0	1.636	1439.0	2.77	1509	0.88	1.603	558.7	16.89	920	0.85	19.76	615.7	1003	6.12	41471	42184	92.25	91.83
Mix	6	262	76.7	14.453	56.0	0	1.707	1472.9	2.93	1686	0.92	1.656	559.4	17.62	950	0.88	20.54	664.3	1040	6.02	44742	45495	93.52	93.35
Mix	7	261	76.1	14.454	56.0	0	1.771	1482.4	3.11	1643	0.95	1.686	566.5	18.16	967	0.90	21.27	704.8	1066	5.85	47467	48263	94.83	94.74
Sep	8	258	72.1	14.466	55.3	0	1.293	1261.7	1.37	1036	0.62	1.487	546.4	16.80	838	0.77	18.17	481.8	853	12.27	32453	32969	85.36	85.00
Sep	9	259	71.7	14.466	55.3	0	1.400	1294.8	1.70	1196	0.72	1.600	545.1	18.56	907	0.85	20.26	586.3	931	10.93	39492	40120	88.68	88.46
Sep	10	260	72.9	14.464	55.6	0	1.507	1328.6	2.00	1331	0.80	1.694	546.5	19.74	955	0.90	21.74	670.3	992	9.88	45145	45871	91.18	91.19
Mix	1	244	61.3	14.479	56.2	0.24	1.363	1341.9	1.93	1170	0.89	1.406	527.2	14.53	766	0.71	16.46	416.2	813	7.54	28031	19057	75.51	74.51
Mix	2	245	59.9	14.482	56.6	0.24	1.430	1370.0	2.19	1267	0.74	1.458	529.7	15.34	806	0.75	17.53	470.6	864	7.02	31663	22160	78.38	77.49
Mix	3	246	62.5	14.480	56.0	0.24	1.494	1386.3	2.40	1346	0.79	1.495	536.8	15.71	837	0.78	18.11	508.6	904	6.56	34271	24450	80.82	79.73
Mix	4	247	64.3	14.474	55.8	0.24	1.558	1410.7	2.56	1423	0.83	1.553	540.6	16.59	876	0.82	19.14	564.5	949	6.49	38021	27876	83.13	81.89
Mix	5	250	65.5	14.470	55.7	0.24	1.630	1443.3	2.75	1506	0.87	1.597	546.5	17.03	906	0.85	19.78	608.4	990	6.20	40975	30319	85.27	84.07
Mix	6	251	65.2	14.469	55.6	0.24	1.703	1465.6	2.92	1580	0.92	1.654	548.9	17.76	939	0.88	20.67	661.7	1030	6.08	44570	33462	86.98	85.97
Mix	7	254	69.8	14.483	55.2	0.24	1.771	1485.2	3.06	1646	0.96	1.707	555.0	18.30	972	0.91	21.35	708.9	1068	5.99	47749	36318	75.73	87.67
Sep	8	257	69.0	14.466	55.5	0.24	1.291	1259.0	1.34	1032	0.62	1.483	547.9	16.61	837	0.77	17.95	475.0	851	12.41	31989	22245	88.67	75.81
Sep	9	256	70.6	14.469	55.1	0.24	1.384	1291.4	1.57	1174	0.70	1.596	548.9	18.47	908	0.85	20.04	578.4	929	11.74	36955	28121	79.47	79.41
Sep	10	255	68.9	14.467	55.4	0.24	1.506	1329.8	1.97	1330	0.80	1.699	550.5	19.77	964	0.90	21.74	673.7	997	10.04	45376	33676	82.81	82.85
Mix	4	248	62.8	14.474	55.6	0.28	1.558	1418.5	2.54	1427	0.83	1.552	542.4	16.45	876	0.82	18.99	560.6	950	6.48	37760	25694	82.30	80.81
Mix	5	249	62.6	14.471	55.8	0.28	1.631	1440.7	2.72	1506	0.88	1.611	544.3	17.31	913	0.85	20.03	618.4	993	6.36	41652	28954	84.31	82.98
Mix	6	252	64.7	14.468	55.8	0.28	1.701	1465.3	2.92	1578	0.91	1.648	551.4	17.59	938	0.86	20.51	656.4	1029	6.02	44209	31238	86.32	84.96
Mix	7	253	66.0	14.467	55.5	0.28	1.770	1499.2	3.05	1650	0.95	1.707	553.7	18.34	971	0.91	21.39	709.8	1067	6.01	47810	34311	87.84	86.70

A6 - Aeroacoustic Data Summary of E<sup>3</sup> Nozzles

Test Date: Feb-95  
 Test Site: Cell 41  
 Config. No.: 4  
 Nozzle: Skewed Mixer (F12A)

Model Size, sq.in.: 45.7  
 Engine Size, sq.in.: 3078  
 Distance, ft.: 1500

Definition			Test Cell			Freejet	Model Core					Model Fan					Model Total				Engine Total			
Operating Line	Point No.	Reading No.	Relative Humidity	Ambient Pressure (Pamb, psf)	Ambient Temp. (Tamb, °F)	Mach No. (Ma)	Pressure Ratio (PR)	Total Temp (TTc, °R)	Weight Flow (Wc)	Velocity (Vc)	Mach No. (Mc)	Pressure Ratio (PRF)	Total Temp (TTF, °R)	Weight Flow (WF)	Fan Velocity (VF)	Mach No. (MF)	Weight Flow (WF)	Thrust (F)	Mixed Velocity (Vmix)	Bypass Ratio	Ideal Thrust	Ideal Net Thrust FN/5	PNL <sub>max</sub> dB	EPNL dB
			RELHUM	PSB105	TTCHA1	TERMAC	CORRAV	TTCAVG	OFLOW	CVELAV	CORMAV	FANRAV	TTF AVG	FLOW	FVELAV	FANMAV	TOTFLO	FGTOT	Vmix	BPR				
Mix	1	239	40.6	14.622	40.9	0	1.362	1349.2	2.05	1172	0.89	1.400	531.6	14.35	765	0.71	19.41	416.1	818	7.00	28022	28163	86.56	85.36
Mix	2	235	46.1	14.622	40.7	0	1.426	1367.2	2.30	1260	0.74	1.447	534.8	14.95	802	0.75	17.25	462.0	863	6.50	31179	31335	89.05	87.59
Mix	3	215	58.2	14.588	37.2	0	1.493	1387.1	2.46	1345	0.79	1.489	518.9	15.70	819	0.78	18.16	502.4	880	6.37	33840	34080	90.51	89.13
Mix	4	234	44.1	14.626	41.2	0	1.558	1417.7	2.63	1426	0.83	1.545	537.1	16.38	868	0.81	19.01	558.7	946	6.23	37628	37810	92.47	91.52
Mix	5	233	44.8	14.623	40.2	0	1.625	1448.6	2.78	1506	0.87	1.597	540.1	17.06	901	0.85	19.85	608.2	986	6.13	40965	41171	93.90	93.23
Mix	6	232	51.5	14.626	39.5	0	1.698	1489.3	2.96	1578	0.91	1.647	540.3	17.78	928	0.88	20.73	658.0	1021	6.02	44315	44527	95.38	94.96
Mix	7	231	42.9	14.624	41.3	0	1.771	1491.5	3.09	1648	0.95	1.702	537.8	18.53	954	0.91	21.62	709.0	1053	6.00	47682	47917	96.50	96.57
Sep	8	228	43.7	14.624	41.1	0	1.294	1258.2	1.61	1037	0.62	1.471	534.7	16.22	818	0.76	17.63	464.5	838	10.05	31285	31439	86.66	85.63
Sep	9	229	49.3	14.627	39.8	0	1.391	1286.6	1.88	1181	0.71	1.589	533.7	18.20	891	0.84	20.08	573.1	918	9.67	38598	38779	90.03	89.63
Sep	10	230	41.9	14.620	42.4	0	1.506	1321.6	2.25	1326	0.79	1.681	535.5	19.36	942	0.89	21.81	659.4	982	8.60	44411	44643	93.09	92.77
Mix	1	238	39.1	14.625	42.7	0.24	1.358	1343.8	2.08	1163	0.88	1.400	532.2	14.29	765	0.71	16.37	415.1	816	6.88	27956	18846	90.80	78.98
Mix	2	236	40.5	14.623	42.5	0.24	1.428	1367.3	2.29	1263	0.74	1.450	532.6	15.03	802	0.75	17.32	464.8	863	6.56	31309	21673	83.22	81.46
Mix	3	216	57.4	14.586	38.0	0.24	1.490	1393.0	2.47	1345	0.79	1.485	519.4	15.53	816	0.77	18.00	487.2	889	6.29	39490	23546	85.12	83.14
Mix	4	217	56.3	14.590	38.3	0.24	1.549	1427.1	2.55	1422	0.83	1.559	521.7	16.72	864	0.82	19.27	561.7	938	6.56	37834	27195	86.30	84.76
Mix	5	220	53.5	14.600	38.5	0.24	1.629	1444.1	2.85	1506	0.87	1.595	534.1	17.00	895	0.84	19.86	606.4	983	5.96	40843	29673	88.60	86.97
Mix	6	221	54.2	14.607	38.3	0.24	1.698	1488.8	2.94	1578	0.91	1.651	539.1	17.73	930	0.88	20.87	656.8	1022	6.02	44224	32796	90.04	88.57
Mix	7	224	48.2	14.614	40.1	0.24	1.767	1490.6	3.05	1644	0.95	1.697	545.5	18.21	959	0.90	21.20	698.3	1057	5.97	47034	35277	91.25	90.24
Sep	8	227	44.0	14.624	40.6	0.24	1.292	1257.3	1.56	1033	0.62	1.480	535.0	16.35	825	0.77	17.91	489.3	843	10.52	31807	21645	80.46	79.11
Sep	9	226	48.8	14.628	39.8	0.24	1.385	1291.9	1.82	1176	0.71	1.594	535.0	18.26	895	0.84	20.08	574.7	921	10.03	38706	27547	83.85	82.65
Sep	10	225	54.1	14.622	38.7	0.24	1.500	1327.8	2.18	1323	0.79	1.690	538.2	19.49	949	0.90	21.67	664.4	986	8.92	44747	32728	88.58	85.76
Mix	4	218	58.2	14.593	38.0	0.28	1.549	1417.9	2.58	1417	0.82	1.545	525.0	16.42	858	0.81	19.00	551.6	934	6.37	37149	24859	86.27	84.30
Mix	5	219	56.1	14.598	38.6	0.28	1.624	1439.3	2.77	1499	0.87	1.601	528.3	17.14	893	0.85	19.91	604.9	978	6.20	40739	27867	88.15	86.33
Mix	6	222	53.4	14.608	39.0	0.28	1.698	1467.6	2.95	1578	0.91	1.648	541.4	17.61	930	0.88	20.55	653.4	1023	5.97	44008	30707	89.22	87.77
Mix	7	223	49.6	14.613	39.8	0.28	1.769	1485.5	3.11	1642	0.95	1.706	543.9	18.38	961	0.91	21.49	707.8	1060	5.91	47673	33771	90.52	89.32

REPORT DOCUMENTATION PAGE			Form Approved OMB No. 0704-0188	
Public reporting burden for this collection of information is estimated to average 1 hour per response, including the time for reviewing instructions, searching existing data sources, gathering and maintaining the data needed, and completing and reviewing the collection of information. Send comments regarding this burden estimate or any other aspect of this collection of information, including suggestions for reducing this burden, to Washington Headquarters Services, Directorate for Information Operations and Reports, 1215 Jefferson Davis Highway, Suite 1204, Arlington, VA 22202-4302, and to the Office of Management and Budget, Paperwork Reduction Project (0704-0188), Washington, DC 20503.				
1. AGENCY USE ONLY (Leave blank)	2. REPORT DATE September 2002	3. REPORT TYPE AND DATES COVERED Final Contractor Report		
4. TITLE AND SUBTITLE  Acoustic and Laser Doppler Anemometer Results for Confluent and 12-Lobed E <sup>3</sup> Mixer Exhaust Systems for Subsonic Jet Noise Reduction		5. FUNDING NUMBERS  WU-781-30-12-00 NAS3-26617		
6. AUTHOR(S)  M. Salikuddin, R.R. Babbitt, H. Shin, S. Wisler, B.A. Janardan, and R.K. Majjigi				
7. PERFORMING ORGANIZATION NAME(S) AND ADDRESS(ES)  General Electric Aircraft Engines Company Mail Drop A411 One Neumann Way Cincinnati, Ohio		8. PERFORMING ORGANIZATION REPORT NUMBER  E-13387		
9. SPONSORING/MONITORING AGENCY NAME(S) AND ADDRESS(ES)  National Aeronautics and Space Administration Washington, DC 20546-0001		10. SPONSORING/MONITORING AGENCY REPORT NUMBER  NASA CR-2002-211597		
11. SUPPLEMENTARY NOTES  Project Manager, James Bridges, Structures and Acoustics Division, NASA Glenn Research Center, organization code 5940, 216-433-2693.				
12a. DISTRIBUTION/AVAILABILITY STATEMENT  Unclassified - Unlimited Subject Categories: 07 and 34 Available electronically at <a href="http://gltrs.grc.nasa.gov">http://gltrs.grc.nasa.gov</a> This publication is available from the NASA Center for Aerospace Information, 301-621-0390.			12b. DISTRIBUTION CODE	
13. ABSTRACT (Maximum 200 words)  The research described in this report has been funded by NASA Glenn Research Center as part of the Advanced Subsonic Technologies (AST) initiative. The program operates under the Large Engine Technologies (LET) as Task Order #3 1. Task Order 31 is a three year research program divided into three subtasks. Subtask A develops the experimental acoustic and aerodynamic subsonic mixed flow exhaust system databases. Subtask B seeks to develop and assess CFD-based aero-acoustic methods for subsonic mixed flow exhaust systems. Subtask B relies on the data obtained from Subtask A to direct and calibrate the aero-acoustic methods development. Subtask C then seeks to utilize both the aero-acoustic data bases developed in Subtask A and the analytical methods developed in Subtask B to define improved subsonic mixed-flow exhaust systems. The mixed flow systems defined in Subtask C will be experimentally demonstrated for improved noise reduction in a scale model aero-acoustic test conducted similarly to the test performed in Subtask A. The overall object of this Task Order is to develop and demonstrate the technology to define a -3EPNdB exhaust system relative to 1992 exhaust system technology.				
14. SUBJECT TERMS  Acoustic measurement; Laser doppler velocimeters; Noise prediction; Noise reduction; Scale models; Exhaust systems; Subsonic flow; Aeroacoustics; Jet aircraft noise			15. NUMBER OF PAGES 172	
			16. PRICE CODE	
17. SECURITY CLASSIFICATION OF REPORT Unclassified	18. SECURITY CLASSIFICATION OF THIS PAGE Unclassified	19. SECURITY CLASSIFICATION OF ABSTRACT Unclassified	20. LIMITATION OF ABSTRACT	